Rheological study of nuclear glass melts containing Platinum Group Metal aggregates

Norma-Maria Pereira Machado

LRGP – Laboratoire Réactions et Génie de Procédés
Unité de recherche CEA de Marcoule - DES/ISEC/DE2D/SEVT/LDMC

Thèse

Présentée et soutenue publiquement pour l'obtention du titre de

DOCTEUR DE l'UNIVERSITE DE LORRAINE

Mention : Génie des Procédés, des Produits et des Molécules

par **Norma Maria PEREIRA MACHADO**

Sous la direction de Philippe MARCHAL et Cécile LEMAITRE

Rheological study of nuclear glass melts containing Platinum Group Metal aggregates

5 Avril 2022

Membres du jury :

Directeur de thèse :	**Dr Philippe MARCHAL**	Ingénieur de Recherche CNRS - *Université de Lorraine, LRGP UMR CNRS 7274, Nancy*
Co-directrice de thèse :	**Dr Cécile LEMAITRE**	Maitre de Conférences - *Université de Lorraine, LRGP UMR CNRS 7274, Nancy*
Président de jury	**Dr Mohammed MALKI**	Professeur - *Université d'Orléans, CEMHTI-CNRS, Orléans*
Rapporteurs :	**Dr Valérie VIDAL**	Directrice de Recherche CNRS - *ENS de Lyon, Laboratoire de Physique, Lyon*
	Dr Elisabeth LEMAIRE	Directrice de Recherche CNRS - *Université Nice-Sophia Antipolis, Laboratoire InPhyNi, Nice*
Examinateurs :	**Dr Caroline HANOTIN**	Ingénieur Calculs – *IMF Ingénierie, Nancy*
Membres invités :	**Dr Arnaud POULESQUEN**	Ingénieur de Recherche CEA Marcoule - *Bagnols sur Cèze*
	Dr Victor PIOVESAN	Chargé d'affaires R&D - *Orano, Paris*
	Dr Isabelle GIBOIRE	Ingénieur de Recherche CEA Marcoule - *Bagnols sur Cèze*
Encadrante :	**Dr Muriel NEYRET**	Ingénieur de Recherche CEA Marcoule - *Bagnols sur Cèze*

Dedicated to all women and girls who are striving

to make their way in sciences.

Acknowledgements

"Life need not be easy, provided only that it is not empty."

Lise Meitner

First, I would like to thank all the members of the jury for accepting to evaluate this work. I thank Valérie Vidal and Elisabeth Lemaire for reporting the thesis, Mohammed Malki and Carolina Hanotin for examining it. I also thank Arnaud Poulesquen and Victor Piovesan for having accepted our invitation. The fruitful discussions and the very pertinent questions were very important to deepen the perspectives on the subject.

I would also like to thank the great people who led this work: Philippe Marchal, Cécile Lemaitre and Muriel Neyret. You have been present in Nancy or in Avignon and have been very supportive of me in carrying out this work over the last 3 years. It was a pleasure to meet you and work with you! A special thank you goes to Muriel for her help and friendship that started in 2017. Without your kind words, thoughtful attention, and the delicious teas we often shared in your office, I am sure completing the dissertation would have been much more difficult. Thank you very much!

I thank Florence Bart and Isabelle Bisel and then Frédéric Charton and Jacques Lacombe for their kind reception at SEVT. A big thank you also to Olivier Pinet for welcoming me to LDMC and to Isabelle Giboire. Thank you for the tireless way you defy all odds and for your unparalleled attention to all, creating an admirable working environment. Speaking of the working environment, I must not forget to thank the LDMC family (Julia Agullo, Virginie Ansaut, Jean-Gabriel Begos, Thierry Blisson, Flavien Brocheny, Valérie Debono, Leith Ghazzai, Taos Guyot, Jeanini Jiusti, Guillaume Laphitz, Annabelle Laplace, Cloé Laurin, Nais Mercier, Rémi Moles, Sylvain Mure, Muriel Neyret, Damien Perret, François Perrudin, Olivier Podda, Elise Regnier, Lilou Schintu, Alexandre Sierk, Charlène Vallat, Sylvain Vaubaillon, Aliénor Vernay, Eléonore Welcomme, Raphaël Penelope, Morgane Bisel) who have welcomed me so kindly and who have made the long days of work on my dissertation easier for me, both by the scientific exchange and by the pleasant conversations over coffee.

Cloé, what can I say? I could not have a better person to share the office during the thesis. I'll miss our Portuguese classes (não tem geladeira em casa não?), your incessant attempts to teach me names and the smile you bring every day. Even though we ended up not working in the same office, having you in the 208 corridors (and in the streets of Avignon) was of great

importance. Sylvain and Charlène, thank you for your tireless help during the experiments. They were not easy, but you contributed a lot to make them successful! Thank you, Elise, for all the help with the writing. I know how busy you were and yet you always had time for my limitless questions! Being part of the SEVT also allowed me to connect with amazing people outside of LDMC who were of great importance, such as Isabelle Hugon, Maxime Fournier, Emilien Sauvage, Kolani Paraiso, Helène Nonnet, Léa Brunswic, Lionel Campayo, Kamalesh Damodaran. Many thanks to Emilien and Isabelle for important discussions about the process and application of my topic. I would also like to give special thanks to Massine Bettache and Anna Klouzkovà, who did a lot of impeccable work during the time we worked together. I must not forget to thank the great people I met in the short time I spent in Nancy: Adilson, Diego, Andrea and Camila. Thank you for being so warm in a city where it snows even in the spring. ☺

Working at CEA has not only given me the opportunity to work with extraordinary people in the same building, but also to make friendships that I will carry with me forever and that have supported me throughout my work. Thank you, Luiz and Rafael, for all the laughs and scientific advice you all so eagerly gave. The 208 will never be the same after the departure of this first Brazilian dream team! Léa, Aline, Birsen, Miriana, Gabi, Jeanini, Leila I have no words for you my girls! Every drink, every dance, every laugh and every tear we shared is etched in me. We are all far away from our families, but we managed to make this one, Inshallah! Thank you! I also thank the amazing people I have had the pleasure of meeting outside of work, but who have contributed just as much. Anne, Laiza, Lucas and Fabien: what a group! You are a great gift of the coincidences that happen in Avignon, and I could not be happier to have met you! You are an important part of this Avignon family that I can always count on ☺.

Jeanini and Gabi, you both entered my life at the same time and became an integral part of my day. From the Avignon city tours to the long piqueniques, we bonded so much and I will be forever grateful to have had you both! You both gave me so much and I hope that one day I will be able to return the favor!!

Besides the friendships that Avignon has given me, I must also thank the friends who have accompanied me before this work and continue to do so: Gui, Bruna, Rean, Cris, Rhayza, Mari, Leleo, Otavio, Carol, Tosha, Bia, Katy, Julia, Duda, Dudinha, Rhoana, Peds, Queijo, Jeris, Belle. Thank you so much for always being there for me! Bia, we both decided at the same time

to continue our careers in France and since then we have become closer and closer. It's fantastic to have you always by my side, thank you!

A very important cog in everything I do is my family: Rui, Norma, Manuela, Zé and Ana! Even if there is an ocean between us, you managed to be present and be there for me. I will never find enough words to thank you guys!

And finally, I want to thank the little girl I once was and has never given up since, despite all the difficulties. It all started with her, and I am sure she would be proud to see what we have accomplished so far.

Muito obrigada à todos!

Table of Contents

Abstract

In France, borosilicate glass is used as a matrix to immobilize nuclear fission products resulting from spent fuel reprocessing. In the high-temperature vitrification process (1200 °C), most of elements to be contained react chemically with the vitrification additives to form a homogeneous glass melt. Platinum Group Metal (PGM) particles are not soluble in the melt and therefore are present as suspended particles of few microns. These particles exhibit an intense aggregation tendency and consequently the suspensions may present an anomalously high apparent viscosity. These systems are characterized by a shear-thinning and a thixotropic behaviors. The present study aims to provide important inputs for the overall rheological behavior of this system and its features through the characterization of a simulated nuclear glass melt containing 3.0 wt% (1.02 vol%) of PGM particles. A mathematical modeling of the thixotropic behavior of glass melts containing PGM particles is presented for the first time using a model similar to that proposed by Houska (*Houska, 1981*). This predictive model allow to describe experimental results obtained both in steady state and transient conditions. The impact of the shear stress and time on PGM aggregation degree and sedimentation kinetics is determined using an imposed-stress rheometer at high temperature and imaging analyses via Scanning Electron Microscopy (SEM). For the first time, the interplay between the rheological behavior of the system and the aggregation degree is provided, as well as the link with the particles settling. Based on the acquired experimental data, a force balance computation is executed to illustrate the different aggregation scenarios. The work provides a new input for the modeling and control of the vitrification process.

Keywords: Platinum Group Metals (PGM), Thixotropy, Aggregation, Sedimentation, Rheology.

Résumé

En France, les produits de fission nucléaire issus du retraitement des combustibles usés sont conditionnés au sein de matrices de verres borosilicatés. Lors du processus de vitrification à haute température (1200 °C), les éléments à confiner réagissent chimiquement avec les additifs de vitrification pour former un verre homogène. Cependant, parmi ces éléments, les platinoïdes ne sont pas solubles dans le bain de verre et restent en suspension sous forme de particules de quelques microns. Ces particules présentent une forte tendance à l'agrégation et les suspensions peuvent alors présenter une viscosité apparente anormalement élevée. Ces systèmes sont caractérisés par un comportement rhéofluidifiant et thixotrope. La présente étude vise à fournir des données importantes sur le comportement rhéologique global de ces systèmes et leurs propriétés, grâce à la caractérisation d'un verre nucléaire simulé contenant 3,0 % massique (1,02 % en volume) de platinoïdes. Une modélisation mathématique du comportement thixotrope de ce verre est présentée pour la première fois en utilisant un modèle similaire à celui proposé par Houska (*Houska, 1981*). Ce modèle prédictif permet la description des résultats expérimentaux obtenus à partir de mesures en régimes permanent et transitoire. L'impact de la contrainte de cisaillement et du temps sur le degré d'agrégation et la cinétique de sédimentation des particules est déterminé à l'aide d'un rhéomètre à contrainte imposée opéré à haute température et d'analyses d'images obtenues par microscopie électronique à balayage (MEB). Pour la première fois, l'interaction entre le comportement rhéologique du système et le degré d'agrégation est analysé, tout comme le lien avec la sédimentation des particules. Sur la base des données expérimentales acquises, un calcul d'équilibre des forces est réalisé pour illustrer les différents scénarios d'agrégation. Ce travail fournit des nouvelles données pour la modélisation et le contrôle du processus de vitrification.

Mots-clés : Platinoïdes, Thixotropie, Agrégation, Sédimentation, Rhéologie.

Notations

Latin Letters

Symbol	***Definition***	***Units***
1stN	Distance of the SU to their first neighbor	µm
a	Particle radius	µm
a_{eff}	Effective particle radius	µm
A	Constant for VFTH model for viscosity-temperature dependency	Pa.s
B	Constant for VFTH model for viscosity-temperature dependency	°C
C	Torque	Pa
C'	Integration constant	-
C_f	Compactness factor	-
d	Distance between two spheres in the fluid	µm
D	Mean Féret diameter	µm
D1stN	Average distance distribution of the SU first neighbor	µm
D1stNm	Normalized d1stn	µm
d_0	Initial separation distance between two spheres in the fluid	µm
d_c	Critical separation distance between two spheres in the fluid	µm
D_f	Fractal dimension	-
D_m	Normalized D	µm
F	Shear forces	J
F_H	Hydrodynamic force	J
F_{vdW}	Van der Waals potential	J
g	Gravity	$m.s^{-2}$
G	Shear modulus	Pa
h	Mean distance between the particles	µm
k	Dimensionless time constant	-
K	k_1/k_2	-
K_0	Thixotropic model parameter	-
k_1	Parameter of destructuration in the Houska model	-
k_2	Parameter of structuration in the Houska model	-
k_b	Boltzmann constant	$m^2 \cdot kg \cdot s^{-2} \cdot K^{-1}$
K_f	Prefix constant dependent of the radius	-
K_σ	Shear stress calibration constant for the Couette analogy	-
$K_{\dot{\gamma}}$	Shear rate calibration constant for the Couette analogy	-
m	Consistency	-
n	Flow index	-
N	Number of particles	-

n_0	Concentration of impurities in the melt	-
N_B	Number of SUs in the bottom of the crucible	-
n_s	Concentration of impurities in the saturation	-
N_T	Number of SU in the top of the crucible	-
P	Percentage of how many particles settled from the top	%
Pe	Péclet number	-
r	Distance from a point in the cylinder to the axis	µm
R	Aggregate radius	µm
Re	Reynolds number	-
R_e	External cylinder radius	µm
R_H	Hydrodynamic radius	µm
R_i	Internal cylinder radius	µm
R_s	Cluster maximum radius	µm
$R_{//}$	Radius of the parallels larger axis	µm
$R_\perp$	Radius of the perpendicular larger radius	µm
S	Surface	m^2
S'	Number of primary particles contained in a SU	-
SU	Structural unit	-
t	Time	s
T	Temperature	°C, K
t_0	State of homogeneous distribution of particles after pre-shear	s
T_0	Temperature constant for VFTH model for viscosity-temperature dependency	°C
t_c	Critical time of structure reorganization	s
t_m	Normalized experimental time	s
U	Sedimentation speed	$m.s^{-1}$
U_0	Stokes velocity of one single sphere	$m.s^{-2}$
U_{st}	Sedimentation velocity in a shear thinning fluid	$m.s^{-2}$
x	Particle volume fraction	%
x_c	Percolation threshold	%

Notations

Greek Letters

Symbol	*Definition*	*Units*
α	Thixotropic model parameter	-
γ	Shear strain	-
$\dot{\gamma}$	Shear rate	s^{-1}
$\dot{\gamma}_0$	Pre-shear rate	s^{-1}
$\dot{\gamma}_c$	Critical shear rate	s^{-1}
$\dot{\gamma}(r)$	Shear rate at *r* in the cylindrical layer	s^{-1}
η	Viscosity	Pa·s
$[\eta]$	Intrinsic viscosity	Pa.s
η_0	Low shear viscosity	Pa·s
$\eta_{e,0}$	Initial viscosity	Pa.s
$\eta_{e,\infty}$	Equilibrium viscosity	Pa.s
η_f	Viscosity of the continuous phase	Pa.s
η_r	Solvent viscosity	Pa.s
η_s	Relative viscosity of the suspension	Pa.s
η_∞	High shear viscosity	Pa·s
λ	Structure parameter	-
Λ	Hamaker constant	J
λ_0	Structure parameter when t = 0	-
μ	Critical exponent	-
ρ_f	Density of the fluid	$kg.m^{-3}$
ρ_s	Density of the spheres	$kg.m^{-3}$
ρ_p	Density of the suspended particles	$kg.m^{-3}$
σ	Shear stress	Pa
σ_c	Critical shear stress	Pa
σ_e	Electronic conductivity	$\Omega^{-1}.cm^{-1}$
σ_{e0}	Initial electronic conductivity	$\Omega^{-1}.cm^{-1}$
$\sigma(r)$	Shear stress at *r* in the cylindrical layer	Pa
τ	Characteristic time	s
τ_b	Brownian characteristic time	s
τ_h	Hydrodynamic characteristic time	s
φ	Dispersed particles volume fraction	-
Φ	Volume fraction	-
Φ_0	Initial volume fraction	-
Φ_c	Critical volume fraction	-
Φ_{eff}	Effective particle volume fraction	-

Φ_m	Maximum packing fraction for hard spheres	-
Φ_{max}	Hypothetical maximum crystal volume fraction	-
Φ_{meff}	Effective maximum packing fraction	-
Φ_{PK}	Shear dependent maximum packing	-
ψ_0	Rate of flow of the dispersed phase onto the surface of the melt	s
$\psi(t)$	Dynamics of precipitation	s
$\boldsymbol{\Omega}$	Angular velocity	s^{-1}

Introduction

Context and motivation

In France, a majority of pressurized water reactors implements Uranium Oxide (UOX) fuel. At the end of its cycle in the nuclear reactor, the spent fuel still contains recoverable materials, such as uranium (94 to 95%) and plutonium (1%), as well as non-recyclable waste (4%) [1,2]. After the extraction of uranium and plutonium by the PUREX chemical process [3], the remaining waste is dissolved in a nitric acid solution. This high-activity level solution needs to be converted to a monolith to contain radionuclides dissemination and in France is conditioned in a glass matrix. The waste vitrification is a two steps process where the nitrates salts of the waste are first converted into oxides at around 500 °C [4], forming the calcinate that is melted into the glass frit at a temperature between 1100 and 1250 °C [4]. It leads to the production of a homogeneous amorphous material, which is made of around 40 different elements [4]. Currently, the waste is confined in a sodium alumino-borosilicate glass, called R7T7. The crucible, used for glass production, can be heated by direct induction (hot crucible) or indirect induction (cold crucible). The nuclear glass is then poured into metal containers and then stored in ventilated wells before their future storage in deep geological formations [4,5].

During the elaboration at high temperature, most species to be confined react chemically with the vitrification additives to form a homogeneous liquid. However, some elements such as the Platinum Group Metals (PGM: here, Ru, Rh, Pd), do not chemically incorporate into the melt. They can be found as intermetallic of palladium and rhodium with tellurium in a spherical form (1 to 5µm) alongside with needle-like ruthenium oxide particles (10 to 20µm) [6,7]. The presence of these suspended elements has an impact on certain physical properties of the glass melt, such as its viscosity or its electrical conductivity, impacting directly the vitrification process. In addition, even if the PGM particles are in small quantities (3 wt%), their tendency to aggregate and sediment may lead, in degraded stirring conditions, to the formation of high volume fraction layers at the bottom of the crucible which can interfere in the process. Several studies were conducted seeking a better understanding of the PGM particles impact on the physical properties of the nuclear glass melt [8–12].

Investigating the rheological behavior of this system is of great importance considering that it can be strongly affected by the particles aggregation kinetics as well as the flow. The work of Puig *et al.* [11] and Hanotin *et al.* [10] demonstrated the shear thinning and thixotropic behavior of the nuclear glass melt. The phenomenological modeling of the system was well described by a simplified Cross model highlighting the existence of two Newtonian plateaus, at low and high shear rates [11]. According to the authors, at high shear rate, the system behaves as a suspension

containing small clusters and individual particles, and the viscosity is mainly controlled by the viscosity of the glass matrix; thus the suspension viscosity decreases when the temperature increases. On the other hand, at low shear rate and above a certain content of PGM particles, macroscopic aggregates composed of needle-like RuO_2 chains and PdTe spherical particles separated by thin layers of glass matrix are created, which strongly increase the viscosity of the nuclear glass; contrary to what happens at high shear rate, the viscosity increases with the temperature [10,11,13]. The reorganization of the particles can be explained by the interplay between acting forces. At low shear rate the aggregation is promoted by Brownian local reorganizations and van der Waals attraction forces while the hydrodynamic forces remain negligible. At high shear rates, the rheological behavior is then controlled by hydrodynamic forces due to shear flow, which causes the rupture of the aggregates and the drastic decrease of the sample viscosity [11].

The experimental difficulties encountered during the study of the glass melts associated to the involved high temperatures limits the literature on the subject. Although these previous studies accurately illustrate how the rheological behavior of this system is dependent on the shear rate, the temperature and the volume fraction, some questions remain unclear. The thixotropic behavior of the system was highlighted by Puig *et al.* but further analysis on the strong time dependence of the viscosity is still required. Considering that the PGM particle aggregation influences not only the rheological behavior of the material but also the sedimentation kinetics of the particles (through the size of the aggregates) and the electrical properties of the material (through the percolation threshold), it is necessary to update the criteria that determine the aggregation and to characterize it. Furthermore, a deeper investigation on the coupling between aggregation and sedimentation is necessary to the full analysis of the glass melt behavior. The objectives of this thesis are then based on these not fully addressed issues.

Thesis main goals

This PhD thesis takes place in the Laboratory for the Development of Conditioning Matrices of CEA Marcoule, in collaboration with the Center for Chemical Engineering of Rheologically Complex Media (GEMICO) of the Laboratory of Reactions and Process Engineering (LRGP, Nancy), which has developed expertise in dispersions rheology, formulation and associated modeling of rheological behavior of complex fluids. All the experimental work was carried out with the same material: a simulated borosilicate nuclear glass containing 3 wt% PGM particles. The glass was elaborated at 1200 °C on a full-scale pilot unit installed at CEA Marcoule [4].

The present study aims to provide important inputs for the overall rheological behavior of the glass melt containing PGM particle aggregates. The study has three main goals:

i. **Analyze the thixotropic behavior of the glass containing PGM particles**. And in particular, it aims to characterize the impact of the shear rate/ shear stress, time and temperature on the rheological behavior of the melt and to propose a mathematical modeling of the thixotropic behavior.

ii. **Study the aggregation of PGM particles in the glass** considering:
    a. The impacts of time and shear stress on PGM particle aggregation on a wide shear range, besides distinguishing the different aggregation mechanisms.
    b. The interplay between the aggregation degree of PGM particles in the melt and the rheological response of the suspension.

iii. **Establish the link between the rheological behavior and the PGM particle sedimentation**, in particular:
    a. Identifying the impact of the aggregation degree on the particles settling.
    b. Estimating the sedimentation rates as a function of the aggregation degree of the melt and as a function of time and shear stress/rate.

Description of the chapters

The thesis is composed of five different chapters, three of which were written as articles that were submitted to scientific journals on the research domains (chapter II, IV and V).

In the **first chapter**, a **literature review** is presented exploring the waste vitrification background concerning the materials that have been studied, as well as a summary of the latest studies on the behavior of PGM particles in glass. A background of the main concepts of rheology, aggregation and sedimentation is also presented to support the study.

The **second chapter** presents a deep **analysis of the thixotropic behavior of the simulated glass melt containing PGM particles**. To conduct this analysis, techniques adapted to high temperatures were employed in order to characterize the impact of the shear rate, time and temperature (from 1100 to 1250 °C) on the rheological behavior of the melt. A mathematical modeling of the thixotropic behavior of glass melts containing PGM particles is presented for the first time, for a glass melt suspension, using a model similar to that proposed by Houska [14]. The use of the model to describe the thixotropy of the system based on steady state measurements is presented. In particular, it is shown that the model is able to predict the transient behavior of the samples without additional adjustable parameters than those

determined in steady-state regime. In this chapter, the high temperature measurements were conducted by imposing the shear rate in order to fix the characteristic flow time and so to simplify the application of the thixotropic model. This chapter was submitted to the journal Rheologica Acta.

Considering the goal of the thesis to study the aggregation of PGM particles over the widest possible shear rate/stress range, it turns out that stress-imposed tests achieve much lower shear rates than strain-imposed tests. Therefore, the **third chapter** presents a **complementary analysis of the thixotropic behavior of the material** through stress-imposed experiments. More specifically, this chapter focuses on analyzing the evolution of the viscosity of the glass melt with time and temperature (from 1100 to 1250 °C) as a function of the shear stress. The data were analyzed through a phenomenological approach using an exponential model associating the apparent viscosity with a characteristic time to fit the experimental data

Given the insight into the thixotropic behavior of the material and its features, the **fourth chapter** consists in characterizing the **PGM particle aggregation in the glass melt**. The impact of shear stress and time on the degree of PGM aggregation was evaluated using rheological experiments at 1200 °C and imaging analysis via Scanning Electron Microscopy. Given the difficulties of in situ analysis at high temperatures, a post-mortem approach was adopted, in which each sample was first submitted to a different shear stress for a certain time interval and then quenched, so that the PGM particles rearrangement can be investigated. For the first time, the interplay between the rheological behavior of the system and the aggregation degree was described. Based on the acquired experimental data, a force balance computation was executed to illustrate the different aggregation scenarios. This chapter was submitted to the Journal of Nuclear Materials.

The **fifth chapter** investigated the **sedimentation kinetics** of the simulated glass melt at 1200 °C, as well as the impact of the shear stress and time. The samples obtained for the aggregation study presented in the fourth chapter were further analyzed in this chapter. The different degrees of aggregation provided a better understanding of the impact of shear stress and time on sedimentation. Based on the work of Allain *et al*. [15] for settling in diluted systems, the sedimentation velocity of PGM particles was estimated by presenting the interaction between sedimentation and aggregation over a wide range of shear stresses, providing a new input for modeling and controlling particle sedimentation. This chapter was submitted to the Journal of Nuclear Materials.

Finally, an overall conclusion closes the study by presenting the general insights obtained throughout the thesis as well as the perspectives for future research. For practical reasons, each chapter uses its own nomenclature, which is presented at the beginning of the corresponding chapter. The numbering of tables and figures is specific to each chapter and is presented in the following form: "chapter number - figure/table number".

References

[1] Production mondiale d'Électricité - L'énergie nucléaire dans le monde, (n.d.). https://www.cnrs.fr/cw/dossiers/dosnucleaire/darkcartes/1_production-mondiale-d-electricite.php (accessed November 3, 2021).

[2] D. Greneche, Cycle du combustible nucléaire: aval du cycle et questions génériques, Tech. l'Ingénieur. BN3564 V1 (2016).

[3] CEA, Monographie DEN - Le traitement-recyclage du combustible nucléaire usé, 2008.

[4] T. Advocat, J.L. Dussossoy, V. Petitjean, Vitrification des déchets radioactifs et appareillage, Les Tech. l'Ingénieur. 33 (2008) 0–27.

[5] G. Roth, S. Weisenburger, Vitrification of high-level liquid waste: glass chemistry, process chemistry and process technology, Nucl. Eng. Des. 202 (2000) 197–207. https://doi.org/10.1016/S0029-5493(00)00358-7.

[6] K. Uruga, T. Usami, T. Tsukada, S. Komamine, E. Ochi, Viscoplasticity of simulated high-level radioactive waste glass containing platinum group metal particles, J. Nucl. Mater. 452 (2014) 419–424. https://doi.org/10.1016/j.jnucmat.2014.05.062.

[7] R.F. Taylor, Chemical engineering problems of radioactive waste fixation by vitrification, Chem. Eng. Sci. 40 (1985) 541–569. https://doi.org/10.1016/0009-2509(85)80001-4.

[8] B. Luckscheiter, Properties and behavior of the platinum group metals in the glass resulting from the vitrification of simulated nuclear fuel reprocessing waste, J. Mater. Res. 6 (1991) 2535–2546. https://doi.org/10.1557/JMR.1991.2535.

[9] C. Simonnet, A. Grandjean, J. Phalippou, Electrical behavior of platinum-group metals in glass-forming oxide melts, J. Nucl. Mater. 336 (2005) 243–250. https://doi.org/10.1016/j.jnucmat.2004.09.019.

[10] C. Hanotin, J. Puig, M. Neyret, P. Marchal, Platinum group metal particles aggregation in nuclear glass melts under the effect of temperature, J. Nucl. Mater. 477 (2016) 102–109. https://doi.org/10.1016/j.jnucmat.2016.04.033.

[11] J. Puig, C. Hanotin, M. Neyret, P. Marchal, High temperature rheological study of borosilicate glasses containing platinum group metal particles by means of a mixer-type

rheometer, J. Nucl. Mater. 469 (2016) 112–119. https://doi.org/10.1016/j.jnucmat.2015.11.053.

[12] R.B. Nuernberg, N.M.P. Machado, D. Jouglard, L. del Campo, M. Malki, M. Neyret, The origin of hysteresis in the electrical behavior of RuO2-glass composite melts, J. Non. Cryst. Solids. 557 (2021). https://doi.org/10.1016/j.jnoncrysol.2020.120596.

[13] J. Puig, B. Penelon, P. Marchal, M. Neyret, Rheological Properties of Nuclear Glass Melt Containing Platinum Group Metals, Procedia Mater. Sci. 7 (2014) 156–162. https://doi.org/10.1016/j.mspro.2014.10.021.

[14] M. Houška, R. Žitný, Dynamics of Thixotropic Liquids and Time Dependency, in: Adv. Food Rheol. Its Appl., Elsevier, New York, 2017: pp. 47–63. https://doi.org/10.1016/B978-0-08-100431-9.00003-6.

[15] C. Allain, M. Cloitre, F. Parisse, Settling by cluster deposition in aggregating colloidal suspensions, J. Colloid Interface Sci. 178 (1996) 411–416. https://doi.org/10.1006/jcis.1996.0135.

Chapter I

Literature Review

Introduction

In the introductory chapter, we establish the context in which this study is held and present the objectives towards expanding the knowledge concerning the impact of Platinum Group Metal (PGM) particles on the rheological properties of a glass melt. Therefore, this literature review first describes the context of this study that means the energy production in France and the high-level waste vitrification process. Then, the rheology of glass melts is exposed and some necessary concepts such as rheometry and non-Newtonian behaviors are explained. The phenomenological modelling of complex fluids is also reviewed, and a very useful approach is found to understand the rheological behavior of glass melts containing suspended particles. The latest studies concerning the influence of PGM particles on glass rheology as well as their aggregation and sedimentation kinetics and their morphology features are summarized, evidencing a hiatus on the subject. Nonetheless, the former studies on the subject, although scarce, are essential to the development of the thesis.

1 Context of this study: the vitrification of nuclear High Level Waste

1.1 Electricity production in France

Nuclear energy today is one of the lowest greenhouse gas emitting energy sources and is responsible for generating around 10% of the world electricity [1,2]. In France, 70.6 % of the country electricity comes from nuclear with 56 operable Pressurized Water Reactors (PWR) [1]. The French nuclear park started in the 1950s and today is the second largest in the world in terms of power, giving the country today an energy independency [3]. Considering the awareness of the depletion of carbonaceous fossil resources combined with the perspective of global warming, the nuclear option remains an unavoidable energy choice for France to efficiently produce electricity with low CO_2 emissions [4].

The electricity produced by nuclear power plants uses the continuous energy released by the chain fission reaction of heavy nuclei (uranium 235), [5]. The nuclear fuel cycle (Figure I-1) consists in three main parts:

1) preparation of uranium oxide fuel (from the uranium recovery to produce the uranium ore concentrate ("yellowcake") until its enrichment to increase the concentration of uranium 235 and the uranium oxide (UOX) fuel production),
2) use of UOX fuel in nuclear power plants for four to five years to produce electricity,
3) fuel reprocessing. Indeed, only 6 % of the initial fuel is consumed in the nuclear power plant. Therefore, the spent fuel still contains recoverable materials (uranium (94 to 95%) and plutonium (1%)), which can be used to make new nuclear fuel. However, fission reactions that have taken place in the reactor also lead to fission products and other actinides resulting from neutron captures. These fission products and minor actinides constitute the ultimate waste (4%) that constitutes a non-recyclable mater. Thus, this third part of the fuel cycle leads to a "closed cycle" of the uranium oxide cycle, and, after conditioning (see §1.3), to the final disposal of the ultimate waste [6,7].

1.2 The French reprocessing of nuclear fuel

The process PUREX (Plutonium Uranium Refining by Extraction) set up in La Hague has been developed to reprocess the spent fuel in France. It consists in extracting the uranium and the plutonium still present in the spent fuel and allows therefore to reduce the radioactivity of the final waste [8]. Plutonium thereby extracted is then used to make Mixed Oxide (MOX) fuel [7]. This fuel is being considered in particular for future fast neutron reactors and to date, it is used in about thirty PWRs in Europe. In France, the majority of PWRs still implements Uranium

Oxide (UOX) fuel [7]. At the end of the fuel reprocessing, fission products and minor actinides remain in the obtained nitric acid waste solution. This final waste, which is a High Level Waste (HLW), needs to be contained to prevent the dissemination of radionuclides in the environment.

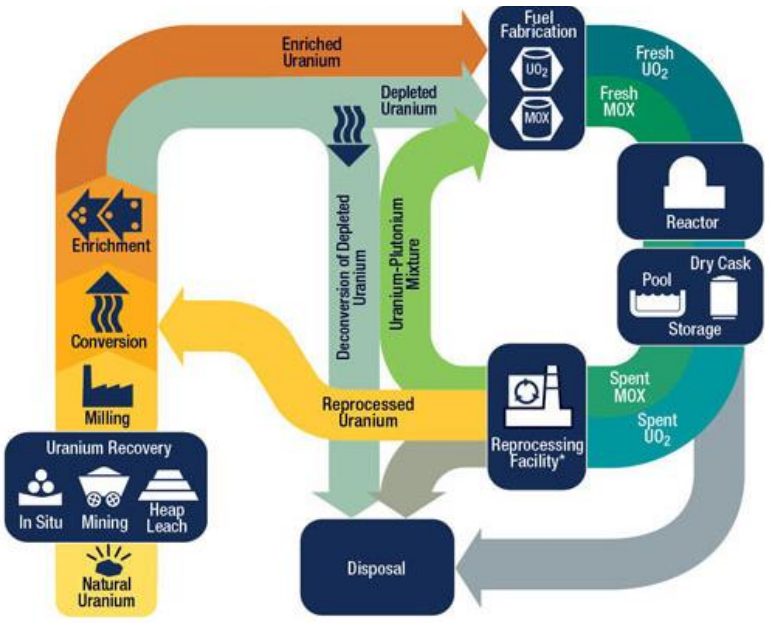

Figure I-1 - Representation of the "closed" nuclear fuel cycle [9].

This high level waste (HLW) corresponds to a small part of the French radioactive waste in term of volume (0.2 vol%). Nonetheless, it is characterized by a high radioactivity contributing to 95% of the radioactivity level of the waste stockpile in the country, according to ANDRA (Agence Nationale pour la Gestion des Déchets Radioactifs) [10]. Thus, in the1960s, the vitrification of these waste solutions was chosen and developed over the years. The conditioning of this HLW is further explained in the next section.

1.3 High-level waste (HLW) conditioning

In France, ANDRA classifies the nuclear waste accordingly to two main criteria: their level of radioactivity and their half-life. The level of radioactivity relates to the amount of radiation emitted by the radioactive elements (radionuclides) contained in the waste. It can be separated in four levels: high activity (HA for “Haute Activité” in French), average activity (MA for “Moyenne Activité” in French), low activity (FA for “Faible Activité” in French) and very low activity (TFA for “Très Faible Activité” in French). The half-life quantifies the time at which the initial activity of a radionuclide is halved. ANDRA thus distinguishes short-life waste, that mainly contains radionuclides with a half-life shorter than or equal to 31 years) and long-life waste, that mainly contains radionuclides with a half-life longer than 31 years) [11]. This

classification allows ANDRA to choose the appropriated waste management system based on their characteristics. Since the decay is the only way radioactivity become innocuous, HLW must be safety stored for thousands of years in order to protect the environment and the public. In the 1960s, after different attempts of solidifying the complex waste solutions containing more than 40 chemical elements in different materials, the glass proved to be an effective conditioning matrix for the waste. Indeed, the highly disordered structure of the glass allows the incorporation of a large number of different elements by creating chemical bonds with the glass forming oxides without jeopardizing its physical-chemical properties [12].

From there, the French waste vitrification process has been developed from laboratory scale to industrial scale. This process is a two steps process (Figure I-2) where the nitrates salts of the waste solution are first converted to oxides at 400 °C, forming the calcinate that is then melted with the glass frit in a furnace heated at high temperature (ab. 1100°C). In France, the crucible is fed almost continuously and can be heated by direct (hot crucible) or indirect induction (cold crucible). The nuclear glass is then poured into metal containers and then stored in wells before their future storage in deep geological formations [13]. Casting is done discontinuously: the stainless steel containers are filled in two 200 kg pours. A homogeneous amorphous material containing around 40 different elements is produced [12,13]. The glass composition selected for the HLW conditioning is a sodium alumino-borosilicate glass (called “R7T7 glass” because of the name of the plant where they are produced) and presents good properties in term of long-term behavior [14].

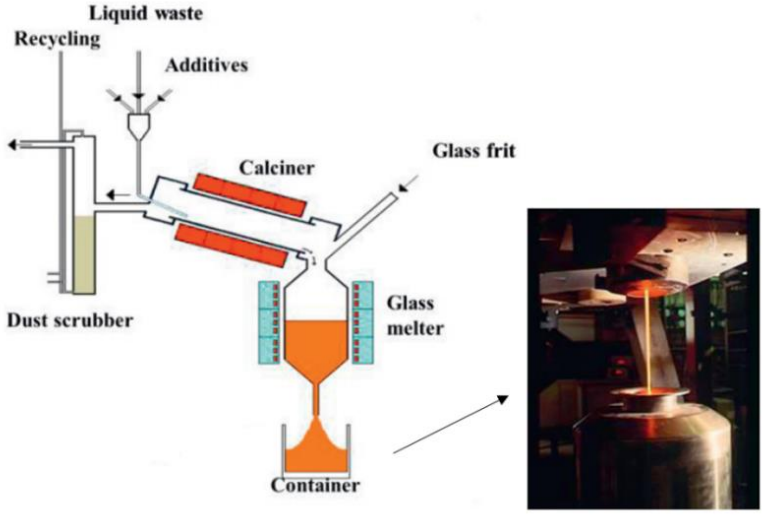

Figure I-2 - Scheme of the French two-step vitrification process [15].

1.4 French vitrification furnaces

The “Hot Crucible” consists in introducing the calcinate and the glass frit into a metal crucible that is afterwards heated at about 1100°C thanks to the induction heating of the furnace which transfers its heat to the glass bath by thermal conductivity. The “Cold Crucible” induction melter technology (Figure I-3) is innovative in the sense that the induced currents, do not circulate in the walls of the crucible but directly in the glass melt [15,16]. The walls are again metallic, but separated in small sections by insulating layers, in order to make them transparent to the magnetic field. To improve the longevity of the furnace, the walls are cooled by a circulation of cold water, thus creating a protective layer of frozen glass called auto-crucible. This glass layer of a few millimeters thick acts as a thermal barrier. The cold glass layer also serve as an electrical insulator for the various metal structures of the furnace. This technology allows the glass to be processed at 1200°C or even 1300°C. As glass is an insulating material, the initiation of the fusion of the glass frit is done by a titanium ring [13,15].

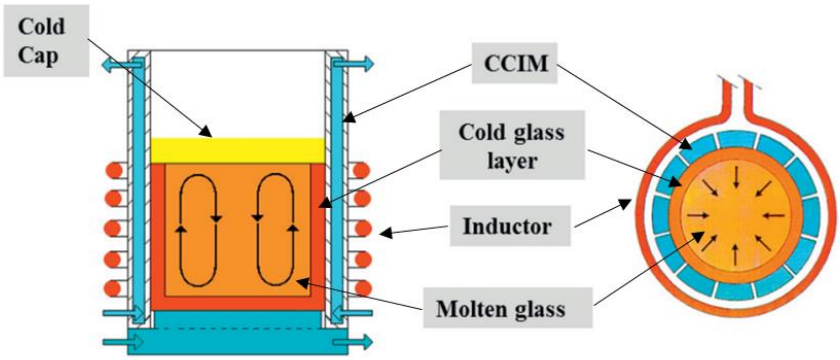

Figure I-3 - The cold crucible induction melter (CCIM) [15].

1.5 PGM particles in the vitrification furnaces

During the elaboration at high temperature, most radionuclides contained in the liquid waste react chemically with the vitrification additives to form a homogeneous liquid. However, among these radionuclides, elements from the Platinum Metal Group (Ru, Rh, Pd) do not chemically incorporate into the melt because of their very low solubility limits [17,18]. Therefore, these elements can be found as alloys of palladium-rhodium-tellurium in a spherical form (balls of 1 to 5 µm) alongside with needle-like ruthenium oxide particles (10 to 20 µm). The presence of these suspended elements has an impact on certain physical properties of the glass melt such as its viscosity or its electrical conductivity, then affecting the vitrification process [19]. In addition, their tendency to aggregation and sedimentation is likely to form layers of high volume fraction at the bottom of the crucible, which can interfere in the process.

In order to minimize the sedimentation and aggregation phenomena, a mechanical agitation system coupled with a bubbling system have been implemented [13,19]. The impact of these undissolved elements in the overall behavior of nuclear melts will be further discussed in this chapter and is the focus of this study.

Conclusion

The first part of this literature review listed the main facts on waste vitrification aiming to clarify the background of this work. The context of nuclear energy in France as well as the nuclear waste management was detailed. The importance of studying the behavior of glasses containing PGM particles comes from the impact these particles may have on the conditioning glass for high-level waste. This section combined with the next section which describes the rheology of glass melts serve as a base for the following sections which detail the impacts of the suspended particles on the glass melt properties.

2 Rheology of glass melts

2.1 Rheology: An overview

The word *Rheos* means "flow" in Greek. Rheology is the name given by Eugene Bingham to the study of flow and deformation of matter. It is known as a multidisciplinary science that relies on the understanding of a material response to external applied forces [20]. It has a wide range of applications in fields that go from cosmetics to metallurgy. Over the years, different theories describing the behavior of solid and liquids were derived providing mathematical representations. Elasticity theory is based on Hooke's Law (Eq.(1)) to describe mechanical properties of elastic solids where the stress applied (σ) in a material is proportional to the deformation γ and to a constant G (Shear Modulus), the material elasticity modulus. On the other hand, Newton-Stokes' Law (Eq. (2)) describes the properties of viscous liquids where the shear stress (σ) is proportional to the shear rate ($\dot{\gamma}$) and the viscosity (η), which is a coefficient of proportionality that measures the fluid resistance to flow [21]. Materials that follow these laws are known as Hookean and Newtonian, respectively.

$$\sigma = G\gamma \tag{1}$$

$$\sigma = \eta\dot{\gamma} \tag{2}$$

However, many materials exhibit more complex behavior, and rheology comes as a tool to formulate new models to describe these materials and improve their characterization. In glass science, several techniques are applied to analyze the rheological behavior of the glass melt during steps of production (melting, fining, forming, and annealing) but also in order to understand the relaxation and the glass transition of super cooled liquids[22][23][24]. Most glasses present a Newtonian behavior, described by Eq. (2), with a viscosity independent of the applied force; and mathematical models have been proposed to predict viscosity as a function of temperature, composition and thermal history [22]. Still, some glassy systems under different conditions and compositions exhibit non-Newtonian behavior [23,25], a topic that will be explored in this work . In the next sections, the main concepts and parameters of rheology will be defined.

2.2 Main definitions

To understand the main parameters involved in a rheological study, it is important to know the different types of flow that a material may undergo as illustrated in Figure I-4. Shear flow and extensional flow are the two basic kinds that involve the movement of adjacent particles. In the former kind, particles or elements flow over or past each other; in the latter kind, the elements flow towards or away from each other [26].

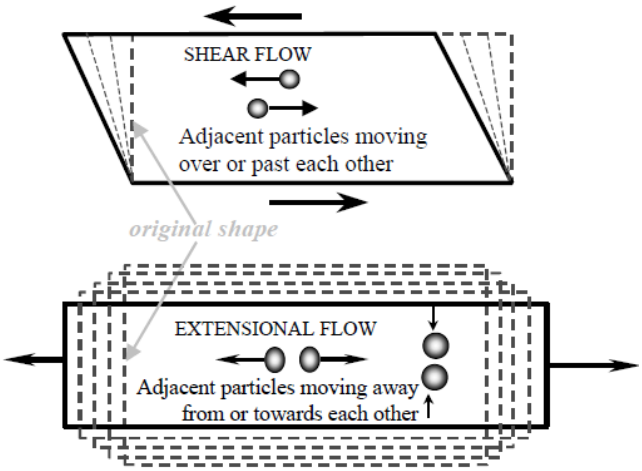

Figure I-4 - Scheme for a Shear and an Extensional flow [26].

- Shear Stress (σ)

A shear flow is also characterized by the sliding of layers over each other, creating a laminar movement that leads to the deformation of the material [26]. During a laminar flow, friction

forces acts tangentially to the layer surface (S), these forces are called "shear forces" (F). Thus, the shear stress (σ) can be defined as:

$$\sigma = \frac{dF}{dS} \tag{3}$$

where force is expressed in Newtons (N) and surface in square meters (m^2), so that the shear stress unit is Pascal (Pa).

- Shear Strain (γ) and Shear Rate ($\dot{\gamma}$)

The movement of the layers causes a gradient of velocity. In a simple case, the speed increases linearly from one layer to the other. The uppermost layer moves at a higher velocity than the lowermost [26]. The deformation of a fluid particle caused by this movement is called shear strain and can be defined as:

$$\gamma = \frac{dx}{dz} \tag{4}$$

Where *dx* is the differential distance travelled by a particle and *dz* is the differential thickness of the flow layers. This way, the shear rate ($\dot{\gamma}$) is the rate of the strain in which the material undergoes. It can be obtained by deriving the strain over time, obtaining the following relation:

$$\dot{\gamma} = \frac{dv}{dz} \tag{5}$$

Where dv is the differential velocity between two adjacent fluid layers. The shear rate has the units of velocity divided by distance, i.e. units of one over seconds (s^{-1})[27].

- Viscosity (η)

Viscosity is a transport property that can be generally defined as a resistance to the flow. When considering a laminar shear flow, a fluid passes between two layers with an internal friction force that is represented as the necessary energy for it to move while the layers slide over each other. If the layer, with surface *S*, moves parallel to another at a speed *v*, a force *F* per unit area *S* shall be applied to maintain the displacement, such as in Eq.(3). The higher this force, the more viscous the fluid [26].

$$\frac{dF}{dS} = \eta\left(\frac{dv}{dz}\right) \tag{6}$$

The unit of viscosity is Pascal divided by reciprocal seconds, which leads to Pascal seconds (Pa.s). When the fluid is non-Newtonian, the ratio of shear stress over shear rate, which is equals to the viscosity, is not constant, so that the viscosity, which is then called "apparent viscosity", is not constant and depends in particular on the shear rate. Furthermore, the viscosity is strongly dependent on the temperature and several equations can model this dependency. The main equation used for super cooled liquids is the Vogel-Fucher-Tammann-Hesse (VFTH) equation that considers three constants (*A*, *B* and T_0) and the absolute temperature *T*, as follows [28]:

$$\log_{10}\eta = A + \frac{B}{T - T_0} \tag{7}$$

The VFTH equation was used for glass as the standard viscosity equation for years since it works well for strong glass-forming liquids, for example, oxide glasses, however it performs more poorly for fragile systems [22]. Other parameters that influence the viscosity are the chemical nature of the fluid, the phase concentration in solutions, the applied pressure, the time and the shear rate [29] . Moreover, it is important to notice that the two last mentioned parameters strongly influence the behavior of non-Newtonian fluids. The characteristics of these materials will be discussed further in another section.

2.3 Rheometry

Rheometry is a group of experimental techniques developed to determine the rheological properties of materials. The technique choice will depend on the property to be explored [30]. To understand the behavior of the fluid, it is necessary to know several rheological properties and not only a viscosity value. Except for Newtonian fluids, the rheological behavior will depend on the flow characteristics [31]. It is possible to separate the most used techniques in three groups [30]: capillary technique, falling/rolling ball technique and rotational technique. The latter is the most used to characterize non-Newtonian fluids, such as suspensions and complex fluids, which is the base of this study [32]. It consists in submitting the fluid to a shear between two surfaces (one at rest and the other mobile) which geometry may vary. The next sections will discuss in more details the main geometries and the aspects of this technique.

2.3.1 Rotational Technique- Parallel-plates Geometry

The parallel plates geometry consists of two coaxial parallel discs of radius *R*, where one of the discs is fixed and the other is rotating at a known angular speed **Ω** (Figure I-5). The fluid is confined between the two plates in a gap of thickness *h*, settled by the operator. This kind of measurement can be advantageous due to its adaptability to several fluids and the small fluid volume required for the experiments. Nonetheless, if the fluid is too viscous or if it sediments easily, this kind of geometry is not recommended [31]. The shear rate gradient is not constant in the gap; it reaches a maximum value at the periphery and a zero value at the center. This phenomenon affects directly the measurement especially when dealing with non-Newtonian fluids [31].

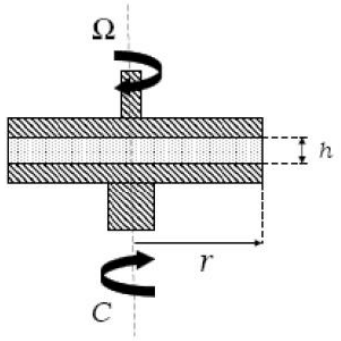

Figure I-5 - Parallel plate's geometry [33].

2.3.2 Rotational Technique- Couette Geometry

The name Couette comes from the famous physicist Maurice Couette. His name is given to designate the shear flows usually created between two walls that move parallel to each other, as well as for the geometry of concentric cylinders, some of the base of his research [34]. In the concentric cylinder's configuration, the gap between the cylinders is filled with the material to be measured (Figure I-6). This configuration allows the study of very fluid materials, which cannot remain within the plane geometries during the tests [35]. The applied torque (C) and the stress in this layer can be obtained by:

$$C = 2\pi r^2 L\sigma \quad \rightarrow \quad \sigma(r) = \frac{C}{2\pi r^2 L} \tag{8}$$

where L is the height of the cylinders, r is the distance from a point to the axis and $\sigma(r)$ is the shear stress at r in the cylindrical layer. Eq.(8) shows that shear stress varies as the inverse of the distance r, resulting in a shear rate that is not homogeneous in the gap between the cylinders. The smaller is the gap, the larger is the shear rate for a given angular velocity [33]. For a non-

Newtonian fluid which viscosity follows a power law $\eta = m\dot{\gamma}^{n-1}$, the shear rate is expressed by

$$\dot{\gamma}(r) = \frac{4\pi N}{n} \frac{(R_e/r)^{(2/n)}}{(R_e/R_i)^{(2/n)} - 1} \tag{9}$$

where R_e and R_i are respectively the external and internal cylinder radius and speed N is the angular speed of the rotating cylinder.

2.3.3 Couette Analogy – Mixer-type rheometry

Rheological studies of complex systems often find challenges in the conventional geometries available for analyses. In this scenario, the systemic rheology is born to integrate the known rheology with other disciplines, such as process engineering, to study complex systems in their real conditions of production, packaging and implementation [36]. Therefore, to overcome the limitations of regular rheometers, the mixer-type was created coupling a mixing device to a cylinder tank, making possible to analyze heterogeneous fluids with continuous mixing without phase separation. The torque and rotational speed are monitored and can evidence the rheological behavior of the mixture. Nonetheless, to extract from these data the viscosity/shear-rate curves, the Couette analogy is necessary [37]. The analogy consists in determining the inner cylinder radius R_i of a virtual Couette system with the same height L as the mixer, in which at the angular speed N, the torque C generated in the tank (cylinder of radius R_e) is identical to the one generated in the real system mixer-tank (Figure I-6) [38], the external radius R_e being the same for the real and virtual external cylinder.

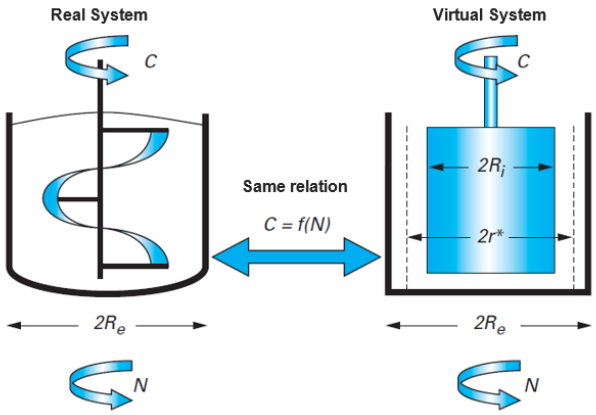

Figure I-6 - The Couette analogy principle, where a real system is considered analogous to the traditional Couette geometry [36].

In such a geometry, the shear stress at a given position *r* in the gap is obtained directly from the *r*,θ-component of shear stress, related to the torque C [37]:

$$\sigma(r) = \frac{C}{2\pi L r^2} \tag{10}$$

The internal radius of the mixing device is obtained by solving hydrodynamic equations in the particular case of a generalized Newtonian fluid obeying a power law $\eta = m\dot{\gamma}^{n-1}$, where *m* and *n* are the consistency and the flow index respectively. In most cases, *n* is smaller than one, corresponding to shear-thinning or pseudoplastic behavior. The expression of the internal radius is written as [39]:

$$R_i = R_e \Big/ \left[1 + \frac{4\pi N}{n}\left(\frac{2\pi m L {R_e}^2}{C}\right)^{\frac{1}{n}}\right]^{\frac{n}{2}} \tag{11}$$

It was demonstrated that the internal radius varies slightly with index *n*, hence a calibration procedure can be performed using a Newtonian fluid or any other well-characterized power law fluid. With the established R_i, it is possible to determine the shear rate variation as a function of r and n:

$$\dot{\gamma}\,(r,n) = \frac{4\pi N}{n}\frac{(R_e/r)^{(2/n)}}{(R_e/R_i)^{(2/n)}-1} \tag{12}$$

Eq. (12) demonstrates that, even in a large gap, there is a narrow region around a value *r** where the shear rate range is nearly independent of n. The optimum *r** can be calculated assuming two extreme values of the flow index (n and n'), considering only shear thinning fluids:

$$r^* = \left[\frac{n'}{n}\frac{(R_e/R_i)^{2/n'-1}}{(R_e/R_i)^{2/n-1}} {R_e}^{(2/n-2/n')}\right]^{\left(\frac{1}{2/n-2/n'}\right)} \tag{13}$$

In the particular case of n=1, the shear rate at particular position *r* = *r** is proportional to the angular speed *N*, *i.e.* $\dot{\gamma} = K_{\dot{\gamma}} N$ [40]. To calculate the apparent viscosity, it is necessary to divide the shear stress and the shear rate calculated at position *r** for n = 1 in Eq.(9) and Eq.(10), obtaining the following relations for the calibration constants:

$$K_\sigma(r) = \frac{\sigma}{C} = \frac{1}{2\pi L r^2} \tag{14}$$

$$K_{\dot{\gamma}}(r,n) = \frac{\dot{\gamma}}{N} = (2/n)\frac{(R_e/r)^{2/n}}{(R_e/R_i)^{2/n} - 1} \quad (15)$$

Several authors [32]–[44] used the Couette analogy for non-conventional geometries and complex fluids showing its efficiency in translating the experimental data obtained in the rheological profile of the material.

2.3.4 Glass rheometry - High temperature measurements

One of the main parameters that influence the rheological behavior of a material is temperature. Nonetheless, the apparatus available for rheological analysis are mainly designed to operate with high accuracy at room temperature, with a margin of a few degrees, which is enough to see changes in the behavior of several materials [45]. For materials such as glasses, higher temperatures (above 700°C) are necessary to make rheological analysis in the molten state. These conditions restrict the choices of design and the method should be chosen considering the chemical and physical properties of the material. Glass viscosity can vary by twelve or more orders of magnitude with temperature. Since some techniques are limited to a specific range of temperature and viscosity, several techniques are necessary to study the rheological behavior of the material in a wide thermal range [46][47]. Figure I-7 shows a correlation between viscosity at some important glass processing temperatures and the main techniques to measure it.

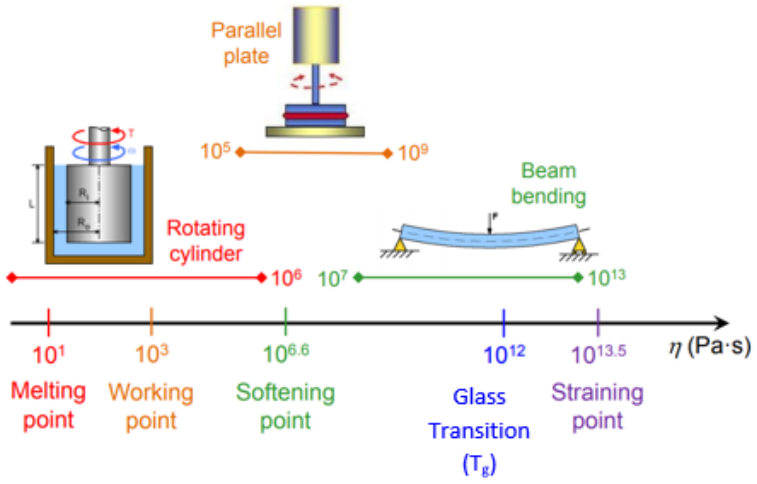

Figure I-7 - Correlation between the viscosity at some of the important glass processing temperatures and the main techniques to measure it [48].

In the viscosity range above 10^{12} Pa.s, the glass is under its glass transition temperature, where it can be used for structural applications without permanent deformation (straining point) or

relieved from internal stresses with heat treatments (annealing point, above the glass transition). In this range, the recommended technique is the beam bending viscometer [47]. It consists in applying a load in the center of a beam placed in a three-point bending configuration. The viscous deflection rate of the beam is measured under a given load at the midpoint between the supports. The viscosity-temperature relationship and the dependence of the viscosity on the thermal history of the sample can be determined [49]. The parallel plate viscometer is one of the methods that is widely used to characterize the glass between the softening and the glass transition (10^5 to 10^9 Pa.s) [50,51], especially to determine the viscosity-temperature relationship of the material. Others techniques can be used in this range, such as cone and plate, penetration viscometer and fiber elongation [22,23,25].

The rotating cylinder technique, as mentioned in the earlier section, is one of the most used techniques for complex fluids [36], which makes it a good alternative to measure the viscosity of glass melts (10^1 to 10^6 Pa.s). However, it is requested to adapt the device by using materials that can resist to temperatures above 1400°C, such as platinum and platinum alloys [47]. Apart from this aspect, the measurement are the same as at room temperature, where the relation between the shear rate and the applied torque leads to the material viscosity.

2.4 Non-Newtonian behaviors

As mentioned in an earlier section, a fluid is considered Newtonian when its viscosity is constant under different shear stress or shear rates, at a given temperature or pressure. On the other hand, it is called non-Newtonian when an experience comes to contradict the forecasts that one can establish by the Newtonian behavior [52]. Several studies are dedicated to understand the non-Newtonian behavior and establish models and/or empiric relations to describe these kinds of fluids [53–56]. Glasses may also show non-Newtonian behavior, especially when the mix involves the addition of heterogeneities that play a role as suspended elements in the glass melt [19,57–59]. In this section, the non-Newtonian behaviors will be classified in two major groups: time-independent and time-dependent behaviors. The first designates the materials which rheological properties do not depend on the flow history. Nonetheless, the variation of rheological properties of time-dependent materials, as the name suggests, is not only function of shear but also associated to a variation through time.

2.4.1 Time-independent behavior

- Shear Thinning

Shear thinning or pseudoplastic are the names given to materials which apparent viscosity decreases when the imposed shear increases. From the structural point of view, this behavior is seen as the progressive disintegration or reorganization of aggregates, freeing the immobilized fluid suspended in it [60]. Several empiric relations describe this type of materials but normally these equations depend on some parameters that are hard to interpret physically. One of these relations is the Ostwald De Waele model, also known as power-law model, described by Eq.(16), where *m* is the consistency index and *n* is the flow index. The value of n dictates the degree of pseudoplasticity of the material since it usually ranges from 1 (Newtonian liquids) to 0, for shear-thinning liquids [26]. The power-law can describe the flow in most of cases, it is not suited to describe materials exhibiting one or two Newtonian plateaus at low and/or high shear rates. In this case, other models involving more than two parameters are necessary to describe the rheological behavior [61]. One example is the Cross model, Eq. (17), where η_0 is the viscosity on the first Newtonian plateau (low shear rate), η_∞ is the viscosity in the second plateau (high shear rate), τ is a characteristic time and *n* the flow index. This equation is largely used to model the flow of complex fluids [62]. For fluids exhibiting only one viscosity Newtonian plateau at high shear rates, the equation can be reduced to Sisko's law.

$$\eta = k.\dot{\gamma}^{\,n-1} \tag{16}$$

$$\frac{\eta - \eta_\infty}{\eta_0 - \eta_\infty} = \frac{1}{1 + (\tau.\dot{\gamma})^m} \tag{17}$$

- Shear Thickening

For some materials, called dilatants, when the shear is imposed the apparent viscosity of the materials increases. This non-linear behavior is called shear thickening. At low shear rates, the fluid has low viscosity, acts as a lubricant and flows easily. However, when an impact is applied (at higher shear rates), the fluid adopts a solid-like state leading to a rapid increase in viscosity and becomes less penetrable [63]. A power law like the shear thinning behavior can describe the behavior, but in this case, the flow index is bigger than one. An empiric relation that can describe it is the Chaffey model (Eq.(18)), where η_0 is a limiting value towards which the low-shear viscosity can be extrapolated; *w* and *c* are dimensionless parameters and τ is the

characteristic time. The index n is fixed at 0.5, but τ and *c* depends on the particle volume fraction of the suspension [64].

$$\frac{\eta}{\eta_0} = 1 + \frac{\cosh(\, c\tau^w\dot{\gamma}^w)}{\tau^w\dot{\gamma}^w} \tag{18}$$

- Yield Stress fluid

Yield stress fluids are known to behave like viscoelastic solids under a stress lower than a threshold value whereas they flow like fluids when the intensity of the applied stresses exceeds the threshold. These fluids have in common a complex and disordered structure and can be of different natures and found in food industry (mayonnaise), construction (cement) or cosmetics (gel) [65]. It is important to mention that for a long time many shear-thinning fluids were confused with yield stress fluids because of experimental limitations. Actually, the sudden increase of viscosity as the shear was decreased seemed to be as a material solid-like response but in fact, there was a slow and continuous steady deformation when the stress was imposed for a long time. With new equipment that could reach low stresses for longer, it is possible to clarify the existence or not of the apparent yield stress. At the lowest stresses, this creep behavior for solids, soft solids and structured liquids can be described by a Newtonian-plateau viscosity [62]. Nonetheless, these advancements in experimental analysis helped to initiate a long debate around the existence or not of the yield stress in measurements performed under $10^{-7}s^{-1}$ [66–68]. The most known equation to describe this behavior is the Bingham behavior law (Eq.(19)). It considers that below a certain threshold stress σ_c, the fluid does not flow at all, behaving as an elastic solid and that, above the threshold, the deformation velocity varies linearly with the stress. For fluids which do not vary linearly above the threshold, the Herschel-Bulkley model (Eq.(20), a generalization of the Bingham model where η_p is the plastic viscosity [62], may be used.

$$\sigma = \sigma_c + \eta_p.\dot{\gamma} \tag{19}$$

$$\sigma = \sigma_c + \eta_p.\dot{\gamma}^n \tag{20}$$

2.4.2 Time-dependent behavior

- Thixotropy

A current definition of thixotropy is "the continuous decrease of viscosity with time when flow is applied to a sample that has been previously at rest and the subsequent recovery of viscosity in time when the flow is discontinued" [69]. Hence, it is a time related phenomenon associated with modifications in the "inner structure" of the material [70]. These modifications are known as the "build up" and the "break down" of the structure (Figure I-8). The break down is produced by the flow stresses while the build-up is due to in-flow collisions, Brownian motion and van der Waals attractive forces [71]. Weakly connected particles form flocs, which evolve to networks that can be destructed by the shear. Thus when the shear is increased, the size of these flocs is decreased. However, at rest and under low shear, the growth of the flocs restarts due to Brownian motion and attractive forces between the particles, which helps the floc network to rebuild. The whole process is reversible and can take hours to happen depending on the structure [71] [72].

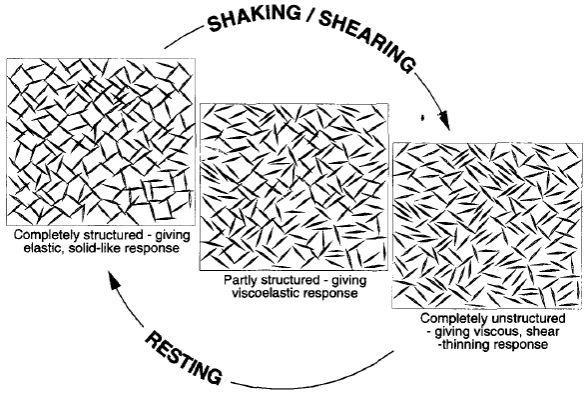

Figure I-8 - Scheme of the thixotropy dynamics related to the structure breakdown and build-up [71].

Only few data can be found in the literature, which seriously hampers progress in the field [73]. On the other hand, several authors propose different models to describe the phenomenon and, according to Mewis *et al.* [69], it is possible to divide these models in three categories: the microstructural, the continuum mechanics, and the structural kinetics models. One way to obtain experimental time-depending data is to use *loop* tests. It consists in successive sweeping up and down stresses, and the area between the obtained curves is sometimes used as a measurement of thixotropy. But since thixotropy both depends on time and shear rate, experiments where both variables are changed simultaneously, are not recommended as a trustful result. Nonetheless, an interesting technique consists in imposing a constant shear to

the sample until it reaches the equilibrium and then change the shear to another value as quick as possible, measuring changes from one steady state to another. The obtained behavior, in terms of viscosity, can be described by the exponential model [26,72]:

$$\eta = \eta_{e,0} + \left(\eta_{e,\infty} - \eta_{e,0}\right).\left(1 - e^{-\frac{t}{\tau}}\right) \tag{21}$$

where $\eta_{e,0}$ is the initial viscosity (very influenced by the inertia problems in viscometers), $\eta_{e,\infty}$ the viscosity at equilibrium and τ is a time constant, function of both the original and the final shear rate. This model was applied by Maingonnat *et al.* [74] to experimental data obtained for suspensions of montmorillonite clay and carboxymethylcellulose (Figure I-9a).

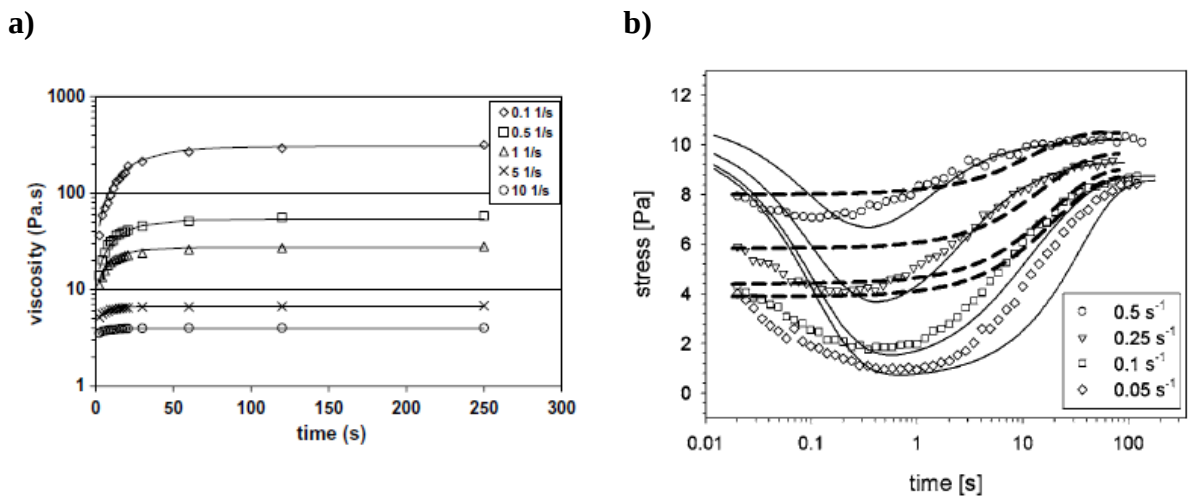

Figure I-9 – a) Viscosity of the model fluid as a function of time of exposure to low shear rates (points), fitted by the exponential model (full lines) [74]. b) Predictions of the Houska model (dashed lines) and of Coussot (solid lines) for build-up experiments [73].

Houska *et al.* [75] also established a mesoscopic structural model well suited for the study of thixotropic materials where the structure is described by a scalar parameter λ obeying a kinetic law:

$$\frac{\partial \lambda}{\partial t} + u_i \frac{\partial \lambda}{\partial x_i} = -k_1 \dot{\gamma} \lambda + k_2 (1 - \lambda) \tag{22}$$

with u_i the component of the fluid velocity vector, $\dot{\gamma}$ the shear rate. The first term of the right hand side of Eq.(22) indicates the breakdown of the network due to sample shear; the second term is responsible for build-up of the network. The values of k_1 and k_2 can be obtained by

rheological experiments. When λ tends to zero, the structure is completely unstructured, but when it tends to one, it is intact [75]. This model is can be used in fluid mechanics simulation codes, such as in Derksen *et al*. [76]. Coussot's model Eq.(23) also shows accurate fitting for different thixotropic systems [77] using a structural parameter λ. In Eq.(23), λ increases at a constant rate with $1/\tau$ where τ is the characteristic time of the microstructure. The second part of the equation, involving a dimensionless parameter α, is related to the structure breakdown. The parameter *n* is the flow index. For $n < 1$, the fluid does not have a yield stress and for $n > 1$, the fluid does not have a real yield stress threshold but it tends to an infinite viscosity with time [65].

$$\begin{cases} \eta = \eta_0(1+\lambda^n) \\ \dfrac{\partial\lambda}{\partial t} = \dfrac{1}{\tau} - \alpha\dot{\gamma}\lambda \end{cases} \tag{23}$$

Dullaert *et al*. [73] used both Houska and Coussot models (Eq.(22) and Eq.(23), respectively) to describe the mixture of fumed silica particles in a Newtonian paraffin oil with poli(isobutylene). The Coussot model has well described the build-up phenomena for the system, but at the same time, it has shown deviations for the breakdown. For this system, the Coussot model showed a better fit than the Houska model (Figure I-9b).

2.5 Phenomenological modeling of complex fluids

One way to interpret the complex rheological behavior of glasses containing insoluble particles is to analyze it as a complex fluid, *i.e*, a suspension of dispersed Structural Units (SUs) in a glass matrix [78]. Due to its structural complexity, the rheological study of these fluids is extremely difficult. Even the simplest suspension composed of identical hard spheres shows rather complex rheological phenomena [79]. Nonetheless, the area has evolved in experimental and computational techniques [80] and such advancements produce a better background for the phenomenological modeling of the rheological behavior of some of these fluids. Some important concepts to this approach will be detailed in this section.

2.5.1 Structural Units (SUs)

The similarities between any concentrated dispersions rely mainly on the fact that all of them have internal structures observed at all length scales that are changed by shear. These structures start with small elements that evolve to groups and can eventually arrive to a sample spanning structure. These groups are the Structural Units (SUs) and their size depend on the applied shear. As presented in Figure I-10, large SUs can be reduced to small flocs then to single

particles, by the increased shear. Nonetheless, the figure also explains the plastic behavior when analyzing the evolution of a sample-spanning network, which also reduce the size of its SUs in function of the increased shear [81]. This progressive SU size reduction often produces a shear-thinning behavior.

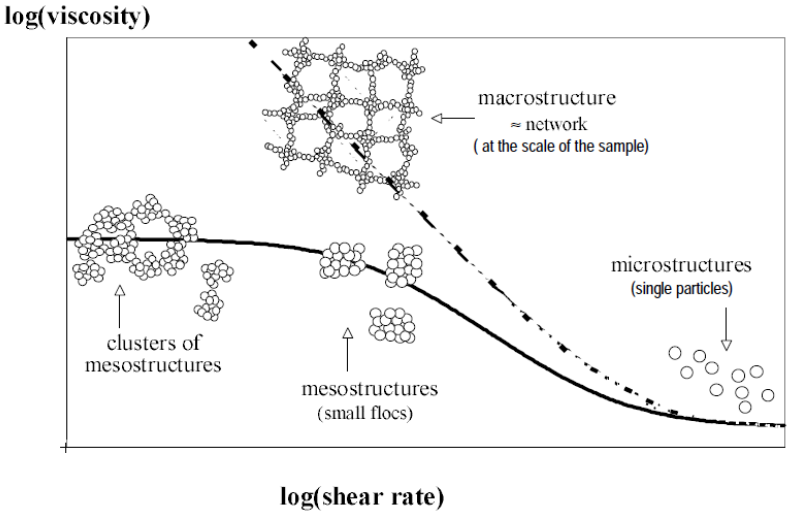

Figure I-10 - Structural interpretation of shear-thinning and plastic behaviors [81].

Three main forces may act of the SUs of these suspensions: hydrodynamic, Brownian and colloidal [82]. The intensity of these forces and therefore the rheological properties of the suspension depend on the size of the particles. For example, for particles larger than 10µm, there is a dominance of hydrodynamic forces, but for particles between 10^{-3} and 10^{1} µm, there is a combination of hydrodynamic, Brownian and interparticle forces [83]. Genovese *et al*. separated the suspensions according to the type of discrete phase, *i.e*. according the structural units shapes are interactions (schematic details can be seen in Figure I-11): hard-sphere suspensions (Figure I-11a and b); repelling particles suspensions (Figure I-11c and d); aggregated suspensions (Figure I-11e and f).

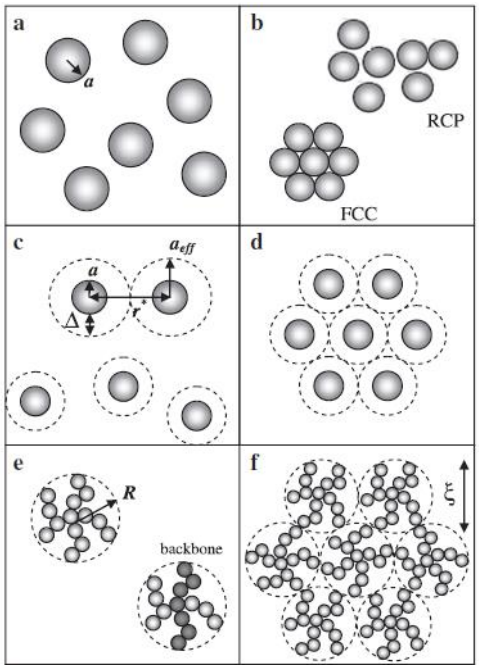

Figure I-11 - Schematic representation of a) isolated hard-spheres, b) caged and packed monodisperse spheres at random close packing (RCP), and face centered cubic array (FCC), c) isolated repelling particles (dashed line represents the range of the repulsive potential), d) caged repelling particles, e) isolated fractal clusters of aggregated particles (dashed line represents the smallest enclosing sphere), f) network of fractal clusters. Adapted from van der Werff *et al.* [82].

2.5.2 Structural models

Structural models involve structural changes in the material and are the most suitable for rheological characterization of fluids with shear-dependent structures. Although these systems are complex, the approach considers a minimum number of parameters with physical significance starting from simpler models before it can be generalized to a more complex one [84]. Quemada stated four essential steps to elaborate a structural model: define a set of dimensionless structural variables; choose the kinetic equations which governs the structural variables and describes the rupturing and restoring of the structure induced by the flow; determine shear-dependency of kinetic constants involved in kinetic equations and select an explicit form of the viscosity-structure relation [85]. In general, the viscosity of the suspension (η) is directly proportional to the viscosity of the continuous phase (η_f), so that most rheological models are expressed in terms of the relative viscosity of the suspension $\eta_r = \eta/\eta_f$ [82]. Einstein's efforts in calculating the viscosity of a dilute suspension of hard spheres [79] is the base for the advances in describing more concentrated systems, considering the interactions

between the SUs. Einstein's model is given by Eq. (24), where η_s is the solvent viscosity and Φ the volume fraction

$$\eta(\Phi) = \eta_s(1 + 2.5\Phi) \tag{24}$$

An example that follows these specifications is the model proposed by Krieger *et al.* [86] that describes the shear thinning behavior of suspensions of small spheres. He assumed a viscosity-structure relation (Eq. (25)) where η_∞ and η_0 are the limiting steady state viscosities when $\dot{\gamma}/\dot{\gamma}_c$ tends respectively to infinity and to zero, with $\dot{\gamma}$ is the shear rate and $\dot{\gamma}_c$ the characteristic shear rate above which the material no longer behaves linearly. These limits correspond to relative viscosities (η_r) that are expressed as a function of the volume fraction of the particles (Eq. (26)), where Φ_m is the maximum volume fraction, $[\eta] = \lim_{\Phi \to 0} \eta - \eta_c/\Phi\eta$ is the intrinsic viscosity (Einstein's limit for a suspension of spheres $[\eta]$ = 2.5 in a much-diluted media) [78].

$$\eta = \eta_\infty + \frac{\eta_0 - \eta_\infty}{1 + \dot{\gamma}/\dot{\gamma}_c} \tag{25}$$

$$\eta_r = \left[1 - \frac{\Phi}{\Phi_m}\right]^{-q} \; where \; q = [\eta]\Phi_m \tag{26}$$

2.5.3 Effective volume fraction (Φ_{eff})

The hard sphere model such as in Figure I-11a, in which the hydrodynamic forces are the only significant forces, reflects only approximately the real systems. However, in the case of a suspension with net repulsive forces (Figure I-11c and d), it is possible to introduce an effective radius a_{eff} which defines the equivalent hard spheres (HS) radius, where $a_{eff} = a + \delta$, with *a* the particle radius. If polymers are present in the suspension, δ is the thickness of the polymer layer grafted or adsorbed on the particle surface. The HS approximation permits to apply Eq. (26) by considering an effective volume fraction (Φ_{eff}). It can be calculated as shown in Eq. (27) where *N* is the number of particles [87].

$$\Phi_{eff} = \frac{4\pi}{3} N a_{eff}^3 = \left(\frac{a_{eff}}{a}\right)^3 \Phi \tag{27}$$

The effective volume fraction concept is largely used in the literature but its use can be limited [79,88,89]. The idea of SUs results from regrouping smaller elements and irreducible aggregates formed at higher shear rates. However, smaller individual particles are not included in the SU [78]. This way, a new volume fraction is taken into account; the shear-dependent maximum packing (Φ_{PK}). This adjustable parameter regroups the characteristics of the

hydrodynamic volume of the particles and their maximum packing. It can be written as shown in Eq. (28), where *S'* is the total number density of primary particles contained in all the SUs and C_f is compactness factor ($C_f = \varphi^{-1} - 1$, where φ is the dispersed particles volume fraction), directly related to the mean compactness of SUs [78].

$$\Phi_{PK} = \frac{\Phi_m}{1 + C_f S'} \tag{28}$$

Conclusion

This section aimed to present an overview on the main concepts involved in rheology of glass melts. The most used rheometry techniques were described as well as the challenges of high temperature measurements. The Non-Newtonian behaviors that exist among materials and their differences are explored leading to the explanation of the complex fluid theory serving as background for the following sections where the rheological behavior of glasses containing PGM particles will be explored.

3 Influence of PGM particles in glass rheology

3.1 Platinum group metals (PGM)

Platinum group metals (PGM) is the name given to classify the six transition metals from the periodic table that are chemically, physically, and anatomically similar to platinum. The group is composed of platinum, palladium, rhodium, ruthenium, iridium and osmium. They are characterized by their high density and melting point, as shown in Table I-1 [90]. Due to their chemical stability they are often used as catalysts for the petroleum industry, but their use is varied since according to the International Platinum Group Metals Association (IPA), one-quarter of all manufactured goods either contains a PGM or has a PGM playing a key role in its production [90].

Table I-1 - Density and melting point of the Platinum Group Metals.

	Platinum(Pt)	Palladium(Pd)	Ruthenium(Ru)	Rhodium(Rh)	Iridium(Ir)	Osmium(Os)
Density (g/cm3)	21.45	12.02	12.45	12.41	22.65	22.61
Melting Point (ºC)	1769	1554	2310	1960	2443	3050

Some of these elements are present in the high-level nuclear waste concentrates (HLWC), originated from the reprocessing of spent nuclear fuels. The conditioning of this type of waste

consists in immobilizing the components in a stable borosilicate glass matrix before its final disposal in a geological site. Several oxides come from the high-level waste and are added to the glass melt to form the nuclear waste glass. Most of the waste oxides are dissolved in the melt and become structural elements of the glass when cooled. However, it does not totally apply for PGM present in the waste such as ruthenium (Ru), rhodium (Rh), and palladium (Pd) that do not dissolve, but precipitate as particles in the glass along with Tellurium. These high density PGM precipitate and may settle and accumulate during the melting, which impacts some of the glass properties [91–93].

3.1.1 Influence on the physical properties of the glass

In France, the reference content of PGM particles in nuclear waste glasses is between 1.5 %wt (~ 0.5 %vol.) and 3 %wt (~ 1 %vol.), but even though it is a low quantity, their impact on the glass properties is considerable. Depending on the temperature and the glass composition, PGM particles solubility in a glass melt can be very low. Mukerji *et al.* showed that the solubility of ruthenium in a simple borosilicate glass is of a few ppm and it depends on the sodium content of the glass [94]. In complex systems that simulate the nuclear glass, the solubility can vary from 0 to 250ppm in a temperature range from 1000º to 1400ºC [95–97]. This insolubility affects directly the material since the presence of precipitates can change the electrical, thermal and rheological properties of the glass.

The shape and size of the PGM particles influence the glass properties such as the flow, sedimentation, and so on [88]. The precipitates are mainly spherical $PdRh_xTe$ alloys and needle shaped RuO_2 particles (Figure I-12a) as mentioned earlier, but nonetheless, polyhedral forms can also be found. If the calcinate is depleted in sodium nitrate, the RuO_2 particles will be polyhedral. On the contrary, if the calcinate is rich in sodium nitrate, the formation of a reaction intermediate of Na3RuO4 type favors the formation of acicular morphology. The size of RuO_2 can vary from 10 to 200 µm and the PdRhTe from 1 to 5µm diameter, depending on the temperature and the melting time which can also lead to a coarsening of the PGM particles, as shown in Figure I-12b [59,93]. The PGM particles may be found in the form of dense aggregates and/or sediment in the glass depending on the melting conditions. These two phenomena influence the properties of the melt and will be more explored in the next sections.

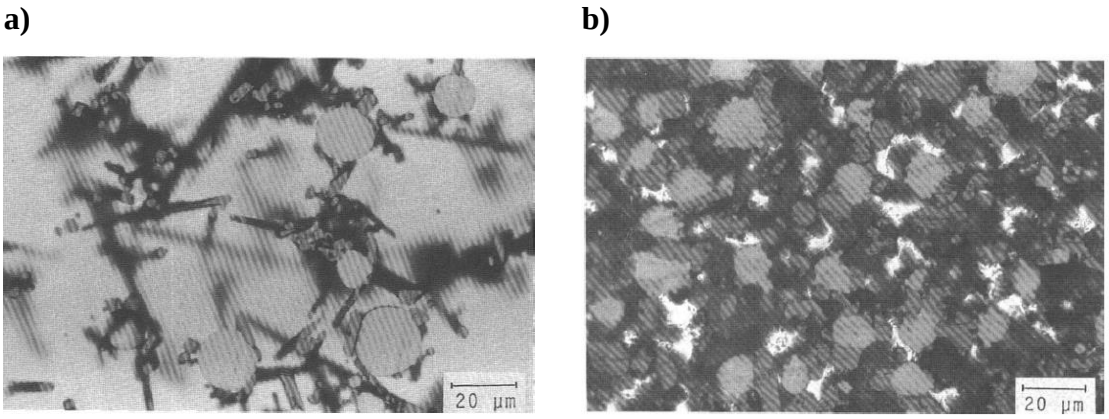

Figure I-12 - a) PdRhTe droplets surrounded by RuO_2 needles. b) Coarse RuO_2 and PdRhTe particles [50].

In the vitrification process such as the cold crucible or the ceramic melter, the electrical conductivity plays an important role in the process control. The PGM particles are also a key element in the electrical properties of the glasses. Some authors showed that a PGM content increase leads to an increase of the glass conductivity [16,59,98,99]. All these authors agree that this increase occurs because an electronic conductivity (σ_e) is added to the ionic conductivity of the glass matrix due to the presence of interconnected chains of ruthenium oxide. This way, according to Simonnet *et al.*, the conductivity increases with the PGM content above a threshold, which depends on the particles morphology [100]. For glasses with needles like RuO_2, the particles touch each other by their extremities to form the chain. But for glasses with polyhedral shapes, the hypothesis is that even though the particles do not touch each other, there is a thin glass layer between them that would help the electron transport by tunnel effect [101]. This effect can only happen if the glass layer is very thin (~1 nm) to form an insulating interparticle barrier in which electron transfer could be enhanced by soluble ruthenium impurities and if the PGM content is high enough to entail this scenario [102].

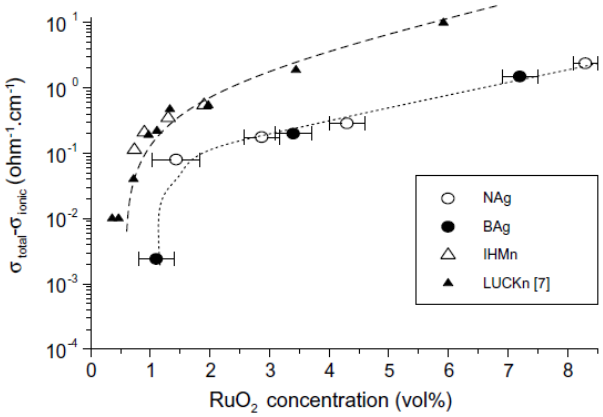

Figure I-13 - Electronic conductivity of a nuclear glass containing particles of ruthenium oxide, at 1100 ° C, as a function of the volume fraction in RuO_2. The "NAg" and "BAg" series represent data acquired for particles in the form of polyhedra and the series "IHMn" and "LUCKn" represent data acquired for particles in the shape of needles [102].

Simonnet *et al*. showed that, by subtracting the ionic conductivity of a molten glass matrix to the electrical conductivity of the molten composite RuO_2-matrix, it is possible to determine the electronic conductivity. It would produce two groups of data independent from the matrix and characteristic of the electrical percolation phenomena. In Figure I-13, the electronic conductivity due to the presence of RuO_2 particles is represented as a function of the concentration of these particles, for surrogates of HLW glasses with needle-like particles or with polyhedral particles. There is a volume fraction (percolation threshold) above which the electronic conductivity appears. This threshold corresponds to the appearance of a chain of interconnected particles of RuO_2. The experimental points are perfectly adjusted by a percolation model of the type [100]:

$$\sigma_e = \sigma_{e0}(x - x_c)^{\mu} \tag{29}$$

with σ_{e0} the initial electronic conductivity, x the volume fraction of RuO_2 particles, x_c the percolation threshold and μ a critical exponent.. For needle particles (triangular symbols in Figure I-13), the percolation threshold is estimated at $x_c = 0.5 \pm 0.2\%\ vol$ at 1100 °C. For polyhedral particles (circular symbols), this threshold is evaluated at $x_c = 0.9 \pm 0.2\%\ vol$. The value of the exponent μ is around 5. The percolation threshold of polyhedral chains is larger than that of needles chains since the latter morphology facilitates the formation of interconnected chains [16].

As well as other physical properties, the PGM particles also lead to significant changes in the rheological behavior of the glass. The literature on the subject is limited due to the difficulties of high temperature rheological measurements, as explained in earlier sections. Nonetheless, all authors discovered an increase of the PGM glass viscosity and a non-Newtonian behavior of the material [43,57–59,93]. At first, the observed behavior was that of a yield stress fluid and classical models were used to describe it such as Bingham, Hershel- Bulkley and Casson models. Studies that came later started to focus on the morphology and microstructures and connect it with the rheology. Krause [59] studied the viscosity of borosilicate nuclear waste glasses containing needle-shaped RuO_2 particles and spherical $PdRh_xTe_y$ alloys. The study showed that the viscosity decreased with higher temperatures (Figure I-14) but increased with the PGM content. He also showed that the material displays an increase of viscosity and exhibits an evident non-Newtonian behavior when the size of the PGM particles increases, especially when they are aggregated; nonetheless, in experiments at higher temperatures and lower viscosities the particles were dispersed, which raised the hypothesis of disaggregation under flow [59].

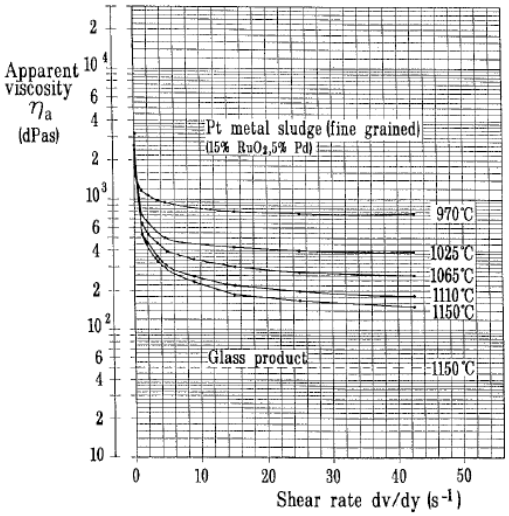

Figure I-14 - Apparent viscosity as a function of shear rate at different temperatures of fine-grained platinum group metal sludge prepared in the laboratory.

Grünewald *et al*. [93] studied the properties and rheological behavior of a PGM sludge formed during the vitrification of simulated high level liquid waste by a Joule heated liquid fed ceramic lined glass melter (LFCM). They observed that when imposing a shear stress in the PGM glass melt the needle-like RuO_2 particles orient themselves in the flow direction, lowering the viscosity, which makes it flow more easily out of the melter [93]. Uruga *et al*. [57] analyzed

the shear rate dependency of the viscosity of three simulated high-level radioactive waste glasses containing 10 wt % of sodium and 15%wt of non-radioactive fission products, including different PGM contents (0, 1.2 and 4.5 wt% PGM particles). The composition of the glass was the same as in the Tokai Vitrification Facility (TVF), in Japan. The studies showed the decrease of the viscosity with the increased shear rate and temperature (Figure I-15). The authors also raised the idea that the PGM particles in the melt might also form aggregates at low shear rates and that the aggregate would break down to individual particle at a high shear rate. Nonetheless, the shear range was limited (10^{-2} to 100 s^{-1}), not exploring the behavior of the material at lower shear rates [57].

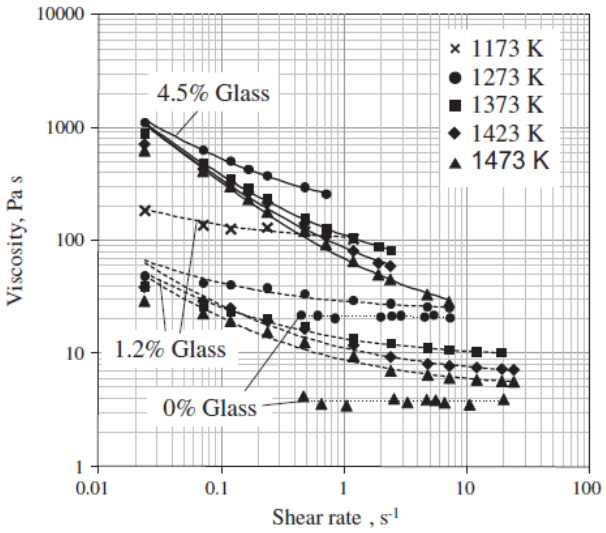

Figure I-15 - Viscosity of Japanese glasses containing PGM particles as a function of the shear rate for different PGM contents and different temperatures. The solid lines represent the adjustment of the data by Casson's model [57].

Aiming to explore a broader shear rate range needed for the development of cold crucible melter, recent studies with nuclear simulant glasses proposed a new phenomenological model for the rheological behavior of these materials. Puig *et al.* [43] and Hanotin *et al.* [19] studied the viscosity of simulated nuclear glasses containing PGM particles over a wide range of shear stress, as a function of the particles content and the temperature. The scheme in Figure I-16 summarizes what happens to the material: at high shear rate, the system behaves as a suspension of small clusters and individual particles and its viscosity is entirely controlled by the viscosity of the glass matrix, this way the viscosity decreases with increasing temperatures. At low shear rate, above a certain content of PGM particles, the apparition of macroscopic aggregates, made up of RuO_2 particles chains separated by thin layers of glass matrix, strongly increases the

viscosity of the nuclear glass that, contrary to what happens at high shear rate, also increases with the temperature [19].

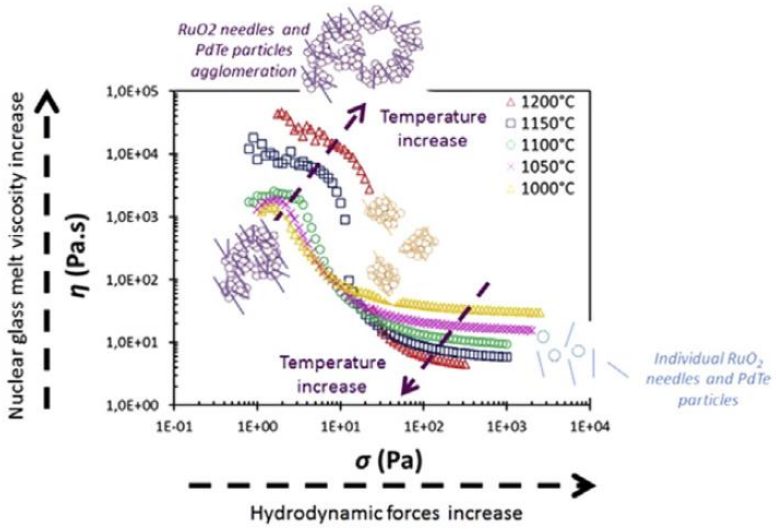

Figure I-16 - Scheme summarizing the rheological behavior of the glass containing PGM particles in a wide shear range and different temperatures.

The work of Puig *et al.* [43] and Hanotin *et al.* [19] showed that the shear thinning behavior of the nuclear glass can be well described by a simplified Cross model with n =1 since this model highlights the existence of two Newtonian plateaus [43]. The $K.\dot{\gamma}$ factor in the equation can be replaced by $\dot{\gamma} / \dot{\gamma}_c$ where $\dot{\gamma}_c$ is the critical shear rate from which the viscosity decreases and is used to find the critical stress $\sigma_c = \eta_0.\dot{\gamma}_c$. Table I-2 shows the parameters used to fit the experimental data at 1200°C. The authors' hypothesis is that, on the Newtonian plateau at low shear rate, the rheological behavior of the nuclear glass is controlled by Brownian local reorganizations of these clusters and the flow regime is linear as long as the hydrodynamic forces remain negligible. When the shear stress reaches the critical stress σ_c, the behavior is then controlled by hydrodynamic forces due to shear flow, which causes the rupture of the aggregates and the drastic decrease of the sample viscosity [43].

Table I-2 - Parameters used for the fit of the experimental data at 1200°C by a simplified Cross model [43].

PGM (wt%)	η_0 (Pa.s)	η_∞ (Pa.s)	$\dot{\gamma}_C$ (s^{-1})	$\sigma_c = \eta_0.\dot{\gamma}_C$ (Pa)
0	3.6	3.6	0	0
1.6	58	4	1.1E-01	6.4
2.1	1096	4.2	5.8E-03	6.3
3	2724	4.3	3.3E-03	9.0
4.2	29708	4.4	7.2E-04	21.3
5.2	63045	4.7	5.7E-04	35.9

Figure I-17a shows the high shear regime of the samples at different PGM volume fractions and temperatures: the viscosity increases with the PGM content at all temperatures. Einstein's law does not model correctly this increase since the particles involved are not spherical as assumed in this model. This is why Quemada approach is adopted, considering the hydrodynamic volume of the needle-like particle, *i.e.* the effective volume fraction Φ_{eff}. For an ellipsoidal particle of diameter $2d$ and length 2ℓ, the excluded volume is a puck of radius ℓ and thickness $2d$ and the effective volume fraction is defined by $\Phi_{eff} \approx \beta\Phi_0$, with $\beta = \ell/d$. For a given PGM content the viscosity also depends on the temperature (Figure I-17b) following the same behavior as the glass without PGM particles. Combining these two dependencies, the rheological behavior at high shear stress can be describe by

$$\eta_\infty = A\exp\left(\frac{B}{T-T_0}\right)\left(1-\frac{\Phi}{\Phi_{PK}}\right)^{-2} \tag{30}$$

where A, B and T_0 are constants, η_∞ is viscosity on the high shear plateau, T the temperature, Φ the volume fraction in particles and Φ_{PK} the maximum effective volume fraction [19].

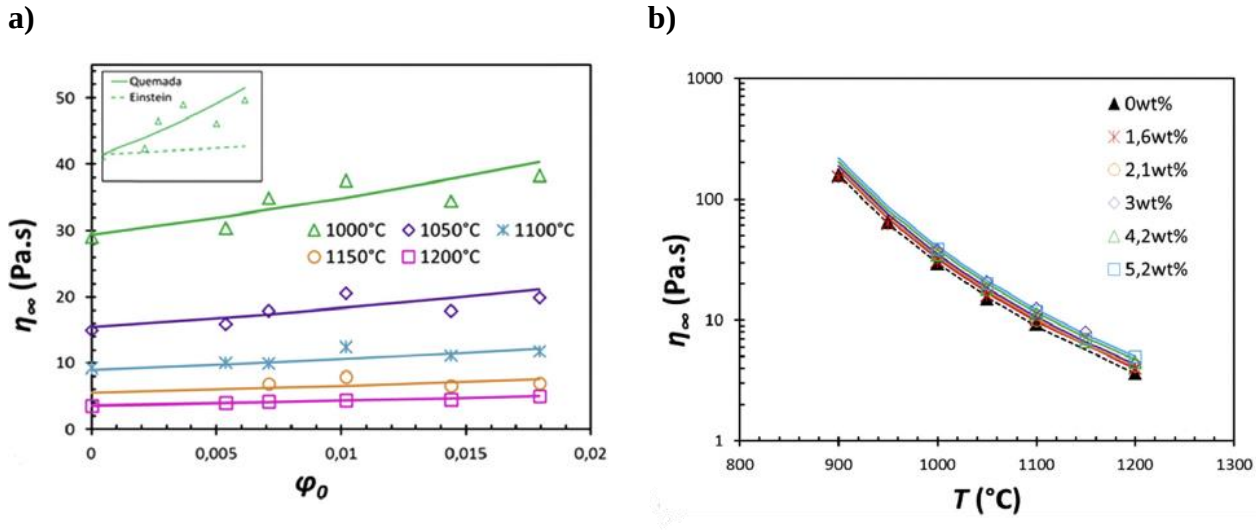

Figure I-17 - a) High shear viscosity plateau (η_∞) as a function of the initial volume fraction in PGM particles for six simulated nuclear glasses at different temperatures. b) High shear viscosity plateau as a function of the temperature for different values of initial PGM content. The data is fitted with the Eq.(30) [19].

Figure I-18 shows the evolution of the low-shear viscosity η_0: contrary to the high shear viscosity, it increases over 3 decades (Figure I-18a) with the volume fraction of PGM. Above 1.6 wt% of PGM, η_0 increases with the temperature (Figure I-18b). The work showed that the temperature increase favors aggregation via the decrease of the viscosity of the glass matrix [19].

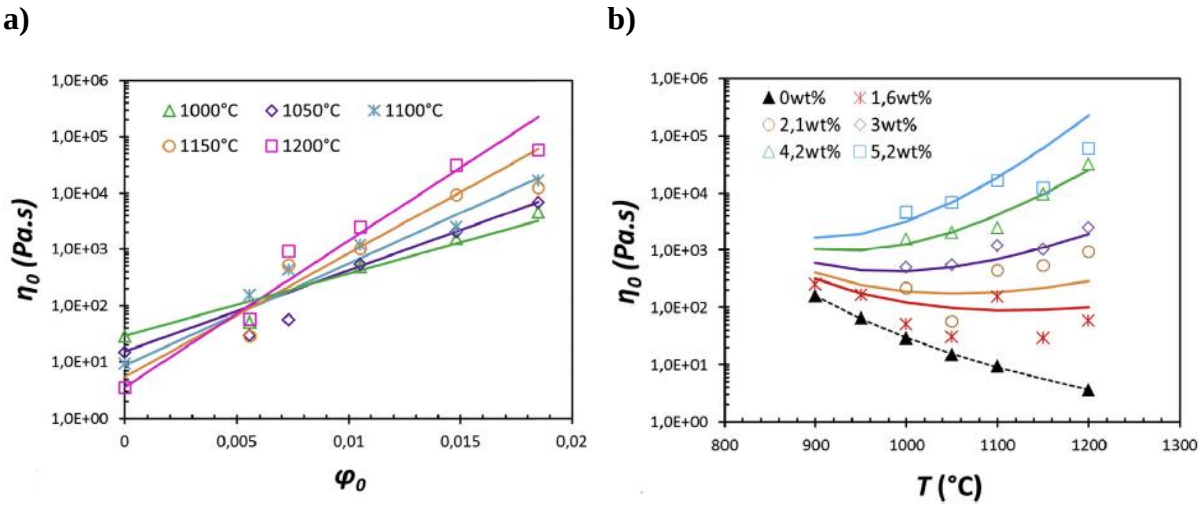

Figure I-18 - a) Low shear viscosity plateau (η_0) as a function of the initial volume fraction in PGM particles for six simulated nuclear glasses at different temperatures b) Low shear viscosity plateau as a function of the temperature for different values of initial PGM content [19].

The aggregates will trap part of the fluid which will be transported in a block hence the importance of the effective volume fraction [103,104]. Systems in which aggregates undergo rotations due to shear rate, which is the case with the present system, tend to develop a fractal structure. The hydrodynamic radius of the clusters was estimated using the relationship proposed by Allain *et al*. [103] that compares the hydrodynamic shear forces, which tend to break the aggregates, with the binding forces. This way, in the case of fractal clusters of radius R composed of elementary particles of size a, the effective volume fraction will be given by [104]:

$$\Phi_{eff} = \Phi\left(\frac{R}{a}\right)^{3-D_f} = \Phi\left(\frac{C}{\eta_f}\right)^{3-D_f/2} \tag{31}$$

with R the radius of the clusters, a the radius of the elementary particles and D_f the fractal dimension of the cluster and $Q = \frac{\Lambda}{a12h^2\dot{\gamma}}$. The experimental data acquired at low shear can then be adjusted by a free volume type model in the form $\eta = \eta_f \exp\left(\frac{\phi_{eff}}{\phi_c}\right)$ that gives:

$$\eta_0 = \eta_f \exp\left[\frac{\phi}{\phi_c}\left(\frac{Q}{\eta_f}\right)^{3-D_f/2}\right] = A\exp\left(\frac{B}{T-T_0}\right) \exp\left[\frac{\phi}{\phi_c}\left(\frac{Q}{A\exp\left(\frac{B}{T-T_0}\right)}\right)^{3-D_f/2}\right] \tag{32}$$

where *A*, *B*, *Q* and T_0 are constants, η_0 is the low shear viscosity, η_f the viscosity of the continuous phase, *T* the temperature and Φ_c the critical volume fraction. Considering Eq.(30) and (32) , the viscosity of a glass melt containing PGM particles can be defined by the following phenomenological model:

$$\eta(T,\phi,\dot{\gamma}) = \eta_\infty(T,\phi) + \frac{\eta_0(T,\phi) - \eta_\infty(T,\phi)}{1 + \frac{\dot{\gamma}}{\dot{\gamma}_c(\phi)}} \quad (33)$$

Conclusion

This chapter aimed to present the PGM particles and their impact on the rheology of glass melts. It started by showing the characteristics of these metals and how their presence affects the physical properties of the glass, such as their electrical conductivity and viscosity. It also explored in more details the past studies about the rheological behavior of PGM glasses and the models proposed along the years to describe the very shear-thinning behavior of such materials. The model proposed by Hanotin et al. [19] *is the most suitable for instance to predict the behavior of this material, combining the simplified Cross model with the evolution of particles aggregation on both Newtonian plateaus exhibited by the glass melt, at low and high shear rates.*

4 PGM particles aggregation kinetics

4.1 Particles aggregation

4.1.1 Mechanisms and Kinetics

Aggregation is a process in which particles interact to create connection and form clusters called aggregates. It can be induced by external and internal factors, but the aggregation is an inherent behavior of any particle system, though the extent to which this aggregation prevails may largely differ depending on its nature [105]. In some cases, it is possible to consider aggregation as an irreversible phenomenon since it is the result of particles collision and adhesion. With an effective shock, a strong bond can be formed and, in this case, only the growth of aggregates is studied. However, in many cases, aggregation is reversible. Therefore, during aggregation, several mechanisms are likely to modify the concentration of aggregates, such as the flow and interparticle forces. The size of an aggregate results from a balance between the internal cohesion forces and the hydrodynamic constraints applied to its surface [106].

To define the rupture of these aggregates, it is therefore necessary to understand the physicochemical phenomena governing the cohesion of the aggregates (identify and quantify them) but also to understand the effect of the hydrodynamic constraints on the aggregates. As long as the particles are transported, either by Brownian or hydrodynamic forces, they are submitted to attractive or repulsive forces. The electrostatic forces lead particles of opposite charge to attract each other, while particles of same charge will repulse one another. Another important interaction is the van der Waals force that originates in the interaction between the electromagnetic field of the particles created by permanent or induced atom dipoles. Van der Waals interaction prevails at very small interparticle distances (r = 1–10 nm), resulting in a minimum net interaction potential energy where the attractive forces are large enough to give permanent particle contact, or irreversible aggregation [83,85].

The frequency of collisions controls the aggregation rate, so that the mass balance of the aggregation depends on the collision frequencies and the probabilities of bonding between the particles [107]. To facilitate the studies, the kinetics of aggregation processes are usually examined for monodisperse particles in the absence of nucleation, dissolution, and aggregate breakage. There are three main transport mechanisms: perikinetic aggregation, orthokinetic aggregation and differential sedimentation [108–110]. The first mechanism consists in particle aggregation solely driven by diffusion, *i.e.* Brownian motion. Orthokinetic qualifies the aggregation mechanism where the collision rate between the particles is increased by the flow. Finally, a suspension composed of particles of different size and density is an environment favorable to aggregation by differential sedimentation, since the particles sediment at different speeds and thus come into contact.

It is possible to determine the predominant aggregation mechanism by the ratio between the characteristic Brownian time and the hydrodynamic characteristic time, τ_b and τ_h respectively. The dimensionless number is called Péclet number (*Pe*) and is obtained by $Pe = \tau_b / \tau_h$. If $Pe < 1$ the predominant mechanism is perikinetic and if $Pe > 1$, it is orthokinetic [109]. The characteristic hydrodynamic time is the inverse of the shear rate. The Brownian time is given by a relation between the particle radius and the coefficient of Brownian diffusion. Consequently, the expression for *Pe* reads:

$$Pe = \frac{6\pi\eta_f a^3}{k_B T}.\dot{\gamma} \tag{34}$$

with a as the spherical particle radius, η_f the fluid viscosity and k_B the Boltzman constant [109].

4.1.2 Structural approach

The morphology of aggregates depends on their physicochemical properties and on the conditions in which they were produced. On the other hand, the dynamic of aggregates formation depends on their morphology during collision. This reciprocal situation leads to the importance of the correct prediction of the aggregates structure since normally they have a non-traditional aspect that cannot be described by conventional mathematical equations. This way, the typically irregular morphology of aggregates can be described as fractal like. Fractals are objects composed of small and approximate copies of the whole object that can be split into smaller copies of themselves (Figure I-19); a property which is called self-similarity [105]. The introduction of these models makes the approach more realistic from a geometrical point of view and allows a more satisfactory theoretical representation of the transport of aggregates by the fluid, their hydrodynamic and physicochemical interactions, their fragmentation, and so on [83].

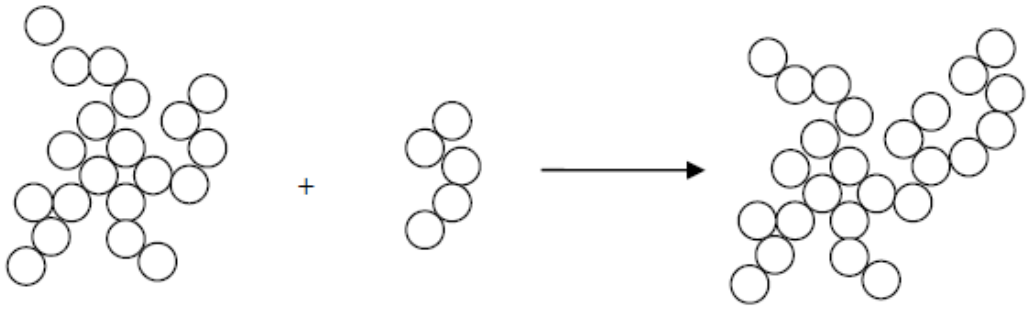

Figure I-19 - Scheme showing the fractal form and growth mechanism [105].

A way to classify and compare the fractals is the "fractal dimension" (D_f). According to Gmachowski, the characterization of an aggregate is made by its fractal dimension since it determines the aggregate hydrodynamic size and therefore, its coefficient of translation friction. This value is crucial in determining transport properties such as the sedimentation and diffusion. The fractal dimension reflects the internal structure of the aggregate (it is proportional to the aggregate density) and depends on the type of aggregation [111]. Its value may range from almost 3 for the most dense, close-packed aggregates (D_f = 3 simply would mean a packing like in a crystal lattice), to lower values for more open structures [83]. It can be calculated by the following expression:

$$N = K_f \left(\frac{R}{a}\right)^{D_f} \tag{35}$$

where N is the average number of elementary particles in a fractal aggregate, R the average radius, a is the radius of the primary spherical particle and K_f is a prefix constant that depends on the definition of R, which could be the hydrodynamic radius, the collision radius, the radius of gyration, or the radius of the circumscribed sphere [83]. The models that are more representative in simulating the relationship between the fractal dimension of aggregates and their growth mechanism are those of the "Cluster-Cluster" type [106]. When there is no barrier of repulsive energy between the particles, i.e. each collision leads to the formation of an irreversible bond between the two particles, the aggregates will have a loose structure and the experimental measurements will give fractal dimension values between 1.7 and 1.8. Contrarily, if the probability of bonding between the particles is very low, then the aggregates are more compact, and the values obtained are between 2.05 and 2.1. Thus, two main types of mechanisms are defined: DLCA (Diffusion-Limited Clusters Aggregation) and RLCA (Reaction-Limited Clusters Aggregation) [112].

The DLCA mechanism proposes that aggregation kinetics is limited by the time that the aggregate takes to diffuse in the medium towards another particle or another aggregate which leads to a small fractal dimension (D_f ~ 1.7). On the other hand, the RLCA mechanism considers that a small fraction of collision results in the formation of bridges. Then the aggregation speed is not limited by diffusion but by the time needed for the aggregate to form a bridge. The fractal dimension is then greater for the RLCA mechanism (D_f ~ 2.1). Clusters are supposed to behave as spheres composed of particles in contact with trapped fluid. This way, the phenomena will increase the volume of the discrete phase so the effective volume fraction will be considered (volume of the constituent particles plus the trapped fluid). Eq. (31) is commonly used and includes the fractal dimension of the cluster [83,113]. This expression also considers the radius of the clusters, one of the main important geometric parameters to physically characterize an aggregate.

There are two important radii: the radius of gyration that depends only on the geometrical arrangement of the particles in the cluster, which can be obtained by experimental techniques, and the hydrodynamic radius, which is the radius of the equivalent sphere experiencing the same hydrodynamic drag as the cluster itself, and is accessed through both experiments and simulations [114]. Many authors have established different relations for the hydrodynamic

radius of clusters, as shown in Table I-3 [103,104,115]. Lattuada *et al.* [115] proposed the calculus of the hydrodynamic radius of clusters thanks to the description of the effect that the different spheres constituting an aggregate have on its hydrodynamic behavior. Snabre *et al.* [104] focused on finding the mean radius of clusters in a shear field, considering the particles interaction forces, where the exponent *m* mainly depends on the structure of the aggregates, and their mechanism of deformation and breakup under the action of external stresses. Allain *et al.* [103] formulates the equation based on a comparison between hydrodynamic shear forces (which tend to break up aggregates) and attractive forces.

Table I-3 - Different relations for the hydrodynamic radius of clusters.

Author	Equation	Parameters
SNABRE [104]	$R = a(1 + \left(\frac{\sigma_c}{\sigma}\right)^m)$	m: Dimensionless constant a: Radius of the elementary particles of the cluster σ_c: Characteristic stress for cluster break-up or cohesion σ: Shear stress
ALLAIN [103]	$R = a\left(\frac{\Lambda}{a12h^2\eta_f\dot{\gamma}_c}\right)^{1/2}$	Λ: Hamaker constant h: Average distance between particles η_f: Viscosity of the continuous phase
LATTUADA [115]	$R = \frac{2(D_f - 1)}{D_f}.R_s$	R_s: Cluster maximum radius

4.1.3 Aggregation influence on rheology

The rheological behavior of a fluid can be strongly influenced by the particles aggregation kinetics as well as the flow, which has an impact on the particles collision and clusters destruction or formation. The particle-particle interactions that lead to the aggregation have dramatic effects on viscosity since not only are the aggregates larger than individual particles, and hence more resistant to flow, but they also enclose, and so immobilize some of the liquid phase, increasing the effective volume fraction, resulting in a higher viscosity at low shear rates [116]. When the aggregates in a suspension are weakly connected, the flow breaks these clusters, which are restored due to the attractive force field combined to Brownian motion. At a given shear stress or shear rate, the steady state is reached when a dynamical equilibrium is established between breakdown and reformation of the aggregates, leading to a mean equilibrium of the clusters radius. It will reach its maximum equilibrium size at the maximum imposed stress that it can support without breaking [26,83,104]. This radius will decrease as the shear stress increases, and consequently the viscosity will also decrease, which is associated to the shear- thinning behavior of suspensions. This way, the aggregate size is set by a competition

between cohesive forces and rupture forces caused by the flow [117]. Snabre *et al.* [118] proposed a model to associate the relative viscosity of the suspension with the aggregate volume fraction (Eq. (36)):

$$\eta_r = \left\{1 - \frac{\phi}{\phi_m}\left[1 + \left(\eta_r . \frac{\eta_f \dot{\gamma}_c}{\sigma_c}\right)^{-m}\right]^{3-D_f}\right\}^{-2} \tag{36}$$

Where η_r and η_f are the relative and the continuous phase viscosity, respectively. Figure I-20 shows the relative viscosity versus a dimensionless shear rate of weakly aggregated suspensions, predicted by Eq. (36), at different particle volume fractions. For a given volume fraction, the viscosity decreases at increasing shear rates, due to the decrease in the equilibrium cluster size (and its effective volume fraction). At infinite shear rates, the clusters are reduced to the primary particles and the viscosity reaches a plateau corresponding to a hard-sphere suspension [83,104]. Hence, the changes on the suspended aggregates to reach an equilibrium size after reorganization are not instantaneous and require a finite time to happen. This non-equilibrium nature of the structure implies that the rheology of weakly aggregated suspensions can be affected by shear history [26], which can be described by thixotropic models [83].

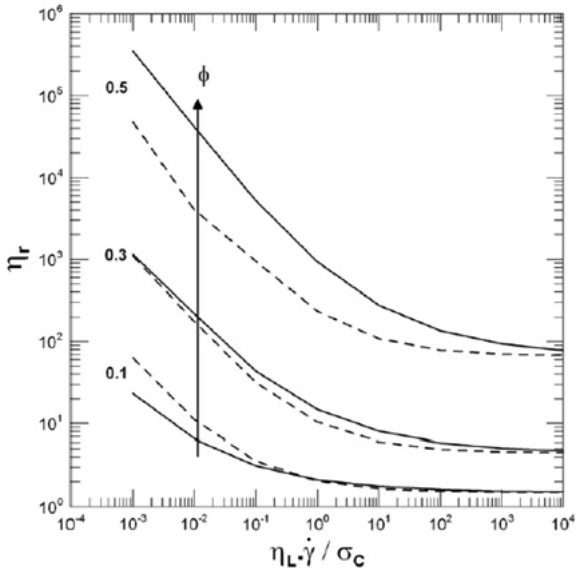

Figure I-20 - Relative viscosity vs. dimensionless shear rate of weakly aggregated suspensions, predicted by Eq. (36), at different particle volume fractions at equilibrium [83].

4.2 PGM particles aggregation

As mentioned in earlier sections, the Platinum Group Metals are often found in glass in the form of dense aggregates, which can be crucial for some of the glass properties such as the rheological behavior. Some studies were conducted aiming to understand the mechanism behind this particle aggregation and its impact on the material behavior [19,119]. During the vitrification process of nuclear glasses containing PGM particles, the aggregation followed by the sedimentation of clusters is one of the concerns since it can change dramatically the smooth continuation of the process. Cobb *et al*. [119] were interested in the RuO_2 behavior in the glass and in understanding how the clusters found in the bottom of the crucibles were created; whether by the settling of particles aggregates or by the reorganization of dispersed particles after settling. They analyzed crucibles containing glass with RuO_2 maintained at 1050°C for different times (from 15 minutes to 140 hours). It was observed that some aggregates appear in the upper half of the melt, indicating that aggregation happens before the sedimentation. The aggregates were created within the melt meniscus and above due to high velocity gradients formed by surface tension that bring the particles into contact. In the glass melter this aggregation may happen due to existing velocity gradients coupled with the accumulation of particles transported by bubbles, even though the latter were never noticed in the crucibles [119].

The work of Hanotin *et al*. [43] laid on the structural approach to describe the rheological behavior of glasses containing PGM particles. As mentioned in section 3.1.1, the authors stated that the PGM particles aggregation during flow happens through the effect of van der Waals forces combined with Brownian reorganizations at low shear, leading to changes in the viscosity of the system. In addition, the effects of PGM content and temperature on the aggregation were analyzed. The hypothesis was that at low shear, the increase in temperature leads to the acceleration of diffusional processes of the particles, which favors aggregation. This way, a crucible containing a glass sample with a PGM content of 3%wt was subjected to a shear rate of 10^{-3} s^{-1} for 1 hour at 1000ºC and 1200ºC. Afterwards, the sample was cut in several sections and analyzed by SEM. Figure I-21 shows, after image treatment, that the size of the clusters is larger at 1200°C, which supports the hypothesis that the temperature favors aggregation at low shear and therefore leads to a viscosity growth [19]. More studies are needed to model the mechanism of PGM particles aggregation over time and link it to the rheological behavior.

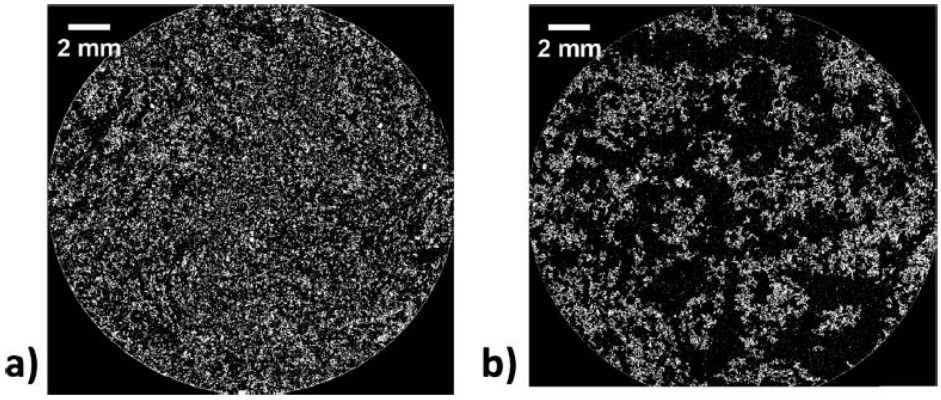

Figure I-21 - SEM images, obtained after image processing, of a chip extracted from the simulated nuclear glass containing 3 wt% of PGM particles, sheared for 1 hour in the crucible at 10-3 s-1 and heating up to a) 1000ºC and b) 1200ºC. The white pixels correspond to the PGM particles (RuO2 needles and PdTe spheres) [19].

Conclusion

The study of PGM particles aggregation allows relating the structural behavior of the glass to its rheological behavior. In this section, the basic mechanisms of this phenomenon were presented in the context of generic suspensions. For glass melts containing suspended particles, aggregation can be studied using these same mechanisms thanks to several models available in the literature. Nonetheless, there are still only few studies on this topic for PGM glasses.

5 PGM particles sedimentation kinetics

5.1 Particles sedimentation

5.1.1 Mechanisms and kinetics

Sedimentation happens when the forces acting on the particles and in the fluid are unbalanced leading to the settling of the particles. The most common sedimentation type is due to the gravity, when the fluid and particle densities are different. Macroscopic particles dispersed in a fluid are submitted to gravitational and surface forces produced by the fluid, considered as a continuous medium [120]. The sedimentation velocity is expressed nondimensionnally through the Reynolds number (Re)

$$Re = \frac{\rho_f L U}{\eta} \tag{37}$$

where ρ_f is the fluid density, L the length of the particle, U is the sedimentation speed and η the fluid viscosity [61]. In a suspension, each particle that settles drives the fluid around it along

which makes the particles in the neighborhood settle faster. At the same time, due to the presence of the recipient walls, when the particle reaches the bottom, it moves the fluid in the other direction, slowing down the other particles that sediment. The effect of local backflow during the sedimentation of a suspension of spheres is called hindered sedimentation (Figure I-22).

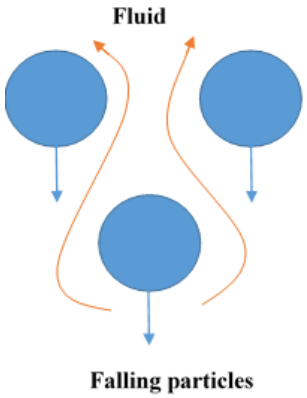

Figure I-22 - Effect of local backflow during the sedimentation of a suspension of spheres.

Considering the case of an isolated particle in a fluid, it is possible to calculate the relation between the displacement speed and the acting forces by the Stokes relation, which is valid for low Reynolds number. It considers a sphere of radius a and density ρ_s, left in a viscous fluid of viscosity η, which will tend to its limit speed. The viscous friction of the fluid will act on the particle and influence its falling speed through the viscous drag force. The sedimentation velocity (U) can be derived from the following equation [61]:

$$F = \frac{4}{3}.\pi.(\rho_s - \rho_f).g.a^3 = 6.\pi.a.U.\eta \tag{38}$$

leading to

$$U_0 = \frac{2a^2(\rho_s - \rho_f)}{9\eta}.g \tag{39}$$

For a more complex case where the particle is an elongated ellipsoid with the dimensions *a* and *b* (*a* > *b*), the relation will depend on the orientation of the larger axis in relation to the vertical. Eq.(38) would consider the hydrodynamic radius (R_H) instead of the particle radius. Supposing the case that the axis is vertical, (*i.e.* particle and sedimentation axis are parallel); the radius would be $R_{//}$ (Eq.(40)). If they are perpendicular, the radius would be $R_{\perp}$ (Eq.(41)). Both equations involve the aspect ratio α = *a*/*b*:

$$R_{//} = \frac{2a}{3} \cdot \frac{1}{\ln(2\alpha) + 1/2} \tag{40}$$

$$R_{\perp} = \frac{4a}{3} \cdot \frac{1}{\ln(2\alpha) + 1/2} \tag{41}$$

From these two relations it is observed that the viscous drag force is two times greater when the displacement speed is perpendicular to the larger axis of the ellipsoid. This same relation can be applied to cylindrical particles where the length will be of great importance to determine the viscous resistance of the fluid to sedimentation [61].

In the case of dispersion of multiple particles, the acting forces differ from isolated particles since they interfere with each other, resulting in a different velocity. Considering a statistically homogeneous dispersion of identical rigid spherical particles of radius *a* in a Newtonian fluid. The Stokes velocity of one single sphere U_0 is calculated from expression (39), considering an infinite fluid and falling under gravity [121]. On the other hand, for a sphere in a suspension the velocity *U* follow the Batchelor expression:

$$U = U_0(1 - pc) \tag{42}$$

where *c* is the volume fraction of the spheres in the suspension and *p* is a theoretical parameter that normally is approximately 5 for volume fraction smaller than 10% [121]. For more concentrated dispersion the relation of Richardson and Zaki is the most used [122], considering also that *p* is of the order of 5:

$$U = U_0(1 - c)^k \tag{43}$$

Both equations, indicates that the sedimentation speed decreases when the particles concentration increases. This is observed during the settling of a suspension when a transition zone is created. This zone is composed of the settled suspension and above it the fluid with a lower concentration. The particles that settle from this fluid will be faster and will catch up other particles creating a sedimentation front that separates the clear fluid from the concentrated suspension [61]. These transition zones also appear with suspensions containing particles of different types and shapes since the sedimentation speed will differ between them, creating layers separated by the different settling velocity.

5.1.2 Sedimentation in non-Newtonian fluids

Most of sedimentation studies are conducted considering the kinetics in a Newtonian fluid even though the phenomenon differs for non-Newtonian fluids. Studies show that for non-Newtonian

fluids, nonhomogeneous structures are created during sedimentation that are induced by particle aggregation. Moreover, the sedimentation rate in such fluids is not constant in time: the suspensions first settle rapidly, and the process then slows down [123]. The drag force exerted on single spheres in non-Newtonian fluids cannot be generalized since there are several rheological parameters that influence this force. The influence of normal stress differences and extensional viscosity can also be crucial. The Reynolds number is as well an important parameter to be considered since, as in a Newtonian fluid, inertia can modify the settling of a single particle [124]. The sedimentation velocity in a shear-thinning fluid (U_{st}) can be calculated by a relation based on the Stokes velocity U_0 (Eq.(39)) of a single sphere (radius a) and the average distance between two neighbor spheres in the fluid (d):

$$U_{st} = U_0(1 + \frac{3}{2}.\frac{a}{d}) \tag{44}$$

For shear thinning fluids, there is a critical separation distance (d_c) under which the particles interact. Daugan *et al*. [124] showed that for an initial separation distances d_0 larger than d_c, two neighbor particles settle at the same velocity. When d_0 is smaller than d_c, the second particle falls faster than the first one and finally chains with it, resulting in a stable cluster. The higher velocity of the second particle results from the creation of a corridor of reduced viscosity in the wake of the first particle that shears the fluid, which vanishes when the fluid relaxes [123].

5.1.3 Aggregation and Sedimentation

Colloidal suspensions are composed of particles, with diameters ranging between 10^{-9} m and 10^{-7} m, suspended in a continuous phase. If the particles of a colloidal suspension do not aggregate, gravity does not have a big effect and the particles remain dispersed. But if aggregation occurs and the aggregates size exceeds a critical size, the Brownian motion diminishes and it leads to the aggregates sedimentation [61]. Figure I-23 shows a scheme of the behavior of a strongly aggregated colloidal suspension submitted to gravity as a function of the volume fraction of the particles. When Φ is small ($\Phi < \Phi^*$), the settling of individual aggregates happens until the clusters reach a reasonable size followed by deposit onto the bottom. At this point, the cluster growth is solely controlled by Brownian diffusion. On the other hand, when the volume fraction is large ($\Phi > \Phi^{**}$), no settling occurs; the suspension forms a stable colloidal gel, i.e. a close packing of aggregates filling the whole cell, that does not separate under the action of gravity. In the intermediate regime, when $\Phi^* < \Phi < \Phi^{**}$, a gel forms very rapidly but this gel is fragile and collapses under its own weight [125].

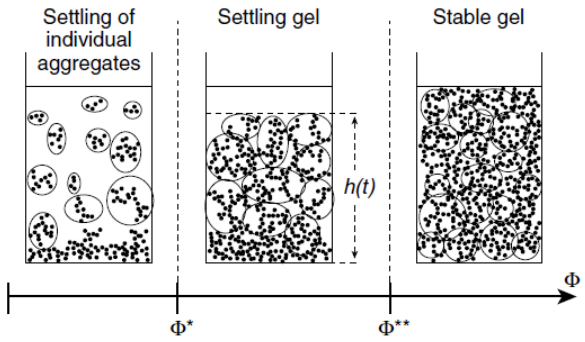

Figure I-23 - Schematic representation of the behavior of a strongly aggregating colloidal suspension submitted to gravity as a function of the volume fraction of the particles [125].

Allain *et al*. [126] found experimentally that for a calcium carbonate gel, Φ*= 3.10-3 and Φ**= 5.10-2. They showed for this system that, if the aggregates do not reach the critical size for sedimentation, the kinetics is governed by the aggregation, but when these aggregates get larger, the kinetics changes and will couple both phenomena, without a sedimentation front. The sedimentation speed (U) of an aggregate results from the balance between the aggregate weight and the hydrodynamic friction force, leading to the following expression [61]:

$$U = \frac{2}{9}\frac{\Delta\rho g a^2}{\eta}\left(\frac{R}{a}\right)^{D_f-1} \tag{45}$$

where, D_f is the fractal dimension, R is the fractal radius, a is the particle radius, g is the gravity, η is the viscosity and $\Delta\rho$ is the density variation. Therefore, the aggregation kinetics influence directly the sedimentation kinetics of a suspension. Figure I-24 shows a table with the effects some basic aggregation variables have in sedimentation such as the primary particle size, aggregate diameter, and fractal dimension is shown. These variables affect directly two important sedimentation parameters: the gel point and settling rate. For example, for the same primary particle size and fractal dimension, increasing the aggregate diameter results in an increased settling rate, a trend that is similar for solid spherical particles. On the other hand, for the same aggregate diameter and fractal dimension, increasing the primary particle size increases the solids density of the aggregate resulting in an increased settling rate. Finally, increasing the fractal dimension with constant primary particle and aggregate sizes results in an increased settling rate. Thus, primary particle size, fractal dimension, and aggregate size must all be known to predict the settling behavior of colloidal suspensions [127].

Primary Diameter	Agglomerate Diameter	Fractal Dimension	Gel Point (vol%)	Settling Rate (cm/hr)
0.01 μm	100 μm	1.8	0.32%	0.07
1 μm	100 μm	1.8	2.7%	18
0.01 μm	100 μm	2.5	3%	72
1 μm	100 μm	2.5	10%	3000
0.01 μm	1 μm	2.5	10%	0.036
0.01 μm	10 μm	2.5	7%	1.4
0.01 μm	100 μm	2.5	3%	72
100 μm	100 μm	3.0	16%	6000

Figure I-24 - Dependence of sedimentation velocity on aggregation properties [104].

5.2 PGM particles sedimentation

As mentioned before, the PGM particles are insoluble in the glass melt and must be considered as suspended particles. The PGM can be found as spherical alloys of palladium and rhodium with tellurium (1 to 5 μm) and ruthenium oxide in a needle-like form (length ~10 μm). Hence, PGM particles are not strictly speaking colloidal, but their sizes remain close to 1μm, so that Brownian motion still has a significant action on them. Moreover, during the vitrification process, these particles tend to aggregate and sediment to the bottom of the melter. Some studies were carried out to model this mechanism and predict the settling velocity of these particles. Cobb *et al.* showed that the clusters found in the bottom of crucibles were not created only by sedimentation but by a previous aggregation followed by settling [119]. Kashcheev *et al.* developed a mathematical model to predict the growth and sedimentation of dispersed phase during the vitrification of liquid radioactive waste [95]. Both of these phenomena (growth and sedimentation) depend on the structure of the aggregates and thus on the aggregate fractal dimension. The study relies on the hypothesis of a supersaturated solution without mixing, in which the clusters growth is due to supersaturation and not from the particle collision. Based on it, the dynamics of precipitation $\psi(t)$ on a unit area at the bottom of a tank at a certain time is given by the following equation [95]:

$$\psi(t) = \psi_0(t) + (n_0 - n_s).L.\left[1 - \exp\left(-\frac{t}{\tau}\right)\right] \quad (46)$$

where n_0 and n_s are the concentration of impurities in the melt and in the saturation, respectively; L is the depth of the melt, ψ_0 is rate of flow of the dispersed phase onto the surface of the melt and τ is a characteristic time. n_s is a function of the temperature and composition

of the melt. This sedimentation was analyzed neglecting the convective flows in the glass melt [95].

Puig *et al.* [58] also studied the sedimentation dynamics of a glass containing PGM particles under low shear rate. The work was dedicated to understand the mechanisms that affects the rheological behavior of simulated nuclear glasses containing PGM particles. Therefore, the PGM particles sedimentation was analyzed during a characterization of the non-Newtonian behavior of the glass. A glass sample with 3 %wt of PGM particles was stirred under low shear rate at 1200°C during 21.5 hours in a platinum crucible and another for 25 hours without stirring. After the mixing, a cooled glass cylinder was extracted from each crucible and cutted horizontally in several pellets which were then characterirized by image analysis and density measurements [58]. These experiments proved that the particles aggregation at low shear rate had an accelerating effect on the PGM settling.

There is not a lot of data available on the sedimentation of PGM particles due to experimental difficulties. On the other hand, in the same nuclear waste management context, American researchers deepened the studies on the spinels sedimentation in the vitrification furnaces of high-level waste in the Waste Treatment and Immobilization Plant (WTP) at the Hanford site, becoming a reference in the particle sedimentation studies in glass. In order to overcome the challenge to carry out in-situ experiments at high temperature, model suspensions were developed to represent the glass melts. Guillen *et al*. performed experiments at room temperature on model systems in a scale 1 prototype of the casting system [128]. A silicone oil and magnetite system (75-125 μm) was used to simulate molten glass containing spinels, at a maximum volume fraction of 0.1%. However, the density ratio of magnetite and oil is not representative of that of the spinel and glass system. The experimental system consisted of a discharge riser and throat attached to a feed tank that allowed visual observation of the particles behavior. The particle settling speed was measured optically, by video and image analysis, but also calculated based on empirical modifications of Stokes law. Figure I-25 shows a table comparing the different settling velocities and time obtained experimentally and theoretically. Batchelor's approach, considering a settling cloud of particles, was the most suitable for this diluted suspension. Indeed, the experimental and calculated sedimentation rates were very close (in the order of 10^{-4} $m.s^{-1}$), if a correction considering the effect of the walls is applied. Stokes' law on the other hand underestimates the sedimentation rate by two orders of magnitude [128].

Methodology	Settling velocity (m/s)	Settling time (min)
Stokes	3.66×10^{-6}	1793
Hindered Stokes	3.69×10^{-6}	1779
Cloud	6.95×10^{-4}	9
Wall-corrected cloud	1.06×10^{-4}	62
Experiment	1.1×10^{-4}	60

Figure I-25 - Settling velocity and time for the different theoretical approximations compared with experimental data [128].

Conclusion

This chapter focused on the sedimentation mechanisms and kinetics and on the relation of aggregation and sedimentation, previously described in the literature. The comprehension of how the sedimentation occurs in glasses containing PGM particles is important to predict (and if necessary adapt) the glass melt behavior during the vitrification. In particular, some recent studies on the topic showed the challenges in predicting the sedimentation speed for high temperature experiments, leading to qualitative rather than quantitative analysis. Just as for aggregation, the analysis of sedimentation relies on the understanding of the PGM containing glass as a complex fluid. The section also showed that one way to overcome the challenges of high temperature measurements is to work with model suspensions.

6 Conclusion

In this state of the art chapter were described the latest studies related to the behavior of PGM particles in glass as well as prepare a background in the main concepts of waste management, rheology, aggregation and sedimentation in a nuclear context. An overview on waste vitrification in the French nuclear system was given in the first section of this chapter. The rheology of glass melt was explored next, establishing the main definitions, showing the most common rheometry techniques for glass melts and defining the different non-Newtonian behaviors. It also explored the behavior of complex fluids, which can be used to approach the study of glass with suspended PGM particles. Considering the complexity of this system, it gives the proper tools to a phenomenological modelling of the PGM particle glass rheological behavior.

The following section relied on the impact of PGM particles in a glass melt. It started by showing the properties of these metals and then the great influence they have on the physical properties of glass such as increasing electrical conductivity and viscosity. It also explored in more details the past studies on the rheological behavior of PGM glasses and the last models used to model the very shear-thinning behavior of such materials. The model proposed by Hanotin et al. is the most suitable for instance to predict the behavior of this material combining the simplified Cross model with the evolution of particles aggregation in both Newtonian plateaus exhibit by the glass, at low and high shear rates.

The aggregation and sedimentation topics approached the basic mechanisms of the phenomena in the suspension context. By considering the glass as a complex fluid, the analysis of grouping and settling particles becomes more viable thanks to several available models. These sections also showed recent studies in the area, showing that are still only a few studies in these topics for PGM glasses. Hanotin and Puig gave a good overview in the subject, creating the base for the studied carried in this work establishing the impact of time, temperature and shear on the rheological behavior of the simulated nuclear glass as well as the impact on the aggregation and sedimentation kinetics.

References

[1] Nuclear Power Today | Nuclear Energy - World Nuclear Association, (n.d.). https://world-nuclear.org/information-library/current-and-future-generation/nuclear-power-in-the-world-today.aspx (accessed November 3, 2021).

[2] Intergovernmental Panel on Climate Change, Technology-specific Cost and Performance Parameters, Clim. Chang. 2014 Mitig. Clim. Chang. (2015) 1329–1356. https://doi.org/10.1017/cbo9781107415416.025.

[3] C.E. Velasquez, F.B.G.L. e Estanislau, A.L. Costa, C. Pereira, Assessment of the French nuclear energy system – A case study, Energy Strateg. Rev. 30 (2020). https://doi.org/10.1016/j.esr.2020.100513.

[4] Production mondiale d'Électricité - L'énergie nucléaire dans le monde, (n.d.). https://www.cnrs.fr/cw/dossiers/dosnucleaire/darkcartes/1_production-mondiale-d-electricite.php (accessed November 3, 2021).

[5] J.G. Tyror, Nuclear Reactor Physics, Phys. Bull. 12 (1961) 323–323. https://doi.org/10.1088/0031-9112/12/11/012.

[6] J.-M. GRAS, Cycle du combustible nucléaire - Introduction, Tech. l'ingénieur. 33 (2016) 1–2.

[7] D. Greneche, Cycle du combustible nucléaire: aval du cycle et questions génériques, Tech. l'Ingénieur. BN3564 V1 (2016).

[8] J.E. Birkett, M.J. Carrott, O.D. Fox, C.J. Jones, C.J. Maher, C. V. Roube, R.J. Taylor, D.A. Woodhead, Recent developments in the purex process for nuclear fuel reprocessing: Complexant based stripping for uranium/plutonium separation, Chimia (Aarau). 59 (2005) 898–904. https://doi.org/10.2533/000942905777675327.

[9] Stages Of The Nuclear Fuel Cycle | NRC.gov, (n.d.). https://www.nrc.gov/materials/fuel-cycle-fac/stages-fuel-cycle.html (accessed November 3, 2021).

[10] ANDRA, Inventaire national des déchets radioactifs, Les Essentiels. 53 (2020) 26. www.inventaire.andra.fr.

[11] Waste classification | Andra international, (n.d.).

https://international.andra.fr/radioactive-waste-france/waste-classification (accessed November 4, 2021).

[12] T. Advocat, J.L. Dussossoy, V. Petitjean, Vitrification des déchets radioactifs et appareillage, Les Tech. l'Ingénieur. 33 (2008) 0–27.

[13] G. Roth, S. Weisenburger, Vitrification of high-level liquid waste: glass chemistry, process chemistry and process technology, Nucl. Eng. Des. 202 (2000) 197–207. https://doi.org/10.1016/S0029-5493(00)00358-7.

[14] S. Peuget, J.N. Cachia, C. Jégou, X. Deschanels, D. Roudil, V. Broudic, J.M. Delaye, J.M. Bart, Irradiation stability of R7T7-type borosilicate glass, J. Nucl. Mater. 354 (2006) 1–13. https://doi.org/10.1016/j.jnucmat.2006.01.021.

[15] É. Vernaz, J. Bruezière, History of Nuclear Waste Glass in France, Procedia Mater. Sci. 7 (2014) 3–9. https://doi.org/10.1016/j.mspro.2014.10.002.

[16] C. Simonnet, A. Grandjean, J. Phalippou, Electrical behavior of platinum-group metals in glass-forming oxide melts, J. Nucl. Mater. 336 (2005) 243–250. https://doi.org/10.1016/j.jnucmat.2004.09.019.

[17] R.F. Taylor, Chemical engineering problems of radioactive waste fixation by vitrification, Chem. Eng. Sci. 40 (1985) 541–569. https://doi.org/10.1016/0009-2509(85)80001-4.

[18] C. Laurin, E. Régnier, S. Gossé, A. Laplace, J. Agullo, S. Mure, E. Brackx, M. Toplis, O. Pinet, Redox behavior of ruthenium in nuclear glass melt: ruthenium dioxide reduction reaction, J. Nucl. Mater. 545 (2021). https://doi.org/10.1016/j.jnucmat.2020.152650.

[19] C. Hanotin, J. Puig, M. Neyret, P. Marchal, Platinum group metal particles aggregation in nuclear glass melts under the effect of temperature, J. Nucl. Mater. 477 (2016) 102–109. https://doi.org/10.1016/j.jnucmat.2016.04.033.

[20] D.I. Wilson, What is rheology?, Eye. 32 (2018) 179–183. https://doi.org/10.1038/eye.2017.267.

[21] H. Murata, Rheology - Theory and Application to Biomaterials, in: A.D.S. Gomes (Ed.), Polymerization, InTech, 2012. https://doi.org/10.5772/48393.

[22] Q. Zheng, J.C. Mauro, Viscosity of glass-forming systems, J. Am. Ceram. Soc. 100 (2017) 6–25. https://doi.org/10.1111/jace.14678.

[23] Y. Yue, R. Brückner, A new description and interpretation of the flow behaviour of glass forming melts, J. Non. Cryst. Solids. 180 (1994) 66–79. https://doi.org/10.1016/0022-3093(94)90398-0.

[24] J.C. Mauro, D.C. Allan, M. Potuzak, Nonequilibrium viscosity of glass, Phys. Rev. B - Condens. Matter Mater. Phys. 80 (2009) 1–18. https://doi.org/10.1103/PhysRevB.80.094204.

[25] J.H. Simmons, R. Ochoa, K.D. Simmons, J.J. Mills, Non-Newtonian viscous flow in soda-lime-silica glass at forming and annealing temperatures, J. Non. Cryst. Solids. 105 (1988) 313–322. https://doi.org/10.1016/0022-3093(88)90325-0.

[26] H.A. Barnes, A Handbook of Elementary Rheology, The University of Wales- Institute of Non-Newtonian Fluid Mechanics, Department of Mathematics, Avaiable online, 2000.

[27] RheoTec, Introduction to rheology, in: Germany, 2013: p. 48.

[28] M.L.F. Nascimento, C. Aparicio, Data classification with the Vogel-Fulcher-Tammann-Hesse viscosity equation using correspondence analysis, Phys. B Condens. Matter. 398 (2007) 71–77. https://doi.org/10.1016/j.physb.2007.04.074.

[29] D. Dupuis, Mesure de la viscosité - Principes généraux Mesure de la viscosité, Tech. l'ingénieur. 33 (2008).

[30] Y.Y. Hou, H.O. Kassim, Instrument techniques for rheometry, Rev. Sci. Instrum. 76 (2005) 1–19. https://doi.org/10.1063/1.2085048.

[31] D. Dupuis, Mesure de la viscosité - Viscosimètres et rhéomètres, Tech. l'ingénieur. r2351 (2008).

[32] T.G. Mezger, 8. Oscillatory tests, in: Rheol. Handb., 2nd revise, Vincentz Network, Hannover, Germany, 2019: pp. 135–212. https://doi.org/10.1515/9783748600367-009.

[33] J. Guillemin, Rhéologie de suspensions concentrées de matériaux énergétiques recyclables – Modélisation du temps de coulée, Thesis. (2008).

[34] J.-M. Piau, M. Piau, Le Prix Maurice Couette du GFR, Rheologie. 8 (2005) 1–4.

[35] P. Coussot, C. Ancey, Rhéophysique des pates et des suspetions, EDP Sciences, Les Ulis, 1999.

[36] L. Choplin, P. Marchal, Rhéologie et Produits Formulés Complexes, Tech. l'ingénieur. Réf. : J21 (2010) 1–21.

[37] A. Aït-kadi, P. Marchal, L. Choplin, M. Bousmina, Quantitative Analysis of Mixer-Type Rheometers, Can. J. Chem. Eng. 80 (2002) 1166–1174.

[38] L. Choplin, P. Marchal, L. Choplin, D. Langevin, C. Baravian, P. Marchal, L. Choplin, La rhéologie systémique ou une rhéologie au service d'un génie des procédés et des produits, Rhéologie. 12 (2007) 9–18.

[39] Bousmina M.; A. Aït-Kadi and J.B. Faisant, Determination of Shear Rate and Viscosity from Batch Mixer Data: Theoretical and Experimental Results, J. Rheol. 43 (1999) 1999.

[40] S. Gotoh, M. Nishikawa, H. Tada, H. Hirabayashi, Power consumption of mixing impellers in bingham plastic liquids, J. Chem. Eng. JAPAN. 3 (1970) 237–243. https://doi.org/10.1252/jcej.3.237.

[41] V.V. and J.J.U. Chavan, Power Correlations for Close Clearance Helical Impellers in Non-Newtonian Liquids, Ind. Eng. Chem. Process Des. Dev. 12 (1973) 472–476.

[42] P. Estellé, C. Lanos, A. Perrot, S. Amziane, Processing the vane shear flow data from Couette analogy, Appl. Rheol. 18 (2008) 1–14.

[43] J. Puig, C. Hanotin, M. Neyret, P. Marchal, High temperature rheological study of borosilicate glasses containing platinum group metal particles by means of a mixer-type rheometer, J. Nucl. Mater. 469 (2016) 112–119. https://doi.org/10.1016/j.jnucmat.2015.11.053.

[44] J.P. Guillemin, Y. Menard, L. Brunet, O. Bonnefoy, G. Thomas, Development of a new mixing rheometer for studying rheological behaviour of concentrated energetic suspensions, J. Nonnewton. Fluid Mech. 151 (2008) 136–144. https://doi.org/10.1016/j.jnnfm.2007.12.007.

[45] S. Vargas, Straw and Coal Ash Rheology, Technical University of Denmark, Thesis, 2001.

[46] H. Fukuyama, Y. Waseda, High-Temperature Measurements of Materials, Springer,

Sendai, Japan, 2009.

[47] J.E. Shelby, M. Lopes, Viscosity of glass formaing melts, in: J.E. Shelby (Ed.), Introd. to Glas. Sci. Technol., Royal Society of Chemistry, Cambridge, 2007: pp. 111–137. https://doi.org/10.1039/9781847551160-00111.

[48] Juejun Hu, Lecture on Amorphous Materials: Viscosity of glass, in: Dep. Mater. Sci. Eng. - Massachusetts Inst. Technol., 2017. https://doi.org/10.11410/kenbikyo1950.35.198.

[49] International Organization for Standardization, ISO 7884-4. Glass - Viscosity and viscometric fixed points - Part 4: Determination of viscosity by beam bending, Part 4 (1987). http://www.isostandards.com.au/.

[50] H. Jiang, B. Bochtler, M. Frey, Q. Liu, X. Wei, Y. Min, S.S. Riegler, D. Liang, R. Busch, J. Shen, Equilibrium viscosity and structural change in the Cu47.5Zr45.1Al7.4 bulk glass-forming liquid, Acta Mater. 184 (2020) 69–78. https://doi.org/10.1016/j.actamat.2019.11.039.

[51] Y. Song, C. Won, S. hoon Kang, H. Lee, S.J. Park, S.H. Park, J. Yoon, Characterization of glass viscosity with parallel plate and rotational viscometry, J. Non. Cryst. Solids. 486 (2018) 27–35. https://doi.org/10.1016/j.jnoncrysol.2018.02.003.

[52] J. Piau, Fluides non-newtoniens, Tech. l'ingénieur. 33 (1979).

[53] A.Y. Malkin, Non-Newtonian viscosity in steady-state shear flows, J. Nonnewton. Fluid Mech. 192 (2013) 48–65. https://doi.org/10.1016/j.jnnfm.2012.09.015.

[54] A.E. Kaiser, A.L. Graham, L.A. Mondy, Non-Newtonian wall effects in concentrated suspensions, J. Nonnewton. Fluid Mech. 116 (2004) 479–488. https://doi.org/10.1016/j.jnnfm.2003.11.004.

[55] T.Y. Na, A.G. Hansen, Radial flow of viscous non-Newtonian fluids between disks, Int. J. Non. Linear. Mech. 2 (1967) 261–273.

[56] V. Thai Son, Rhéologie des suspensions non newtoniennes, Université Paris-Est, Thesis, 2011. tel-00598310⟩.

[57] K. Uruga, T. Usami, T. Tsukada, S. Komamine, E. Ochi, Viscoplasticity of simulated high-level radioactive waste glass containing platinum group metal particles, J. Nucl.

Mater. 452 (2014) 419–424. https://doi.org/10.1016/j.jnucmat.2014.05.062.

[58] J. Puig, B. Penelon, P. Marchal, M. Neyret, Rheological Properties of Nuclear Glass Melt Containing Platinum Group Metals, Procedia Mater. Sci. 7 (2014) 156–162. https://doi.org/10.1016/j.mspro.2014.10.021.

[59] B. Luckscheiter, Properties and behavior of the platinum group metals in the glass resulting from the vitrification of simulated nuclear fuel reprocessing waste, J. Mater. Res. 6 (1991) 2535–2546. https://doi.org/10.1557/JMR.1991.2535.

[60] D. Quemada, Rheological modelling of complex fluids. I. The concept of effective volume fraction revisited, Eur. Phys. J. Appl. Phys. 1 (1998) 119–127. https://doi.org/10.1051/epjap:1998125.

[61] B. Ildefonse, C. Allain, P. Coussot, Des grands écoulements naturels à la dynamique du tas de sable: introduction aux suspensions en géologie et en physique., 1st ed., Cemagref, 1999.

[62] G.P. Roberts, H.A. Barnes, P. Carew, Modelling the flow behaviour of very shear-thinning liquids, Chem. Eng. Sci. 56 (2001) 5617–5623. https://doi.org/10.1016/S0009-2509(01)00291-3.

[63] J. Ding, P.J. Tracey, P.G. Whitten, Review on Shear Thickening Fluids and Applications, Text. Light Ind. Sci. Technol. 2 (2013) 161–173.

[64] I. Wagstaff, C.E. Chaffey, Shear thinning and thickening rheology. I. Concentrated acrylic dispersions, J. Colloid Interface Sci. 59 (1977) 53–62. https://doi.org/10.1016/0021-9797(77)90338-1.

[65] J. Paiola, Écoulement d ’ un fluide à seuil dans un milieu poreux, Université Paris-Saclay, Thesis, 2017. https://tel.archives-ouvertes.fr/tel-01563941.

[66] A.N. Alexandrou, N. Constantinou, G. Georgiou, Shear rejuvenation, aging and shear banding in yield stress fluids, J. Nonnewton. Fluid Mech. 158 (2009) 6–17. https://doi.org/10.1016/j.jnnfm.2009.01.005.

[67] M.M. Denn, D. Bonn, Issues in the flow of yield-stress liquids, Rheol. Acta. 50 (2011) 307–315. https://doi.org/10.1007/s00397-010-0504-3.

[68] P.C.F. Møller, A. Fall, D. Bonn, Origin of apparent viscosity in yield stress fluids below

yielding, Epl. 87 (2009). https://doi.org/10.1209/0295-5075/87/38004.

[69] D.Z. Gunes, R. Scirocco, J. Mewis, J. Vermant, Flow-induced orientation of non-spherical particles: Effect of aspect ratio and medium rheology, J. Nonnewton. Fluid Mech. 155 (2008) 39–50. https://doi.org/10.1016/j.jnnfm.2008.05.003.

[70] H. Giesekus, M.F. Hibberd, eds., Progress and Trends in Rheology II, Steinkopff, Heidelberg, 1988. https://doi.org/10.1007/978-3-642-49337-9.

[71] H.A. Barnes, Thixotropy—a review, J. Nonnewton. Fluid Mech. 70 (1997) 1–33. https://doi.org/10.1016/S0377-0257(97)00004-9.

[72] J. Mewis, Thixotropy - a general review, J. Nonnewton. Fluid Mech. 6 (1979) 1–20. https://doi.org/10.1016/0377-0257(79)87001-9.

[73] K. Dullaert, J. Mewis, Thixotropy: Build-up and breakdown curves during flow, J. Rheol. (N. Y. N. Y). 49 (2005) 1213–1230. https://doi.org/10.1122/1.2039868.

[74] J.F. Maingonnat, L. Muller, J.C. Leuliet, Modelling the build-up of a thixotropic fluid under viscosimetric and mixing conditions, J. Food Eng. 71 (2005) 265–272. https://doi.org/10.1016/j.jfoodeng.2005.01.036.

[75] M. Houška, R. Žitný, Dynamics of Thixotropic Liquids and Time Dependency, in: Adv. Food Rheol. Its Appl., Elsevier, New York, 2017: pp. 47–63. https://doi.org/10.1016/B978-0-08-100431-9.00003-6.

[76] J.J. Derksen, Simulations of thixotropic liquids, Appl. Math. Model. 35 (2011) 1656–1665. https://doi.org/10.1016/j.apm.2010.09.042.

[77] P. Coussot, A.I. Leonov, J.M. Piau, Rheology of concentrated dispersed systems in a low molecular weight matrix, J. Nonnewton. Fluid Mech. 46 (1993) 179–217. https://doi.org/10.1016/0377-0257(93)85046-D.

[78] D. Quemada, Rheological modelling of complex fluids: II. Shear thickening behavior due to shear induced flocculation, EPJ Appl. Phys. 2 (1998) 175–181. https://doi.org/10.1051/epjap:1998170.

[79] C.I. Mendoza, I. Santamaría-Holek, The rheology of hard sphere suspensions at arbitrary volume fractions: An improved differential viscosity model, J. Chem. Phys. 130 (2009). https://doi.org/10.1063/1.3063120.

[80] J.M. Krishnan, A.P. Deshpande, P.B.S. Kumar, eds., Rheology of Complex Fluids, Springer New York, New York, NY, 2010. https://doi.org/10.1007/978-1-4419-6494-6.

[81] D. Quemada, Rheological modelling of complex fluids: IV: thixotropic and "thixoelastic" behaviour. Start-up and stress relaxation, creep tests and hysteresis cycles, EPJ Appl. Phys. 5 (1999) 191–207. https://doi.org/10.1051/epjap:1999128.

[82] J.C. van der Werff, C.G. de Kruif, Hard-sphere Colloidal Dispersions: The Scaling of Rheological Properties with Particle Size, Volume Fraction, and Shear Rate, J. Rheol. (N. Y. N. Y). 33 (1989) 421–454. https://doi.org/10.1122/1.550062.

[83] D.B. Genovese, Shear rheology of hard-sphere, dispersed, and aggregated suspensions, and filler-matrix composites, Adv. Colloid Interface Sci. 171–172 (2012) 1–16. https://doi.org/10.1016/j.cis.2011.12.005.

[84] D. Quemada, Vieillissement , rajeunissement et thixotropie dans les fluides complexes Evolution de la viscosité au repos et sous cisaillements constants, 6 (2004) 1–16.

[85] D. Quemada, Rheology of concentrated disperse systems and minimum energy dissipation principle - I. Viscosity-concentration relationship, Rheol. Acta. 16 (1977) 82–94. https://doi.org/10.1007/BF01516932.

[86] I.M. Krieger, T.J. Dougherty, A Mechanism for Non-Newtonian Flow in Suspensions of Rigid Spheres, Trans. Soc. Rheol. 3 (1959) 137–152. https://doi.org/10.1122/1.548848.

[87] D. Quemada, C. Berli, Energy of interaction in colloids and its implications in rheological modeling, 2002. https://doi.org/10.1016/S0001-8686(01)00093-8.

[88] N. Koumakis, A. Pamvouxoglou, A.S. Poulos, G. Petekidis, Direct comparison of the rheology of model hard and soft particle glasses, Soft Matter. 8 (2012) 4271–4284. https://doi.org/10.1039/c2sm07113d.

[89] B.J. Maranzano, N.J. Wagner, The effects of interparticle interactions and particle size on reversible shear thickening: Hard-sphere colloidal dispersions, J. Rheol. (N. Y. N. Y). 45 (2001) 1205–1222. https://doi.org/10.1122/1.1392295.

[90] M. ElGuindy, Platinum Group Metals: Alloying, Properties, and Applications, Encycl. Mater. Sci. Technol. (2001) 7117–7121. https://doi.org/10.1016/b0-08-043152-6/01260-2.

[91] B. Luckscheiter, M. Nesovic, Development of glasses for the vitrification of High Level Liquid Waste (HLLW) in a joule heated ceramic melter, Waste Manag. 16 (1996) 571–578. https://doi.org/10.1016/S0956-053X(97)88231-1.

[92] T. Hartmann, H. Pentinghaus, The ternary system palladium-rhodium-tellurium: A Study to understand phase formation in the vitrification process of high-level waste concentrates (HLWC), J. Nucl. Mater. 422 (2012) 124–130. https://doi.org/10.1016/j.jnucmat.2011.12.029.

[93] W. Grünewald, G. Roth, W. Tobie, K. Weiß, S. Weisenburger, The role of the platinum group elements ruthenium, rhodium and palladium in the vitrification of radioactive high level liquid waste using joule heated ceramic lined waste glass melters, Glas. Technol. Eur. J. Glas. Sci. Technol. Part A. 49 (2008) 266–278.

[94] J. Mukerji, Behavior of Ruthenium in Glass, Ind. Eng. Chem. Prod. Res. Dev. 11 (1972) 178–183. https://doi.org/10.1021/i360042a010.

[95] V.A. Kashcheev, P.P. Poluéktov, A. V. Demin, Modeling of the sedimentation of heterogeneous phases accompanying the vitrification of liquid radioactive wastes, At. Energy. 78 (1995) 210–213. https://doi.org/10.1007/BF02407492.

[96] T. Akai, J. Nishii, M. Yamashita, H. Yamanaka, Chemical behavior of platinum-group metals in oxide glasses, J. Non. Cryst. Solids. 222 (1997) 304–309.

[97] H.D. Schreiber, F.A. Settle, P.L. Jamison, J.P. Eckenrode, G.W. Headley, Ruthenium in glass-forming borosilicate melts, J. Less-Common Met. 115 (1986) 145–154. https://doi.org/10.1016/0022-5088(86)90379-6.

[98] R. Pflieger, M. Malki, Y. Guari, J. Larionova, A. Grandjean, Electrical conductivity of ruo2-borosilicate glasses: Effect of the synthesis route, J. Am. Ceram. Soc. 92 (2009) 1560–1566. https://doi.org/10.1111/j.1551-2916.2009.03088.x.

[99] A. Grandjean, M. Malki, C. Simonnet, D. Manara, B. Penelon, Correlation between electrical conductivity, viscosity, and structure in borosilicate glass-forming melts, Phys. Rev. B - Condens. Matter Mater. Phys. 75 (2007) 1–7. https://doi.org/10.1103/PhysRevB.75.054112.

[100] C. Simonnet, Conductivité électrique des verres et fontes d'oxydes : effet de l'incorporation de particules de RuO2, Université de Montpellier II, PhD thesis, 2004.

[101] C. Simonnet, A. Grandjean, Mixed ionic and electronic conductivity of RuO2-glass composites from molten state to glassy state, J. Non. Cryst. Solids. 351 (2005) 1611–1618. https://doi.org/10.1016/j.jnoncrysol.2005.04.049.

[102] R. Pflieger, L. Lefebvre, M. Malki, M. Allix, A. Grandjean, Behaviour of ruthenium dioxide particles in borosilicate glasses and melts, J. Nucl. Mater. 389 (2009) 450–457. https://doi.org/10.1016/j.jnucmat.2009.02.034.

[103] C. Allain, M. Cloitre, F. Parisse, Settling by cluster deposition in aggregating colloidal suspensions, J. Colloid Interface Sci. 178 (1996) 411–416. https://doi.org/10.1006/jcis.1996.0135.

[104] P. Snabre, P. Mills, Rheology of concentrated suspensions of viscoelastic particles, Colloids Surfaces A Physicochem. Eng. Asp. 152 (1999) 79–88. https://doi.org/10.1016/S0927-7757(98)00619-0.

[105] F. Babick, Suspensions of Colloidal Particles and Aggregates, Springer International Publishing, Dresden, Germany, 2016. https://doi.org/10.1007/978-3-319-30663-6.

[106] M. Tourbin, Caractérisation et comportement de suspensions concentrées de nanoparticules sous écoulement: Application aux processus d'agrégation et de rupture, (2006) 294. http://ethesis.inp-toulouse.fr/archive/00000505/.

[107] M. Tourbin, C. Frances, Monitoring of the aggregation process of dense colloidal silica suspensions in a stirred tank by acoustic spectroscopy, Powder Technol. 190 (2009) 25–30. https://doi.org/10.1016/j.powtec.2008.04.067.

[108] A.A. Potanin, On the mechanism of aggregation in the shear flow of suspensions, J. Colloid Interface Sci. 145 (1991) 140–157. https://doi.org/10.1016/0021-9797(91)90107-J.

[109] P.A. Arp, S.G. Mason, Orthokinetic collisions of hard spheres in simple shear flow, Can. J. Chem. 54 (1976) 3769–3774. https://doi.org/10.1139/v76-541.

[110] Q. Jiang, B.E. Logan, Fractal Dimensions of Aggregates Determined from Steady-State Size Distributions, Environ. Sci. Technol. 25 (1991) 2031–2038. https://doi.org/10.1021/es00024a007.

[111] L. Gmachowski, Calculation of the fractal dimension of aggregates, Colloids Surfaces A Physicochem. Eng. Asp. 211 (2002) 197–203. https://doi.org/10.1016/S0927-

7757(02)00278-9.

[112] F.L. Braga, O.A. Mattos, V.S. Amorin, A.B. Souza, Diffusion limited aggregation of particles with different sizes: Fractal dimension change by anisotropic growth, Phys. A Stat. Mech. Its Appl. 429 (2015) 28–34. https://doi.org/10.1016/j.physa.2015.02.050.

[113] C. Allain, M. Cloitre, The effects of gravity on the aggregation and the gelation of colloids, Adv. Colloid Interface Sci. 46 (1993) 129–138. https://doi.org/10.1016/0001-8686(93)80038-D.

[114] M. Lattuada, Journal of Colloid and Interface Science Retarded hydrodynamic properties of fractal clusters, J. Colloid Interface Sci. 429 (2014) 8–16. https://doi.org/10.1016/j.jcis.2014.05.003.

[115] M. Lattuada, H. Wu, M. Morbidelli, Hydrodynamic radius of fractal clusters, J. Colloid Interface Sci. 268 (2003) 96–105. https://doi.org/10.1016/j.jcis.2003.07.028.

[116] W.R. Richmond, R.L. Jones, P.D. Fawell, The relationship between particle aggregation and rheology in mixed silica-titania suspensions, Chem. Eng. J. 71 (1998) 67–75. https://doi.org/10.1016/S1385-8947(98)00105-3.

[117] V.A. Tolpekin, M.H.G. Duits, D. Van Den Ende, J. Mellema, Aggregation and breakup of colloidal particle aggregates in shear flow, studied with video microscopy, Langmuir. 20 (2004) 2614–2627. https://doi.org/10.1021/la035758l.

[118] P. Snabre, P. Mills, II. Rheology of Weakly Flocculated Suspensions of Viscoelastic Particles, J. Phys. III. 6 (1996) 1835–1855. https://doi.org/10.1051/jp3:1996216.

[119] W. T. Cobb and P. Hrma, Behavior of RuO2 in a glass melt, Ceram. Trans. 23 (1986) 233–237.

[120] K. Höfler, Simulation and modeling of mono- and bidisperse suspensions, Thesis. (2000). http://elib.uni-stuttgart.de/opus/volltexte/2000/663/.

[121] G.K. Batchelor, Sedimentation in a dilute dispersion of spheres, J. Fluid Mech. 52 (1972) 245–268. https://doi.org/10.1017/S0022112072001399.

[122] O.J.I. Kramer, P.J. de Moel, E.T. Baars, W.H. van Vugt, J.T. Padding, J.P. van der Hoek, Improvement of the Richardson-Zaki liquid-solid fluidisation model on the basis of hydraulics, Powder Technol. 343 (2019) 465–478.

https://doi.org/10.1016/j.powtec.2018.11.018.

[123] S. Daugan, L. Talini, B. Herzhaft, Y. Peysson, C. Allain, Sedimentation of suspensions in shear-thinning fluids, Oil Gas Sci. Technol. 59 (2004) 71–80. https://doi.org/10.2516/ogst:2004007.

[124] S. Daugan, L. Talini, B. Herzhaft, C. Allain, Aggregation of particles settling in shear-thinning fluids. Part 2 - Three-particle aggregation, Eur. Phys. J. E. 9 (2002) 55–62. https://doi.org/10.1140/epje/i2002-10054-8.

[125] D. Senis, L. Talini, C. Allain, Settling in Aggregating Colloidal Suspensions, Oil Gas Sci. Technol. 56 (2001) 153–159. https://doi.org/10.2516/ogst:2001016.

[126] C. Allain, M. Cloitre, M. Wafra, Aggregation and sedimentation in colloidal suspensions, Phys. Rev. Lett. 74 (1995) 1478–1481. https://doi.org/10.1103/PhysRevLett.74.1478.

[127] D.R. Rector, B.C. Bunker, Effect of Colloidal Aggregation on the Sedimentationand Rheological Properties of Tank Waste, Pacific Northwest Lab. (1995).

[128] D.P. Guillen, A.W. Abboud, K. Fox, Particle settling in a simulated melter discharge riser, Mater. Lett. 236 (2019) 38–41. https://doi.org/10.1016/j.matlet.2018.10.028.

Chapter II

Thixotropic behavior of a glass melt of nuclear interest containing Platinum Group Metal particles

This second chapter is dedicated to further investigate the thixotropic behavior of the melt containing PGM particles. Previous studies presented the Non-Newtonian behavior of the melt and indicated the impact of time on the rheological behavior. Nonetheless, for the first time a mathematical modeling of the thixotropic behavior of the glass melt containing 3 %wt of PGM particles was made. The goal was to investigate the impact of shear rate, temperature and time on the overall rheological behavior of the melt. In particular, the study shows that the modeling allows predicting the transient behavior of the samples without additional adjustable parameters than those determined in steady-state regime.

Norma Maria Pereira Machado; Muriel Neyret; Cécile Lemaître; Philippe Marchal.

Submitted to Rheologica Acta

Abstract

Platinum Group Metals particles (PGM) are generally found in nuclear borosilicate glasses resulting from the melting, at 1200°C, of a glass precursor and fission products issued from spent fuel reprocessing. Contrary to some other elements such as Iron, Nickel and Chromium, these particles are not incorporated chemically in molten glasses. During the melting step, the presence of these metals as suspended particles of a few microns has an impact on the rheological properties of the material, leading to a Non-Newtonian behavior. Their impact on the process is the object of characterization and modeling of many studies that have established that the melt presents a shear-thinning and thixotropic behavior. In this work, a deeper analysis of the thixotropic behavior of a simulated nuclear glass melt containing 3.0 wt% (1.02 vol%) of PGM particles is presented. Steady and transient state rheological measurements were performed over a wide shear rate range using a stress-imposed rheometer at temperatures ranging from 1100 to 1250 °C. A mathematical modeling of the thixotropic behavior of the glass is presented for the first time, for a glass melt suspension, using a thixotropic model akin to that proposed by Houska. This model is found to explain and predict successfully the rheological behavior of the material. In particular, it allows predicting the transient behavior of the samples from steady-state experiments, without additional adjustable parameters. The present study thus provides an important input for the modeling of the vitrification process.

Keywords: Melt, Platinum Group Metals (PGM), Thixotropy, Houska.

1. Introduction

In France, pressurized water reactors are in majority operating with Uranium Oxide fuel (UOX). At the end of its cycle in the nuclear reactor, the spent fuel still contains recoverable material, such as uranium (94 to 95%) and plutonium (1%), as well as high-level radioactive non-recyclable waste (4%). After the extraction of uranium and plutonium, the vitrification of the high-level radioactive waste is the standard immobilization treatment [1]. The vitrification consists in melting the nitrates salts of the waste (mostly converted to oxides in the calcination furnace heated at 400°C) and the glass frit in a melter, leading to the production of a complex amorphous material, which contains around 40 different elements [2], [3]. Currently, the material is confined in a sodium alumino-borosilicate glass, called R7T7. The vitrification technology is based on the use of induction, in the crucible (hot crucible melter) or directly in the glass (cold crucible melter) [1]. The nuclear glass is then poured into metal containers and then stored in wells before their future storage in deep geological formations [4].

During the elaboration at high temperature, most species to be confined react chemically with the vitrification additives to form a homogeneous liquid. Some elements, such as the Platinum Group Metals (PGM: RuO_2, Pd, Rh) and their oxides, do not chemically incorporate into the nuclear glass melt and in the cast glass [5]. They can be found in the form of spherical alloys of palladium and rhodium with tellurium (1 to 5 µm) and ruthenium oxide in a needle-like form (length ~10 µm). Even in small amounts (3 %wt), the PGM particles lead to significant modifications of the physical properties of the material, such as its viscosity and electrical conductivity [6]. Previous work has shown that they tend to aggregate and settle down, creating layers at the bottom of the crucible that can interfere with the process [7]–[9].

In view of the impact of the PGM particles on the physical properties of the nuclear glass melt, a deeper understanding of these modifications is needed. In particular, the rheological behavior of a fluid can be strongly affected by the particles aggregation kinetics as well as the flow. Nonetheless, studies on the impact of PGM particles on the rheological behavior of a glass melt are limited due to experimental difficulties linked to the very high temperature required to perform rheological measurements. Despite existing devices designed to operate accurately from room temperature up to a few hundred degrees, few apparatus exist that can reach the temperatures needed to study molten glass [10]. Nevertheless, some studies have already shown that the glass melt viscosity is increased by the presence of PGM particles leading to a non-Newtonian behavior [6], [7], [9], [11].

In this context, Puig *et al*. designed an innovative device that combines a rheometer with an oven allowing rheological characterization of molten glass containing PGM particles over a broader shear stress and rate range, exploring the system with different platinum contents and at different temperatures up to 1300 °C. It enabled the development of a new phenomenological model describing the rheological behavior of these materials [9], [12], [13]. The model was conceived from rheological measurements of simulated nuclear glass melts containing PGM particles, both in steady-state and transient regime. Figure II-1 shows the rheograms from the work of Hanotin *et al*. for a simulated nuclear glass containing 4.2 wt% of PGM particles at different temperatures. They exhibit a shear-thinning behavior and two Newtonian plateaus at low and high shear rates, well described by a Cross model:

$$\eta = \eta_\infty + \frac{\eta_0 - \eta_\infty}{1 + \left(\dot{\gamma}/\dot{\gamma}_c\right)^m} \quad (1)$$

with $m = 1$ where η_∞ and η_0 are the viscosity at the high and low shear plateaus respectively, $\dot{\gamma}_c$ is the critical shear rate [9]. At low shear rates and above a certain content of PGM particles, macroscopic aggregates appear. They are made of RuO_2 and Pd-Te chains, separated by thin layers of liquid and they strongly increase the viscosity of the systems. In this first case, an increase in temperature lowers the viscosity of the matrix and favors aggregation through Brownian motion leading to an overall increase of the viscosity of the whole system. In contrast, at high shear rates, the system behaves as a suspension of small clusters and individual particles and its viscosity decreases classically by increasing temperature since it is then mainly controlled by the viscosity of the matrix [9].

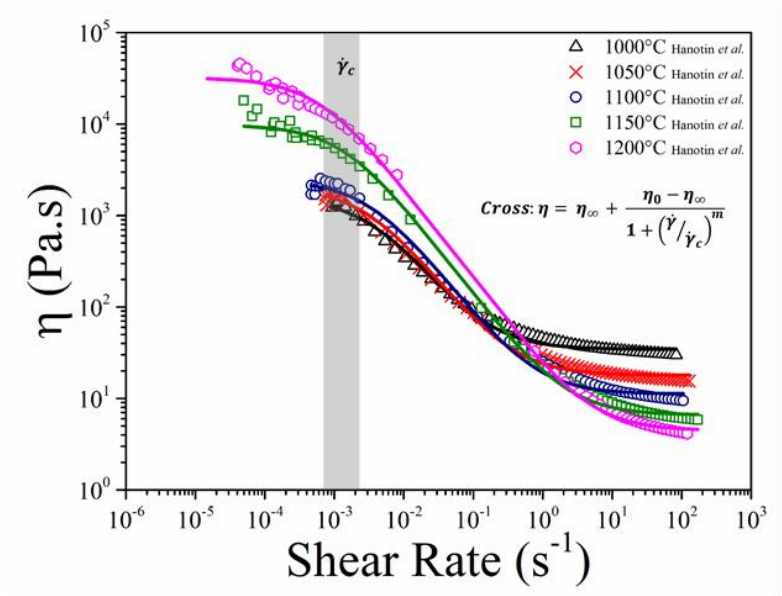

Figure II-1 - Steady-state viscosity (η) of a simulated nuclear glass containing 4.2 %wt PGM particles as a function of the shear rate for different temperatures, extracted from Hanotin *et al.* [9]. The data were fitted with a simplified Cross model (Eq. (1)) (continuous lines).

The study also showed a thixotropic behavior of the glass melt that increased with the PGM content, associated to the non-instantaneous breakage of the aggregates under shear [13]. Differently from the shear thinning behavior, thixotropy is a time-related phenomenon associated with progressive modifications of the internal structure of the material and is commonly observed for many substances such as concentrated suspensions, polymer gels, foams. These modifications are generated by the competition of shear-induced destructuration and restructuring processes induced by flow and Brownian motion [14], [15]. Thus, experimental difficulties are encountered during the study of such systems is due to their physicochemical complexity coupled with the mechanical inertia of the available apparatus which makes it difficult to find reliable experimental data on the matter [16]. However, many studies addressed the mathematical modeling of the thixotropic behavior and may be classified, according to Mujumdar *et al.*, under three different approaches: the phenomenological approach, the direct microstructure approach and the indirect microstructure approach [17].

In this work, a deep analysis of the thixotropic behavior of a simulated glass melt containing PGM particles is presented. Techniques adapted to high temperatures are employed in order to characterize the impact of the shear rate, time and temperature on the rheological behavior of the melt. A mathematical modeling of the thixotropic behavior of glass melts containing PGM particles is presented for the first time using a similar approach of that proposed by

Houska [18]. It can be viewed as a mesoscopic structural model and it follows an indirect microstructure approach, well suited for the study of thixotropic materials. This new thixotropic model is found to explain and predict successfully the rheological behavior of the material. In particular, it will be shown that the model is able to predict the transient behavior of the samples without additional adjustable parameters than those determined in steady-state regime. The present study thus provides a significant improvement of the modeling of the rheological behavior of nuclear glass melts.

2. Materials and Methods

2.1 Materials

The borosilicate glass containing PGM particles used in this work was elaborated on a full-scale pilot unit installed at CEA Marcoule [4]. The unit follows the two-step calcination-vitrification protocol and was equipped with a cold-crucible melter working at 1200°C. The chemical composition of this simulated nuclear glass containing 3 wt% PGM particles is pointed in Table II-1. The glass was cooled at room temperature and the studied material was extracted from the middle of the canisters. The PGM particles appear under the form of needle-like RuO_2 ranging from 10 to 50µm while the Pd-Te alloys particles exhibited spherical shapes with diameter ranging from 1 to 10µm.

Table II-1 - Chemical composition of the simulated nuclear glass samples containing 3 wt% of PGM particles.

Glass 3 wt% PGM									
SiO_2 (wt%)	B_2O_3 (wt%)	Na_2O (wt%)	Al_2O_3 (wt%)	Alkali metal oxides (wt%)	Alkaline earth metal oxides (wt%)	Rare earth oxides (wt%)	RuO_2 (wt%)	Pd (wt%)	Others (wt%)
43.7	13.2	9.2	4.2	3.3	5.0	7.0	1.8	1.2	11.4

2.2 Rheological measurement at high temperatures

Due to the high temperatures needed for the characterization of a glass melt, an innovative device conceived in the laboratory [13] was used for all the rheological characterization presented in this work. The equipment, illustrated in Figure II-2 [9], consists of a stress-imposed rheometer (Rheometrics Scientific SR5000) above a tubular furnace that can be heated up to 1500°C. A specific tool designed for this purpose, showed in Figure II-2a, ensures the transmission of the torque from the rheometer to the crucible without disturbances. The characterization cell consists of a platinum-rhodium crucible (27 mm

diameter; 40 mm height) located in the center of the furnace. The rotor is composed of a 30 cm long rod with the measurement geometry on the edge. The multiblade geometry chosen for this work allows a uniform distribution of the particles in the glass and prevents their sedimentation [13]. The crucible is filled with the shattered glass and heated to 1200 °C previously to the measurement. From the top to the bottom of the crucible, the temperature gradient is lower than 2 °C.

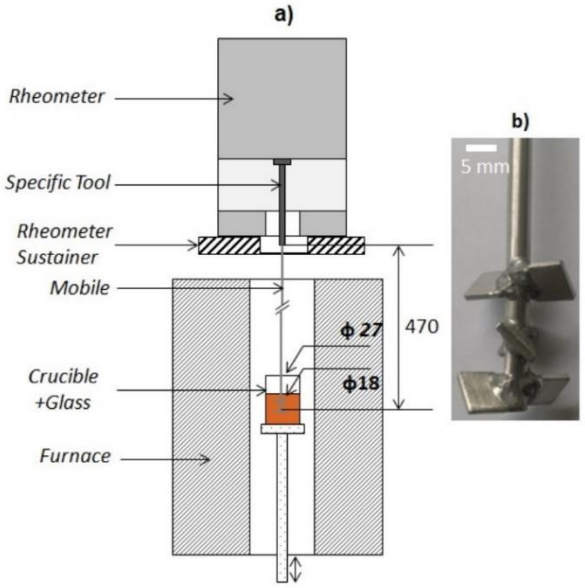

Figure II-2 - a) High temperature measurement equipment (dimensions in mm), b) Mobile with a multiblade geometry.

The measured parameters such as torque (C) and angular velocity (Ω) are linked to the shear stress (σ), shear rate ($\dot{\gamma}$), through geometrical factors K_σ and $K_{\dot{\gamma}}$ such as $\sigma = K_\sigma\, C$ and $\dot{\gamma} = K_{\dot{\gamma}}\, \Omega$. To determine K_σ and $K_{\dot{\gamma}}$ the mixing device (multiblade + crucible) has been calibrated via a Couette analogy leading to K_σ = 8.79 10^4 ± 4.10^2 Pa N^{-1} m^{-1} and $K_{\dot{\gamma}}$ = 2.1 ± 0.01 rad^{-1} with an equivalent annular gap of 4.5 mm [19], [20]. The use of this analogy has shown efficiency in translating the experimental data into the rheological behavior of the materials [21]–[24]. Puig *et al* [13] provided a complete description of the equipment and calibration procedure. The rheological measurements were carried out in steady-state and transient regime to further investigate the thixotropic behavior occurring in nuclear glass melts.

The steady-state measurements were conducted by imposing successive stresses values from 0.5 to 500 Pa during 600 s. Transient step rate measurements were performed on the melt, varying the shear rate from 0.15 to 100 s^{-1}. Transient tests were performed by imposing

constant shear rates, in order to fix the characteristic shear time $1/\dot{\gamma}$. In that way, it is only necessary to take into account the evolution time of the sample structure under constant shear rate which allows to simplify the modeling. The duration of the experiments were chosen accordingly to the time necessary for the stabilization of the melt viscosity. All tests above were conducted at four different temperatures: 1100, 1150, 1200 and 1250 °C. A pre-shear of 40 s^{-1} during 60 s was applied at the beginning, and between every imposed shear rates, in order to disperse completely the PGM particles in the glass, removing memory effects from previous tests. In shear-rate experiments, because of the length of the cane that support the geometry precession phenomena can appear, leading to small oscillations of the measurements around a well-defined average.

3. Structural Modelling

Houska *et al.* established a model to describe the rheological behavior of thixotropic fluids with a yield stress, via a scalar parameter λ which allows to capture the structural evolution of the samples through a kinetic equation coupled to a rheological law [18]. The value of this parameter varies between 0 and 1 depending on whether the material is respectively in its most destructured or structured state, depending on the experimental conditions. The glass containing PGM particles is a complex system which undergoes different physicochemical transformations with temperature such as volatilization and electrical conductivity variations [25]–[28]. Therefore the structure parameter takes globally those changes into account since it can affect directly the structured/destructured state of the system. This model is known for its effectiveness in describing the behavior of different fluids and is also used in fluid mechanics simulation codes [29].

Glass containing PGM particles do not exhibit a yield stress and the rheological equation that best described the steady-state flow behavior of the material is the Cross model. This equation accounts for the existence of two Newtonian plateaus: one at low and another at high shear rate. The first Newtonian plateau is reached under very low shear rates, which are difficult to achieve when the measurements are performed in a shear-imposed mode. Hence, for studies carried in a shear rate range higher than the critical shear rate $\dot{\gamma}_c$ corresponding to the limit of the first plateau, Cross model reduces to Sisko model which is a simplified version of Cross one, including only the shear-thinning zone and the high shear Newtonian plateau [30] in such way that

$$\eta = \eta_\infty + k\dot{\gamma}^{n-1} \tag{2}$$

where $k = \eta_o \dot{\gamma}_c^{1-n}$, with *n* as the flow index (*n* = 1 – *m)*. Moreover, the Sisko model must be adapted to take into account the time dependency of the material rheological behavior, due to its thixotropy. Sisko equation is thus modified to include a shear-dependent structure parameter (λ):

$$\eta = \eta_\infty + \lambda K_0 \dot{\gamma}^{\alpha-1} \tag{3}$$

where η_∞ is the plateau viscosity at the high shear rate, *i.e.* the viscosity in a highly dispersed state. Coefficients η_∞, K_0 and α are obtained from viscosity measurements. In Eq. (3), λ depends on $\dot{\gamma}$, contrary to k in Eq. (2), hence α is different from n. The rheological equation (2)(3) is coupled to a kinetic equation governing the time evolution of the structure parameter λ, for a constant temperature:

$$\frac{d\lambda}{dt} = -k_1 \dot{\gamma} \lambda + k_2 (1 - \lambda) \tag{4}$$

Parameters k_1 and k_2 respectively quantify the destructuration and structuration of the system. When t < 0, the imposed shear rate is $\dot{\gamma}_0$ (the pre-shear imposed to the system) and when t > 0, the shear is fixed at $\dot{\gamma}$. Based on this, the structure parameter can be calculated as a function of time (the details of the calculus are presented in the appendix)

$$\lambda(t) = \left\{\lambda_0 - \frac{k_2}{\dot{\gamma} k_1 + k_2}\right\} \exp[-(\dot{\gamma} k_1 + k_2)t] + \frac{k_2}{\dot{\gamma} k_1 + k_2} \tag{5}$$

where λ_0 is the structure parameter when t = 0. At long times λ reaches an equilibrium value

$$\lim_{t \to +\infty} \lambda = \frac{k_2}{\dot{\gamma} k_1 + k_2} \tag{6}$$

which depends on the applied shear rate. If we assume that $\dot{\gamma}_0$ has been applied long enough at negative times, λ would then have reached its equilibrium value at this shear rate corresponding to:

$$\lambda_0 = \frac{k_2}{\dot{\gamma}_0 k_1 + k_2} \tag{7}$$

Therefore, by replacing λ_0 in Eq. (5), the equation for the structure parameter at t > 0 reads

$$\lambda(t) = \left\{\frac{k_2}{\dot{\gamma}_0 k_1 + k_2} - \frac{k_2}{\dot{\gamma} k_1 + k_2}\right\} \exp[-(\dot{\gamma} k_1 + k_2)t] + \frac{k_2}{\dot{\gamma} k_1 + k_2} \quad (8)$$

Considering the modified Sisko equation (3) presented earlier and $K = k_1/k_2$, the apparent viscosity of the system may be written as follows

$$\eta(t) = \eta_\infty + \left(\left\{\frac{1}{\dot{\gamma}_0 K + 1} - \frac{1}{\dot{\gamma} K + 1}\right\} \exp[-k_2(\dot{\gamma} K + 1)t] + \frac{1}{\dot{\gamma} K + 1}\right) K_0 \dot{\gamma}^{\alpha - 1} \quad (9)$$

The model parameters will be then obtained for each temperature from steady-state measurements on glass melt samples.

4. Results and Discussion

4.1 Fitting model parameters in steady-state regime

Steady-state rheological measurements were made to observe the dependency of the viscosity with the shear rate of a technological glass containing 3.0 wt% PGM particles at different temperatures (Figure II-3). The melt showed a shear thinning behavior, with an abrupt decrease of the viscosity. The increase of the temperature led to a decrease of the viscosity, on the studied shear rate range. In the high shear flow regime the PGM aggregates are destructed leading to a rupture of the tridimensional network of PGM aggregates observed at very low shear rates. As a consequence, at medium and high shear rates, the viscosity of the sample is mainly controlled by the viscosity of the matrix and decreases when increasing the temperature, contrary to what happens at low shear rate [9]. Previous work with the glass containing PGM particles demonstrated that the rheological behavior could be described by simplified Cross model, represented also by a shear thinning behavior and two Newtonian plateaus (at low and high shear rates) [9], [13].

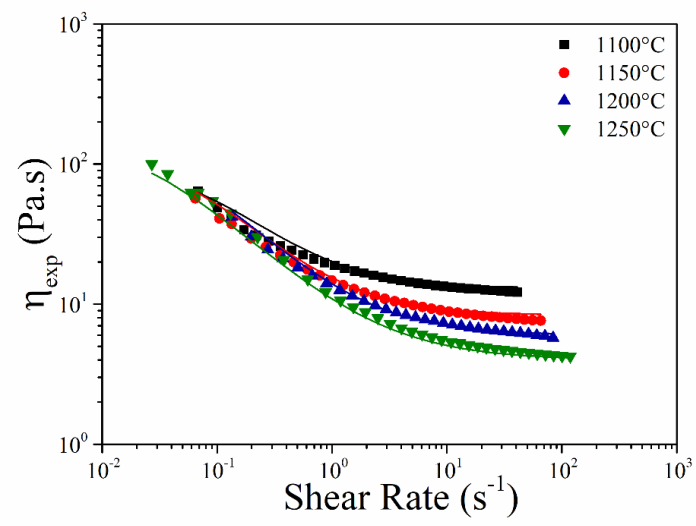

Figure II-3 – Evolution of the glass melt containing 3 wt% of PGM particles steady-state viscosity as a function of the shear rate at 1100, 1150, 1200 and 1250 °C. The experimental data was fitted with the modified Sisko model shown in Eq.(10).

As mentioned in § 2.2, in the current study, the experiments were conducted in a shear-imposed mode, making it difficult to reach very low shear rates. As a consequence, it was not possible to observe the low shear Newtonian plateau, contrary to the high shear plateau that was present for all studied temperatures. The absence of the first Newtonian plateau leads to the use of a modified Sisko model (3) to fit the experimental data. Since the measurements were made in steady-state regime, the viscosity is given by Eq. (10) obtained from equation (9) evaluated at long times ($t \to +\infty$):

$$\eta = \eta_\infty + \left(\frac{1}{\dot{\gamma}K + 1}\right) K_0 \dot{\gamma}^{\alpha - 1} \tag{10}$$

Figure II-3 shows that the Sisko modified equation fitted thanks to an ordinary least square method can describe properly the melt behavior at all studied temperatures. Table II-2 shows the parameter values obtained for all studied temperatures. Although the four parameters (η_∞, K, K_0 and α) for each temperature were obtained in the steady-state regime, they can be used in the thixotropic model (3 - 4), to describe the transient regime of the samples.

Table II-2 – Parameters of thixotropic model (3 - 4).

Parameters	**1100 °C**	**1150 °C**	**1200 °C**	**1250 °C**
$\boldsymbol{\eta_\infty}$	13	8.0	6.0	4.0
$\boldsymbol{K}$	15	24	35	57
$\boldsymbol{K_0}$	115	177	285	400
$\boldsymbol{\alpha}$	1.05	1.08	1.11	1.18

4.2 Analysis of the model parameters

The temperature has a great impact on the viscosity of the melt containing PGM particles. Depending on the applied shear rate range, it can either favor the particles aggregation or their dispersion. At low shear rate and high temperature, hydrodynamic forces are low and do not prevent particle aggregation. This tends to increase the viscosity of the suspension even if an increase of temperature tends to decrease the viscosity of the matrix. In the other hand, at high shear rates, the particles are dispersed due to the hydrodynamic forces leading to a breaking of the tridimensional network of PGM particles so that the viscosity of the suspension evolves similarly to that of the matrix with temperature. Hence the understanding of the model parameters dependency with the temperature is essential for the study of the thixotropic behavior of the glass melt. Figure II-4 shows that all parameters evolve monotonically with the temperature. The dotted lines are drawn to provide a visual aid.

In Figure II-4a, the fitting parameter η_∞ corresponding to the viscosity on the high shear plateau (η_∞) for all studied temperatures is observed to decrease gradually with the temperature, agreeing with the experimental data shown in Figure II-3. As mentioned before, at high shear rate the hydrodynamic forces contribute to the dispersion of the aggregates formed in the glass melt and consequently to a decrease of the viscosity with the temperature. Hanotin *et al*. derived an equation that describes the evolution of η_∞ as a function of temperature for PGM glass melts [9]. Even if the PGM aggregates are destroyed, the non sphericity of PGM particles implies that the rotation of the particles leads to a trapping of the suspending fluid around them. So this feature has to be taken into account through an effective hydrodynamic volume fraction $\varphi_{eff} = \beta\varphi_0$ of the particles larger than the real volume fraction φ_0 (β >1). Hence, Quemadas's model was used to describe the viscosity in high shear flow coupled with the Vogel-Fulcher-Tamann's (VFT) law that represents the behavior of the continuous phase:

$$\eta_\infty = A\left(1 - \frac{\varphi_{eff}}{\varphi_m}\right)^{-2} exp\left(\frac{B}{T - T_0}\right) = A\left(1 - \frac{\varphi_0}{\varphi_{meff}}\right)^{-2} exp\left(\frac{B}{T - T_0}\right) \quad (11)$$

where A, B and T_0 are dimensional constants, φ_0 is the initial solid volume fraction (in this case φ_0= 1.02 %) and $\varphi_{meff} = \varphi_m/\beta$ the effective maximum packing fraction. In Figure II-4a the experimental data are well fitted by Eq. (11) with φ_{meff} = 10.2 %, A=0.008 Pa.s, B = 4977 °C and T_0= 402 °C. The values obtained may vary slightly from those obtained by Hanotin *et al.* due to the differences from a glass batch to another. Figure II-4b and c show the

increase of K_0 and α with the temperature, indicating a strong dependency of both parameters with temperature.

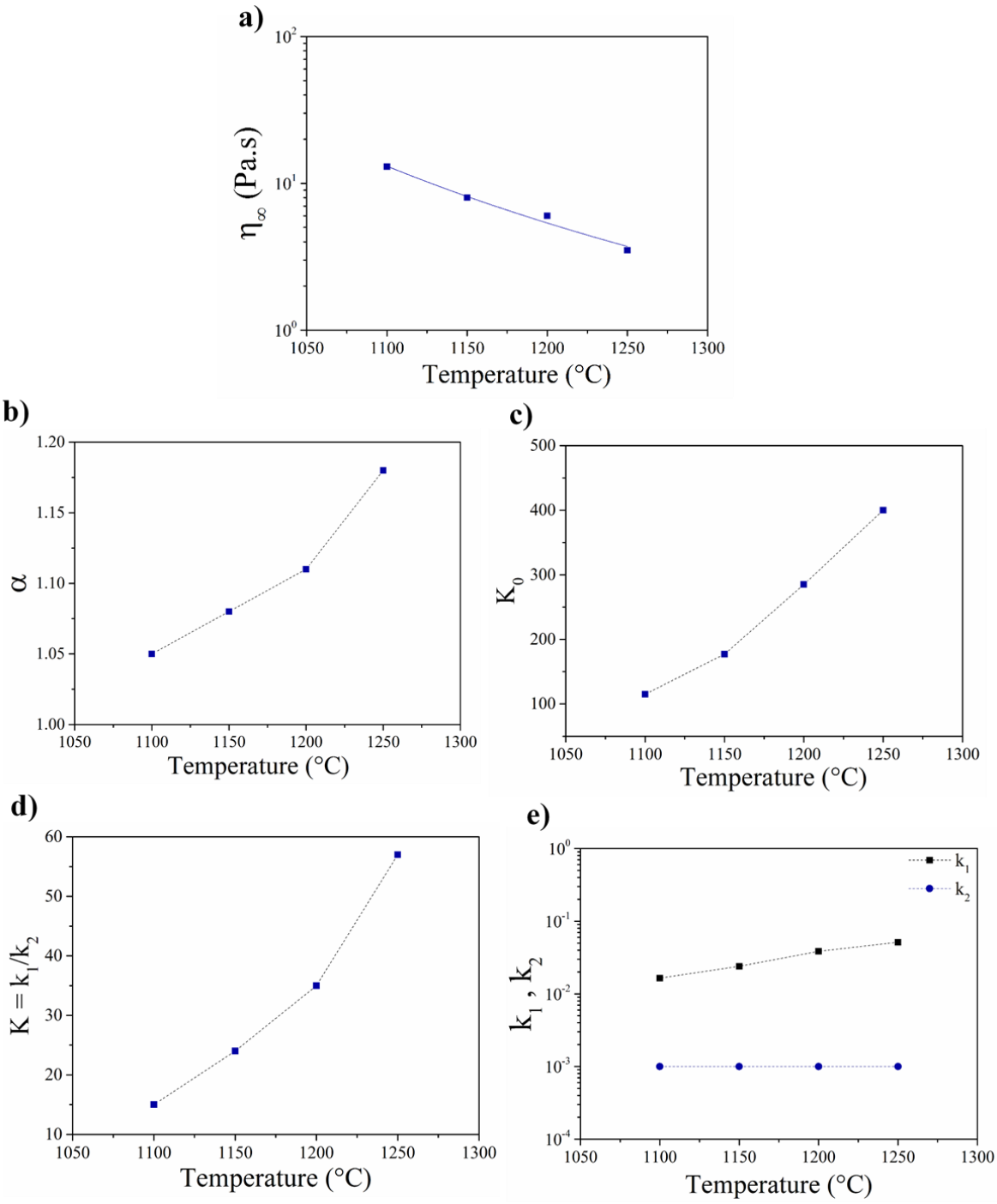

Figure II-4 - Parameters of model (3-4) as a function of the temperature: a) Viscosity on the high shear rate plateau η_∞ fitted with Eq. (11), b) K_0, c) α, d) Ratio between k_1 and k_2 (K) and e) evolution of k_1 and k_2. The dotted lines are drawn for visual aid.

As shown in Figure II-4d, the ratio between k_1 and k_2 (K) is also observed to depend strongly on the temperature. Although the steady-state measurements allow to determine K, in order to

predict the material transient state behavior, it is essential to know k_1 and k_2 separately since both are connected to the system structure evolution. The reorganization of the system structure is the result of a balance between the forces acting on the PGM particles and the impact of the matrix fluidity. Thus, these changes are intrinsically related to the variation of the rheological behavior of the melt. The critical turning point where the material changes from linear to non-linear behavior is characterized by the critical shear rate ($\dot{\gamma}_c$) at which the viscosity begin to decrease. At this point, the Péclet number is close to unity which corresponds to a balance between thermal and hydrodynamic forces. This allows to estimate a critical time t_c, characteristic of the reorganization of the structure, considering $Pe = t_c\dot{\gamma}_c = 1$ which leads to $t_c = 1/\dot{\gamma}_c$.

Figure II-4displays in grey the critical shear rate range at which the viscosity of the melt begins to decrease, changing its behavior from Newtonian to shear thinning, for the simulated glass containing 4.2 wt% PGM particles at five different temperatures [9]. The graph shows that the temperature does not impact significantly $\dot{\gamma}_c$, which varies little in the studied temperature range. It means that the range of particle-particle interactions do not depend significantly on the temperature. The change on the rheological behavior of the melt related to the reorganization of the structure is more impacted by the volume fraction, as investigated in the study of Puig *et al.* [13]. The study explored the variation of the critical shear rate $\dot{\gamma}_c$ for several compositions at 1200 °C, obtained via the simplified Cross model. Based on both studies [9] and [13], a typical value of 10^{-3} s^{-1} was adopted for $\dot{\gamma}_c$, for the present glass containing 3 wt% PGM particles, for all temperatures. As mentioned earlier, it is linked to the structuration of the system and is not influenced by the shear rate as exhibited in Eq.(4). Furthermore, it has the dimension of inverse time. Hence, k_2 may be related to t_c. Therefore, k_2 was considered a constant for all temperatures and equal to the critical shear rate, since $k_2 = 1/t_c = \dot{\gamma}_c = 10^{-3}$ s^{-1}, as displayed in Figure II-4e.

Nonetheless, the five parameters ($\eta_\infty, K_0, \alpha, k_1, k_2$) alone are not enough to elucidate the evolution of the particles rearrangement. Hence, the calculation of lambda is essential to have an overall perspective of the structure over time and to correlate the dependency of the rheological parameters with the temperature. Figure II-5 shows the evolution of the structure parameter over time on a wide shear rate range for all studied temperatures. As mentioned earlier, when λ tends to zero, the material is in its most unstructured state and in its most structured state when it tends to one. For all temperatures, λ grows in time until it reaches a constant value. This behavior characterizes the build-up phenomena common to thixotropic

fluids after a period of high shear rate [15]. The PGM particles have the tendency of aggregating at low shear rates due to the weakness of hydrodynamic forces compared to the effects of Brownian motion and attractive van der Waals forces [9]. Hence, the pre shear at a higher shear rate disperses the particles in the melt. On the contrary, low shear allows the formation of aggregates leading to an increase of the viscosity associated to the structuration of the system, followed by its stability when it reaches a maximal structuration given the applied conditions. Figure II-5 also shows consistently that λ decreases with the shear rate.

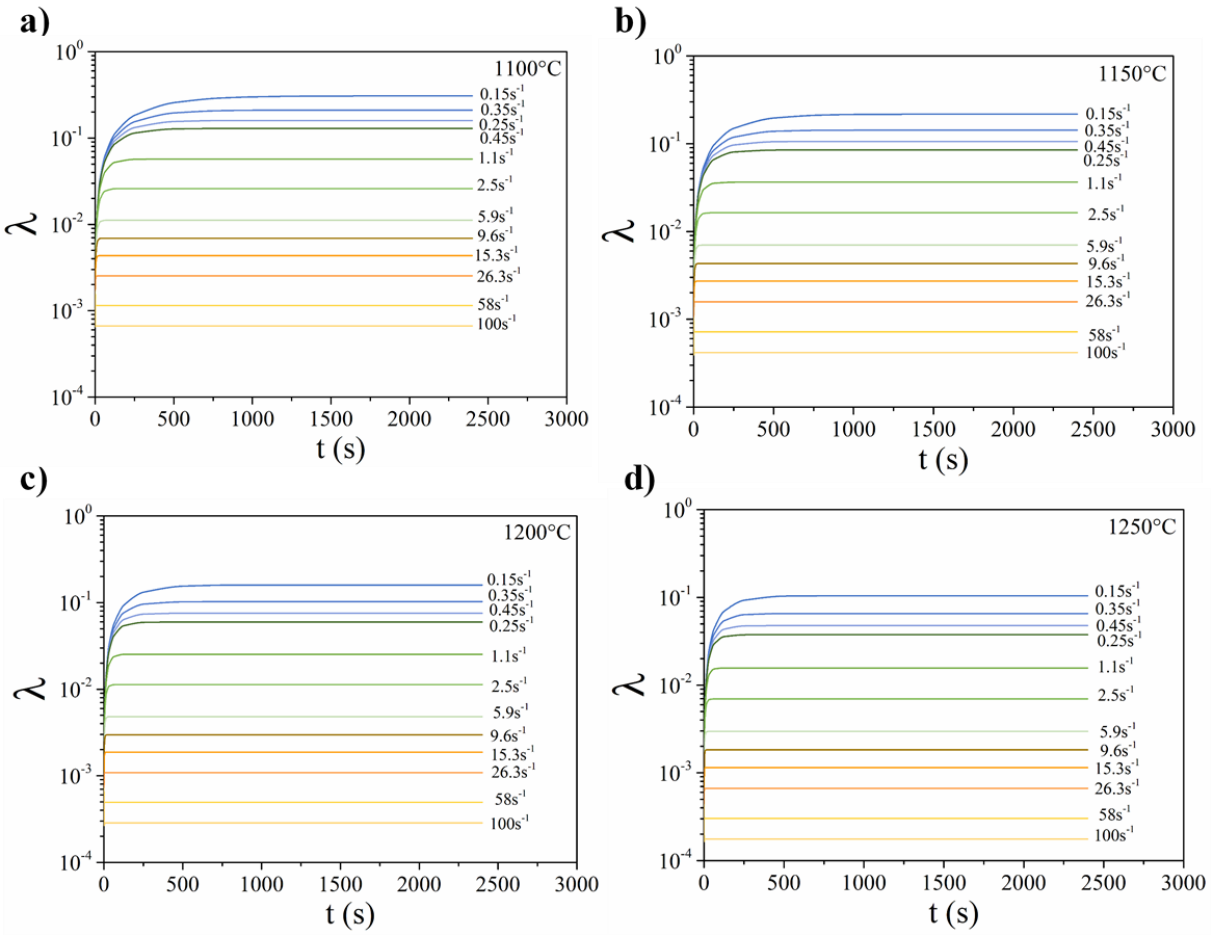

Figure II-5 –Calculated λ as a function of time for all studied shear rates at a) 1100 °C, b) 1150 °C, c) 1200 °C and d) 1250 °C.

The value of λ at an arbitrary long time (t = 2500 s) was calculated as a function of the shear rate for all temperatures using Eq. (5) and was plotted in Figure II-6. As the shear rate tends to zero, the λ curves reaches a plateau of height 1. At low shear rate, the formation of clusters is intensified. Indeed, particle-particle interactions leading to PGM aggregation are enhanced at low shear rate [31], helping cluster formation, which causes an increase of the structuration of the system, leading to an increase of viscosity for all temperatures. As a consequence, at low

shear rate the rheological behavior of the system is controlled by the cluster network and it demonstrates to be insensitive to the temperature. This is why λ tends to one for all studied temperatures. In contrast, at high shear rates, the system behaves as a suspension of small clusters and individual particles and its viscosity decreases by increasing temperature since it is then entirely controlled by the viscosity of the matrix. Figure II-6 indicates that a less structured system (λ tends to 0) is formed with higher temperatures.

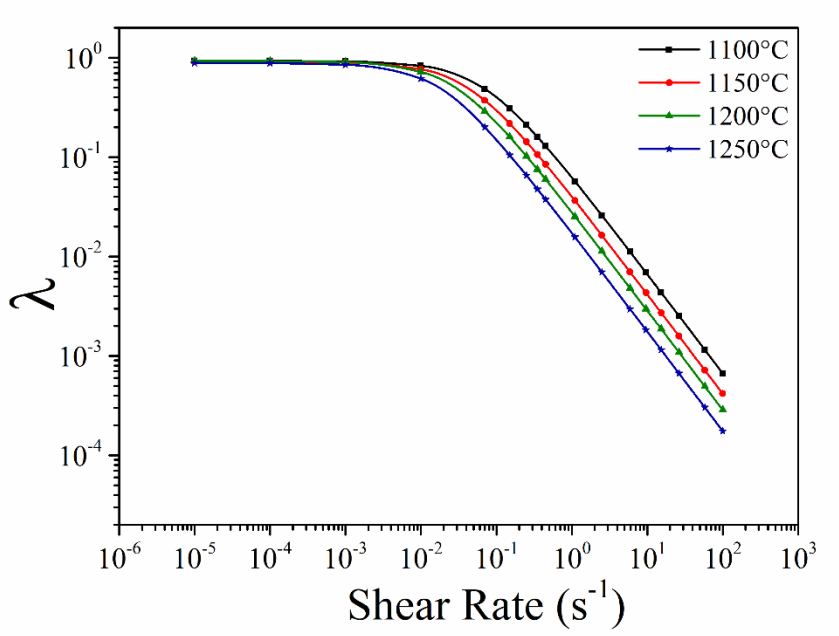

Figure II-6 – Evolution of calculated λ with the shear rate at an arbitrary long time (t = 2500 s) for all studied temperatures.

4.3 Prediction of the transient regime – Comparison with experimental results

One of the main difficulties to characterize the thixotropic behavior of a system lies in the experimental difficulties due to the complexity of the phenomena encountered [14], [15]. However, transient step rate experiments offer an interesting approach to investigate this behavior since they allow a temporal analysis of the viscosity evolution at constant shear rate. Therefore, experimental data in transient regime were also performed for the PGM glass melt for comparison with model (3-4). Figure II-7 shows the experimental evolution of viscosity over time (symbols) for all four studied temperatures at different shear rates. As mentioned earlier, rheological experiments may exhibit artifacts, especially under extreme conditions. The graphs of Figure II-7 illustrate these artifacts as oscillations for low shear rate results (under 0.35 s^{-1} for example) at all temperatures. They are due to the precession of the rheometer axis resulting from its long length inside the oven (Figure II-2). For all experiments, the melt viscosity increases over time until it reaches a stable value, just as λ

was found to increase over time as shown in Figure II-5. The growth of both parameters (η and λ) is indicative of the build-up of the suspension. For the experiments where the initial shear rate is smaller than the applied shear rate, the phenomenon is the opposite: the viscosity decreases until it reaches a stable value, corresponding to the breakdown of the structure.

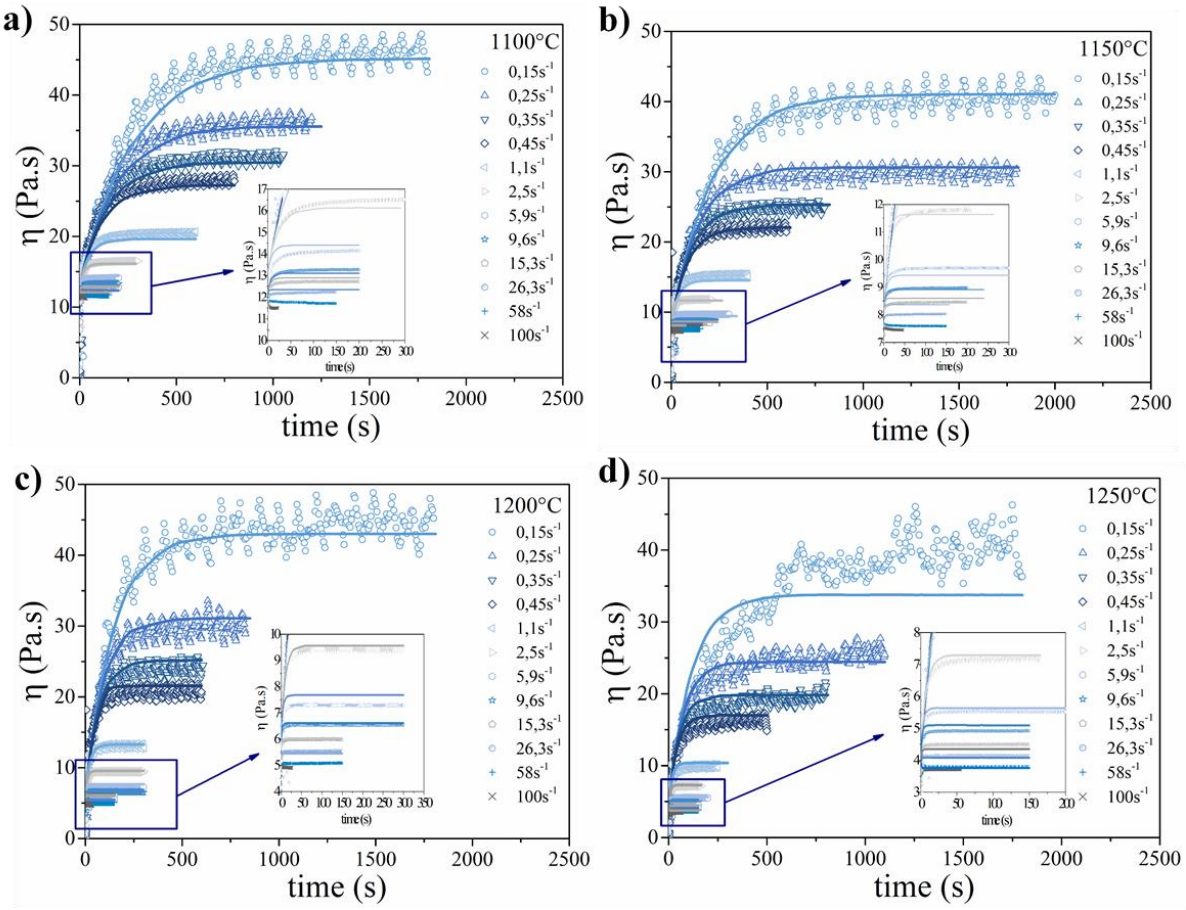

Figure II-7 – Evolution of viscosity over time for different values of shear rate, varying from 0.07 s^{-1} to 100 s^{-1} at all studied temperatures. The lines correspond to the calculated apparent viscosity using Eq. (9) and the symbols correspond to the experimental data: a) 1100 °C, b) 1150 °C, c) 1200 °C and d) 1250 °C.

The parameters of thixotropic model (3-4) were all obtained from steady-state measurements. With these parameters, it was possible to predict the temporal evolution of the sample viscosity in transient regime by applying Eq. (9) without any additional fitting parameter. The continuous lines in Figure II-7 represent the calculated viscosity of the melt for the four studied temperatures. It is worth noting the very close agreement between the prediction of the model and the experimental results in transient regime over a very wide range of shear rates (0.15 to 100 s^{-1}). The calculated viscosity follows the same behavior observed for the experimental data, increasing over time until it reaches an equilibrium plateau. Houska-like model (3- 4) thus proves its efficiency not only in describing the steady-state rheological

behavior of the glass melt, but also in predicting the thixotropic behavior of the PGM glass in transient regime. Therefore, the proposed model and the associated characteristic parameters allow to describe and quantify with accuracy the thixotropic behavior of the glass melt.

5. Conclusions

The thixotropic behavior of a simulated nuclear glass melt containing 3 wt% PGM particles was studied in this paper. Steady-state and transient measurements were conducted to disclose the rheological profile of the material. The impact of shear rate, time and temperature on the melt viscosity was evaluated using a stress-imposed rheometer, working at high temperatures ranging from 1100 °C to 1250 °C. The initial analysis in the steady-state regime showed a shear thinning behavior of the melt, associated to a decrease of the viscosity with an increase of the temperature. Given the range of shear rate covered in this study, a modified version of the Sisko model proved to be adequate to describe the rheological behavior of the glass melt in the experimental conditions.

A mathematical modeling of the thixotropic behavior of the system was derived for the first time to describe the rheological behavior of a suspension in a glass melt. The thixotropic model, similar to that of Houska, combines a modified Sisko model involving a parameter λ describing the structure of the material, coupled with a kinetic equation governing the temporal evolution of λ. The model coefficients were optimized to fit at the best the experimental data. The structure parameter λ calculated with the thixotropic model allows to quantify at a mesoscopic scale the thixotropic behavior of the samples by numerically describing the structural state of the material. The evolution of λ over time evidenced a build-up phenomenon in the melt where PGM particles aggregates are formed over time due to Brownian motion associated to attractive forces, leading to an increase of the viscosity of the melt, until the material structure reaches a dynamic equilibrium. This is particularly evident at low shear rates where the weakness of hydrodynamic forces favors particles aggregation.

The value of the structural parameter was extrapolated at lower shear rates at an equilibrium time (t = 2500 s) for all temperatures. Regardless of the temperature, λ exhibits a plateau close to one corresponding to a fully structured sample. This is consistent with the fact that, at low shear rate, the material is more structured than at high shear rate. The parameters of the thixotropic model were all calculated from steady-state measurements. The resulting model was then compared with experimental data obtained in transient regime for all studied temperatures. The model showed to predict extremely well, both qualitatively and

quantitatively, the thixotropic behavior of the PGM glass in the transient regime. It is so, not only descriptive but also explicative and predictive of the rheological behavior of the simulated nuclear glass containing PGM particles. These observations are crucial for the rheological study of the glass melt not only because they are limited in the literature due to the extreme experimental conditions, but also on account of their strong impact on the vitrification process itself and its modeling.

6. Appendix

*Calculation of the structure parameter (λ) from the Houska-like model for thixotropic fluids***:**

At t < 0, the fluid is subjected to a constant shear rate $\dot{\gamma}_0$. At t = 0, the shear is abruptly increased to a new constant value $\dot{\gamma}$. Equation (4) may then be reordered as

$$\frac{d\lambda}{dt} + (\dot{\gamma}k_1 + k_2)\lambda = k_2 \tag{12}$$

As $\dot{\gamma}$ is a constant, equation (12) is a first-order linear ordinary differential equation. Hence, the solution is presented as follows

$$\lambda(t) = C' \exp(-(\dot{\gamma}_c k_1 + k_2)t) + \frac{k_2}{(\dot{\gamma}_c k_1 + k_2)} \tag{13}$$

where *C'* is an integration constant that can determined using an initial condition, i.e. at t = 0.

$$\lambda(0) = C' \exp[-(\dot{\gamma}_c k_1 + k_2) \times 0] + \frac{k_2}{\dot{\gamma}_c k_1 + k_2} \tag{14}$$

If we note λ_0 the structure parameter when t = 0, the calculated integration constant reads

$$C' = \lambda_0 - \frac{k_2}{\dot{\gamma}_c k_1 + k_2} \tag{15}$$

Replacing C' in Eq. (13) we obtain

$$\lambda(t) = \left\{\lambda_0 - \frac{k_2}{\dot{\gamma}k_1 + k_2}\right\} \exp[-(\dot{\gamma}k_1 + k_2)t] + \frac{k_2}{\dot{\gamma}k_1 + k_2} \tag{8}$$

7. References

[1] É. Vernaz and J. Bruezière, "History of Nuclear Waste Glass in France," *Procedia Mater. Sci.*, vol. 7, pp. 3–9, 2014, doi: 10.1016/j.mspro.2014.10.002.

[2] G. Roth and S. Weisenburger, "Vitrification of high-level liquid waste: glass chemistry, process chemistry and process technology," *Nucl. Eng. Des.*, vol. 202, no. 2–3, pp. 197–207, Dec. 2000, doi: 10.1016/S0029-5493(00)00358-7.

[3] R. F. Taylor, "Chemical engineering problems of radioactive waste fixation by vitrification," *Chem. Eng. Sci.*, vol. 40, no. 4, pp. 541–569, 1985, doi: 10.1016/0009-2509(85)80001-4.

[4] T. Advocat, J. L. Dussossoy, and V. Petitjean, "Vitrification des déchets radioactifs et appareillage," *Les Tech. l'Ingénieur*, vol. 33, pp. 0–27, 2008.

[5] T. Akai, J. Nishii, M. Yamashita, and H. Yamanaka, "Chemical behavior of platinum-group metals in oxide glasses," *J. Non. Cryst. Solids*, vol. 222, pp. 304–309, 1997.

[6] B. Luckscheiter, "Properties and behavior of the platinum group metals in the glass resulting from the vitrification of simulated nuclear fuel reprocessing waste," *J. Mater. Res.*, vol. 6, no. 12, pp. 2535–2546, 1991, doi: 10.1557/JMR.1991.2535.

[7] W. Grünewald, G. Roth, W. Tobie, K. Weiß, and S. Weisenburger, "The role of the platinum group elements ruthenium, rhodium and palladium in the vitrification of radioactive high level liquid waste using joule heated ceramic lined waste glass melters," *Glas. Technol. Eur. J. Glas. Sci. Technol. Part A*, vol. 49, no. 6, pp. 266–278, 2008.

[8] T. Hartmann and H. Pentinghaus, "The ternary system palladium-rhodium-tellurium: A Study to understand phase formation in the vitrification process of high-level waste concentrates (HLWC)," *J. Nucl. Mater.*, vol. 422, no. 1–3, pp. 124–130, 2012, doi: 10.1016/j.jnucmat.2011.12.029.

[9] C. Hanotin, J. Puig, M. Neyret, and P. Marchal, "Platinum group metal particles aggregation in nuclear glass melts under the effect of temperature," *J. Nucl. Mater.*, vol. 477, pp. 102–109, 2016, doi: 10.1016/j.jnucmat.2016.04.033.

[10] S. Vargas, "Straw and Coal Ash Rheology," Technical University of Denmark, Thesis, 2001.

[11] K. Uruga, T. Usami, T. Tsukada, S. Komamine, and E. Ochi, "Viscoplasticity of simulated high-level radioactive waste glass containing platinum group metal particles," *J. Nucl. Mater.*, vol. 452, no. 1–3, pp. 419–424, 2014, doi: 10.1016/j.jnucmat.2014.05.062.

[12] J. Puig, B. Penelon, P. Marchal, and M. Neyret, "Rheological Properties of Nuclear Glass Melt Containing Platinum Group Metals," *Procedia Mater. Sci.*, vol. 7, pp. 156–162, 2014, doi: 10.1016/j.mspro.2014.10.021.

[13] J. Puig, C. Hanotin, M. Neyret, and P. Marchal, "High temperature rheological study of borosilicate glasses containing platinum group metal particles by means of a mixer-type rheometer," *J. Nucl. Mater.*, vol. 469, pp. 112–119, 2016, doi: 10.1016/j.jnucmat.2015.11.053.

[14] H. A. Barnes, "Thixotropy—a review," *J. Nonnewton. Fluid Mech.*, vol. 70, no. 1–2, pp. 1–33, May 1997, doi: 10.1016/S0377-0257(97)00004-9.

[15] J. Mewis, "Thixotropy - a general review," *J. Nonnewton. Fluid Mech.*, vol. 6, no. 1, pp. 1–20, 1979, doi: 10.1016/0377-0257(79)87001-9.

[16] K. Dullaert and J. Mewis, "Thixotropy: Build-up and breakdown curves during flow," *J. Rheol. (N. Y. N. Y).*, vol. 49, no. 6, pp. 1213–1230, 2005, doi: 10.1122/1.2039868.

[17] A. Mujumdar, A. N. Beris, and A. B. Metzner, "Transient phenomena in thixotropic systems," *J. Nonnewton. Fluid Mech.*, vol. 102, no. 2, pp. 157–178, 2002, doi: 10.1016/S0377-0257(01)00176-8.

[18] M. Houška and R. Žitný, "Dynamics of Thixotropic Liquids and Time Dependency," in *Advances in Food Rheology and Its Applications*, New York: Elsevier, 2017, pp. 47–63.

[19] M. Bousmina, A.-S. Chrissemant, L. Choplin, A. Aït-Kadi, and P. Marchal, "Quantitative Analysis of Mixer-Type Rheometers using the Couette Analogy," *Can. J. Chem. Eng.*, vol. 80, no. December, pp. 1166–1174, 2010, doi: 10.1002/cjce.5450800618.

[20] Bousmina M.; A. Aït-Kadi and J.B. Faisant, "Determination of Shear Rate and Viscosity from Batch Mixer Data: Theoretical and Experimental Results," *J. Rheol*, vol. 43, p. 1999, 1999.

[21] S. Gotoh, M. Nishikawa, H. Tada, and H. Hirabayashi, “Power consumption of mixing impellers in bingham plastic liquids,” *J. Chem. Eng. JAPAN*, vol. 3, no. 2, pp. 237–243, 1970, doi: 10.1252/jcej.3.237.

[22] V. V. and J. J. U. Chavan, “Power Correlations for Close Clearance Helical Impellers in Non-Newtonian Liquids,” *Ind. Eng. Chem. Process Des. Dev.*, vol. 12, pp. 472–476, 1973.

[23] P. Estellé, C. Lanos, A. Perrot, and S. Amziane, “Processing the vane shear flow data from Couette analogy,” *Appl. Rheol.*, vol. 18, no. 3, pp. 1–14, 2008.

[24] J. P. Guillemin, Y. Menard, L. Brunet, O. Bonnefoy, and G. Thomas, “Development of a new mixing rheometer for studying rheological behaviour of concentrated energetic suspensions,” *J. Nonnewton. Fluid Mech.*, vol. 151, no. 1–3, pp. 136–144, 2008, doi: 10.1016/j.jnnfm.2007.12.007.

[25] C. Simonnet, A. Grandjean, and J. Phalippou, “Electrical behavior of platinum-group metals in glass-forming oxide melts,” *J. Nucl. Mater.*, vol. 336, no. 2–3, pp. 243–250, 2005, doi: 10.1016/j.jnucmat.2004.09.019.

[26] A. Grandjean, M. Malki, C. Simonnet, D. Manara, and B. Penelon, “Correlation between electrical conductivity, viscosity, and structure in borosilicate glass-forming melts,” *Phys. Rev. B - Condens. Matter Mater. Phys.*, vol. 75, no. 5, pp. 1–7, 2007, doi: 10.1103/PhysRevB.75.054112.

[27] R. Pflieger, L. Lefebvre, M. Malki, M. Allix, and A. Grandjean, “Behaviour of ruthenium dioxide particles in borosilicate glasses and melts,” *J. Nucl. Mater.*, vol. 389, no. 3, pp. 450–457, 2009, doi: 10.1016/j.jnucmat.2009.02.034.

[28] R. B. Nuernberg, N. M. P. Machado, D. Jouglard, L. del Campo, M. Malki, and M. Neyret, “The origin of hysteresis in the electrical behavior of RuO2-glass composite melts,” *J. Non. Cryst. Solids*, vol. 557, no. February, 2021, doi: 10.1016/j.jnoncrysol.2020.120596.

[29] J. J. Derksen, “Simulations of thixotropic liquids,” *Appl. Math. Model.*, vol. 35, no. 4, pp. 1656–1665, 2011, doi: 10.1016/j.apm.2010.09.042.

[30] H. A. Barnes, *A Handbook of Elementary Rheology*. The University of Wales- Institute of Non-Newtonian Fluid Mechanics, Department of Mathematics, Avaiable online,

2000.

[31] W. R. Richmond, R. L. Jones, and P. D. Fawell, “The relationship between particle aggregation and rheology in mixed silica-titania suspensions,” *Chem. Eng. J.*, vol. 71, no. 1, pp. 67–75, 1998, doi: 10.1016/S1385-8947(98)00105-3.

Chapter III

Thixotropic behavior of a glass melt containing PGM particles - Stress imposed experiments

This chapter III follows the same research line as Chapter II, continuing to investigate the thixotropic behavior of a simulated nuclear glass containing PGM particles. Nonetheless, the following chapters (IV and V) will explore the behavior of the material in lower shear ranges that can only be reached when imposing the stress. Hence, in order to construct a base on stress-imposed experiments, the chosen experimental approach for this chapter consists in analyzing stress imposed transient rheological measurements adopting an exponential model to fit the experimental data. The dependency of the model parameters with the shear stress and with the temperature is further explored.

1 Introduction

The choice of using the vitrification as a conditioning method for high level waste is based on its efficiency in containing the fission products in the glass matrix avoiding any release of radionuclides [1]. The Platinum Group Metals (PGM. RuO_2, Pd, Rh), that can be found among these fission products, do not chemically incorporate into the nuclear glass melt which can affect directly some of its physical properties [2]. Previous work has investigated the impacts of these particles in the melt, evidencing their tendency to aggregate and settle, besides the impact on the overall rheological and electrical behavior of the system [3]–[5]. Although studies on the rheological behavior of glass melts containing PGM particles are contemplated, they are limited by experimental difficulties due to the scarcity of devices adapted for analysis at temperatures higher than 1000 °C.

An innovative device that combines a stress imposed rheometer with an oven allowing the rheological characterization of molten glass at different temperatures up to 1300 °C was designed for the study of these materials. The work developed by Puig *et al.* consisted in studying a simulated nuclear glass containing different platinum contents on a broad shear rate range, and led to the proposition of a new phenomenological model for the rheological behavior of these materials [5]–[7]. The glass melt exhibits a shear-thinning behavior and two Newtonian plateaus at low and high shear rates [5]. The existence of those plateaus (see Figure II-1) is directly related to aggregation kinetics of the PGM particles, which at low shear rate and above a certain PGM content have a tendency to aggregate. This aggregation results from a combination of weak hydrodynamic forces, Brownian motion and attractive forces between particles. In contrast, at high shear rates, the system behaves as a suspension of small clusters and individual particles, decreasing the viscosity if compared with the first plateau [5].

The time dependent behavior of the system was also established in Puig's study but further analysis was required to explore the thixotropy of the melt [7]. The work carried out in Chapter II was dedicated to characterize the impact of the shear rate, time and temperature in the rheological behavior of a simulant nuclear glass melt containing PGM particles using techniques adapted to the high temperatures. The approach chosen for the study consisted in deriving a thixotropic model, similar to that proposed by Houska [8], involving a modified Sisko model combined with a kinetic equation, to firstly understand the structure reorganization and secondly predict the PGM behavior in transient regime. Even though the high temperature measurements were conducted in a stress-imposed rheometer, the experiments were conducted

imposing the shear rate to facilitate the application of the thixotropic model. The data collected adds considerably to the existent knowledge by investigating the impact of time on the rheological behavior of the melt. However, the current thesis also investigates the aggregation of PGM particles on a broader range of shear. To achieve very low shear ranges, the measurements are better conducted in stress imposed mode. Hence, the prior investigation of the thixotropic behavior of the melt taking into account the impact of the shear stress is of extreme importance to the continuity of the study. This chapter focuses on analyzing the evolution of the viscosity of the glass melt as a function of time for shear stresses between 6 and 150 Pa and at four different temperatures, in order to understand the build-up of the system. The data are then analyzed by a phenomenological approach, using an exponential model associating the apparent viscosity with a characteristic time to fit the experimental data.

2 Materials and Methods

2.1 Material

For this work, the same simulated nuclear glass as that used in Chapter II was studied (see chemical composition in Table II-1, Chapter II). This borosilicate glass containing 3 wt% of PGM particles was elaborated on a full-scale pilot unit installed at CEA Marcoule [9]. The unit follows a two-step protocol (calcination-vitrification) with an indirect induction furnace heated at 1200 °C. At the end, the glass was poured in a canister and cooled at room temperature. The studied material was extracted from the middle of the canister. PGM particles are in the form of needle-like RuO_2 (length ~10 µm) when Pd-Te alloys appear as spherical particles with diameter ranging from 1 to 5 µm.

2.2 Rheological measurement at high temperatures

The rheological characterization conducted in this work were performed using an innovative device conceived in the laboratory for high temperature measurements [7]. The equipment, showed in Figure III-1a [5], consists of a stress-imposed rheometer (Rheometrics Scientific SR5000) above a tubular furnace that can be heated up to 1500 °C. The transmission of the torque from the rheometer to the crucible is ensured by a specific tool that avoids disturbances effects, as shown in Figure III-1a. The characterization cell is located in the center of the furnace and consists of a platinum-rhodium crucible (27 mm diameter; 40 mm height) in which the temperature gradient is lower than 2 °C from the top to the bottom. The crucible is filled with the shattered glass and heated to 1200 °C previously to the measurement. The rotor is composed of a 30 cm long rod connected with the measurement geometry at its end. To assure a uniform

distribution of the particles in the glass melt and prevent their sedimentation, a multiblade rotor geometry was chosen for this work (Figure III-1b) [7]. The Materials and Methods section of Chapter II along with Puig *et al* [7] provide a complete description of the equipment and calibration procedure.

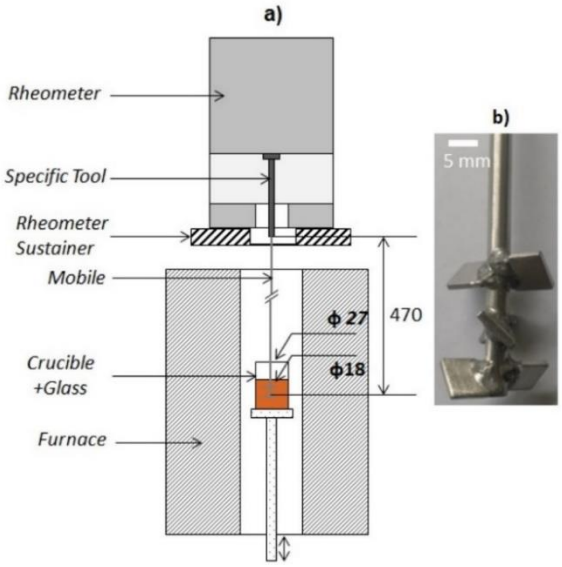

Figure III-1- a) High temperature measurement equipment (dimensions in mm), b) Mobile with a multiblade geometry.

The rheological measurements were carried out in transient regime to further investigate the thixotropic behavior occurring in nuclear glass melts. Transient step stress measurements were performed on the melt, varying from 6 to 150 Pa. The duration of the experiments were chosen accordingly to the time necessary for the stabilization of the melt viscosity. All tests were conducted at four different temperatures: 1100, 1150, 1200 and 1250 °C. A pre-shear was implemented at the beginning and between subsequent tests at 200 Pa during 60 s to disperse completely the PGM particles in the glass, removing memory effects from previous tests.

2.3 Modelling the rheological behavior of the glass melt

As mentioned earlier, the goal is to investigate the build-up phenomenon exhibited by glass melts containing PGM particles. Several models available in the literature are used for this purpose [10]–[12]. In order to use a simpler approach in stress-imposed measurements, an exponential model was chosen (Eq. (1)) to fit the experimental data. The model proved to be suitable for the study of the build-up phenomenon of a Montmorillonite clay [13].

$$\eta(t) = \eta_{e,0} + (\eta_{e,\infty} - \eta_{e,0})(1 - \exp(-t/\tau)) \quad (1)$$

Beside its simplicity, the interest in this model relies on the existence of a characteristic time (τ) in which the viscosity may reach its equilibrium value. The terms $\eta_{e,0}$ and $\eta_{e,\infty}$ represent the glass melt viscosity when the material is completely destructured (just after the pre-shear step at 200 Pa; $t = 0$) and at equilibrium ($t \rightarrow +\infty$), respectively.

3 Results and Discussion

3.1 Fitting model parameters in transient regime

Although assessing the thixotropic behavior of a system may be difficult due to the experimental conditions, transient experiments have proven to be a useful technique for a temporal analysis of the viscosity, as shown in Chapter II [10], [11]. Figure III-2 displays the experimental evolution of viscosity over time (symbols) for all four studied temperatures at different shear stresses. Under extreme conditions such as high temperatures and low shear stresses, the rheological experiments may exhibit oscillations due to the precession of the rheometer axis because of its extensive length. This phenomenon is observed in Figure III-2 at all temperatures for shear stress results under 15 Pa.

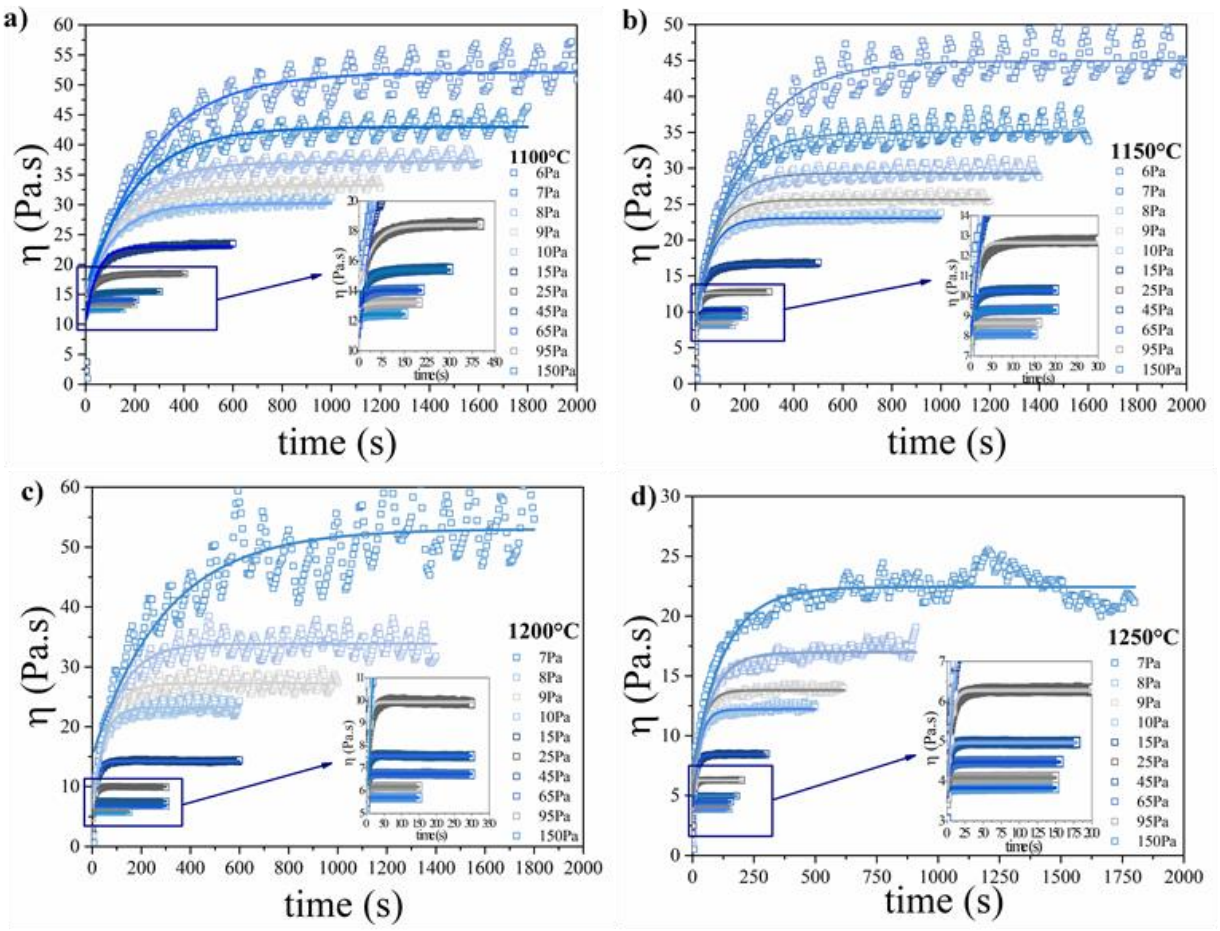

Figure III-2 - Evolution of viscosity over time for shear stress steps of different values, from 6 Pa to 150 Pa at a) 1100 °C, b) 1150 °C, c) 1200 °C and d) 1250 °C. The lines correspond to the fit using the exponential model (Eq.(1)) and the symbols correspond to the experimental data.

A constant increase of the melt viscosity over time is observed for all experiments until it reaches a stable value, characterizing the build-up phenomena common to thixotropic fluids [10]. The rheological behavior of the glasses containing PGM particles is directly affected by the aggregation kinetics of the particles, involving different mechanisms depending on the shear stress value. The PGM particles tendency to aggregate at low shear stresses is due to the weakness of hydrodynamic forces compared to the effects of Brownian motion and attractive van der Waals forces. On the contrary, at high shear stresses, the strong hydrodynamic forces contribute to the dispersion of the particles in the melt, hence the use of a pre-shear at an elevated shear to destructure the sample that will rebuild at lower shear stresses [5]. The structuration of the system leads to an increase of the viscosity, followed by a stabilization when the sample reaches an equilibrium depending on the applied conditions. The lines in Figure III-2 correspond to the fit of the experimental data with the exponential model using damped least squares (DLS) method. The model is found to describe properly the viscosity evolution of the

glass melt over time at all studied temperatures. The evolution of the obtained parameters (τ, $\eta_{e,0}$, $\eta_{e,\infty}$) with the shear for the four studied temperatures is explored in the next section.

3.2 Analysis of the model parameters

The comprehension of how the temperature affects the rheological behavior of a material is largely explored in the literature [14]–[16]. Nonetheless, for complex fluids such as a glass melt containing PGM particles, the thermal impact on the viscosity can be counter intuitive depending on the applied shear range due to the involved aggregation kinetics. At low shear and high temperature, hydrodynamic forces are low and favor the aggregation of the particles promoted by Brownian motion and attractive forces. The presence of clusters leads to an increase of the suspension viscosity even though the high temperatures have a contrary effect on the glass matrix. For higher shear range, the hydrodynamic forces are stronger, promoting a greater dispersion of the particles in the melt, forming a suspension of small clusters and individual particles, and its viscosity decreases by increasing temperature since it is then mainly controlled by the viscosity of the glass matrix [5], [7]. Hence the dependency of the obtained parameters with the temperature is fundamental to understanding the thixotropic behavior of the glass melt.

The initial viscosity ($\eta_{e,0}$) corresponds to the initial viscosity of the melt before the beginning of the build-up of the structure, i.e. the aggregation of the PGM particles in this scenario. This fitting parameter gives the viscosity of the sample when it is completely unstructured considering that a pre-shear at a higher stress has been done previously, which is the case for the conducted measurements. It can be highly affected by the measurement artifacts due to the equipment inertia. Table III-1 shows $\eta_{e,0}$ for all studied temperatures. Given that $\eta_{e,0}$ does not vary with the shear stress and that the pre shear was made at a high shear stress, the viscosity will decrease with the temperature since the material is completely destructured. Indeed, in this case, the melt behaves as a suspension of dispersed particles where the viscosity of the suspension is controlled by the viscosity of the glass matrix.

Table III-1 - The initial viscosity ($\eta_{e,0}$) and the equilibrium viscosity ($\eta_{e,\infty}$) at the Newtonian plateau obtained for the 4 studied temperatures from the exponential model (Eq.(1)).

Temperature (°C)	**1100**	**1150**	**1200**	**1250**
$\boldsymbol{\eta_{e,0}}$ **(Pa.s)**	14 ± 2	8 ± 1	6 ± 3	4 ± 1
$\boldsymbol{\eta_{e,\infty}}$ **(Pa.s)**	44 ± 4	36 ± 4	38 ± 5	18 ± 2

The equilibrium viscosity ($\eta_{e,\infty}$) evolution with shear stress and temperature is showed in Figure III-3. The graph shows the viscosity decreasing both with the shear stress and with the temperature. At this point, the system has already reached its more structured state, which corresponds to the plateau observed in the graphs of Figure III-2. The values of $\eta_{e,\infty}$ are higher than those of $\eta_{e,0}$ which indicates the build-up of the structure. The presented data exhibits less fluctuations when compared to the initial viscosity due to the greater stability of the melt. At high shear rate, the viscosity reaches a Newtonian plateau for all temperatures that is also observed in the steady state measurements presented in Figure II-3 of Chapter II. The value of $\eta_{e,\infty}$ in the plateau is showed in Table III-1. The combination of increasing hydrodynamic forces and higher temperatures is translated in a greater PGM particles dispersion in the melt and the viscosity of the system being controlled by matrix viscosity. Since the shear stress range explored in this work is different from that explored by Hanotin *et al.*, the first Newtonian plateau at low shear rates is not presented [5].

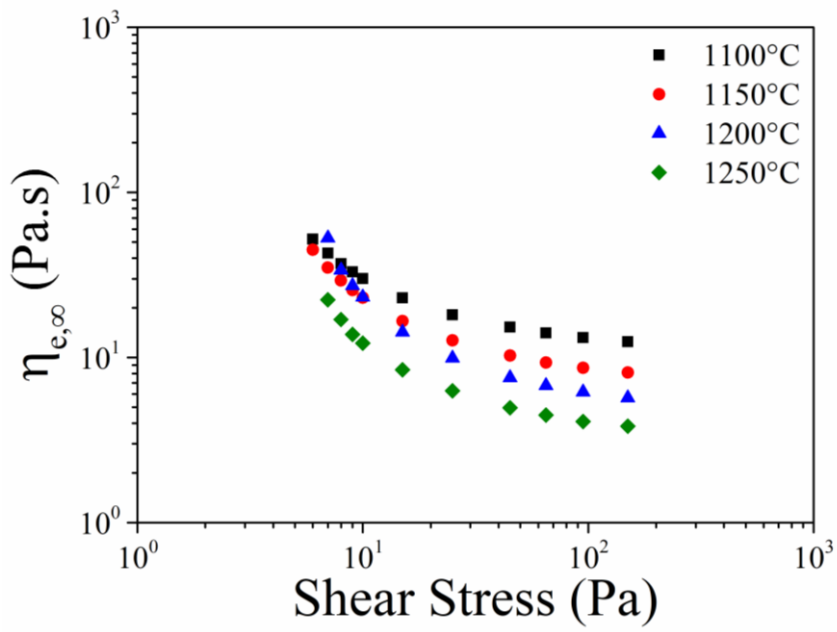

Figure III-3 – Evolution of $\eta_{e,\infty}$ with the shear stress for all studied temperatures.

Figure III-4 exhibits the evolution of the obtained characteristic time (τ) with the shear stress for all studied temperatures. It is observed that τ decreases with the shear stress for all studied temperatures. The thixotropic behavior of the material is thus more visible at low shear stress. At this regime, the weaker hydrodynamic forces coupled with the Brownian motion and attractive forces between the particles enable a stronger PGM particles aggregation. These large aggregates lead to a slow rearrangement kinetics, hence a high characteristic time. It thus takes

longer for the system to reach a stable viscosity. On the contrary, at higher shear stresses, the small aggregates and dispersed particles have a faster rearrangement kinetics, which leads to a small characteristic time. The data presented can be fitted by a power law $\tau = b\sigma^c$ where $b =$ 4.0 ± 0.2 and $c =$ -2.2 ± 0.2. It can indicate an insensibility of the characteristic time to the temperature but further analysis is necessary to explore the dependency. The slope shows that the characteristic time decreases by two orders of magnitude with respect to the shear stress, which implies a strong impact of the shear stress on τ and thus on the thixotropic behavior of the sample.

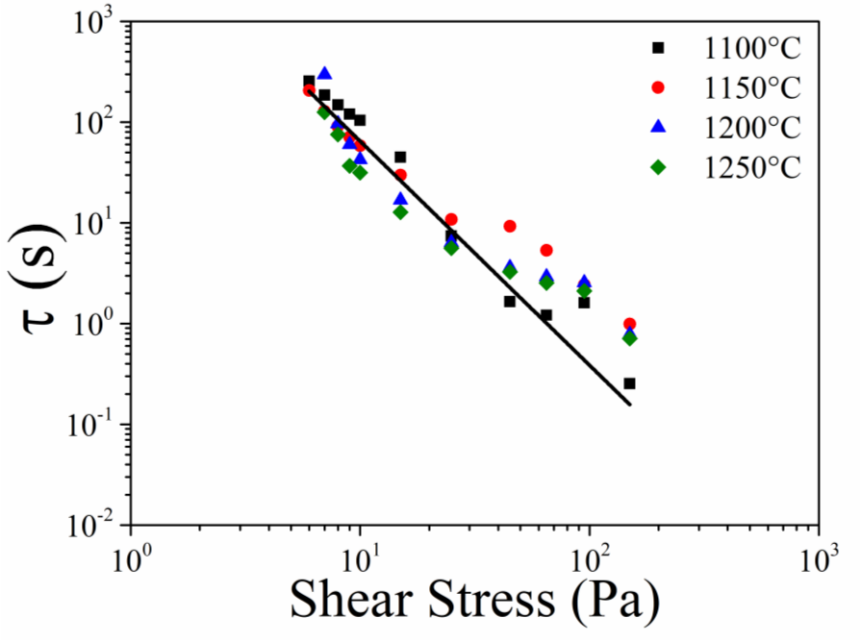

Figure III-4 – Evolution of the characteristic time (τ) with the shear stress for all studied temperatures.

4 Conclusions

This chapter is a continuation of the study on the thixotropic behavior of simulated nuclear glass containing PGM particles. In the previous chapter, a thixotropic model, similar to that of Houska [8], was proposed to represent the rheological behavior of the system in steady-state and transient regimes. All measurements from both chapters were conducted using a stress-imposed rheometer at high temperatures ranging from 1100 to 1250 °C. Nonetheless, for this chapter, the goal was to assess the rheological behavior of the melt using stress-imposed measurements since the following chapters will be focused on stress-imposed analysis to reach low shear regimes.

Transient regime experiments were conducted to investigate the impact of the shear stress, time and temperature on the rheological behavior of the melt. A mathematical modeling of the thixotropic behavior of the system was presented using an exponential model describing the apparent viscosity in terms of a characteristic time. The evolution of the viscosity over time evidenced a build-up phenomenon in the melt due to the PGM particles aggregation kinetics. The association of Brownian motion and van der Walls attractive forces favors the aggregation, leading to an increase of the viscosity until the material structure reaches an equilibrium. The weakness of the hydrodynamic forces favors this phenomenon at low shear stresses. The shear thinning behavior of the melt previously investigated is evidenced by the decrease of the viscosity with the shear stress for all studied temperatures.

The exponential model showed to be efficient to describe the thixotropic behavior of the PGM glass in the transient regime. Only three fitting parameters ($\eta_{e,0}, \eta_{e,\infty}, \tau$) are necessary simplifying the analysis. Before the beginning of the build-up of the structure, the melt viscosity is given by $\eta_{e,0}$ and it decreases with the temperature. Considering it reflects the viscosity of the sample at the beginning of the shearing, the system is close to a fully dispersed state of the PGM particles, which then aggregate, indicating the start of the build-up phenomenon. The equilibrium viscosity ($\eta_{e,\infty}$) on the other hand, decreases with the temperature and the shear stress. The presence of a Newtonian plateau indicates the complete dispersion of the particles in the melt due to the increase of the hydrodynamic forces at high shear stress compared to the Brownian motion and the attractive forces.

Regardless of the temperature, the characteristic time (τ) decreases with the shear stress. The lower the shear stress, the longer it takes the system to reach a stable viscosity due to the structuration of the melt. At higher shear rates, the opposite takes place. The evolution of the characteristic time with the shear can be described by the same power law for all temperatures, indicating, in a first approximation, of an insensibility of the characteristic time to the temperature. It is clear that the shear stress has a strong impact on τ but further analysis is necessary to explore its temperature dependency. These observations are limited in the literature due to the extreme experimental conditions involved, but they create an important background for the following studies on the PGM particles aggregation.

5 References

[1] T. Akai, J. Nishii, M. Yamashita, and H. Yamanaka, “Chemical behavior of platinum-group metals in oxide glasses,” *J. Non. Cryst. Solids*, vol. 222, pp. 304–309, 1997.

[2] B. Luckscheiter, “Properties and behavior of the platinum group metals in the glass resulting from the vitrification of simulated nuclear fuel reprocessing waste,” *J. Mater. Res.*, vol. 6, no. 12, pp. 2535–2546, 1991, doi: 10.1557/JMR.1991.2535.

[3] W. Grünewald, G. Roth, W. Tobie, K. Weiß, and S. Weisenburger, “The role of the platinum group elements ruthenium, rhodium and palladium in the vitrification of radioactive high level liquid waste using joule heated ceramic lined waste glass melters,” *Glas. Technol. Eur. J. Glas. Sci. Technol. Part A*, vol. 49, no. 6, pp. 266–278, 2008.

[4] T. Hartmann and H. Pentinghaus, “The ternary system palladium-rhodium-tellurium: A Study to understand phase formation in the vitrification process of high-level waste concentrates (HLWC),” *J. Nucl. Mater.*, vol. 422, no. 1–3, pp. 124–130, 2012, doi: 10.1016/j.jnucmat.2011.12.029.

[5] C. Hanotin, J. Puig, M. Neyret, and P. Marchal, “Platinum group metal particles aggregation in nuclear glass melts under the effect of temperature,” *J. Nucl. Mater.*, vol. 477, pp. 102–109, 2016, doi: 10.1016/j.jnucmat.2016.04.033.

[6] J. Puig, B. Penelon, P. Marchal, and M. Neyret, “Rheological Properties of Nuclear Glass Melt Containing Platinum Group Metals,” *Procedia Mater. Sci.*, vol. 7, pp. 156–162, 2014, doi: 10.1016/j.mspro.2014.10.021.

[7] J. Puig, C. Hanotin, M. Neyret, and P. Marchal, “High temperature rheological study of borosilicate glasses containing platinum group metal particles by means of a mixer-type rheometer,” *J. Nucl. Mater.*, vol. 469, pp. 112–119, 2016, doi: 10.1016/j.jnucmat.2015.11.053.

[8] M. Houška and R. Žitný, “Dynamics of Thixotropic Liquids and Time Dependency,” in *Advances in Food Rheology and Its Applications*, New York: Elsevier, 2017, pp. 47–63.

[9] T. Advocat, J. L. Dussossoy, and V. Petitjean, “Vitrification des déchets radioactifs et appareillage,” *Les Tech. l’Ingénieur*, vol. 33, pp. 0–27, 2008.

[10] J. Mewis, “Thixotropy - a general review,” *J. Nonnewton. Fluid Mech.*, vol. 6, no. 1, pp. 1–20, 1979, doi: 10.1016/0377-0257(79)87001-9.

[11] H. A. Barnes, “Thixotropy—a review,” *J. Nonnewton. Fluid Mech.*, vol. 70, no. 1–2, pp. 1–33, May 1997, doi: 10.1016/S0377-0257(97)00004-9.

[12] P. R. de Souza Mendes and R. L. Thompson, “Time-dependent yield stress materials,” *Curr. Opin. Colloid Interface Sci.*, vol. 43, pp. 15–25, 2019, doi: 10.1016/j.cocis.2019.01.018.

[13] J. F. Maingonnat, L. Muller, and J. C. Leuliet, “Modelling the build-up of a thixotropic fluid under viscosimetric and mixing conditions,” *J. Food Eng.*, vol. 71, no. 3, pp. 265–272, 2005, doi: 10.1016/j.jfoodeng.2005.01.036.

[14] S. Das, V. S. R. Murthy, and G. S. Murty, “Rheological behavior of discontinuous SiC reinforced borosilicate glass composites at elevated temperatures,” *Mater. Sci. Eng. A*, vol. 241, no. 1–2, pp. 129–136, 1998.

[15] H. Kobayashi, H. Takahashi, and Y. Hiki, “Viscosity of glasses near and below the glass transition temperature,” *J. Appl. Phys.*, vol. 88, no. 6, pp. 3776–3778, 2000, doi: 10.1063/1.1286107.

[16] P. Hrma, “Arrhenius model for high-temperature glass-viscosity with a constant pre-exponential factor,” *J. Non. Cryst. Solids*, vol. 354, no. 18, pp. 1962–1968, 2008, doi: 10.1016/j.jnoncrysol.2007.11.016.

Chapter IV

Influence of Platinum Group Metals particles aggregation on a glass melt rheological behavior

The two previous chapters were dedicated to explore the thixotropy of the glass melt containing PGM particles. The impact of time, temperature, shear rate and shear stress on the rheological behavior of the glass was well described by mathematical models. Nonetheless, the presence of the suspended PGM particles also emerge the aggregation phenomenon in the melt. Hence, this chapter explored the aggregation mechanisms of a simulated nuclear glass melt containing 3.0 wt% (1.02 vol%) of PGM. The impact of the shear stress and time on PGM aggregation degree is determined. For the first time, the interplay between the rheological behavior of the system and the aggregation degree is provided.

Norma Maria Pereira Machado; Luiz Pereira; Muriel Neyret; Cécile Lemaître; Philippe Marchal.

Submitted in Journal of Nuclear Materials

Abstract

Borosilicate glasses are generally used as matrices to immobilize nuclear fission products resulting from spent fuel reprocessing. In the high-temperature vitrification process (1200 °C), most elements to be contained react chemically with the vitrification additives to form a homogeneous glass melt. Platinum Group Metal (PGM) particles are not incorporated chemically in the melt and therefore are present as suspended particles a few microns in size. These particles exhibit an intense aggregation tendency and consequently the suspensions may present an anomalously high apparent viscosity. These systems are characterized by shear-thinning and thixotropic behaviors. However, the interplay between the rheological behavior and the aggregation degree is poorly understood. In this work, the aggregation mechanisms of a simulated nuclear glass melt containing 3.0 wt.% (1.02 vol.%) of PGM particles were investigated. The impact of the shear stress and time on the PGM aggregation degree was determined using an imposed-stress rheometer at high temperature followed by an imaging analysis procedure via Scanning Electron Microscopy (SEM). We present three different aggregation scenarios and their impact on suspension rheology. Based on the experimental data acquired, a force balance computation was performed to illustrate these three scenarios.

Keywords: Melt, Suspension, Platinum Group Metals (PGM), Aggregation, Rheology.

1 Introduction

High-level radioactive waste vitrification is the standard immobilization treatment used in France. After the extraction of uranium and plutonium from spent fuel, the remaining waste is conditioned in a glass matrix in a two-step process. First, the nitrate salts of the waste are converted into oxides at high temperature, yielding calcinate, which is then fed into the melter along with glass frit. This leads to the production of a complex amorphous material that contains around 40 different elements. The melter crucible can be heated by conduction (hot crucible), indirect induction (cold crucible), or in a Liquid Fed Ceramic Melter with electrodes. The nuclear glass is then poured into metal containers and stored in shafts while awaiting future storage in a deep geological repository [1], [2].

Elements and their oxides from the Platinum Group Metals (PGM) (*e.g.*: palladium, rhodium and ruthenium) are insoluble in a nuclear glass melt as well as in the final glass [3]. They are found as palladium-tellurium metallic alloys in a spherical shape (diameter = 1 to 5 μm) together with needle-like ruthenium oxide particles (length ~10 μm), as shown in Figure IV-1. The presence of these suspended particles has an impact on several physical properties of the glass melt such as the suspension viscosity and electrical conductivity [4]–[7]. In addition, even if the PGM particles are in small amounts (*i.e.*: 3 wt.%), their tendency to aggregate and sediment can lead to the formation of high volume fraction layers at the bottom of the crucible. This can interfere in the process [8][9]. It is important to note that authors observed also abnormal behavior linked to particle aggregation in melt systems containing only RuO_2. Thus, one can state that aggregation is not necessarily directly linked to the presence of Pd-Te particles [10], [11].

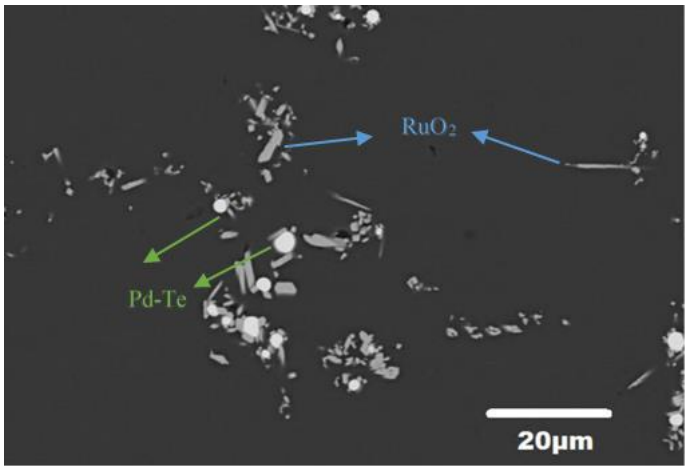

Figure IV-1 –SEM micrographs taken using back-scattered electrons (BSE) mode under 1000X magnification for the technological nuclear glass containing 3 wt.% PGM particles after vitrification.

It is therefore essential to understand the impact of PGM particles on the physical properties of a nuclear glass melt. In particular, the rheological behavior of a fluid can be strongly influenced by the particle aggregation kinetics as well as the flow, which has an impact on the particles collision and on the dynamics of cluster formation/destruction. Although the PGM particles lead to significant changes in the rheological behavior of their suspensions, the literature on this subject is still limited. Nonetheless, some authors have discovered an increase in the system viscosity in the presence of PGM and a non-Newtonian behavior of the material [4], [8], [12]–[14]. In order to explore the broader shear rate range needed for cold crucible melter development, recent studies have proposed a new phenomenological model for the rheological behavior of these materials [4], [5].

Puig *et al.* (2016) and Hanotin *et al.* (2016) studied the viscosity of simulated nuclear glass melts containing PGM particles as a function of their amounts and temperature [4], [5]. These suspensions presented a shear-thinning behavior and two Newtonian plateaus at low and high shear rates, which were well described by a simplified Cross model:

$$\eta = \eta_\infty + \frac{\eta_0 - \eta_\infty}{1 + (\dot{\gamma}/\dot{\gamma}_c)^m} \quad (1)$$

where η_∞ and η_0 are the viscosity at the high and low shear plateaus respectively, $\dot{\gamma}_c$ is the critical shear rate, at which the shear-thinning transition takes place and m controls the slope of this smooth transition. A previous work have suggested that melts containing PGM particles are well described by m = 1 (simplified Cross model) [15]. At low shear rates and above a certain content of PGM particles, macroscopic aggregates appear. They are made of RuO_2 and

Pd-Te chains separated by thin layers of liquid which greatly increase the viscosity of the systems [5]. In this first case, an increase in temperature lowers the viscosity of the melt and improves Brownian diffusion. This in turn favors the particle-particle collision probability leading to an increase of aggregates size and therefore to an overall increase of the suspension viscosity [4]. In contrast at high shear rates, the system behaves as a classical suspension of small clusters and the suspension viscosity is mainly controlled by the liquid phase viscosity that leads to a decrease of the viscosity when the temperature increases.

Particle aggregation can be induced by external and internal factors, but aggregation is an inherent behavior of colloidal systems, even though the extent to which this aggregation prevails may differ widely depending on the particle nature [16]. For molten silicates containing PGM particles, authors [4] have raised a hypothesis that particle aggregation is a result of an interplay of different forces, such as interparticle forces (*e.g.* van der Waals), entropic forces (Brownian motion) and hydrodynamic forces. Several in situ methods are available to study aggregation phenomena by combining rheometry with different characterizations techniques such as ultrasonic velocimetry, X-ray computed tomography, image analysis among others [17]–[19]. Nonetheless, the combination of these techniques is only available at room temperature or below 100 °C, which is much lower than the temperatures of glass melts (900 °C – 1250 °C). In this work, high temperature rheological measurements along with image analyzes was employed to characterize particle aggregation in charged glass melts. The impacts of time and shear stress on PGM particle aggregation were studied for a simulated nuclear glass melt at 1200 °C. We present here an in-depth analysis of the aggregates and their contribution to the proposed rheological model based on the phenomenology of the system by varying the imposed shear stress and the experiment durations. In this work, we also explore the interplay between the aggregation degree of PGM particles in the melt and the rheological response of suspension.

2 Experimental Method

2.1 Materials

The material used in this study was a simulated nuclear glass containing 3 wt.% of PGM particles. The glass was produced in the full-scale pilot unit installed at CEA Marcoule [20]. The process followed a two-step vitrification protocol at 1200 °C, using the indirect induction technology. The glass was cooled at room temperature and the material studied was extracted

from the middle of the canisters. During vitrification, RuO_2 was present in the glass as needle-like of ~10 µm, while Pd-Te alloy appeared as spherical particles with diameters ranging from 1 to 5 µm (Figure IV-1). The theoretical chemical composition of the nuclear glass is shown in Table IV-1.

Table IV-1 – Chemical composition of the nuclear glass samples containing 3 wt.% of PGM particles.

Glass with 3 wt% PGM									
SiO_2 (wt.%)	B_2O_3 (wt.%)	Na_2O (wt.%)	Al_2O_3 (wt.%)	Alkali metal oxides (wt.%)	Alkaline earth metal oxides (wt.%)	Rare earth oxides (wt.%)	RuO_2 (wt.%)	Pd (wt.%)	Others (wt.%)
43.7	13.2	9.2	4.2	3.3	5.0	7.0	1.8	1.2	11.4

2.2 Rheological measurements

Different aggregation degrees were generated by submitting the samples to several shear stresses during different time intervals at 1200 °C, followed by a fast cooling of the sample to "freeze" the particle rearrangements for further image analyses. The high temperature experimental apparatus used for this work is showed in Figure IV-2 [5]. It consists of a stress-imposed rheometer (Rheometrics Scientific SR5000) above a tubular furnace that could be heated up to 1500 °C. A tool was designed to ensure torque transmission from the rheometer to the crucible without disturbance effects. The characterization cell consisted of an alumina crucible (diameter, height, and wall thickness equal to 27, 40, and 2 mm respectively) previously filled with glass, and centered inside the furnace. The rotor was a multiblade agitator, used in order to maintain a uniform distribution of particles in the glass and avoid settling phenomena [5]. From the top to the bottom of the crucible, the temperature gradient was lower than 2 °C. For these experiments, disposable alumina crucibles were used so that the hardened glass and the crucible could be cut at the end of the experiment in order to analyze the PGM distribution in the glass. The rheological parameters such as shear stress (σ) and shear rate ($\dot{\gamma}$) are linked to measured parameters, namely the torque (C) and the angular velocity (Ω) through geometrical factors K_σ and $K_{\dot{\gamma}}$,

$$\sigma = K_\sigma \, C \qquad \dot{\gamma} = K_{\dot{\gamma}} \, \Omega$$

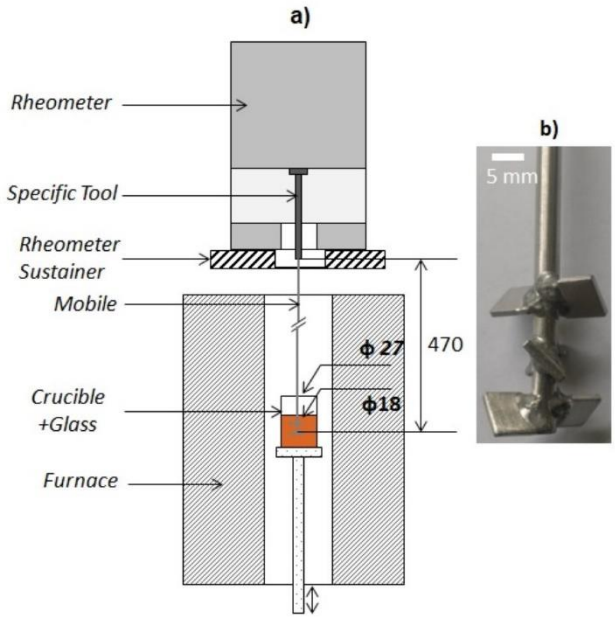

Figure IV-2- a) High temperature rheological experimental set-up (dimensions in mm), b) Multiblade rotor. [5]

The combination of the crucible and the multiblade geometry formed a virtual Couette cell, therefore factors K_σ and $K_{\dot{\gamma}}$ were determined through a Couette analogy [21] by solving the equation of motion. In the case of Newtonian fluid or a well-characterized power law fluid, the boundary conditions were imposed by the geometrical dimensions of a virtual inner cylinder (the rotor) and the outer cylinder (the crucible) [22]. A complete description of the equipment and calibration procedure was provided in Puig *et al* [5].

In order to establish the overall rheological behavior of the material, a first measurement was made in steady state regime by imposing successive shear stress values, from 0.3 to 300 Pa for 600 s in order to reach equilibrium values. The temporal evolution of the aggregates was then investigated along with the viscosity. In order to create the different aggregation degrees, the measurements were carried out in transient regime by imposing different shear stresses for different times. All samples were first submitted to a pre-shear of 200 Pa for 300 s in order to disperse the PGM particles within the glass melt, which will be referred as the pre-shearing stage. One crucible that was only submitted to the pre-shear stage was considered as the reference for this study. Then the samples were subjected to a given shear stress, between 0.1 to 200 Pa. The experiment duration for each selected stress was chosen considering the thixotropic behavior of the glass melt. For a given stress level, experiments were performed for 3 to 4 different experimental durations (varying from 300 s to 7200 s). Table IV-2 shows the shear stresses and time intervals implemented. Each stress/time pair corresponds to a different experiment and to a new crucible, with a total of twenty different experiments.

Table IV-2 – Operating conditions (shear stress level and duration) for the 20 experiments.

Stress (Pa)	**Duration (s)** (All samples were first pre-sheared at 200Pa for 300s)				
0.1	-	1200	3600	-	7200
2	-	1200	3600	5400	7200
5	300	1200	3600	-	-
10	300	1200	3600	-	-
100	300	1200	3600	-	7200
200	300	1200	3600	-	-

At the end of the rheological tests, the rotor was lifted out of the crucible at a low velocity of 8 $mm.min^{-1}$ to avoid significant changes of particle rearrangement during the withdrawal. The same rotor removal velocity and the same constant speed of crucible cooling were used for all the samples. The crucible was located on an alumina holder that was extracted from the bottom of the furnace. To ensure a compromise between a quick temperature drop and the prevention of thermal shock [23], this descent was conducted at a speed of 2 $cm.min^{-1}$, equivalent to a cooling rate of 35 $°C.min^{-1}$. At this rate, no significant changes in the particle rearrangement were expected, due to the rapid increase in the glass viscosity induced by the drop of temperature. In order to observe the impact of withdrawing the rotor on PGM particle distribution, two crucibles were placed in the furnace following the same conditions. The difference between them was that the first one was placed with no rotor and no agitation and the second one with the rotor but with no applied shear stress.

2.3 Sample preparation

To relieve residual internal stresses introduced in the system during the cooling and to avoid breakage during the sample preparation, the glass underwent annealing at 580 °C for 2 h followed by a slow cooling at 10 $°C.h^{-1}$ until room temperature. To observe the PGM particle distribution in the crucible, it was filled with epoxy resin and cut in half with a circular diamond saw as displayed in Figure IV-3. One of the halves was cut again horizontally and covered with epoxy resin to fit and to facilitate its support within the SEM measurement cell. The analyzed face was polished and coated with a thin film of carbon for SEM analysis. Each experiment thus produced two samples: the top and the bottom of the crucible (P1 and P2, as shown in Figure IV-3). The second half of the crucible was kept in case further characterization was needed.

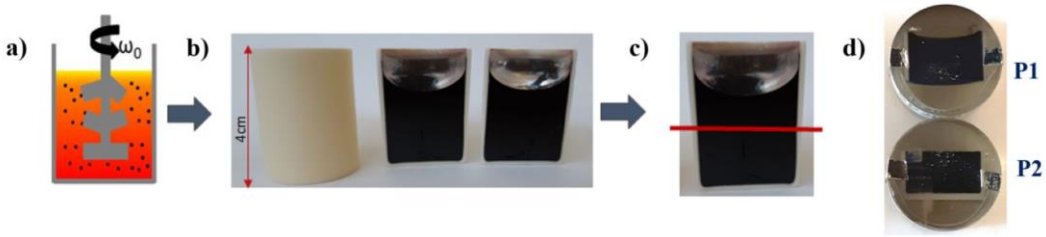

Figure IV-3 – Samples preparation protocol: the glass melt in the alumina crucible was sheared for a certain time (a). After annealing, the crucible was cut vertically (b), and then cut again horizontally (c), yielding two samples for each crucible (d): top (P1) and bottom (P2).

2.4 Scanning Electron Microscopy imaging

The Scanning Electron Microscopy was performed using a Zeiss Supra 55 FEG. The image of the whole surface was reconstructed from a mosaic of small images automatically acquired using commercial SEM software to describe the PGM particles rearrangement in the most representative area. The most representative zones of P1 and P2 were then selected. To ensure a standardization of the procedure, the same rectangular region of each crucible was chosen for all experiments. A final area of 1.75 cm² was selected for the bottom and the top samples. The combination of the bottom and top selected surfaces corresponds to the middle of the crucible, *i.e.*, the zone where the rotor was located during the rheological measurement. The analyzed area of the upper sample P1 was located 0.3 cm below the crucible top while the analyzed area of the lower sample P2 was 0.3 cm above the crucible bottom. Each image making up the mosaic was acquired using the back-scattered electron (BSE) mode under a × 100 magnification, a voltage of 15 kV and a 1024 × 768-pixel resolution. Each mosaic contained an average of 320 images, with an acquisition time of ~10 s/image. Due to the size of the sample, a compromise was made between image capture time and resolution. The Fiji software was used for the image processing. The methodology of image acquisition and treatment was derived from crystallization studies involving image analysis found in the literature [24][25]. Subsequently, the information obtained on the PGM particle positions was used as input data to a Python script, developed to quantify the aggregation degree of the samples for different situations under study.

3 Results and Discussion

3.1 Generation of different aggregation degrees

From the first steady state viscosity measurements performed on the glass with 3.0 wt.% of PGM at 1200 °C (Figure IV-4), six different conditions were selected, expected to produce six different aggregation degrees. The viscosity curve shows three distinct zones displayed in Figure IV-4: a Newtonian plateau at low shear rates (in blue as M1), a shear-thinning behavior at intermediate shear rates (in green as M2) and a second Newtonian plateau at higher shear rates (in red as M3). Two shear stresses were chosen in each zone, yielding six different representative stress values, marked with grey stars: 0.1 Pa and 2 Pa in zone M1, 5 Pa and 10 Pa in M2, and 100 Pa, and 200 Pa in M3.

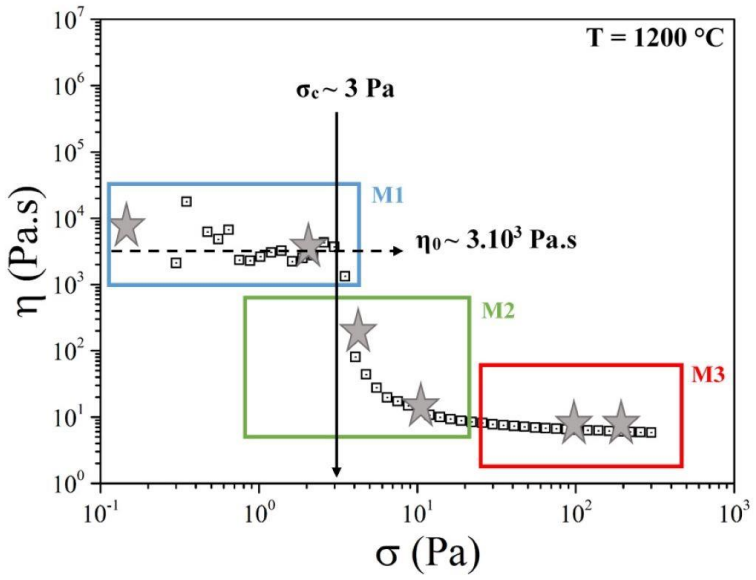

Figure IV-4 - Evolution of the glass melt viscosity as a function of the shear stress for 3 wt.% of PGM particles at 1200 °C. Stars represent the shear stresses selected for the aggregation analysis.

One of the main limitations of non “in situ” measurements is guaranteeing the reproducibility of the experiment, since for each combination of stress and time, a different sample (in a new crucible) was submitted to the protocol. This is why the tests were repeated at least 3 times, leading to twenty experiments in all. Figure IV-5 shows the evolution of the suspension viscosity under a shear stress of 5 Pa for three different times: 300, 1200, and 3600 s. These three curves overlap indicating that the three experiments gave the same rheological response so that the methodology reproducibility is guaranteed. It also shows that three main events were captured by the experiments: a sharp increase in viscosity, followed by a more progressive

increase and, finally, a stabilization. The thixotropic behavior is more pronounced for the lower stresses, but all the samples studied showed the same reproducibility.

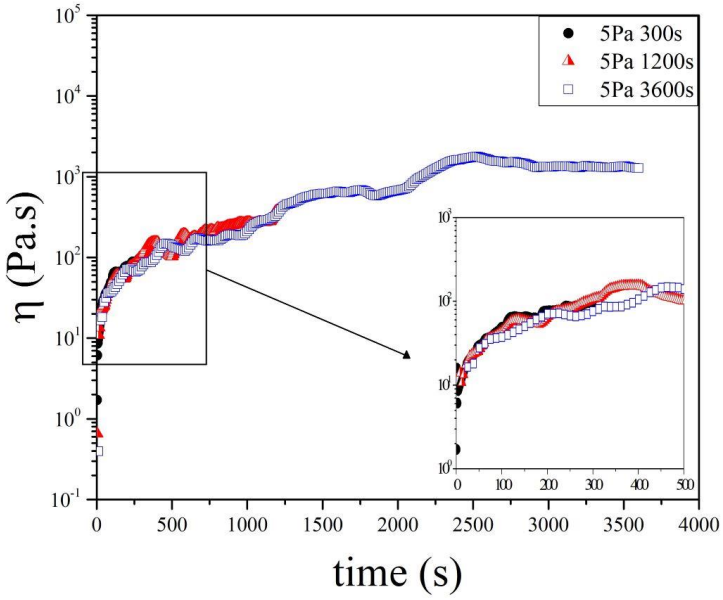

Figure IV-5 – Evolution of viscosity with time at the imposed stress of 5 Pa for three different samples tested for 300 s, 1200 s and 3600 s. The zoom focuses on the overlap of the three curves, indicating the reproducibility of the experiments.

3.2 Determination of the aggregation degrees

All samples were analyzed using scanning electronic microscopy imaging. For each experiment, images were extracted from the bottom and from the top of the crucible, as mentioned. Although the SEM images give details of the PGM particles in the glass, it is difficult to identify the aggregates only visually. The RuO_2 needles and the Pd-Te spheres were dispersed in the glass matrix normally in groups, as shown in Figure IV-6a. They are rarely found separately. Therefore, even in the most disaggregated state (after the pre-shearing stage), small clusters composed of RuO_2 needles and Pd-Te spheres remains. It is believed that the pre-shearing scenario (200 Pa, 300s) was not enough to break them all apart. In this current study, these entities are called structural units (SU), and, an aggregate will be a group of SUs close to each other. Thus, if the goal is to observe the aggregation degree of a sample, image processing is necessary to detect the assemblage of these SUs. For this work, the aggregation and dispersion mechanisms will always concern to the union or dispersion of SUs, not the individual RuO_2 and Pd-Te. Given that the average diameter size of the SUs measured by SEM in the glass

was ~ 50 µm [14], when the image processing detected larger SUs, it will be considered as a group of SUs, *i.e.* an aggregate.

The image treatment consisted in detecting the contours of these SUs so that they could be counted and characterized by the software (Figure IV-6c). Using the image analyzing, important characteristics of the sample were obtained, such as the total areas and positions of the SUs. Since they did not have a specific shape when grouped, the SUs were analyzed in terms of Féret characteristics (Figure IV-6d), where their diameters were calculated, as well as the perimeters, mass centers, positions and circularity. These properties obtained by image processing could be used as an approach for defining the aggregation degree of the samples as will be specified later on.

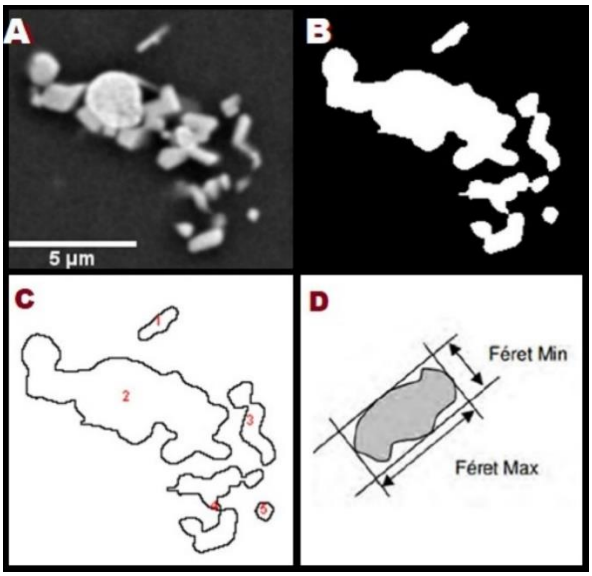

Figure IV-6 – Example of the image processing applied to the SEM images to identify the structural units of PGM particles: a) Raw image from SEM. b) The same image after processing with the Fiji program. c) Contours of the SUs after processing. d) An example of the Féret form.

Another advantage of the image treatment is the contrast created between the particles and the glass matrix by binarizing the mosaic. It produced useful way to visually analyze the aggregation degree of the samples. Figure IV-7 shows the mosaics for three samples: i) a sample with no agitation and without rotor (Figure IV-7a), ii) a sample without agitation and with rotor (Figure IV-7b), and iii) a sample equivalent to the pre-shear stage (Figure IV-7c). Based on a visual analysis, a difference in the PGM particle reorganization can be noticed when the rotor was removed from the crucible compared to when there is no rotor (Figure IV-7a and b). The withdraw causes a homogenization of the particles compared to the first scenario. At the same time, the pre-shear lead to a homogeneous dispersion of the SUs in the

glass matrix. Although removing the rotor can cause disruption in the PGM reorganization imposed on the sample, it does not produce more aggregation. The only homogenous state that can be considered for all the samples is the pre-shear since it can be imposed on all the crucibles before the measurements.

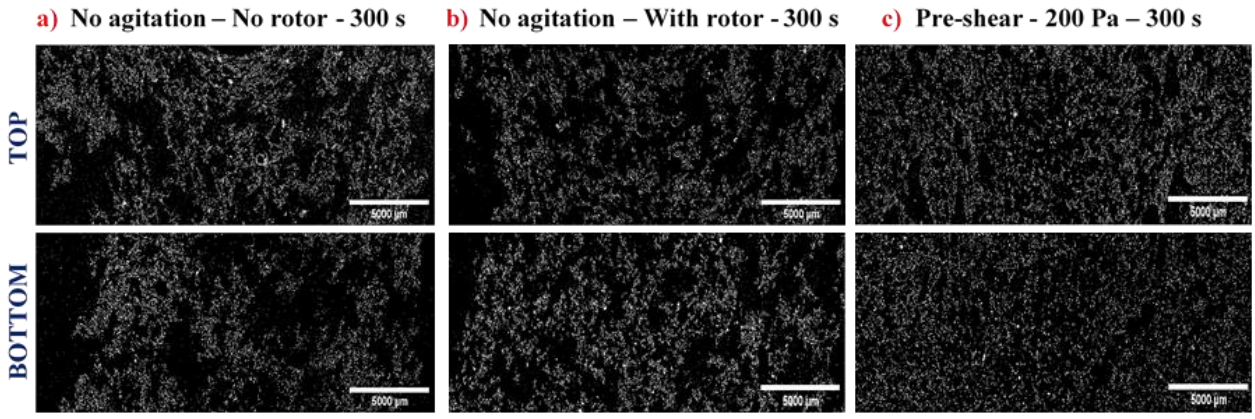

Figure IV-7 - SEM images of the top and bottom half of the samples, binarized via image processing. a) sample with no rotor and no agitation for 300 s, b) sample with the rotor and no agitation for 300 s, and c) sample submitted to the pre-shear of 200 Pa for 300s. Images b and c were obtained after removing the rotor.

Figure IV-8 shows an example of the mosaics obtained after image processing for samples subjected to a 5 Pa stress for three different durations (300, 1200, and 3600 s). In the images, the PGM SUs are shown in white (in green on the Cartesian representation) and the glass matrix is black (in white on the Cartesian representation). All samples started from a dispersed state after the pre-shear step (200 Pa for 300 s). As shown in Figure IV-8a, after 300 s at 5 Pa a slight rearrangement of the SUs started, but the sample was still homogenous compared to the pre-shear (Figure IV-7c). The PGM particles regroup more significantly after 1200 s, as shown in Figure IV-8b, where a large glass matrix area (black) is observed, separating the SUs in large groups. Furthermore, the top and the bottom of the crucible are more heterogeneous than the previous situation. For the last sample (5 Pa stress imposed for 3600 s), the sample is mostly aggregated and the difference between the top and bottom clearly indicates a sedimentation of the particles (Figure IV-8c). For all the stresses studied, image mosaics were made for each time step (300, 1200 and 3600 s), but the SU evolutions were different. This highlights different mechanisms. The aggregation kinetics were strongly influenced by the imposed stress and the forces acting in the melt. For stresses in a narrow range, these differences may be hard to distinguish using only SEM images. The surface percentage as a function of the SUs diameters was obtained via the image treatment for each sample as shown in the fourth column in Figure IV-8. Although it exemplifies the increase in the SUs diameter over time with a maximum size

of 200 μm at 300 s reaching 400 μm at 3600 s, the data is not enough conclusive in how aggregate the sample is. Hence, a numerical tool was necessary to deepen the analysis.

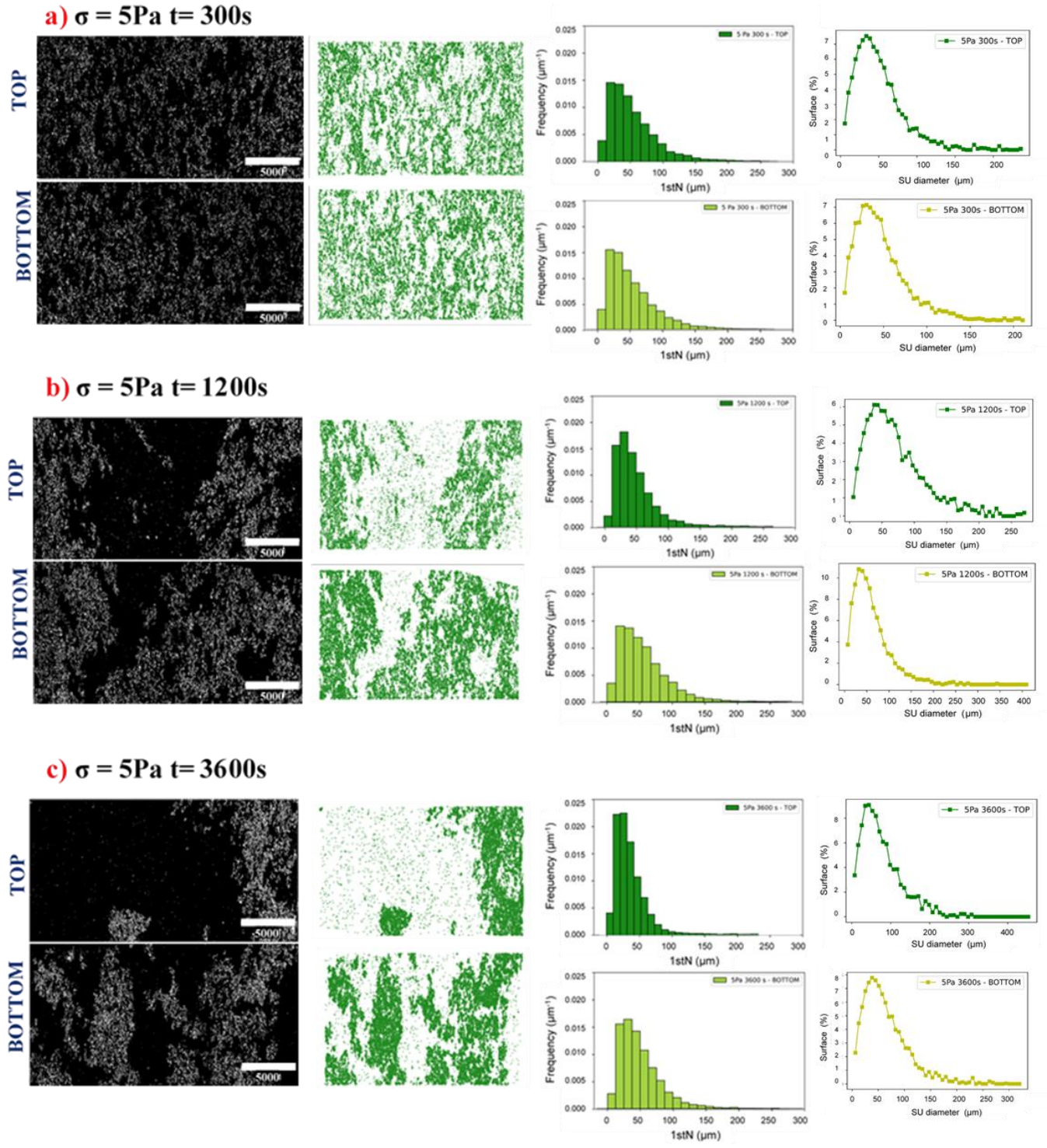

Figure IV-8 – Top and bottom data of the sample subject to 5 Pa stress for 3 different durations. SEM images (first column) binarized via image processing, along with their corresponding Cartesian representations (second column) of the PGM structural units positioning. Distance of the SUs to their first neighbor (1stN)as a function of their frequency of occurrence (third column) and the surface percentage as a function of the SU diameters (fourth column). Durations of the tests: a) 300 s b) 1200 s, and c) 3600 s.

3.3 Impact of time and shear stress on the aggregation degrees

A Python script was developed to post-process the treated SEM images, in order to quantify the aggregation and the macrostructural characteristics of the suspension. This script uses the Cartesian coordinates of the SUs in the images as input and aggregation parameters are obtained through spatial geometry calculations, in particular the average distance distribution of the SUs to their first neighbor (D1stN). This distance distribution provides an idea of the level of PGM rearrangement and gives information regarding the aggregation degree. In fact, the aggregates are formed by a grouping of SUs that do not necessarily touch one another. The script consists in three steps:

1. Reading the SU positions from the treated SEM image in a Cartesian plane (x,y), and plotting these points as shown in Figure IV-8 (microstructure in green).
2. Random selection of n SUs belonging to the plotted population of particles.
3. Calculation of the average distance distribution of the SU first neighbors (D1stN) among the chosen n points

The amount of SUs in each image was around 40000 for each of the experiments. In order to limit the computational effort required to evaluate such a large matrix, the calculations were based on n = 8000 random SUs. This value was chosen based on a compromise between the associated error and the required computation time. Since this random number is large enough to represent the whole sample, both aggregated areas and depleted areas in SUs were considered in the computation. The calculation was repeated five times for each image and the standard error associated was calculated. For each stress, two samples were produced from which two D1stN were calculated: one for the top (T) and one for the bottom (B) of the crucible. Figure IV-9a presents the results for the 5 Pa samples over time. The starting point for all the samples, *i.e.* t = 0, is the pre-shear. Therefore the D1stN was calculated for the top and the bottom of the crucible submitted to 200 Pa for 300s. As previously mentioned, when analyzing the 5 Pa images a difference was found between the top and the bottom of the crucibles, probably due to sedimentation effects. Nonetheless, the D1stN shows the same evolution in time for both parts of the crucible. If considering the aggregation shown in Figure IV-8 for the same samples, it is coherent that the distance decreases with time since the SUs are approaching each other. The longer the crucible is submitted to 5 Pa, the more the SUs rearrange to form larger and fewer aggregates.

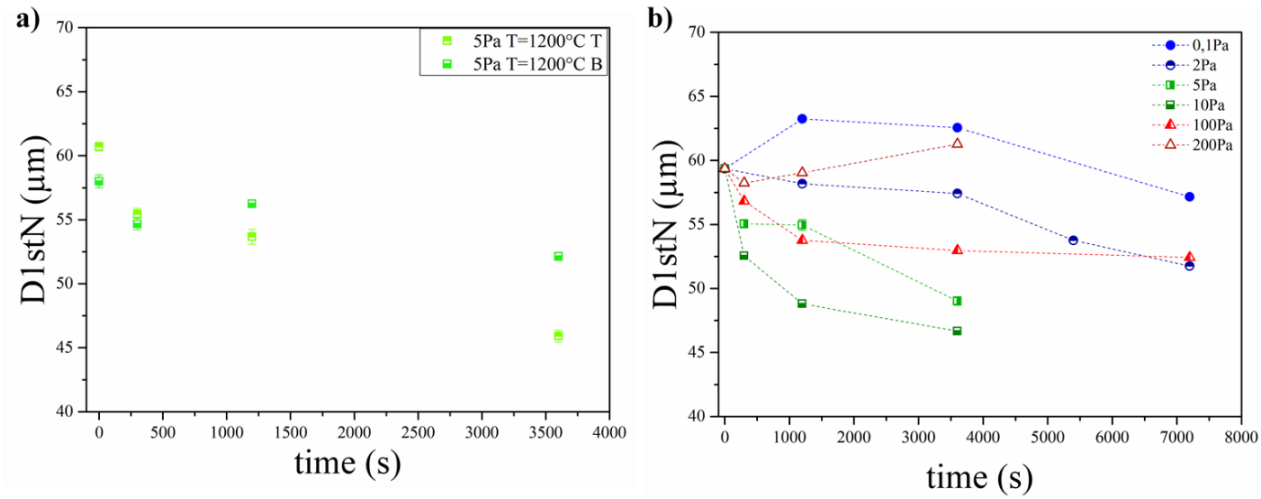

Figure IV-9- a) Average distance distribution of the SUs first neighbor for the 5 Pa samples as a function of time for the top (T) and the bottom (B) of the crucible. b) Average distance distribution of the SUs first neighbor for all the stresses studied as a function of time.

For all the samples analyzed, both top and bottom of the crucible exhibited the same tendency. The average D1stN was thus calculated for the two crucible parts to indicate the general behavior of the sample. In Figure IV-9b, the D1stN is shown as a function of the experimental time for all the experiments. All samples start from the pre shear. Firstly, a decreasing of the D1stN with time and with stress can be seen for stresses up to 10 Pa, with the exception of 0.1 Pa which firstly increases and then decreases after two hours under shear. For an imposed stress of 100 Pa, a fast decrease occurred first followed by a stabilization of the D1stN. Lastly, at 200 Pa, the D1stN value increased with time from the beginning of the experiment, and after 3600 s it reached a higher D1stN than the pre shear. By comparing these results with the obtained images, it can be concluded that different aggregation mechanisms govern the PGM particle behavior in the glass melt. The next section will explain these mechanisms in detail.

3.4 Aggregation mechanisms

As shown in Figure IV-4, the experiments can be separated into three different shear regimes: low shear (M1), medium shear (M2), and high shear (M3). They also represent the different aggregation mechanisms involved in the glass melt. Image analysis alone did not distinguish the aggregation kinetics that the material underwent at each imposed stress. By associating the images with the D1stN, a detailed situation becomes clearer. Figure IV-10 presents the average distance distribution of the SU first neighbors for all the stresses, in three separate groups. The distance value is normalized by the initial distance (D1stNm) (at time t = 1200 s for 0.1 Pa and 2 Pa, Figure IV-10a; and t = 300 s for the other stress values, Figure IV-10b and c) versus the

normalized time (t/t_m). t_m is the final experimental time for each situation investigated. The distance points are illustrated by the associated images produced via the Python code as described in section 3.2.

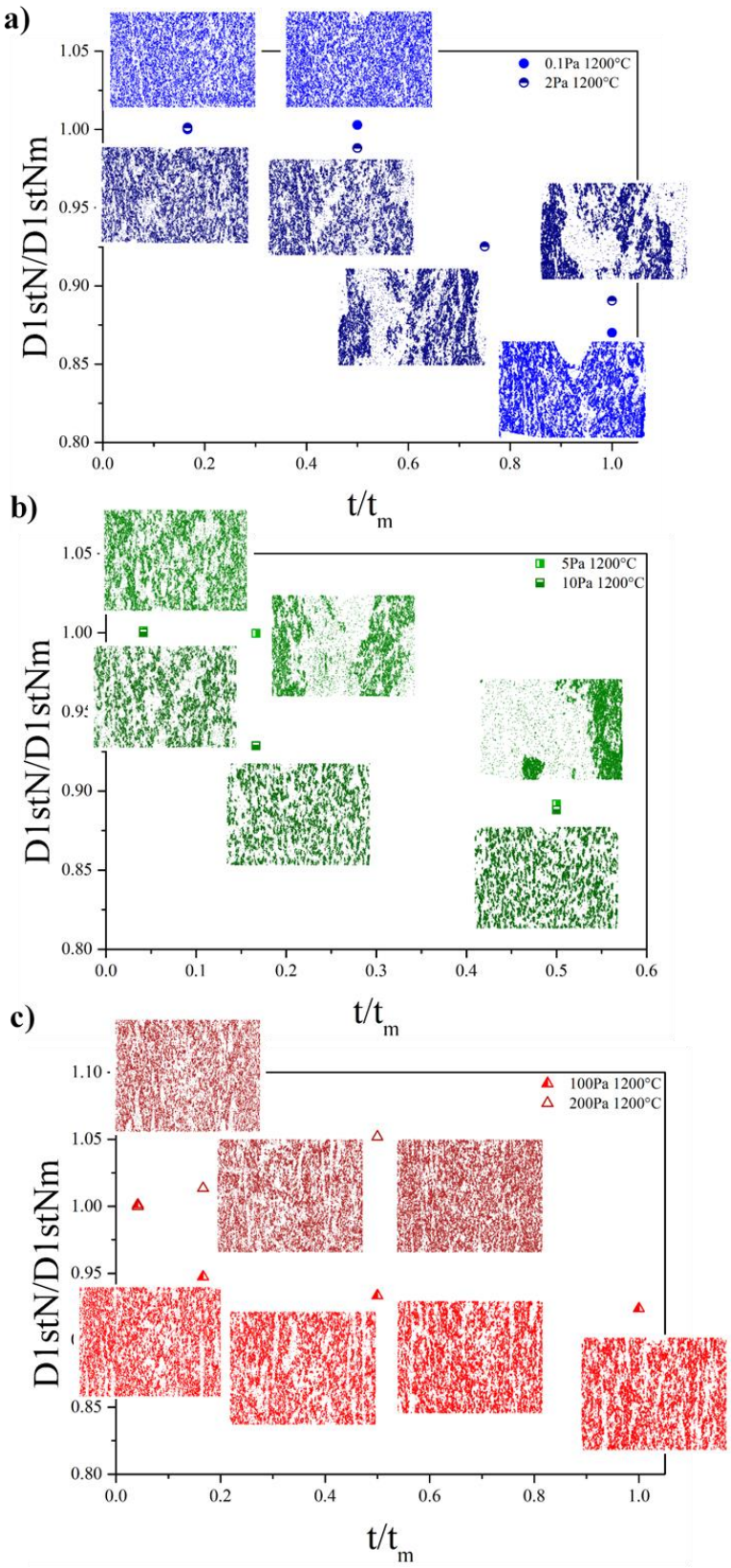

Figure IV-10 – Normalized D1stN as a function of the normalized time for all stresses studied, separated into three flow regimes, along with the Cartesian representation of the PGM structural unit positioning: a) low shear stress (M1), b) medium shear stress (M2) and c) high shear stress (M3).

To interpret the behavior, this discussion is based on the so-called DLVO (Derjaguin, Landau, Verwey, and Overbeek) theory [26], [27]. This theory was developed to explain the aggregation of aqueous dispersions. In the DLVO theory, aggregation of dispersed particles is explained by the interplay between the attractive van der Waals and the repulsive electrostatic double-layer force. Van der Waals forces between identical particles are always attractive and consequently promote aggregation, while electrostatic double-layer force stabilizes the dispersion, keeping identical particles apart. Their intensities do not depend on the external shear rate imposed by the rheometer. Thus once aggregation is taking place it can be seen that attractive forces predominate over repulsive ones. However, in the case studied here, the shear stress imposed by the rheometer generated hydrodynamic forces that, depending on their intensities, could either favor or prevent the aggregation of PGM particles, as will be shown next.

For the low shear stress regime (M1, Figure IV-10a), a decrease in the normalized D1stN with time can be noted for both stresses. In this regime, the hydrodynamic forces imposed by the rheometer are weak and not strong enough to push the particles away from each other, so that van der Waals attraction dominates in this situation. Therefore in the M1-scenario, SUs could undergo aggregation and large clusters were formed. Focusing on the images at $t/t_m = 1$ under low shear stresses, the sample at 2 Pa exhibits an obvious heterogeneity. This indicates that for this shear stress range, the low hydrodynamic forces promote collisions and favor aggregation. In this first regime, the higher the stress, the quicker the aggregation kinetics leading to a smaller distance between the SUs (D1stN). This rearrangement is correlated with the Newtonian plateau at low shear, which was observed in the steady state rheological tests (Figure IV-4). Particle-particle interactions that lead to aggregation have dramatic effects on viscosity, since the resulting aggregates are larger than individual particles and so immobilize some of the liquid phase, increasing their effective volume fraction. This results in a higher viscosity at low shear rates that increases with temperature despite the resulting decrease in the matrix viscosity [28][29].

Figure IV-10b shows the results for the medium shear stress regime (M2). This shear range is characterized by a decrease in viscosity with increasing shear stress when compared to the low shear regime M1. However, the same trend as the one previously described for the M1 regime can be observed: for a given shear stress, D1stN decreases with the run duration. Although the dependence is the same, the difference lies in the kinetics of the phenomenon. When the shear is increased above a critical stress, hydrodynamic forces increase enough to counteract the aggregation phenomena, controlled by Brownian diffusion. The shear stress imposed is not high

enough to completely disperse the SUs, but it enhanced the local reorganizations. Unlike the first mechanism, when the stress increased, the aggregate size reached after one hour decreased.

At a given shear stress or shear rate, the steady state is reached when a dynamical equilibrium is established between the breakdown and building of aggregates, leading to a mean equilibrium of the radius. The aggregate will reach its maximum equilibrium size at the maximum imposed stress that it can support without breaking [30]–[32]. This radius will decrease as the shear increases, and consequently the viscosity will also decrease. Even though the aggregates are smaller, the distance between SUs keeps decreasing. This is due to a competition between cohesive forces caused by the fluid and rupture forces caused by the flow [33].

The results concerning the third regime (regime M3) are presented in Figure IV-10c. This regime is also characterized by a Newtonian plateau at high shear on the steady state rheograms. Contrary to mechanism M1 explained earlier, in which aggregation dominates, at high shear flow scenarios, the hydrodynamics forces are higher than the interparticle forces controlling then the behavior of the suspension, leading to the rupture of the aggregates [34]. The distance between the SUs stabilizes over time at this range. As shown in Figure IV-10c, the PGM SUs are completely dispersed in the glass matrix. This dispersion leads to greater first neighbor distances for the SUs compared to the other regimes.

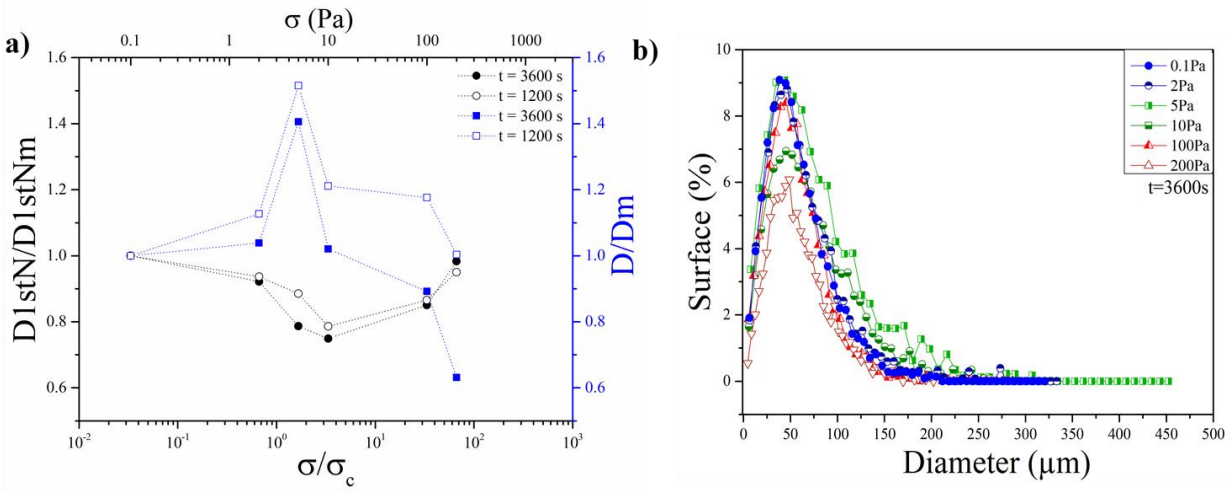

Figure IV-11 – a) Normalized D1stN and normalized Féret diameter (D) as a function of the normalized shear stress for experimental durations t = 3600 s and t = 1200 s. b) Surface percentage as a function of the SU diameters for all the 3600s-samples studied.

In order to analyze the overall impact of shear stress in the material aggregation degree, the three regimes were compared at two experimental durations for varying applied shear stress. Figure IV-11a shows the dependency of the normalized D1stN (D1stN/D1stNm) as well as the normalized Féret diameter (D/Dm) versus the normalized shear stress (σ/σ_c) at two different experimental times: t = 1200 s and t = 3600 s. The first neighbor distance was normalized by the initial value (D1stNm) of sample σ = 0.1 Pa and the mean diameter is normalized by the initial value (Dm) of sample σ = 0.1 Pa. The critical shear stress was chosen at the end of the first Newtonian plateau, σ_c = 3 Pa as shown in Figure IV-4. The distance to the first neighbor decreased with the stress for the low and medium shear flows. For both regimes M1 and M2, as previously mentioned, aggregation predominated, unlike the high shear regime (M3) for which the first neighbor distance started to increase again. Figure IV-12 shows the corresponding Cartesian representations for each case presented in Figure IV-11a. It can be seen that the particle aggregation increases with the shear stress up to 10 Pa; above 10 Pa, a further increase in the stress produced SU dispersion as shown in Figure IV-11a, even though images at 10, 100 and 200 Pa seem similar in Figure IV-12.

At this point, it is important to recall the definition of the structural units previously proposed. If we consider the SUs as small clusters composed of a few RuO_2 needles and Pd-Te spheres, the aggregates are clusters composed of SUs. Hence, the aggregates exhibit larger radii than the SUs. With image analysis, it was possible to extract the size of the SUs present in the sample, or more precisely their maximum Féret diameter. In Figure IV-11b, the surface percentage occupied by the SUs as a function of their diameters is plotted for all the 3600 s samples. At first, all samples show a similar size distribution. This confirms the SU hypothesis since all samples would have a majority of the surface occupied by small SUs of approximately 50 µm diameter dispersed in the matrix, corresponding to the average SU size previously measured by SEM in the glass [14]. It is paradoxically found that the average distance to the first neighbor at low and high shear scenarios are similar. However, it can be clarified by analyzing Figure IV-11b. For the medium and low shear stresses, contrary to the high shear stress regime, SUs present diameters greater than 300 and 450 µm, that is to say aggregates, can be observed. The same trend appears when the normalized mean diameter of the SUs (D/Dm) is plotted in Figure IV-11a as a function of the normalized shear stress for the 1200 and 3600 s experiments. After reaching a maximum size at 5 Pa the diameters drop, reaching a smaller SU size than at 0.1 Pa. Therefore, when comparing the D1stN for the low and high shear stress regimes, the values

correspond to the D1stN between aggregates and structural units, respectively. Even though the values are similar, for higher shear stresses, the structure is a collection of small SUs.

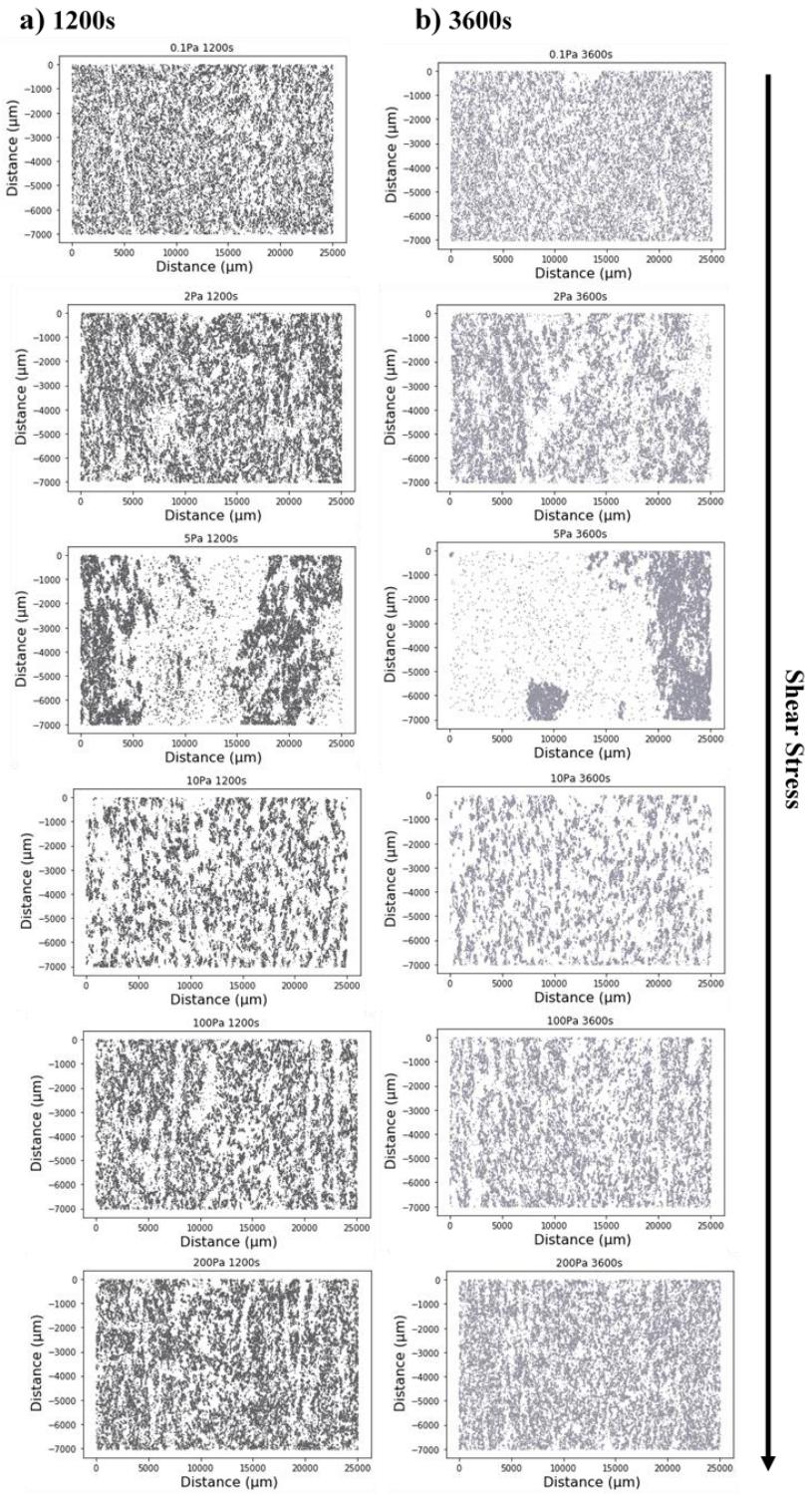

Figure IV-12 - Cartesian representations of the PGM structural units positioning in the top of the glass samples for all stresses at a) 1200 s and b) 3600 s.

3.5 Force balance and aggregation mechanisms

As mentioned earlier, the aggregation mechanisms studied in this work can be explained based on the DLVO theory [26], [27]. Although the three different mechanisms involve a balance between the forces acting on the material, for this work only two were considered: the hydrodynamic forces generated by the shear flow and the attractive van der Waals potential between the particles. It goes against the background of DLVO since double layer forces were ignored due to the difficulty in their evaluation [35][36]. Hydrodynamic and van der Waals forces were estimated through the relations provided by Allain *et al.* [35]. The hydrodynamic force was calculated as $F_H = \eta_f \dot{\gamma} R^2$, where η_f is the viscosity of the continuous phase, $\dot{\gamma}$ is the shear rate and R is the aggregate radius. For the van der Waals potential, the relation $F_{vdW} = \frac{\Lambda a}{12h^2}$, was considered, where Λ is the Hamaker constant, a is the particle radius and h is the mean distance between the particles.

Figure IV-13 shows the ratio between both forces as a function of $\dot{\gamma}/\dot{\gamma}_c$, where $\dot{\gamma}_c = \sigma_c/\eta_0$ is the critical shear rate at which the viscosity abruptly decreases (the critical stress σ_c and the low shear viscosity η_0 are indicated in Figure IV-4). The forces were approximated using the data obtained for the 3600 s experiments at all the shear stresses studied. To adapt the equations to experimental reality, the viscosity of the continuous matrix was considered as the viscosity of the simulated nuclear molten glass without PGM particles (η_f = 3.6 Pa.s) and the radius of the particles a as the mean size of the SUs ($a = 25\ \mu m$). The aggregate radius (R) and the mean distance between the particles (h) are the mean Féret radius of the SUs and the D1stN for the 3600 s experiments, respectively (shown in Figure IV-11a). Since there is a lack of information on the Hamaker constant for silicate melts in the literature, a range of values was scanned.

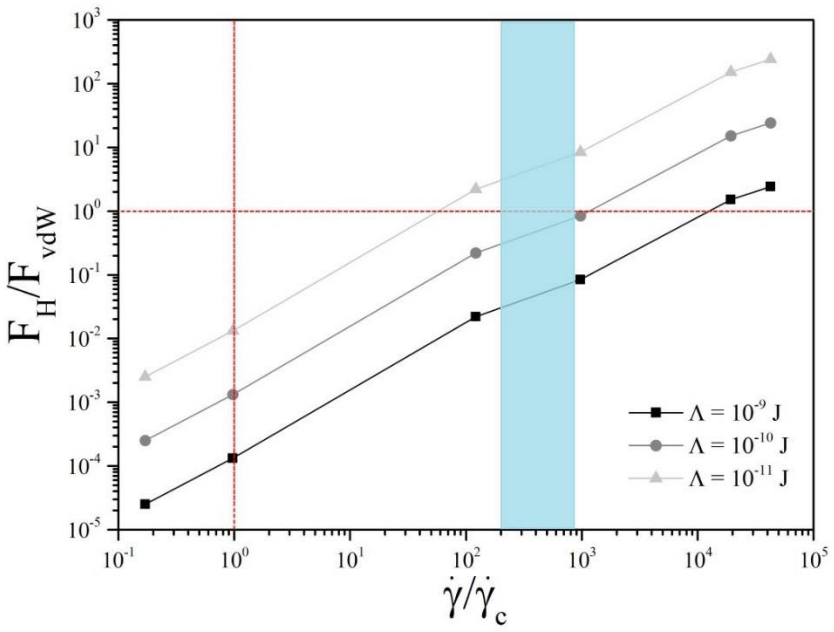

Figure IV-13 – The ratio between the hydrodynamic forces (F_H) and the van der Waals potential (F_{vdW}) as a function of $\dot{\gamma}/\dot{\gamma}_c$, for three different Hamaker constants. $\dot{\gamma}_c$ is the critical shear rate when the viscosity abruptly decreases.

When analyzing the graph, it can be seen that below the critical shear rate ($\dot{\gamma}/\dot{\gamma}_c \leq 1$), the van der Waals potential has a greater impact on the melt, as predicted for mechanism M1. For a shear above the critical value, the impact of the hydrodynamic force increases but the ratio F_H/F_{vdW} is still lower than one, indicating that hydrodynamic forces are not strong enough to break apart the aggregates completely and van der Waals attraction still dominates for particle reorganization in the melt. Hence the critical shear rate indicates only the limit between the two recognized rheological behaviors of the material (Newtonian and shear thinning). Note that the shear thinning behavior can be first induced by the orientation and organization of the aggregates and is not necessarily directly connected to the moment when the hydrodynamic forces surpass the binding forces between particles. Considering a Hamaker constant value between 10^{-10} and 10^{-11} J, the force balance corresponds to the hypothesis that the increase in the hydrodynamic forces and the beginning of the mechanism M3 occur when the shear is more than a hundred times the critical shear, corresponding to the shaded region of the graph. In terms of shear stress, it corresponds to more than 10 Pa, giving the smaller aggregates shown in Figure IV-12 that were formed after 3600 s due to the competition between the aggregation and dispersion of the SUs in the melt. It is important to stress that these Hamaker constant values are overestimated because the repulsive EDL force was neglected in the calculation. The introduction of this repulsive forces deserves a deeper investigation in the future.

4 Conclusions

The aggregation mechanisms of a simulated nuclear glass melt containing 3 wt.% of PGM particles were studied in this paper. The impact of the shear stress and time on the PGM particle aggregation degree was determined using a stress-imposed rheometer, working at high temperature, and an SEM image analysis method. Given the difficulties of in situ analysis at 1200 °C, a post-mortem approach was used after each sample was submitted at 1200 °C to different shear stresses and for different durations. These duration times were used to follow the evolution of the particles rearrangement with the viscosity, from the early stages of the regime to the steady state. For the same stress applied for different durations, the samples showed the same rheological behavior as a function of time, validating the reproducibility of the protocol implemented.

The image mosaics obtained for each sample were submitted to image analysis protocol in order to highlight the structural units (SUs) made of RuO_2 needles and Pd-Te spherical particles, and their distribution within the glass. This image analysis was an important tool to evidence the aggregation degree of each sample, highly influenced by the experiment time. Although visually the aggregation was clear, a numerical approach was developed in order to turn the distance between the first near neighbor of the SUs into a parameter to quantify the aggregation in each sample. The overall data showed that the PGM glass behaved in three different ways depending on the flow regime imposed *i.e.*, low, medium and high shear flow regime. An explanation of the three mechanisms has been proposed in this work.

The three mechanisms are differentiated by the intensity of the forces acting on the particles. For the first regime, a combination of the low hydrodynamics forces and van der Waals attractive forces on the PGM particles contributes to the aggregation phenomenon, translated by the decrease in the distance between SUs. It affects the viscosity by increasing the effective volume fraction, leading to a higher viscosity at low shear rates. At a medium flow, the same forces are acting on the particles, but in a different ratio than the low shear regime: the hydrodynamic forces also have an impact by enhancing local reorganizations but are not strong enough to dissipate the SUs in the glass. The viscosity decreases significantly, but aggregation still occurs, which is shows by the continuous drop in distance values. At high shear flow, the SUs are completely dispersed in the melt due to the effects of the hydrodynamic forces, leading to a greater distance between the SUs and a lower viscosity. The experimental challenges of observing the aggregation kinetics of PGM particles in a glass melt were overcome thanks to a

numerical approach that allows quantification of the evolution of aggregation and its impact to construct the general idea of what influences the phenomena. A balance between the hydrodynamic forces and the van der Waals potential was estimated using the data obtained to support our study's hypothesis. The information collected can be linked directly to the rheological behavior of the PGM glass, contributing to a deeper understanding of the material and consequently of the vitrification process.

5 References

[1] E. Vernaz, S. Gin, and C. Veyer, “Waste glass,” *Compr. Nucl. Mater.*, vol. 5, no. January, pp. 451–483, 2012, doi: 10.1016/B978-0-08-056033-5.00107-5.

[2] R. F. Taylor, “Chemical engineering problems of radioactive waste fixation by vitrification,” *Chem. Eng. Sci.*, vol. 40, no. 4, pp. 541–569, 1985, doi: 10.1016/0009-2509(85)80001-4.

[3] T. Akai, J. Nishii, M. Yamashita, and H. Yamanaka, “Chemical behavior of platinum-group metals in oxide glasses,” *J. Non. Cryst. Solids*, vol. 222, pp. 304–309, 1997.

[4] C. Hanotin, J. Puig, M. Neyret, and P. Marchal, “Platinum group metal particles aggregation in nuclear glass melts under the effect of temperature,” *J. Nucl. Mater.*, vol. 477, pp. 102–109, 2016, doi: 10.1016/j.jnucmat.2016.04.033.

[5] J. Puig, C. Hanotin, M. Neyret, and P. Marchal, “High temperature rheological study of borosilicate glasses containing platinum group metal particles by means of a mixer-type rheometer,” *J. Nucl. Mater.*, vol. 469, pp. 112–119, 2016, doi: 10.1016/j.jnucmat.2015.11.053.

[6] C. Simonnet, A. Grandjean, and J. Phalippou, “Electrical behavior of platinum-group metals in glass-forming oxide melts,” *J. Nucl. Mater.*, vol. 336, no. 2–3, pp. 243–250, 2005, doi: 10.1016/j.jnucmat.2004.09.019.

[7] R. B. Nuernberg, N. M. P. Machado, M. Malki, and M. Neyret, “Electrical behavior of RuO2-glass composites: The effect of RuO2 particle size on the percolation threshold,” *J. Nucl. Mater.*, vol. 546, p. 152777, 2021, doi: 10.1016/j.jnucmat.2020.152777.

[8] W. Grünewald, G. Roth, W. Tobie, K. Weiß, and S. Weisenburger, “The role of the platinum group elements ruthenium, rhodium and palladium in the vitrification of radioactive high level liquid waste using joule heated ceramic lined waste glass melters,” *Glas. Technol. Eur. J. Glas. Sci. Technol. Part A*, vol. 49, no. 6, pp. 266–278, 2008.

[9] F. Pacaud, C. Fillet, and N. Jacquet-Francillon, “Effect of platinoids on French LWR reference glass properties,” *Mater. Res. Soc. Symp. Proc.*, vol. 257, no. 3, pp. 161–167, 1992.

[10] R. B. Nuernberg, N. M. P. Machado, D. Jouglard, L. del Campo, M. Malki, and M. Neyret, “The origin of hysteresis in the electrical behavior of RuO2-glass composite melts,” *J. Non. Cryst. Solids*, vol. 557, no. February, 2021, doi:

10.1016/j.jnoncrysol.2020.120596.

[11] L. Pereira *et al.*, "A Feedback Mechanism Between Crystals and Bubbles in a RuO2-Bearing Melt," *J. Non. Cryst. Solids*, 2022, doi: 10.1016/j.jnoncrysol.2022.121456.

[12] K. Uruga, T. Usami, T. Tsukada, S. Komamine, and E. Ochi, "Viscoplasticity of simulated high-level radioactive waste glass containing platinum group metal particles," *J. Nucl. Mater.*, vol. 452, no. 1–3, pp. 419–424, 2014, doi: 10.1016/j.jnucmat.2014.05.062.

[13] J. Puig, B. Penelon, P. Marchal, and M. Neyret, "Rheological Properties of Nuclear Glass Melt Containing Platinum Group Metals," *Procedia Mater. Sci.*, vol. 7, pp. 156–162, 2014, doi: 10.1016/j.mspro.2014.10.021.

[14] B. Luckscheiter, "Properties and behavior of the platinum group metals in the glass resulting from the vitrification of simulated nuclear fuel reprocessing waste," *J. Mater. Res.*, vol. 6, no. 12, pp. 2535–2546, 1991, doi: 10.1557/JMR.1991.2535.

[15] Y. Yue and R. Brückner, "A new description and interpretation of the flow behaviour of glass forming melts," *J. Non. Cryst. Solids*, vol. 180, no. 1, pp. 66–79, 1994, doi: 10.1016/0022-3093(94)90398-0.

[16] F. Babick, *Suspensions of Colloidal Particles and Aggregates*, vol. 20. Dresden, Germany: Springer International Publishing, 2016.

[17] C. Bower, C. Washington, and T. S. Purewal, "The use of image analysis to characterize aggregates in a shear field," *Colloids Surfaces A Physicochem. Eng. Asp.*, vol. 127, no. 1–3, pp. 105–112, 1997, doi: 10.1016/S0927-7757(96)03945-3.

[18] A. Kurokawa, V. Vidal, K. Kurita, T. Divoux, and S. Manneville, "Avalanche-like fluidization of a non-Brownian particle gel," *Soft Matter*, vol. 11, no. 46, pp. 9026–9037, 2015, doi: 10.1039/c5sm01259g.

[19] S. Deboeuf, N. Lenoir, D. Hautemayou, M. Bornert, F. Blanc, and G. Ovarlez, "Imaging non-Brownian particle suspensions with X-ray tomography: Application to the microstructure of Newtonian and viscoplastic suspensions," *J. Rheol. (N. Y. N. Y).*, vol. 62, no. 2, pp. 643–663, 2018, doi: 10.1122/1.4994081.

[20] T. Advocat, J. L. Dussossoy, and V. Petitjean, "Vitrification des déchets radioactifs et appareillage," *Les Tech. l'Ingénieur*, vol. 33, pp. 0–27, 2008.

[21] M. Bousmina, A.-S. Chrissemant, L. Choplin, A. Aït-Kadi, and P. Marchal, "Quantitative Analysis of Mixer-Type Rheometers using the Couette Analogy," *Can. J. Chem. Eng.*, vol. 80, no. December, pp. 1166–1174, 2010, doi: 10.1002/cjce.5450800618.

[22] Bousmina M.; A. Aït-Kadi and J.B. Faisant, "Determination of Shear Rate and Viscosity from Batch Mixer Data: Theoretical and Experimental Results," *J. Rheol*, vol. 43, p. 1999, 1999.

[23] W. L. Wang, J. Q. Bi, K. N. Sun, M. Du, N. N. Long, and Y. J. Bai, "Thermal shock resistance behavior of alumina ceramics incorporated with boron nitride nanotubes," *J. Am. Ceram. Soc.*, vol. 94, no. 8, pp. 2304–2307, 2011, doi: 10.1111/j.1551-2916.2011.04658.x.

[24] O. Delattre, E. Régnier, S. Schuller, M. Allix, and G. Matzen, "Image analysis study of crystallization in two glass compositions of nuclear interest," *J. Non. Cryst. Solids*, vol. 379, pp. 112–122, 2013, doi: 10.1016/j.jnoncrysol.2013.07.029.

[25] J. Fournier-Renaud, "Cinétiques de dissolution des cristaux dans les silicates fondus – contexte des verres nucléaires," Université Montpellier, 2017.

[26] B. Derjaguin and L. Landau, "Theory of the stability of strongly charged lyophobic sols and of the adhesion of strongly charged particles in solutions of electrolytes," *Prog. Surf. Sci.*, vol. 43, no. 1–4, pp. 30–59, 1993, doi: 10.1016/0079-6816(93)90013-L.

[27] C. E. Marshall, "'Theory of the stability of lyophobic colloids. The interaction of particles having an electric double layer.' E. J. W. Verwey and J. T. G. Overbeek, with the collaboration of K. van Ness. Elsevier, New York-Amsterdam, 1948, 216 pp.," *J. Polym. Sci.*, vol. 4, no. 3, pp. 413–414, Jun. 1949, doi: 10.1002/pol.1949.120040321.

[28] W. R. Richmond, R. L. Jones, and P. D. Fawell, "The relationship between particle aggregation and rheology in mixed silica-titania suspensions," *Chem. Eng. J.*, vol. 71, no. 1, pp. 67–75, 1998, doi: 10.1016/S1385-8947(98)00105-3.

[29] D. Quemada, "Rheological modelling of complex fluids: II. Shear thickening behavior due to shear induced flocculation," *EPJ Appl. Phys.*, vol. 2, no. 2, pp. 175–181, 1998, doi: 10.1051/epjap:1998170.

[30] H. A. Barnes, *A Handbook of Elementary Rheology*. The University of Wales- Institute of Non-Newtonian Fluid Mechanics, Department of Mathematics, Avaiable online,

2000.

[31] D. B. Genovese, “Shear rheology of hard-sphere, dispersed, and aggregated suspensions, and filler-matrix composites,” *Adv. Colloid Interface Sci.*, vol. 171–172, pp. 1–16, 2012, doi: 10.1016/j.cis.2011.12.005.

[32] P. Snabre and P. Mills, “Rheology of concentrated suspensions of viscoelastic particles,” *Colloids Surfaces A Physicochem. Eng. Asp.*, vol. 152, no. 1–2, pp. 79–88, 1999, doi: 10.1016/S0927-7757(98)00619-0.

[33] V. A. Tolpekin, M. H. G. Duits, D. Van Den Ende, and J. Mellema, “Aggregation and breakup of colloidal particle aggregates in shear flow, studied with video microscopy,” *Langmuir*, vol. 20, no. 7, pp. 2614–2627, 2004, doi: 10.1021/la035758l.

[34] S. Herminghaus, *Wet Granular Matter*, vol. 6. WORLD SCIENTIFIC, 2013.

[35] C. Allain, M. Cloitre, and F. Parisse, “Settling by cluster deposition in aggregating colloidal suspensions,” *J. Colloid Interface Sci.*, vol. 178, no. 2, pp. 411–416, 1996, doi: 10.1006/jcis.1996.0135.

[36] F. E. Torres, W. B. Russel, and W. R. Schowalter, “Floc structure and growth kinetics for rapid shear coagulation of polystyrene colloids,” *J. Colloid Interface Sci.*, vol. 142, no. 2, pp. 554–574, 1991, doi: 10.1016/0021-9797(91)90086-N.

Chapter V

Sedimentation of PGM particles in a glass melt

As mentioned before, the glass containing PGM particles is likely to endure, during the different process operations, not only aggregation but also sedimentation of the suspended particles. The previous chapter explored the aggregation mechanisms of a simulated nuclear glass melt containing 3.0 wt% (1.02 vol%) of PGM, determining the impact of the shear stress and time on PGM aggregation degree. By reconsidering the samples at different degrees of aggregation studied earlier, Chapter V addresses the sedimentation of the PGM particles at 1200 °C, which is correlated to the different aggregation mechanisms. An estimated sedimentation rate is calculated and the impacts of shear stress and time on the particles settling is explored.

Norma Maria Pereira Machado; Muriel Neyret; Cécile Lemaître; Philippe Marchal.

In process of submission in Journal of Nuclear Materials

Abstract

In order to immobilize nuclear fission products issued from spent fuel reprocessing, a high-temperature vitrification process (1200 °C) is adopted. Most of the species contained are in a calcined solution as they react chemically with the vitrification additives to form a homogeneous glass melt. Some exceptions, such as the Platinum Group Metal particles (PGM) are not incorporated chemically in the melt and are present as suspended particles of a few microns. The presence of these metals and their tendency to aggregate and settle has an impact on the rheological properties of the material and is the object of characterization and modeling of many studies. The PGM bearing melt presents a shear-thinning and thixotropic behavior. In the present work, the particles sedimentation kinetics is investigated in a simulated nuclear glass melt containing 3.0 wt% of PGM. Samples from a previous study with different aggregation degrees obtained at 1200 °C via a post-mortem approach were analyzed. The impact of the shear stress and time on PGM sedimentation is determined by analyzing images obtained via Scanning Electron Microscopy (SEM). A quantification of the particles sedimentation over time is proposed. The interplay between sedimentation and aggregation is presented considering the first order expression proposed by Allain *et al*. for diluted systems. Based on the experimental data, the sedimentation velocity of the PGM particles is estimated for the three identified different aggregation scenarios. This work provides a new input for the modeling and control of particles sedimentation.

Keywords: Melt, Platinum Group Metals (PGM), Sedimentation, Rheology.

1 Introduction

The efficiency of the high temperature vitrification process to immobilize high-level radioactive waste has made it the standard conditioning treatment in France. In the back end of the "closed" nuclear fuel cycle, after the passage in the reactor, the spent nuclear fuel is reprocessed and the high-level waste is disposed [1,2]. This remaining waste is conditioned in a glass matrix in a two steps process that combines the calcination of the nitrates salts of the waste and the mixture with the glass frit to feed the melter, generating a complex amorphous material that contains around 40 different elements [3,4]. However, some elements from the waste are insoluble in the nuclear glass melt, such as the Platinum Group Metals (PGM: RuO_2, Pd, Rh). These elements are found as alloys of palladium and tellurium in a spherical form (1 to 5 μm) alongside with needle-like ruthenium oxide particles (~10 μm).

The presence of these suspended elements affects directly the physicochemical characteristics of the melts such as their electrical and rheological properties [5–7]. Previous studies have also shown that the PGM particles have a strong tendency to aggregate and sediment leading to the formation of high volume fraction layers at the bottom of the crucible that interfere with the process even in small amounts (3 wt%) [7–9]. Thus, an understanding of the effects of these particles on the material is essential to control the process. In particular, the rheological behavior of the melt can be strongly influenced by the particles aggregation kinetics. Although studies on the rheological behavior of glass melts containing PGM particles are contemplated, they are limited due to the difficulties linked to the required very high temperatures [10]. Nonetheless, authors explored the increase of the melt viscosity in the presence of the PGM particles, as well as a non-Newtonian behavior of the material [5,7,8,11,12].

The work conducted by Puig *et al*. and Hanotin *et al*. not only evidenced the shear thinning and thixotropic behavior of the material but also associated the dynamics of aggregation and disaggregation to the rheological behavior as a function of the particles content and the temperature [5,12]. The two Newtonian plateaus that the system presents are linked to the formation of macroscopic PGM aggregates induced by Brownian motion associated to attractive forces at low shear rates and to the destruction of these same aggregates with the increase of hydrodynamic forces at high shear rates [12]. Due to the interplay of different forces, at low shear rates, an increase of temperature lowers the viscosity of the matrix but favors aggregation leading to an increase of the overall viscosity of the suspension. In contrast, at high shear rates, the system behaves as a suspension of small clusters and individual particles and its

viscosity decreases by increasing temperature since it is then essentially controlled by the viscosity of the matrix [5]. The phenomenological modeling of the system gathers crucial information on the overall aggregation kinetics in the system even though it lacks in understanding the impact of time and shear rate on particles reorganization and settling.

Sedimentation occurs when a solid particle is placed in a fluid in which the whole system is subjected to a field exerting an unbalanced distribution of forces [13]. It is often the gravity field that gives rise to sedimentation, if the particles and the fluid present different densities. In particular, gravity effects have to be taken into account when dealing with complex structures as aggregates, since, depending on the forces compensating gravity and on the values of the characteristic times for aggregation and settling, a wide variety of situations can be encountered [13,14]. The literature dealing with PGM particles sedimentation in a glass melt is limited due to the difficulty of investigating the phenomenon at high temperature or formulating alternative equivalent suspensions exhibiting similar rheological behavior at customary temperatures. Nonetheless, some studies were carried out to model and predict the settling velocities of these particles, linking the creation of clusters in the bottom of the crucible to previous aggregation followed by settling in the vitrification of liquid radioactive waste. However these studies assumed an absence of stirring [15,16]. Puig *et al*. observed as well the settling of PGM particles in a glass melt but under low shear rate; they found that the settling rate was increased compared to a system without shearing Considering that aggregation is favored under low shear rate, aggregates grow bigger over time, which accelerates sedimentation [17]. A deeper investigation of the coupling of aggregation with sedimentation is then necessary to provide a full analysis of the glass melt behavior.

In this context, the present work aims to investigate the sedimentation kinetics in a simulated glass melt containing 3 wt% of PGM particles at 1200 °C. The impact of the shear stress and time on PGM particles settling is investigated using techniques, such as rheometry and image analysis, that where adapted to face the very high temperatures encountered. Samples with different aggregation degrees obtained via a post-mortem approach, described in chapter IV, are analyzed. Each sample was first submitted to a different shear stress for a certain time interval and then quenched, so that the PGM particles rearrangement could be investigated. The impact of the shear stress and shearing time on sedimentation was studied and a quantification over time was performed. Based on the work of Allain *et al*. [18] dealing with settling in diluted systems, the sedimentation velocity of the PGM particles is estimated and the interplay between

sedimentation and aggregation over a wide shear stress range is underlined. This work provides then a new input for the modeling and control of particles sedimentation.

2 Experimental Procedure

2.1 Materials

In the present study, a simulated nuclear glass elaborated on the full-scale pilot unit installed at CEA Marcoule was considered [19]. The archetypal composition of this glass containing 3 wt% of PGM particles is shown in Table V-1. The elaboration process consisted in two steps: a calcification followed by a vitrification at 1200 °C, using the indirect induction technology. The glass was cooled at room temperature and, to guarantee the examination of a representative sample of the glass, the studied samples were extracted from the middle of the canisters after the process. PGM particles appear in the glass as needles of 10 µm for RuO_2, while Pd-Te alloys appear as spherical particles with diameter ranging from 1 to 5 µm.

Table V-1 - Chemical composition of the nuclear glass samples containing 3 wt% of PGM particles.

Glass 3 wt% PGM									
SiO_2 (wt%)	B_2O_3 (wt%)	Na_2O (wt%)	Al_2O_3 (wt%)	Alkali metal oxides (wt%)	Alkaline earth metal oxides (wt%)	Rare earth oxides (wt%)	RuO_2 (wt%)	Pd (wt%)	Others (wt%)
43.7	13.2	9.2	4.2	3.3	5.0	7.0	1.8	1.2	11.4

2.2 Rheological measurements

In order to assess the settling of PGM particles, samples with different aggregation degrees obtained from a previous study (Chapter IV- Experimental Method) were analyzed. The different degrees were generated by submitting the samples to several shear stress values during different time intervals at 1200 °C (Table V-2), followed by a fast cooling of the sample to "freeze" the particles rearrangement for further image analysis. The high temperature experimental apparatus used for this work is showed in Figure V-1 [12].

Table V-2 - Operating conditions (shear stress level and duration) for the 20 performed experiments.

Stress (Pa)	**Durations (s)** (All samples were first pre-sheared at 200Pa for 300s)				
0.1	-	1200	3600	-	7200
2	-	1200	3600	5400	7200
5	300	1200	3600	-	-
10	300	1200	3600	-	-
100	300	1200	3600	-	7200
200	300	1200	3600	-	-

The equipment consists of a stress-imposed rheometer (Rheometrics Scientific SR5000) above a tubular furnace that can be heated up to 1500 °C. As shown in Figure V-1a, the rheometer is connected to the furnace through a specific tool that ensures the transmission of the torque to the rotor. The characterization cell consists of an alumina crucible (diameter, height, and wall thickness equal to 27, 40, and 2 mm respectively) previously filled with glass, located in the center of the furnace. The rotor is composed of a multiblade geometry connected to a 30 cm long rod (Figure V-1b). Considering the tendency of the PGM particles to settle, a geometry that prevents sedimentation was specifically designed to insure an uniform distribution of the suspended particles and analyze their effects during the whole experiments [5]. For these experiments, disposable alumina crucibles were adopted, so that the frozen charged glass and crucible could be cut at the end of the experiment in order to analyze the PGM distribution in the glass.

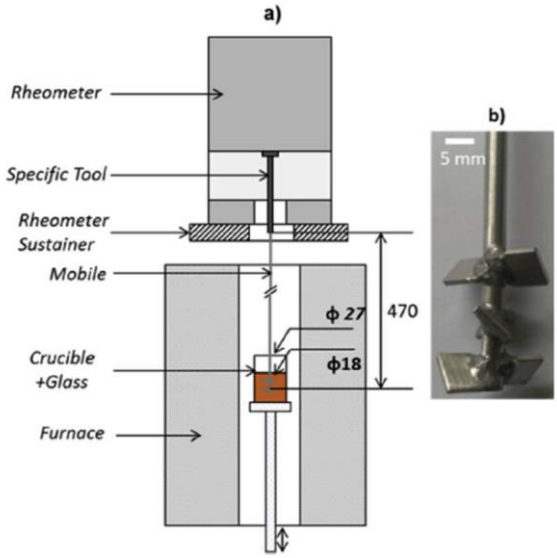

Figure V-1 - a) High temperature rheological experimental set-up (dimensions in mm), b) Multiblade rotor [12].

The instrumental parameters, torque (C) and angular velocity (Ω), are linked to the shear stress (σ) and shear rate ($\dot{\gamma}$) through two geometrical factors K_σ and $K_{\dot{\gamma}}$:

$$\sigma = K_\sigma \, C \qquad\qquad \dot{\gamma} = K_{\dot{\gamma}} \, \Omega$$

To determine K_σ and $K_{\dot{\gamma}}$, the mixing device (multiblade + crucible) has been calibrated via a Couette analogy leading to K_σ = 8.79 10^4 ± 4.10^2 Pa N^{-1} m^{-1} and $K_{\dot{\gamma}}$ = 2.1 ± 0.01 rad^{-1} with an equivalent annular gap of 4.5 mm [20,21]. A complete description of the equipment and calibration procedure was provided in Puig *et al* [12]. Since the goal was to understand the

temporal evolution of the PGM distribution under shear, the measurements were carried out in transient regime by imposing different steps of shear stress to each sample during different time intervals. Seeking an identical initial state for all samples, a pre-shear was systematically applied at 200 Pa during 300 s in order to disperse completely the PGM particles in the glass melt. The shear stress steps ranged from 0.1 to 200 Pa and the time intervals from 300 to 7200 s, as shown in Table V-2. The criteria to choose the different stress/duration combinations are explained in the previous chapter (Chapter IV). Each stress/duration pairs corresponds to a different experiment and to a new crucible, totaling finally twenty different experiments. The crucible is located on an alumina holder that comes out from the bottom of the furnace. A compromise was determined in order to get a quick temperature drop and to prevent a thermal shock at the same time during the descent. To guarantee the reproducibility of the rheological tests, the removing velocity of the rotor from the crucible and the descending velocity of the crucible were the same for all tests and were, respectively 8 $mm.min^{-1}$ and 2 $cm.min^{-1}$. The cooling rate was 35 $°C.min^{-1}$ so that no significant changes in the particles rearrangement were expected due to the rapid increase of the glass viscosity induced by the temperature drop. To relieve residual internal stresses introduced during the cooling and avoid breakage during the sample preparation, the glass was submitted to an annealing at 580 °C for 2 h followed by a slow cooling at 10 $°C.h^{-1}$ until room temperature was reached.

2.3 Sample preparation

Figure V-2 exemplifies the protocol that was chosen to prepare the samples for microscopy analysis. After the annealing, the crucibles were filled with epoxy resin and cut vertically with a circular diamond saw in two halves to allow the observation of the PGM distribution in the glass. The halves were cut again horizontally and covered with epoxy resin to fit and to facilitate its support in the SEM measurement cell. Each crucible produces two samples (P1 and P2) corresponding to the top and bottom of the crucible. Theses samples were polished and coated with a thin film of carbon for SEM analysis. The second half of the crucible was kept apart, in the case further characterizations were needed.

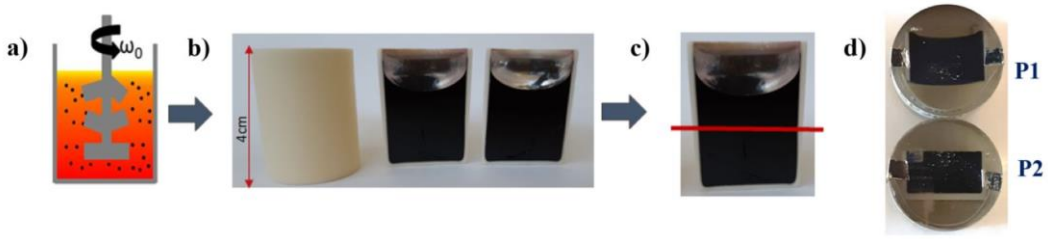

Figure V-2 - Samples preparation protocol: (a) the glass melt in the alumina crucible is sheared for a certain time. (b) After annealing, the crucible is cut vertically, (c) and then cut again horizontally, yielding two samples for each crucible, (d) one from the top (P1) and one from the bottom (P2).

2.4 Scanning Electron Microscopy (SEM) imaging

To have a complete vision of the particles reorganization in the glass after the rheological measurement, the samples were investigated using Scanning Electron Microscopy (SEM). The analysis were performed using a Zeiss Supra 55 FEG. An image of a representative area of each sample was reconstructed from a mosaic of small images automatically acquired using the commercial SEM software. To ensure a standardization of the procedure, the same rectangular region of each crucible was chosen for all experiments. A final area of 3.75 cm² was selected for each sample, corresponding to almost 90 % of its total area filled with glass (neglecting the alumina walls of the crucible). Each image that composes the mosaic was acquired in BSE mode under a magnification of x 45, a voltage of 15 kV and a 1024 × 768-pixel resolution. Each mosaic contained an average of 120 images, with an acquisition time of 10.3 s/image. A compromise was necessary between image capturing time and resolution due to the size of the sample. The Fiji software was used for imaging processing of all mosaics. The methodology of image acquisition and treatment was derived from crystallization studies involving image analysis found in the literature [22,23].

3 Results and Discussion

3.1 Generation of different aggregation degrees – particles settling

As mentioned earlier, the particles settling is linked to particles aggregation. Hence, the first step of the present work consisted in analyzing the samples for which different aggregation degrees were achieved. Based on the steady state measurements of the glass with 3.0 wt% of PGM at 1200 °C, six different shear stresses along with different experiment durations were selected, leading to twenty different aggregation degrees, as indicated in Table V-2. The choice of these specific values is further explained in Chapter IV. All samples were analyzed via SEM

and images were extracted from the top and bottom of each crucible, as explained in section 2.4. The RuO_2 needles and the Pd-Te spheres are rarely found separately in the melt. They are generally combined in small groups forming structural units (SU) which may in turn aggregate with other SUs (Figure V-3a). Hence, considering the importance to highlight the particles aggregates in the study, the obtained SEM images follow afterward an image treatment so that these individual SUs are detected (Figure V-3b). The image treatment consists in detecting the contours of these SUs that are then counted and characterized by the software (Figure V-3c). This treatment also allows to obtain important characteristics of the sample such as the amount of SUs, the total area and position of the SUs, through image analysis. Since they do not have a specific shape when grouped, the SUs are analyzed as in terms of Féret characteristics (Figure V-3d), such as the SUs diameter, as well as their perimeter, mass center, position, and circularity. These properties are used to characterize not only the aggregation degree of each sample but also as tools for analyzing the overall particles settling.

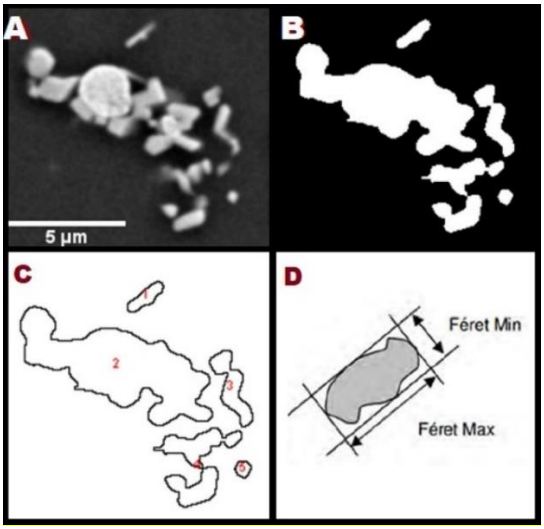

Figure V-3 - Example of the image treatment applied to the SEM images to identify the structural units of PGM particles: a) Raw image from SEM. b) Same image after treatment with the Fiji program. c) Contours of the SUs after treatment. d) An example of the Féret form.

One of the steps of the image treatment is the creation of a contrast between the suspended PGM particles (white) and the glass matrix (black) by binarizing the mosaic. It produces a resourceful way to analyze the results by a visual approach of the particles distribution in each sample. As mentioned earlier, the applied protocol involved *ex-situ* measurements for which reproducibility was proven in Chapter IV. Thus, even though each combination of time and stress was correlated to a different crucible, *i.e.* a different experiment, a straightforward temporal analysis could be adopted to interpret the obtained results. Considering this approach,

the imaging of the top and bottom of the crucibles were analyzed after image treatment. The complete image mosaic of the samples at low, medium and high shear stress ranges are presented, respectively, in Figure V-4, Figure V-5 and Figure V-6. All samples started from a dispersed state after a strong pre-shear (200 Pa during 300 s). As shown in Figure V-4a, b, c for the samples subjected to 0.1 Pa, the difference in the particles distribution over time is only significant after 7200 s of experiment (Figure V-4c), but the top and the bottom of the crucible remain homogeneous and no difference is noticed in the particles fraction. For the samples subjected to 2 Pa, after 3600 s (Figure V-4e) a rearrangement of the particles is noticed, indicating a more aggregated state of the PGM particles. Moreover, a heterogeneity of the top and the bottom of the crucible and an expressive glass matrix area (black) in the upper part is noticed after 7200 s (Figure V-4g), which is a visual sign of particles settling. At this shear stress range, the hydrodynamic forces imposed by the rheometer are not strong enough to push the particles away from each other. Hence, the van der Waals attraction dominates in this situation leading to particles aggregation over time [5]. At the same time, the long periods under low shear stress contributes for the particles to start to settle [15].

Figure V-5 shows the image mosaics for the experiments conducted at 5 Pa and 10 Pa. Differently from what was noticed for lower shear stresses, a difference between the top and the bottom of the crucible is already noticed after 1200 s when submitted to 5 Pa (Figure V-5b). After 3600 s under 5 Pa (Figure V-5c) the sample is completely aggregated and most of the top of the crucible present a large empty area indicative of PGM particles sedimentation. On the other hand, the sample submitted to 10 Pa (Figure V-5d, e and f) seems homogeneous for the three studied periods, even though earlier studies showed that aggregation occurs. At this medium stress range, the imposed shear stress is not high enough to disperse completely the particles but it enhances the local reorganizations at a different kinetics from that determined at low shear stresses. Hence, the visual analysis is not efficient enough to identify aggregation nor the settling of particles. For the third set of SEM images (Figure V-6), corresponding to samples subjected to high shear stresses (100 and 200 Pa), the images show that the particles are completely and homogeneously dispersed in the crucible for all studied durations. It is indicative of a lack of aggregation and makes it difficult to detect sedimentation.

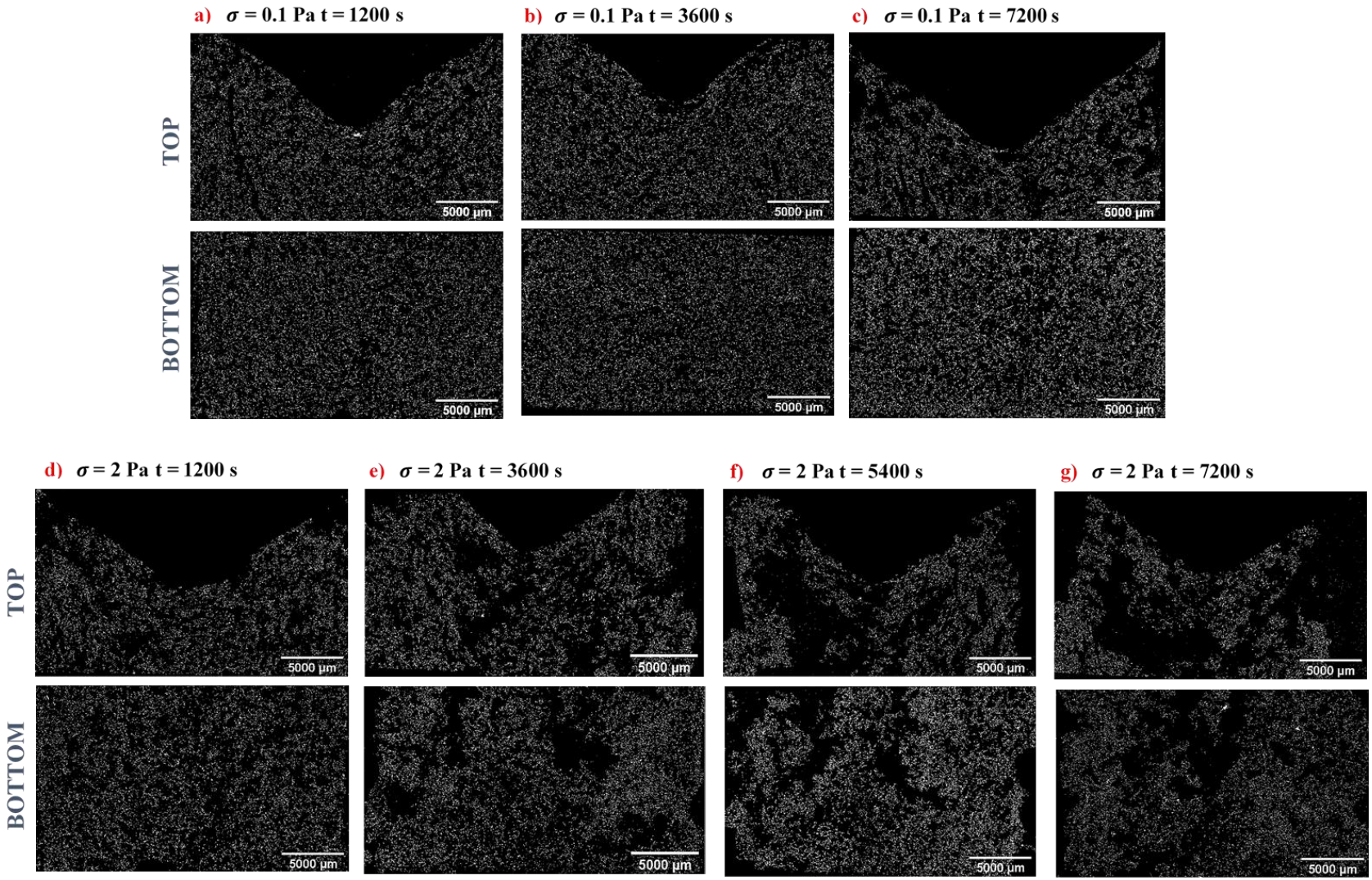

Figure V-4 - Top and bottom SEM images of the samples subject to 0.1 and 2 Pa stress for different durations, binarized via image treatment. Duration of the tests for the 0.1 Pa samples: a) 1200 s, b) 3600 s, and c) 7200 s. Duration of the tests for the 2 Pa samples: d) 1200 s, e) 3600 s, f) 5400 s, and g) 7200 s.

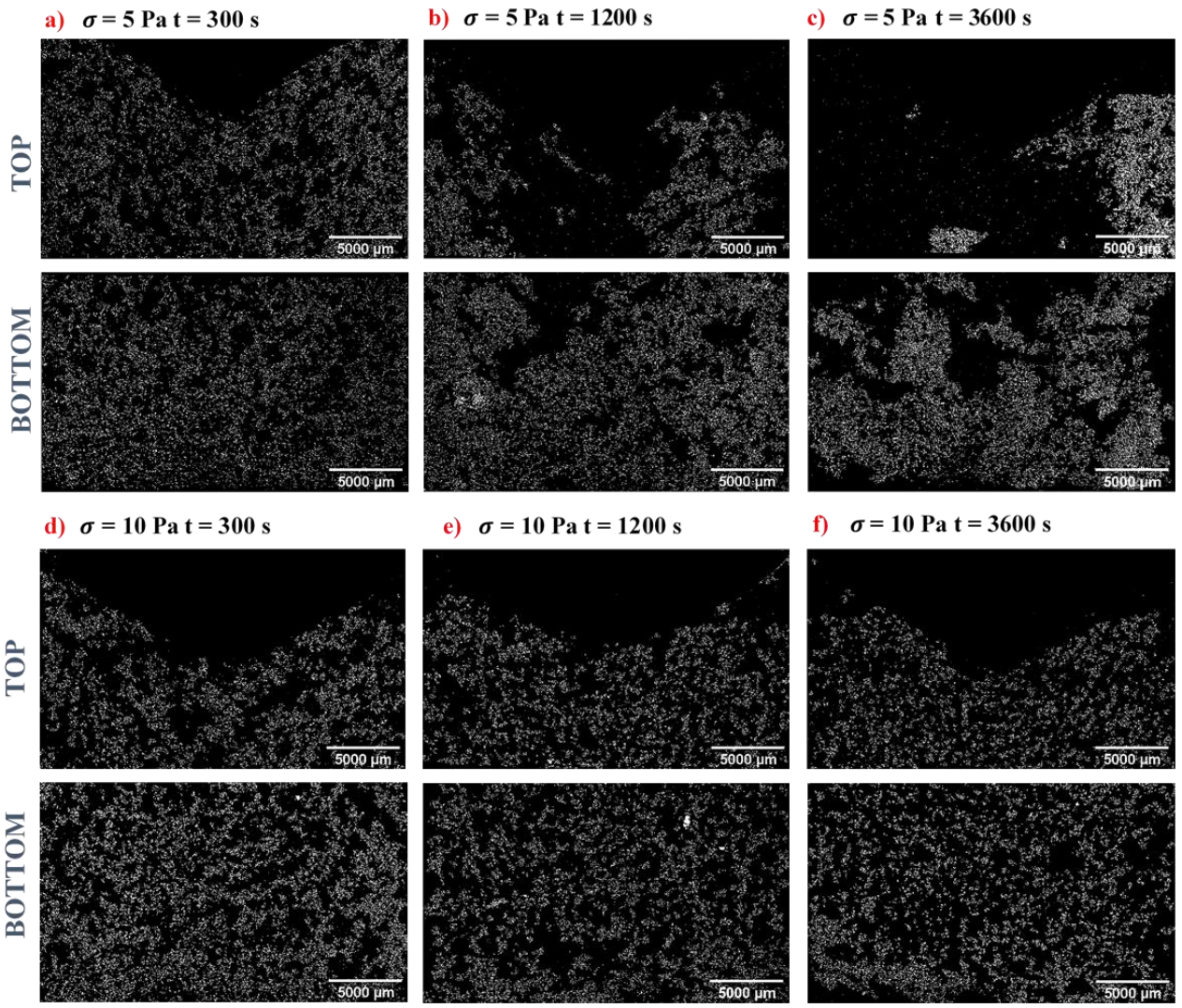

Figure V-5 - Top and bottom SEM images of the samples subject to 5 and 10 Pa stress for different durations, binarized via image treatment. Duration of the tests for the 5 Pa samples: a) 300 s, b) 1200 s, and c) 3600 s. Duration of the tests for the 10 Pa samples: d) 300 s, e) 1200 s, and f) 3600 s.

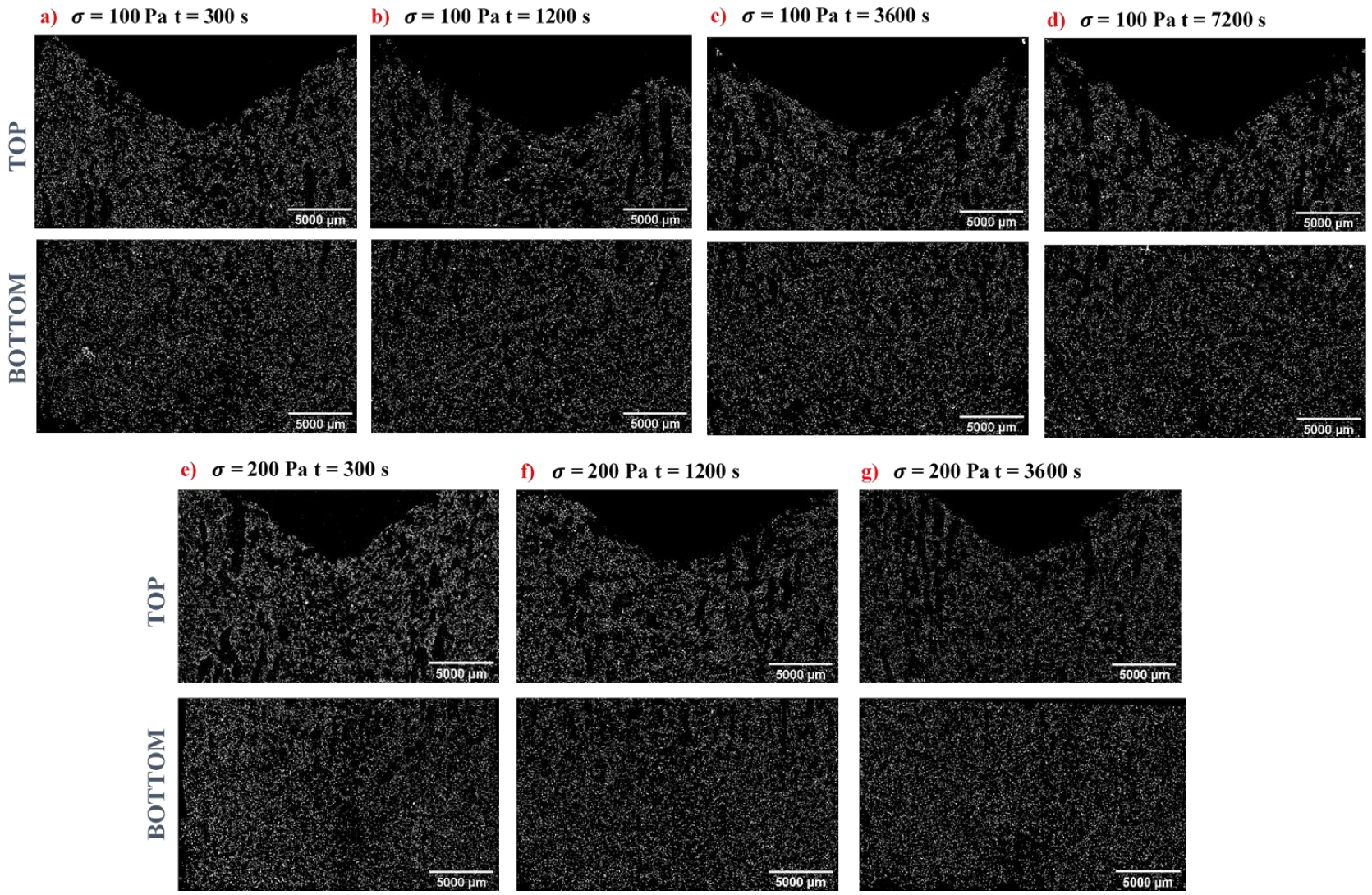

Figure V-6 - Top and bottom SEM images of the samples subject to 100 and 200 Pa stress for different durations, binarized via image treatment. Duration of the tests for the 100 Pa samples: a) 300 s, b) 1200 s, c) 3600 s, and d) 7200 s. Duration of the tests for the 200 Pa samples: e) 300 s, f) 1200 s, and g) 3600 s.

As explained in section 2, the images were taken from different crucibles for each experiment but they seem as if they originate from the same sample observed at different times. Considering the difficulties related to high temperature experiments, this approach helps understanding the impact of time on the rearrangement of the PGM particles. Nonetheless, the method highlights the phenomena when they are significant enough. Otherwise, when examining samples in a close stress range, the effects of time and stress on PGM aggregates may be hard to distinguish using only an imaging tool. Hence, a numerical approach is necessary to deepen the analysis.

3.2 Analysis of particles sedimentation

The SEM images indicate that over time the settling of the PGM particles in the crucible might occur at different scales depending on the shear stress imposed to the sample. However, a quantitative method can inform not only on the occurrence of particles settling but also on its intensity. Considering the *ex-situ* approach involved in this work, one of the possible methods to quantify particle settling is to compare the difference in particles fraction between the top and the bottom of the crucible over time. The image treatment that was performed allows the characterization of the particles by counting the SUs or aggregates in each sample, as explained in earlier sections. Since all the samples were initially subjected to a pre-shear at high shear stress, they all started from the same dispersed state, as represented in Figure V-7 at t_0. At this point, the number of SUs counted in the top (N_T) and the bottom (N_B) is the same due to a homogenous agitation of the melt. Is important to emphasize that both parts of the analyzed crucible have the same surface, which equalizes their particles fraction. For the samples agitated at t_i, where $i > 0$, in case of particle sedimentation, N_T will decrease while N_B will increase with time.

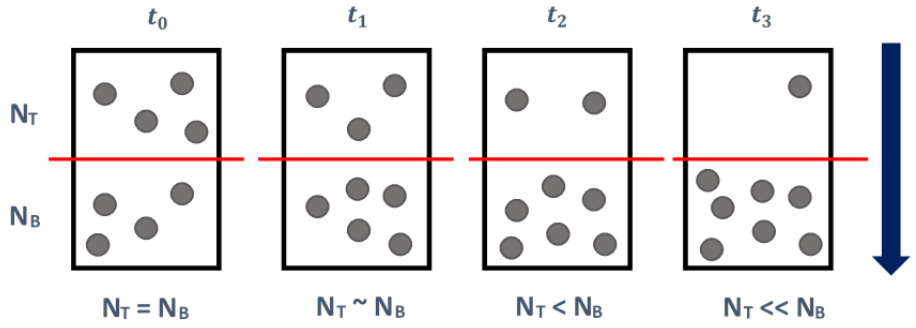

Figure V-7 – Scheme showing the evolution of the SUs number at the top (N_T) and bottom (N_B) of each crucible for a certain shear stress at successive times, starting from a homogeneous distribution at t_0.

Based on the difference between both parts of the crucible, a percentage *P* of particles settled from the top to the bottom could be calculated for each experiment. Assuming that the pre-shear establishes an equal division between the particles in the bottom and the top of the crucible, we consider that each part contains 50% of SUs. Hence, *P* is calculated as presented in Eq. (1), which can be read as the percentage of PGM that settled from the top of the crucible over time, normalized by the total amount of particles in the whole crucible.

$$P = 50 - \left(\left(\frac{N_T}{N_T + N_B}\right).100\right) \quad (1)$$

The percentage of settled SUs for all studied shear stresses over time is presented in Figure V-8. The obtained data gives an overview on the sedimentation intensity of PGM particles over time for each stress range. For the high shear stress range, the difference between top and bottom of the crucible is negligible since for all studied times P remains constant and close to zero for the samples stirred at 100 and 200 Pa. On the other hand, for low and medium shear stresses, a difference is noticeable, especially for the samples submitted to 5 Pa in which, after 1 h, almost 35 % of PGM particles have settled down from the top to the bottom of the crucible. This significant sedimentation is consistent with the observations made by comparing the SEM images, which also presented a strong difference between top and bottom for the samples at 5 Pa. For the low shear stress regime, the sedimentation is also noticeable, reaching 15 % for the 2 Pa samples, but it is not obvious at 0.1 Pa. One hypothesis to explain these differences between flow regimes is the impact that aggregation can have on sedimentation. The weight of the clusters being the driving force of the settling, bigger aggregates will sediment faster than smaller ones. Hence, the sedimentation kinetics is correlated to aggregation. Different models, combining the effects of aggregation and sedimentation to estimate the particles settling velocity, are described in the literature [13,18,24]. In particular, the next section will explore the conditions in which the glass containing PGM particles may follow the mechanism proposed by Allain *et al.* [24] when aggregation and settling are coupled.

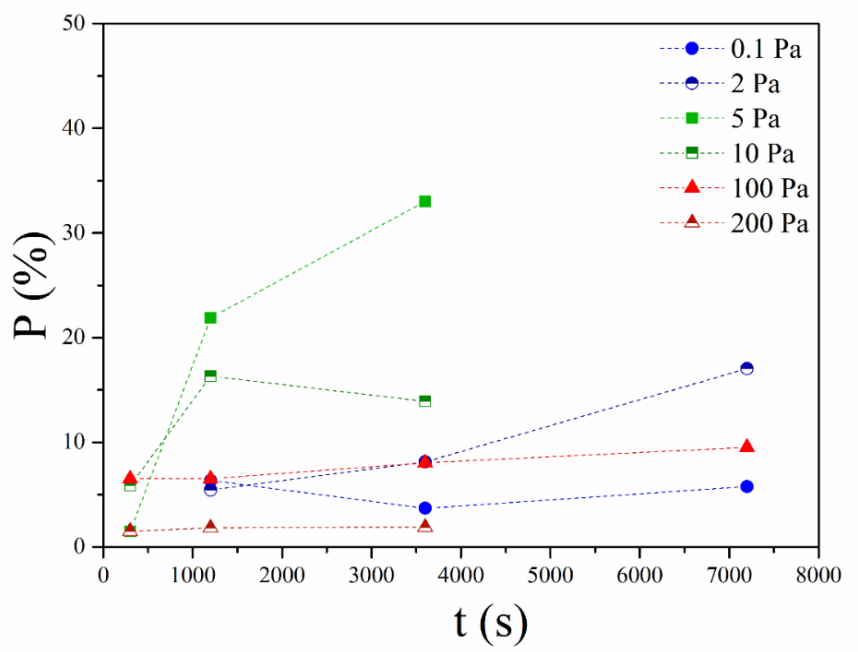

Figure V-8 – Percentage of settled SUs over time for all studied stresses, considering as a start point an equal repartition of particles between both parts of the crucible.

3.3 Sedimentation mechanism

PGM particles sedimentation over time was both, visually and numerically, presented in earlier sections. However, the kinetics at which this phenomenon occurs is not clear. The sedimentation can be complex to investigate in a suspension due to the interactions between particles which influence their settling [13]. Therefore, to establish the settling mechanism it is important to investigate the parameters that impact the particles and their velocity in the melt. At low shear stresses, a combination of weak hydrodynamic forces and attractive van der Waals interactions contributes to a diffusion-limited aggregation of PGM particles over time, as presented in Chapter IV. At medium shear stresses, although the same forces act on the particles, the hydrodynamic forces promote local reorganizations but are not large enough to disperse the SUs. On the contrary, at high shear stresses, particles are completely dispersed in the system due to the effects of hydrodynamic forces. Therefore, as soon as the shear stress is low enough to allow SUs aggregation but large enough to carry the aggregates, they can interact with each other and grow over time.

Considering the effects of gravity, when the SUs reach a certain size, their Brownian motion becomes negligible and they start to sediment. According to Allain *et al.* [24], the settling kinetics of a suspension, in which the aggregation and sedimentation are coupled, is highly dependent on the volume fraction of the particles. For a system with a low volume fraction, the

aggregates will sediment individually, differently from systems of larger solid fractions where a sedimentation front is created [14]. The aggregates formed by the action of van der Waals forces grow until they reach a maximum hydrodynamic radius, beyond which their size does not increase anymore, corresponding to the equilibrium between attractive and hydrodynamic forces [13]. When the aggregates size is lower than this maximum radius, their sedimentation velocity varies according to their radius, following a power law [18]. Since the system is subjected to a homogenous shear promoted by the multi-blade rotor and has a low effective volume fraction of PGM particles ($\varphi_{eff} << 1$) [5], the creation of a sedimentation front is less probable and was not observed in the SEM images (Figure V-4, Figure V-5 and Figure V-6). So, considering the glass melt with PGM particles as a diluted system, the sedimentation velocity (U) can be calculated using the following expression [18]:

$$U = \frac{2}{9}\frac{(\rho_p - \rho_f) g a^2}{\eta_f}\left(\frac{R}{a}\right)^{D_f - 1} \quad (2)$$

where ρ_p is the density of the particles; η_f and ρ_f are the continuous matrix viscosity and density respectively; g is the gravity constant, a the individual particle radius, R the hydrodynamic radius of the aggregate and D_f their fractal dimension. To apply Eq.(2) to PGM suspensions, the viscosity and density of the continuous matrix were considered to be that of the simulated molten glass without PGM particles (η_f = 3.6 Pa.s and ρ_f = 2736 kg.m^{-3}); ρ_p the average density of the PGM particles (ρ_p = 8212 kg.m^{-3}) and the radius of the particles a as the mean size of the SUs (a = 25 µm). The aggregate radius (R) were taken as the mean Féret radius of the SUs, that were obtained for all the studied samples (top and bottom) via the image treatment described in section 3.3. The fractal dimension (D_f) reflects the internal structure of the aggregate and depends on the mode of aggregation [25].

Two main types of "Cluster-Cluster" growth mechanisms may exist: DLCA (Diffusion-Limited Clusters Aggregation) and RLCA (Reaction-Limited Clusters Aggregation). For the DLCA mechanism, the aggregation kinetics is limited by the time that the aggregate takes to diffuse in the medium towards another particle or another aggregate, which leads to a small fractal dimension (D_f ~ 1.7). On the other hand, for the RLCA mechanism the aggregation kinetics is not limited by diffusion but by the time needed for the aggregate to form a bridge, leading to a higher fractal dimension (D_f~ 2.1) [26]. Both mechanisms could occur in the systems considered in the present study, depending on the conditions. Indeed, the applied shear stress

affects the aggregation mechanisms *i.e.*, the force balance to which the PGM particles are submitted. Therefore, three D_f values were chosen between 1.7 and 2.2 (1.76, 1.97 and 2.16). The impact of the shear stress and experiment duration on the settling velocity is explored in the next section.

3.4 Impact of time and shear stress on the settling velocities

Three different aggregation mechanisms of the PGM particles were presented in Chapter IV. They were based on a force balance between attractive van der Waals and hydrodynamic forces imposed by the rheometer, each mechanism corresponding to a different shear stress regime: low, medium and high. By considering the particles sedimentation dependence to the aggregation, the SUs sedimentation velocity (*U*) as a function of time was calculated for a representative shear stress of each one of these mechanisms (Figure V-9) using Eq.(2). *U* was calculated for the top and bottom of each crucible, considering three different fractal dimensions (D_f) values for the aggregates. For all three scenarios, the settling velocity is impacted by the shear stress since the hydrodynamic forces impact directly the aggregates size and so the effects of gravity on the settling process.

The first proposed aggregation mechanism occurs at low shear stress where the Brownian diffusion and the attractive forces between the particles combined with weak hydrodynamic forces promote the SUs reorganization, forming bigger clusters over time. The sample at 2 Pa exhibits a blatant heterogeneity only after 7200 s under shear, as shown in Figure V-4f and g, indicating that for this shear stress range, the low hydrodynamic forces promote collisions and favor aggregation. The resulting aggregates are larger than individual particles and so immobilize some of the liquid phase, increasing their effective volume fraction, having then a direct impact on the rheological behavior of the sample. At low shear rates the melt has a higher viscosity that increases with temperature despite the resulting decrease of the matrix viscosity [5,27,28]. The increase of the SUs radius leads to an increase of *U* over time, as shown in Figure V-9a. Nonetheless, the velocity does not increase rapidly with time, indicating a slow sedimentation kinetics at this shear regime. The difference between the velocities at the top and bottom of the crucible is an indication of the sedimentation of SUs, creating clusters with larger radii over time, which increases the bottom settling velocity.

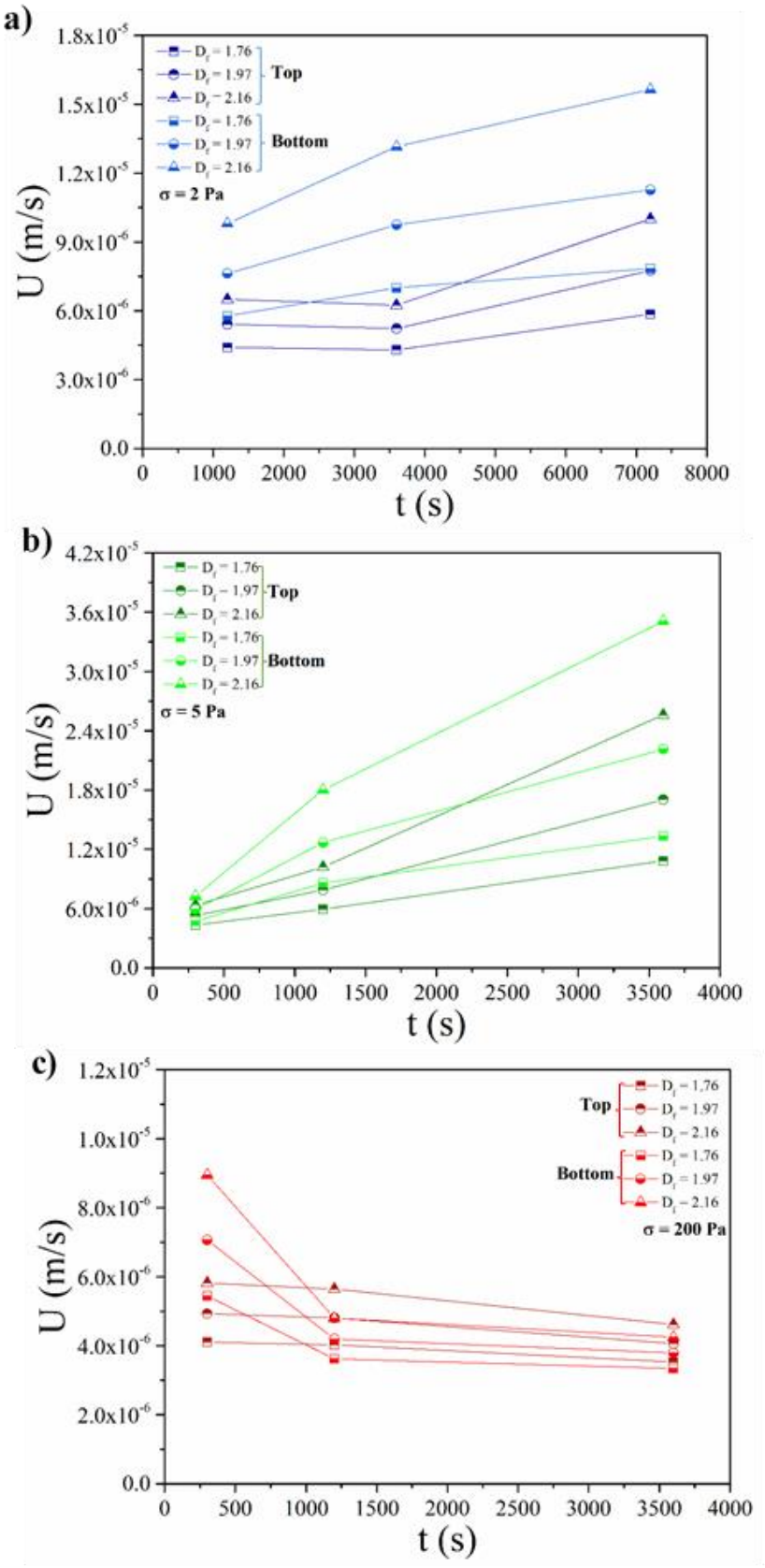

Figure V-9 – Sedimentation velocity (U) calculated for different fractal dimension values (D_f: 1.76, 1.97 and 2.16) in fonction of time for the top and bottom of the samples submitted to different shear stresses: a) 2Pa; b) 5 Pa and c) 200Pa.

Figure V-9b shows the calculated *U* for the sample subject to 5 Pa shear stress, representing the second aggregation mechanisms at medium shear stress. This shear range is characterized by the same trend as the one previously described for the first regime: for a given shear stress, *U* increases with increasing experiment duration. Although the dependence is the same, after 3600 s, the settling velocity of the sample reaches more than five times its value at 300 s and two times the maximum *U* obtained for the 2 Pa sample. The rapid increase of the aggregates radius impacts directly the kinetics of the phenomenon. The difference between the top and the bottom of the sample is more evident than at 2 Pa, which is in agreement with the SEM images shown in Figure V-5b and c where the heterogeneity between the top and bottom samples increases over time both in terms of aggregation and sedimentation. Considering Eq. (2), when the sedimentation dominates the Brownian motion, a collecting effect starts with the bigger aggregates settling faster and absorbing smaller ones, leading then to faster growth which determines the aggregation rate [14]. This phenomenon explains the rapid increase of the sedimentation rate for the 5 Pa sample.

The results concerning the third studied regime (200 Pa sample) are presented in Figure V-9c. For high stress flow, contrarily to both previous mechanisms, the hydrodynamic forces are higher than the van der Waals and double layer forces. Therefore, the behavior of the suspension is controlled by the hydrodynamic forces, leading to the rupture of the aggregates [29]. The sedimentation velocity *U* drops and then stabilizes at a low value for both the top and bottom of the sample. As shown in Figure V-6e, f and g, the PGM SUs are completely dispersed in the glass matrix. For high shear regime, not only the smaller clusters will settle slowly but also will remain suspended in the crucible, leading to a decrease in the difference between the top and the bottom. This regime is also characterized by a Newtonian plateau at high shear on the steady state rheograms, as shown in Chapter IV.

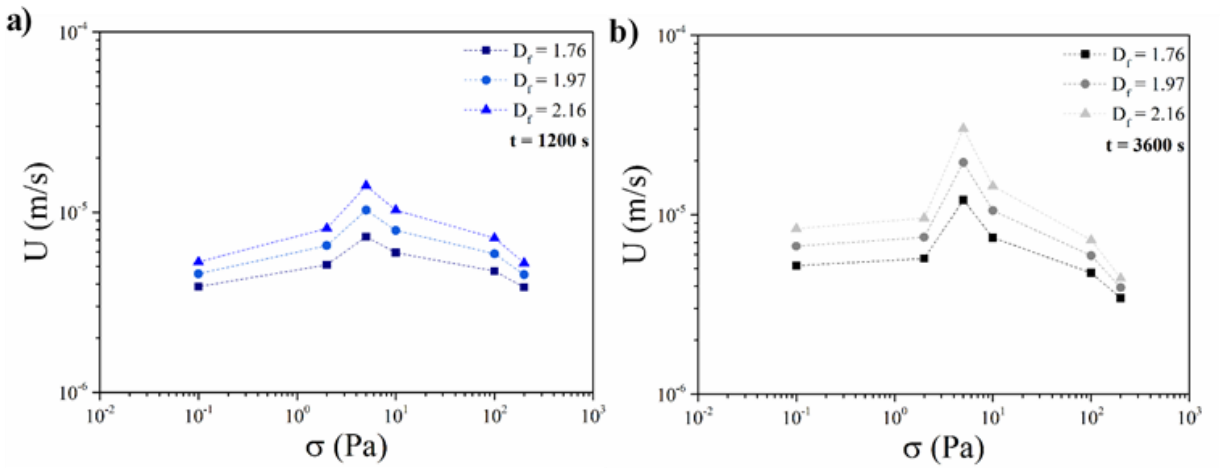

Figure V-10 - Sedimentation velocity (*U*) calculated for different fractal dimension values (D_f: 1.76, 1.97 and 2.16) in fonction of shear stress for the mean radius of each sample submitted to a) 1200 s and b) 3600 s run duration.

Considering the impact of time on the settling velocity, all studied samples were analyzed for two experimental durations: 1200 and 3600 s (Figure V-10). The evolution of *U* with the shear stress was calculated considering the mean radius of the SUs for each sample. Figure V-10a and b show that, the longer the sample undergoes low or medium shear stress, the larger are the aggregates and the higher is the settling velocity. On the contrary, at high shear stress, the longer the sample is subject to shear, the more the SUs are dispersed in the melt and the slower is their settling. For both studied durations (Figure V-10a and b), the sedimentation velocity increases with the shear stress until reaching its maximum size at 5 Pa, *i.e.*, as previously observed in Chapter IV. This maximum size is reached for the shear stress which allows the establishment of a dynamic building /breakage equilibrium that is the most favorable to the growth of the aggregates [30–32]. Beyond this peculiar value, as soon as the shear stress increases, the aggregates radius decrease due to rupture forces caused by the flow, leading to a dispersion of the SUs in the glass matrix. From the settling point of view, the gravity will exert a greater impact on the aggregates as their radius increase, accelerating their sedimentation on the crucible. However, after reaching its maximum, as the size of the aggregates decreases, the forces acting on the aggregates reach a new balance, decreasing the sedimentation rate and leaving the isolated SUs in suspension on the glass.

4 Conclusions

The sedimentation of aggregates in a simulated nuclear glass melt containing 3 wt% PGM particles was investigated in this chapter. Previous study on the aggregation of the same system (Chapter IV) produced samples with different aggregation degrees that were reused in this work to analyze the impact of the shear stress and time on the PGM particles settling. The samples aggregation degree was determined using a stress-imposed rheometer, working at high temperature, and an SEM image analysis method. A post-mortem approach was chosen where each sample was submitted at 1200 °C to different shear stresses and for different durations, capturing the evolution of the particles rearrangement with the viscosity. The reproducibility of the employed protocol was verified in the past chapter.

To observe the settling for each sample, the obtained SEM images were submitted to an image analysis protocol that evidenced the structural units (SUs) made of RuO_2 needles and Pd-Te spherical particles, and their distribution in the glass. The image treatment was an important tool to highlight the aggregation degree of each sample along with the heterogeneous particle distribution in the crucible caused by the settling and influenced by the experimental duration. The visual evolution of the particles settling for all the samples was presented. The experimental challenges of observing the sedimentation kinetics of PGM particles in a glass melt were overcome thanks to a numerical approach quantifying the percentage of settled SUs over time for all studied stresses, considering as a start point an equal repartion of particles between both parts of the crucible. The data showed that the PGM units settling is dependent of time and flow regime, in the same way as the aggregation.

Given that the PGM glass behaves differently at low, medium and high shear stresses due to the intensity of the forces acting on the particles, the settling velocity of the SUs was estimated in the three scenarios using the equations derived by Allain *et al.* [18] first order equation. The model consider the coupling of aggregation and settling for a semi diluted system such as the studied glass melt. For the first regime (low shear stress), a combination of the low hydrodynamics forces and van der Waals attractive forces on the PGM particles tends to favor the aggregation phenomenon, increasing the aggregates radius over time as well as their settling velocity. For the second regime (medium shear stress), the same tendency is observed but the rapid increase of the aggregates radius impacts directly the kinetics of the phenomenon. Considering the collecting effect of larger aggregates over smaller ones, the settling rate for this regime is higher than the first regime, even though the same forces (of different intensities) are

acting on the particles. At high shear stress, the SUs are completely dispersed in the melt due to the effects of the hydrodynamic forces, reducing the impact of gravity. Therefore, the SUs settle slowly and stay suspended due to the continuous flow. Furthermore, since the sedimentation rate depends directly on the size of the aggregates, both increase until they reach their maximum when a dynamic equilibrium is established between building and rupture of the aggregates. As the shear stress continues to increase, the settling velocity decreases due to rupture forces caused by the flow that promote the dispersion of the SUs in the glass matrix. Although all data obtained by image analysis are semi-quantitative, a structural link between rheological behavior, aggregation, and sedimentation of PGM particles is now established. The study and modeling of PGM particle sedimentation and aggregation and its implications thus provide a deeper understanding of the glass melt and the vitrification process.

5 References

[1] J.-M. GRAS, Cycle du combustible nucléaire - Introduction, Tech. l'ingénieur. 33 (2016) 1–2.

[2] D. Greneche, Cycle du combustible nucléaire: aval du cycle et questions génériques, Tech. l'Ingénieur. BN3564 V1 (2016).

[3] E. Vernaz, S. Gin, C. Veyer, Waste glass, Compr. Nucl. Mater. 5 (2012) 451–483. https://doi.org/10.1016/B978-0-08-056033-5.00107-5.

[4] R.F. Taylor, Chemical engineering problems of radioactive waste fixation by vitrification, Chem. Eng. Sci. 40 (1985) 541–569. https://doi.org/10.1016/0009-2509(85)80001-4.

[5] C. Hanotin, J. Puig, M. Neyret, P. Marchal, Platinum group metal particles aggregation in nuclear glass melts under the effect of temperature, J. Nucl. Mater. 477 (2016) 102–109. https://doi.org/10.1016/j.jnucmat.2016.04.033.

[6] C. Simonnet, A. Grandjean, J. Phalippou, Electrical behavior of platinum-group metals in glass-forming oxide melts, J. Nucl. Mater. 336 (2005) 243–250. https://doi.org/10.1016/j.jnucmat.2004.09.019.

[7] B. Luckscheiter, Properties and behavior of the platinum group metals in the glass resulting from the vitrification of simulated nuclear fuel reprocessing waste, J. Mater. Res. 6 (1991) 2535–2546. https://doi.org/10.1557/JMR.1991.2535.

[8] W. Grünewald, G. Roth, W. Tobie, K. Weiß, S. Weisenburger, The role of the platinum group elements ruthenium, rhodium and palladium in the vitrification of radioactive high level liquid waste using joule heated ceramic lined waste glass melters, Glas. Technol. Eur. J. Glas. Sci. Technol. Part A. 49 (2008) 266–278.

[9] F. Pacaud, C. Fillet, N. Jacquet-Francillon, Effect of platinoids on French LWR reference glass properties, Mater. Res. Soc. Symp. Proc. 257 (1992) 161–167.

[10] T. Hartmann, H. Pentinghaus, The ternary system palladium-rhodium-tellurium: A Study to understand phase formation in the vitrification process of high-level waste concentrates (HLWC), J. Nucl. Mater. 422 (2012) 124–130. https://doi.org/10.1016/j.jnucmat.2011.12.029.

[11] K. Uruga, T. Usami, T. Tsukada, S. Komamine, E. Ochi, Viscoplasticity of simulated high-level radioactive waste glass containing platinum group metal particles, J. Nucl. Mater. 452 (2014) 419–424. https://doi.org/10.1016/j.jnucmat.2014.05.062.

[12] J. Puig, C. Hanotin, M. Neyret, P. Marchal, High temperature rheological study of borosilicate glasses containing platinum group metal particles by means of a mixer-type rheometer, J. Nucl. Mater. 469 (2016) 112–119. https://doi.org/10.1016/j.jnucmat.2015.11.053.

[13] B. Ildefonse, C. Allain, P. Coussot, Des grands écoulements naturels à la dynamique du tas de sable: introduction aux suspensions en géologie et en physique., 1st ed., Cemagref, 1999.

[14] C. Allain, M. Cloitre, The effects of gravity on the aggregation and the gelation of colloids, Adv. Colloid Interface Sci. 46 (1993) 129–138. https://doi.org/10.1016/0001-8686(93)80038-D.

[15] W. T. Cobb and P. Hrma, Behavior of RuO2 in a glass melt, Ceram. Trans. 23 (1986) 233–237.

[16] V.A. Kashcheev, P.P. Poluéktov, A. V. Demin, Modeling of the sedimentation of heterogeneous phases accompanying the vitrification of liquid radioactive wastes, At. Energy. 78 (1995) 210–213. https://doi.org/10.1007/BF02407492.

[17] J. Puig, B. Penelon, P. Marchal, M. Neyret, Rheological Properties of Nuclear Glass Melt Containing Platinum Group Metals, Procedia Mater. Sci. 7 (2014) 156–162. https://doi.org/10.1016/j.mspro.2014.10.021.

[18] C. Allain, M. Cloitre, F. Parisse, Settling by cluster deposition in aggregating colloidal suspensions, J. Colloid Interface Sci. 178 (1996) 411–416. https://doi.org/10.1006/jcis.1996.0135.

[19] T. Advocat, J.L. Dussossoy, V. Petitjean, Vitrification des déchets radioactifs et appareillage, Les Tech. l'Ingénieur. 33 (2008) 0–27.

[20] M. Bousmina, A.-S. Chrissemant, L. Choplin, A. Aït-Kadi, P. Marchal, Quantitative Analysis of Mixer-Type Rheometers using the Couette Analogy, Can. J. Chem. Eng. 80 (2010) 1166–1174. https://doi.org/10.1002/cjce.5450800618.

[21] Bousmina M.; A. Aït-Kadi and J.B. Faisant, Determination of Shear Rate and Viscosity

from Batch Mixer Data: Theoretical and Experimental Results, J. Rheol. 43 (1999) 1999.

[22] O. Delattre, E. Régnier, S. Schuller, M. Allix, G. Matzen, Image analysis study of crystallization in two glass compositions of nuclear interest, J. Non. Cryst. Solids. 379 (2013) 112–122. https://doi.org/10.1016/j.jnoncrysol.2013.07.029.

[23] J. Fournier-Renaud, Cinétiques de dissolution des cristaux dans les silicates fondus – contexte des verres nucléaires, Université Montpellier, 2017. https://doi.org/tel-01925448.

[24] C. Allain, M. Cloitre, M. Wafra, Aggregation and sedimentation in colloidal suspensions, Phys. Rev. Lett. 74 (1995) 1478–1481. https://doi.org/10.1103/PhysRevLett.74.1478.

[25] L. Gmachowski, Calculation of the fractal dimension of aggregates, Colloids Surfaces A Physicochem. Eng. Asp. 211 (2002) 197–203. https://doi.org/10.1016/S0927-7757(02)00278-9.

[26] F.L. Braga, O.A. Mattos, V.S. Amorin, A.B. Souza, Diffusion limited aggregation of particles with different sizes: Fractal dimension change by anisotropic growth, Phys. A Stat. Mech. Its Appl. 429 (2015) 28–34. https://doi.org/10.1016/j.physa.2015.02.050.

[27] W.R. Richmond, R.L. Jones, P.D. Fawell, The relationship between particle aggregation and rheology in mixed silica-titania suspensions, Chem. Eng. J. 71 (1998) 67–75. https://doi.org/10.1016/S1385-8947(98)00105-3.

[28] D. Quemada, Rheological modelling of complex fluids: II. Shear thickening behavior due to shear induced flocculation, EPJ Appl. Phys. 2 (1998) 175–181. https://doi.org/10.1051/epjap:1998170.

[29] S. Herminghaus, Wet Granular Matter, WORLD SCIENTIFIC, 2013. https://doi.org/10.1142/8575.

[30] H.A. Barnes, A Handbook of Elementary Rheology, The University of Wales- Institute of Non-Newtonian Fluid Mechanics, Department of Mathematics, Avaiable online, 2000.

[31] D.B. Genovese, Shear rheology of hard-sphere, dispersed, and aggregated suspensions, and filler-matrix composites, Adv. Colloid Interface Sci. 171–172 (2012) 1–16. https://doi.org/10.1016/j.cis.2011.12.005.

[32] P. Snabre, P. Mills, Rheology of concentrated suspensions of viscoelastic particles, Colloids Surfaces A Physicochem. Eng. Asp. 152 (1999) 79–88. https://doi.org/10.1016/S0927-7757(98)00619-0.

Conclusions and perspectives

General conclusions

The present study investigated the overall rheological behavior of a glass melt containing PGM particle aggregates. All the experimental work was carried out using the same composition of simulated nuclear glass containing 3 wt% of PGM particles. The thesis was divided in three main goals:

- present an in-depth analysis of the thixotropic behavior of the glass melt;
- study the PGM particle aggregation kinetics;
- establish a link between the rheological behavior of melts and the PGM particle sedimentation occurring within them.

In particular the impact of shear rate, shear stress, time and temperature in the three aforementioned phenomena (thixotropy, aggregation, sedimentation) was investigated using experimental analysis and modeling tools. Initially, steady-state and transient measurements were conducted to characterize the rheological behavior of the material using a stress-imposed rheometer, at temperatures ranging from 1100 °C to 1250 °C. The impact of time and temperature on the melt viscosity was evaluated for a wide shear rate and shear stress range. Two different mathematical models have been proposed for the first time to describe the thixotropic behavior of a suspension in a glass melt. Both approaches evidenced a build-up phenomenon in the melt where PGM particles aggregates are formed over time due to Brownian motion coupled to attractive forces. This coupling leads to an increase of the viscosity, until the material structure reaches a dynamic equilibrium, especially at low shear rates for which aggregation is favored.

The **first model**, similar to that of Houska [1], allows to **accurately describe the thixotropic behavior of the system**. Although it was established on the basis of steady-state measurements, it **allows the prediction of the transient behavior of the samples without additional fitting parameters** than those determined in steady-state. Consequently, the model is not only descriptive but also explicative and predictive of the rheological behavior of the glass melts. An **exponential model** was also used in the study in order to **describe the transient viscosity under stress-imposed conditions in terms of a characteristic time**. It was shown that, regardless of the temperature, the characteristic time (τ) decreases with the shear stress. The shear stress has a strong impact on τ but further analysis is necessary to explore the temperature dependency of τ. This preliminary study of the thixotropic behavior of melts, taking into

account both the impact of shear rate and shear stress, provides an important input for the study of aggregation.

The second part of the study aimed to determine the **impact of shear stress and time on the degree of aggregation of PGM particles** by combining image analysis and rheological measurements. Given the difficulties of in situ analysis at high temperatures, a reproducible post-mortem approach was implemented after each sample was subjected to different shear stresses and for different durations at 1200 °C. The experimental challenges of observing the aggregation kinetics in a glass melt were overcome thanks to a numerical approach three main scenarios of aggregation were identified depending on the flow regime imposed *i.e.*, low, medium and high shear flow regime.

- At a low shear stress, a combination of the **low hydrodynamics forces, Brownian motion and van der Waals attractive forces** on the PGM particles contributes to the **aggregation of particles**. It affects the viscosity of the melts by increasing the effective volume fraction of the suspension, leading to a higher viscosity at low shear rates.
- At a medium flow rate, the same forces are acting on the particles, but with different intensities than in the low shear regime: **the hydrodynamic forces have an impact by enhancing local reorganizations but are not strong enough to disperse** the SUs in the glass. The viscosity decreases significantly, but aggregation still occurs.
- At high shear flow, the **SUs are completely dispersed** in the melt due to the **dominant effects of hydrodynamic forces**, leading to a lower viscosity.

Considering the samples with different aggregation degrees, the impact of the shear stress and time on the PGM particles settling was then investigated. The image treatment that was applied to all samples was an important tool to highlight the aggregation degree of each sample and the heterogeneous particle distribution in the crucible. These heterogeneities are a consequence of the particles aggregation and sedimentation, which is strongly influenced by the experiment duration. Again, experimental difficulties related to the observation of sedimentation kinetics in molten glass were bypassed by a numerical treatment of the data. It allowed to quantify the percentage of settled SUs over time for all studied stresses, evidencing a strong dependence settling has on time and flow regime, in the same way as the aggregation. In the three distinguished scenarios (low, medium and high shear stress) the settling velocity of the SUs was estimated using Allain *et al*. [2] first order equation, which sustained the hypothesis that the aggregation kinetics influences directly the sedimentation rate. The present study shows:

- For the first regime (low shear stress), the aggregation of the particles is favored, which leads to **an increase of the radius of the SU in time and consequently of their sedimentation speed**.
- In the second regime, at medium shear stress, the same tendency is observed but the rapid increase of the aggregates radius, due to the collecting effect of large aggregates absorbing smaller ones, **increases the settling rate**. Even though, in this regime, the same kind of forces are acting on the particles, their relative intensity is not the same.
- At high shear stress, corresponding to the third zone, the **SUs are completely dispersed in the melt** due to the effects of the hydrodynamic forces, reducing the impact of gravity. As a result, the SU will settle more slowly and **remain in suspension due to the permanent recirculation of the continuous phase**.

The settling velocity is directly dependent of the aggregate size, since both will increase with increasing shear stress, until reaching a maximum corresponding to the establishment of the dynamical equilibrium between the building and breakdown of the aggregates. As the shear continues to increase, the settling velocity decreases due to dominating rupture forces caused by the flow that promote the dispersion of the SUs in the glass matrix.

The complementary approaches implemented during this thesis have allowed an in-depth understanding of the rheological behavior of glass melts. Thus, this work has brought a qualitative and quantitative interpretation of the observed phenomena allowing a deeper understanding of the material behavior and consequently of the vitrification process. The time dependency of the melt viscosity evidences the reorganization of the particles which affects directly the flow. Hence, **the aggregates will gradually increase/ decrease with time, depending on the relative intensities of the forces acting on the particles.** Thus, the constant agitation of the samples does not prevent sufficiently the settling of the aggregates, which increases with time. In conclusion, as presented in Figure 1, the three studied phenomena happen simultaneously and are mutually dependent.

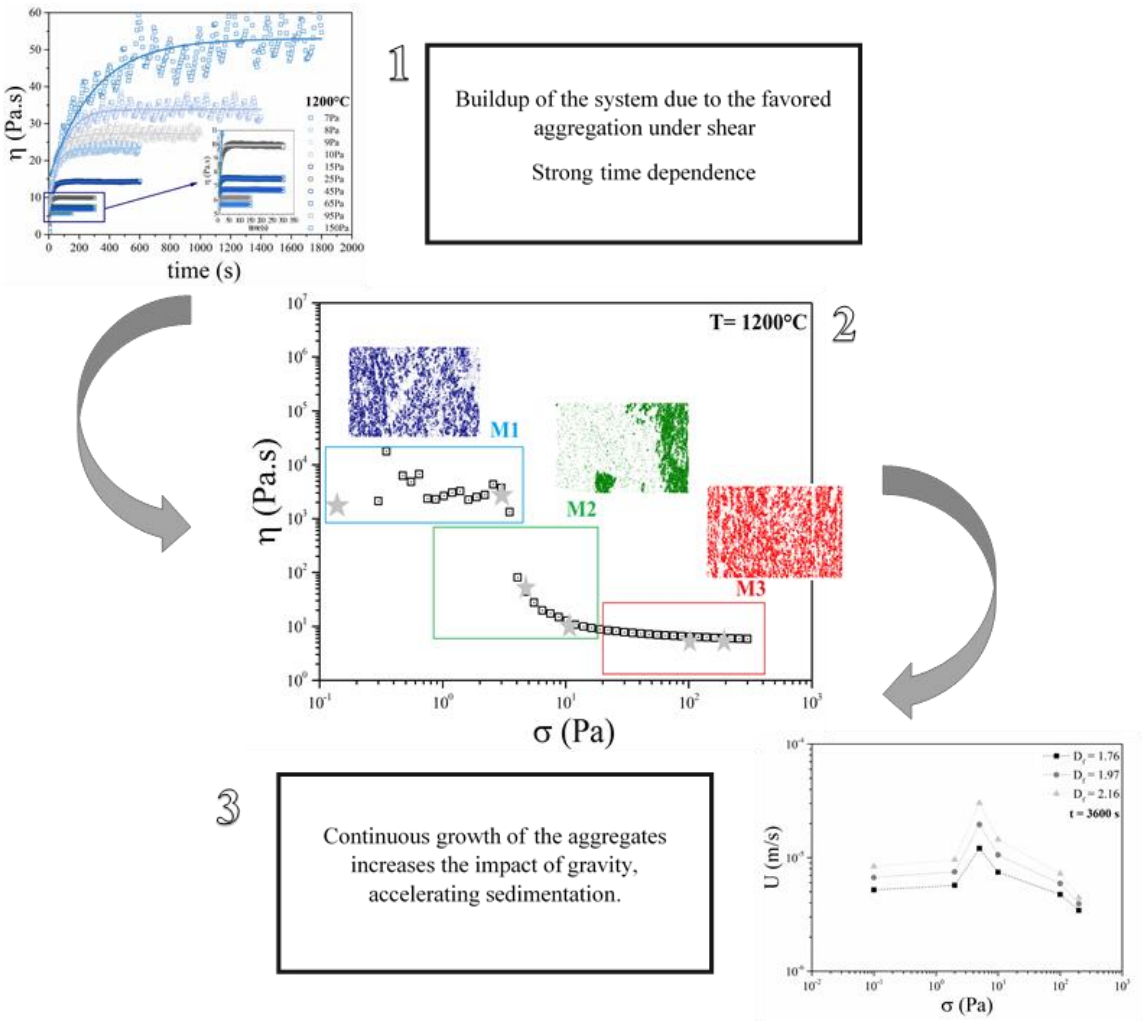

Figure 1 – Scheme of the thesis in a nutshell: Firstly (1), the thixotropic behavior illustrates the reorganization of the particles with time, which is directly linked with their aggregation (2). The PGM aggregation kinetics is dependent of the imposed shear, gradually changing its size and consequently its settling rate (3).

Perspectives for future research

The current study on the rheological properties of nuclear glass melts containing PGM particles is a consequence of previous post-doctoral projects conducted in our research team. The impact of time on aggregation and sedimentation has been explored for the first time, answering important questions on the subject. Nevertheless, this subject may be further deepened. An important perspective for the continuation of this research work would be the development of a global model coupling the steady-state structural model proposed by Hanotin *et al*[3] and the thixotropic transient model proposed in this study, aiming to consolidate the consideration of time in the modelling approach. Future CFD simulation studies taking advantage of the proposed model would then be essential for the optimization of the vitrification process and its control. The choice of the distance between first neighbors, chosen as a mathematical tool to

distinguish the different types of aggregations could be extended by also considering the higher order neighbors (second, third...), in order to quantify more precisely the differences observed by image analysis between the different aggregation scenarios.

Furthermore, the modeling of the aggregates size as a function of time and shear stress could provide more information on the aggregation kinetics. Several parameters can affect the PGM aggregation in the melt. Previous studies analyzed the impact of RuO_2 alone in the glass melt and the effects of bubbles in simpler melt systems [4–8]. Thus, another interesting work for the future would be the coupling between bubble formation and PGM particles aggregation in this type of melt, as well as further comprehension of the Pd-Te intermetallic impact on the overall kinetics of the involved phenomena. Given the limited literature on the PGM particle sedimentation in a glass melt, new experimental studies based on the protocol proposed in this thesis would enhance the study by considering broader shear stress and time ranges.

References

[1] M. Houška, R. Žitný, Dynamics of Thixotropic Liquids and Time Dependency, in: Adv. Food Rheol. Its Appl., Elsevier, New York, 2017: pp. 47–63. https://doi.org/10.1016/B978-0-08-100431-9.00003-6.

[2] C. Allain, M. Cloitre, F. Parisse, Settling by cluster deposition in aggregating colloidal suspensions, J. Colloid Interface Sci. 178 (1996) 411–416. https://doi.org/10.1006/jcis.1996.0135.

[3] C. Hanotin, J. Puig, M. Neyret, P. Marchal, Platinum group metal particles aggregation in nuclear glass melts under the effect of temperature, J. Nucl. Mater. 477 (2016) 102–109. https://doi.org/10.1016/j.jnucmat.2016.04.033.

[4] R.B. Nuernberg, N.M.P. Machado, M. Malki, M. Neyret, Electrical behavior of RuO2-glass composites: The effect of RuO2 particle size on the percolation threshold, J. Nucl. Mater. 546 (2021) 152777. https://doi.org/10.1016/j.jnucmat.2020.152777.

[5] L. Pereira, R.B. Nuernberg, O. Podda, N.M.P. Machado, A. Laplace, F. Pigeonneau, U. Kueppers, K.-U. Hess, D.B. Dingwell, A Feedback Mechanism Between Crystals and Bubbles in a RuO2- Bearing Melt, J. Non. Cryst. Solids. (2022). https://doi.org/10.1016/j.jnoncrysol.2022.121456.

[6] L. Pereira, O. Podda, B. Fayard, A. Laplace, F. Pigeonneau, Experimental study of bubble formation in a glass-forming liquid doped with cerium oxide, J. Am. Ceram. Soc. 103 (2020) 2453–2462. https://doi.org/10.1111/jace.16950.

[7] R.B. Nuernberg, N.M.P. Machado, D. Jouglard, L. del Campo, M. Malki, M. Neyret, The origin of hysteresis in the electrical behavior of RuO2-glass composite melts, J. Non. Cryst. Solids. 557 (2021). https://doi.org/10.1016/j.jnoncrysol.2020.120596.

[8] C. Simonnet, A. Grandjean, Mixed ionic and electronic conductivity of RuO2-glass composites from molten state to glassy state, J. Non. Cryst. Solids. 351 (2005) 1611–1618. https://doi.org/10.1016/j.jnoncrysol.2005.04.049.

French Summary

L’étude rhéologique de fontes verrières nucléaires contenant des agrégats de platinoïdes.

Contexte et motivation

En France, une majorité de réacteurs à eau pressurisée fonctionne à partir de combustible d'oxyde d'uranium (UOX). Après environ 4 ans de fonctionnement dans un réacteur nucléaire, le combustible est usé. Il contient alors des déchets non recyclables (4 %) mais aussi des matières valorisables, telles que l'uranium (94 à 95 %) et le plutonium (1 %) [1,2]. Après l'extraction de l'uranium et du plutonium par le procédé chimique PUREX [3], les déchets restants sont dissous dans une solution d'acide nitrique. Cette solution hautement radioactive doit être transformée en monolithe pour contenir la dissémination des radionucléides. En France, elle est conditionnée dans une matrice de verre. La vitrification des déchets est un processus en deux étapes où les déchets, sous forme de nitrates en solution, sont d'abord transformés en oxydes dans un four rotatif, le calcinateur, chauffé à environ 500 °C. La seconde étape consiste en la fusion du calcinat ainsi obtenu avec une fritte de verre, entre 1050 et 1250 °C [4]. Le four, utilisé pour la fusion du verre, peut être chauffé par induction directe (creuset froid) ou indirecte (creuset chaud). Le verre nucléaire est ensuite versé dans des conteneurs métalliques. Le matériau produit est un alumino-borosilicate de sodium amorphe et homogène, composé d'environ 40 éléments différents [4]. Ce verre est appelé R7T7. Les conteneurs sont entreposés dans des puits ventilés avant leur futur stockage dans des formations géologiques profondes [4,5].

Lors de l'élaboration à haute température, la plupart des espèces à confiner réagissent chimiquement avec les additifs de vitrification pour former un liquide homogène. Cependant, certains éléments tels que les platinoïdes (Ru, Rh, Pd), sont insolubles dans la fonte verrière. Dans les verres, ils sont observés sous forme de billes d'intermétallique de palladium (et de rhodium) avec du tellure (1 à 5 μm de diamètre) et d'aiguilles d'oxyde de ruthénium (et de rhodium) (10 à 20 μm de long) [6,7]. La présence de ces éléments en suspension a un impact sur certaines propriétés physiques de la fonte, telles que sa viscosité ou sa conductivité électrique, impactant directement le processus de vitrification. De plus, même si les platinoïdes sont en faible quantité (3 % massiques), leur tendance à s'agréger et à sédimenter peut conduire, dans des conditions d'agitation dégradées, à la formation de couches de fraction volumique élevée au fond du creuset, pouvant gêner la bonne conduite du procédé. Plusieurs études ont été menées afin de mieux comprendre l'impact des platinoïdes sur les propriétés physiques du verre nucléaire fondu [8–12].

L'étude du comportement rhéologique de ce système est d'une grande importance car il peut être fortement affecté par la cinétique d'agrégation des particules ainsi que par l'écoulement.

Les travaux de Puig *et al.* [11] et Hanotin *et al.* [10] ont démontré le comportement rhéofluidifiant et le comportement thixotrope du verre nucléaire fondu. La modélisation phénoménologique du système a été bien décrite par un modèle simplifié de Cross mettant en évidence l'existence de deux plateaux newtoniens, à faible et à fort taux de cisaillement [11]. Selon les auteurs, à un taux de cisaillement élevé, le système se comporte comme une suspension de petits clusters et de particules individuelles et la viscosité de la suspension est principalement contrôlée par la viscosité de la matrice de verre ; ainsi la viscosité diminue lorsque la température augmente. D'autre part, à faible taux de cisaillement et au-delà d'une certaine teneur en platinoïdes, des agrégats macroscopiques, composés de chaînes d'aiguilles de RuO_2 et de billes de Pd-Te séparées par de fines couches de matrice vitreuse sont créés, ce qui augmente fortement la viscosité de la fonte, contrairement à ce qui se passe à un taux de cisaillement élevé, la viscosité augmente avec la température [10,11,13]. La réorganisation des particules peut être expliquée par l'interaction entre les forces en présence. À faible taux de cisaillement, l'agrégation est favorisée par les réorganisations Browniennes locales et les forces d'attraction de Van der Waals, tandis que les forces hydrodynamiques restent négligeables. A des taux de cisaillement élevés, le comportement rhéologique est alors contrôlé par les forces hydrodynamiques dues au flux de cisaillement, ce qui provoque la rupture des agrégats et la diminution drastique de la viscosité de l'échantillon [11].

Les difficultés expérimentales rencontrées lors de l'étude de la fonte verrière, notamment du fait des hautes températures appliquées, limitent la littérature sur le sujet. Bien que les études précédentes illustrent avec précision la dépendance du comportement rhéologique du système envers le taux de cisaillement, la température et la fraction volumique, certaines questions demeurent. Le comportement thixotropique du système a été mis en évidence par Puig *et al.* mais une analyse plus approfondie de la forte dépendance temporelle de la viscosité est nécessaire. L'agrégation des platinoïdes influençant non seulement le comportement rhéologique du matériau mais aussi la cinétique de sédimentation des particules (par la taille des agrégats) et les propriétés électriques du matériau (par le seuil de percolation), il est nécessaire de mettre au jour les critères qui déterminent l'agrégation et de la caractériser. De plus, une étude plus approfondie du couplage entre agrégation et sédimentation est nécessaire à l'analyse complète du comportement de la fonte verrière.

Objectifs principaux de la thèse

Cette thèse se déroule au sein du Laboratoire de Développement des Matrices de Conditionnement du CEA Marcoule, en collaboration avec le Centre d'Ingénierie Chimique des

Milieux Rhéologiquement Complexes (GEMICO) du Laboratoire de Réactions et Génie des Procédés (LRGP, Nancy), qui possède une expertise en rhéologie des dispersions, formulation et modélisation associée au comportement rhéologique des fluides complexes. Tous les travaux expérimentaux ont été réalisés avec le même matériau : un verre nucléaire borosilicaté simulé contenant 3 % massiques de platinoïdes. Le verre a été élaboré à 1200 °C sur une unité pilote grandeur nature installée au CEA Marcoule [4]. La présente étude vise à fournir des données importantes sur le comportement rhéologique global du verre fondu contenant des agrégats de particules de platinoïdes. L'étude a trois objectifs principaux :

a. **Analyser le comportement thixotropique du bain de verre contenant des platinoïdes**. Et en particulier elle vise à caractériser l'impact du taux de cisaillement / de la contrainte de cisaillement, du temps et de la température sur le comportement rhéologique de la fonte et à proposer une modélisation mathématique du comportement thixotropique.

ii. **Étudier l'agrégation des platinoïdes dans le verre** considéré :
   a. Les impacts du temps et de la contrainte de cisaillement sur l'agrégation des platinoïdes dans une gamme de cisaillement plus large, en plus de distinguer les différents mécanismes d'agrégation.
   b. L'interaction entre le degré d'agrégation des platinoïdes dans la fonte et la réponse rhéologique de la suspension.

iii. **Établir un lien entre le comportement rhéologique et la sédimentation des platinoïdes**, en particulier :
   a. Identifier l'impact du degré d'agrégation sur la décantation des particules.
   b. Estimer le taux de sédimentation en fonction du degré d'agrégation de la fonte en fonction du temps et de la contrainte / du taux de cisaillement.

Description des chapitres

La thèse est composée de cinq chapitres différents, dont trois ont été rédigés sous forme d'articles soumis à des revues scientifiques sur le domaine de recherche (chapitre II, IV et V).

Dans le **premier chapitre,** une **revue de la littérature** est présentée, explorant le contexte de la vitrification des déchets, les matériaux qui ont été étudiés, ainsi qu'un résumé des dernières études sur le comportement des platinoïdes dans une fonte verrière. Un aperçu des principaux concepts de rhéologie, d'agrégation et de sédimentation est également présenté pour étayer l'étude.

Le **deuxième chapitre** présente une **analyse** approfondie du **comportement thixotropique de la fonte simulée contenant des platinoïdes**. Pour réaliser cette analyse, des techniques adaptées aux hautes températures ont été employées afin de caractériser l'impact du taux de cisaillement, du temps et de la température (de 1100 à 1250 °C) sur le comportement rhéologique de la fonte. Une modélisation mathématique du comportement thixotropique des bains de verre contenant des platinoïdes est présentée pour la première fois, en utilisant un modèle similaire à celui proposé par Houska [14]. L'utilisation du modèle pour décrire la thixotropie du système à partir de mesures en régime permanent est présentée. En particulier, il est montré que le modèle est capable de prédire le comportement transitoire des échantillons sans paramètres ajustables supplémentaires que ceux déterminés en régime permanent. Dans ce chapitre, les mesures à haute température ont été réalisées en imposant le taux de cisaillement afin de fixer le temps d'écoulement caractéristique et ainsi simplifier l'application du modèle thixotropique. Ce chapitre a été soumis à la revue Rheologica Acta.

Compte tenu de l'objectif de la thèse qui est d'étudier l'agrégation des platinoïdes sur une plage de taux de cisaillement / contrainte la plus large possible, il s'avère que les essais sous contrainte permettent d'atteindre des taux de cisaillement beaucoup plus faibles que les essais sous déformation. Par conséquent, le **troisième chapitre** présente une **analyse complémentaire du comportement thixotropique du matériau** par le biais d'expériences à contraintes imposées. Plus précisément, ce chapitre se concentre sur l'analyse de l'évolution de la viscosité de la fonte avec le temps et la température (de 1100 à 1250 °C) en fonction de la contrainte de cisaillement. Les données ont été analysées par une approche phénoménologique utilisant un modèle exponentiel associant la viscosité apparente à un temps caractéristique pour ajuster les données expérimentales.

Compte tenu de l'aperçu du comportement thixotropique du matériau et de ses caractéristiques, le **quatrième chapitre** consiste à caractériser l'**agrégation des platinoïdes dans le bain de verre**. L'impact de la contrainte de cisaillement et du temps sur le degré d'agrégation des platinoïdes a été évalué à l'aide d'expériences rhéologiques à 1200 °C et d'analyse d'images obtenues par microscopie électronique à balayage. Étant donné les difficultés de l'analyse in situ à haute température, une approche post-mortem a été adoptée, dans laquelle chaque échantillon a d'abord été soumis à une contrainte de cisaillement différente pendant un certain intervalle de temps, puis trempé pour figer son état à haute température. Ainsi, le réarrangement des platinoïdes a pu être étudié. Pour la première fois, l'interaction entre le comportement rhéologique du système et le degré d'agrégation a été fournie. Sur la base des données

expérimentales acquises, un calcul d'équilibre des forces a été effectué pour illustrer les différents scénarios d'agrégation. Ce chapitre a été soumis au Journal of Nuclear Materials.

Le **cinquième chapitre** étudie la **cinétique de sédimentation des agrégats des platinoïdes dans la fonte verrière** simulée à 1200 °C. Les échantillons obtenus pour l'étude d'agrégation présentée dans le quatrième chapitre ont été analysés dans ce chapitre. Les différents degrés d'agrégation ont permis de mieux comprendre l'impact de la contrainte de cisaillement et du temps sur la sédimentation. Sur la base des travaux d'Allain *et al*. [15] pour la sédimentation dans des systèmes dilués, la vitesse de sédimentation des platinoïdes a été estimée en présentant l'interaction entre la sédimentation et l'agrégation sur une large gamme de contraintes de cisaillement, fournissant une nouvelle entrée pour la modélisation et le contrôle de la sédimentation des particules. Ce chapitre a été soumis au Journal of Nuclear Materials.

Enfin, une conclusion générale clôt l'étude en présentant les enseignements généraux obtenus tout au long de la thèse, ainsi que les perspectives de recherches futures. Pour des raisons pratiques, chaque chapitre utilise sa propre nomenclature, qui est présentée au début du chapitre correspondant. La numérotation des tableaux et figures est spécifique à chaque chapitre et se présente sous la forme suivante : "numéro du chapitre - numéro de la figure/du tableau".

Conclusions générales

La présente étude a examiné le comportement rhéologique global d'une fonte verrière contenant des agrégats de platinoïdes. Tous les travaux expérimentaux ont été réalisés en utilisant la même composition de verre nucléaire simulé contenant 3 % massique de platinoïdes. Cette thèse comporte trois objectifs principaux :

- présenter une analyse approfondie du comportement thixotropique du verre fondu ;
- étudier la cinétique d'agrégation des platinoïdes;
- établir un lien entre le comportement rhéologique des fontes et la sédimentation des particules de platinoïdes.

En particulier l’impact du taux de cisaillement, de la contrainte de cisaillement, du temps et de la température sur les trois phénomènes mentionnés a été investigué en utilisant des outils d'analyse expérimentale et de modélisation. Dans un premier temps, des mesures en régime permanent et transitoire ont été effectuées entre 1100 °C et 1250 °C, à l'aide d'un rhéomètre à contrainte imposée, pour révéler le comportement rhéologique du matériau. L'impact du temps et de la température sur la viscosité de la fonte a été évalué dans une large gamme de taux de cisaillement et de contraintes de cisaillement. Deux modèles mathématiques différents ont été

proposés pour la première fois pour décrire le comportement thixotrope d'une suspension de platinoïdes dans un bain de verre. Les deux approches ont mis en évidence un phénomène d'agrégation de ces particules dans la fonte en raison du mouvement brownien couplé aux forces d'attraction. Ce couplage des phénomènes conduit à une augmentation de la viscosité, jusqu'à ce que la structure du matériau atteigne un équilibre dynamique. Cet effet est spécialement observé à de faibles taux de cisaillement, pour lesquels l'agrégation est favorisée.

Le **premier modèle**, similaire à celui de Houska [14] a permis de **décrire avec précision le comportement thixotropique du système**. Bien qu'il ait été établi sur la base de mesures en régime permanent, il a **permis de prédire le comportement transitoire des échantillons sans paramètre d'ajustement supplémentaire par** rapport à ceux déterminés en régime permanent. Le modèle n'est donc pas seulement descriptif mais aussi explicatif et prédictif du comportement rhéologique des verres fondus. Un **modèle exponentiel** a également été utilisé dans l'étude afin de **décrire la viscosité transitoire dans des conditions de contrainte imposées en termes de temps caractéristique.** Il a été montré que, indépendamment de la température, le temps caractéristique (τ) diminue avec la contrainte de cisaillement. La contrainte de cisaillement a un fort impact sur τ mais des analyses supplémentaires sont nécessaires pour déterminer la dépendance de la température sur τ. Cette étude préliminaire du comportement thixotropique des fontes verrières, prenant en compte à la fois l'impact du taux de cisaillement et de la contrainte de cisaillement, fournit un apport important pour l'étude de l'agrégation des platinoïdes.

La deuxième partie de l'étude visait à déterminer l'**impact de la contrainte de cisaillement et du temps sur le degré d'agrégation des particules de platinoïdes** en combinant analyse d'image et mesures rhéologiques. Compte tenu des difficultés de l'analyse in situ à haute température, une approche post-mortem reproductible a été mise en œuvre après que chaque échantillon ait été soumis à différentes contraintes de cisaillement pendant différentes durées à 1200 °C. Les défis expérimentaux de l'observation de la cinétique d'agrégation dans un verre fondu ont été surmontés grâce à une approche numérique trois scénarios d'agrégation ont été identifiés en fonction du régime d'écoulement imposé, à savoir un régime d'écoulement à faible, moyen et fort cisaillement.

- À faible contrainte de cisaillement, la combinaison des **faibles forces hydrodynamiques, mouvement brownienne et des forces d'attraction de van der Waals** sur les platinoïdes contribue à l'**agrégation des particules**. Elle affecte la

viscosité du verre en augmentant la fraction volumique effective de la suspension, ce qui entraîne une viscosité plus élevée à faible taux de cisaillement.

- À débit moyen, les mêmes forces agissent sur les particules, mais avec une intensité relative différente de celle du régime de faible cisaillement : **les forces hydrodynamiques ont un impact en favorisant les réorganisations locales mais ne sont pas assez fortes pour disperser** les SUs (structural units – unités structurales) dans le verre. La viscosité diminue de manière significative, mais l'agrégation se produit toujours.
- Dans le cas d'un écoulement à fort cisaillement, les **SUs sont complètement dispersés** dans la masse fondue en raison des effets dominante des forces hydrodynamiques, ce qui entraîne une viscosité plus faible.

L'impact de la contrainte de cisaillement et du temps sur la sédimentation des platinoïdes a ensuite été étudié sur les échantillons précédemment obtenus. Le traitement d'image auquel tous ces échantillons ont été soumis a permis de mettre en évidence le degré d'agrégation de chaque échantillon et la distribution hétérogène des particules dans le creuset. Ces hétérogénéités sont une conséquence de l'agrégation et de la sédimentation des particules, qui sont fortement influencées par la durée de l'expérience. Encore une fois, les difficultés expérimentales liées à l'observation de la cinétique de sédimentation dans la fonte ont été contournées par un traitement numérique des données. Il a permis de quantifier le pourcentage de SUs sédimentés au cours du temps pour toutes les contraintes étudiées, mettant en évidence la forte dépendance de la sédimentation avec le temps et le régime d'écoulement, de la même manière que l'agrégation. Dans trois scénarios distincts (contrainte de cisaillement faible, moyenne et élevée), la vitesse de sédimentation des SUs a été estimée en utilisant l'équation du premier ordre d'Allain *et al*. [15] qui soutient l'hypothèse que la cinétique d'agrégation influence directement la vitesse de sédimentation. Cette étude montre que :

- Pour le premier régime (faible contrainte de cisaillement) l'agrégation des particules est favorisée ce qui conduit à **une augmentation du rayon des SUs dans le temps et par conséquent de leur vitesse de sédimentation**.
- Dans le second régime, à une contrainte de cisaillement moyenne, la même tendance est observée mais l'augmentation rapide du rayon des agrégats, due à l'effet de collecte des agrégats les plus petits absorbé par les plus gros**, augmente le taux de sédimentation**. Même si, dans ce régime, les mêmes types de forces agissent sur les particules, leur intensité relative n'est pas la même.

- À une contrainte de cisaillement élevée, correspondant à la troisième zone, les **SUs sont complètement dispersés dans la masse fondue** en raison des effets des forces hydrodynamiques, réduisant l'impact de la gravité. Par conséquent, les SU se déposent plus lentement et **restent en suspension en raison de la recirculation permanente de la phase continue**.

La vitesse de sédimentation dépend directement de la taille des agrégats. Les deux augmentent avec la contrainte de cisaillement jusqu'à atteindre leur maximum et établir un équilibre dynamique entre la construction et la dégradation des agrégats. Lorsque le cisaillement continue à augmenter, la vitesse de sédimentation diminue en raison des forces de rupture dominantes causées par le flux, qui favorisent la dispersion des SUs dans la matrice de verre.

Les approches complémentaires mises en œuvre au cours de cette thèse ont permis une compréhension approfondie du comportement rhéologique des fontes verrières. Ce travail a apporté une interprétation qualitative et quantitative des phénomènes observés, permettant une compréhension plus approfondie du comportement du matériau et par conséquent du processus de vitrification. La dépendance temporelle de la viscosité du verre fondu met en évidence la réorganisation des particules qui affecte directement son écoulement. Ainsi, les **agrégats vont progressivement augmenter/diminuer avec le temps, en fonction de l'intensité relative des forces agissant sur les particules.** Ainsi, l'agitation constante des échantillons n'empêche pas la sédimentation des agrégats, qui augmente avec le temps. En conclusion, comme présenté en Figure 1, les trois phénomènes étudiés se produisent simultanément et sont interdépendants.

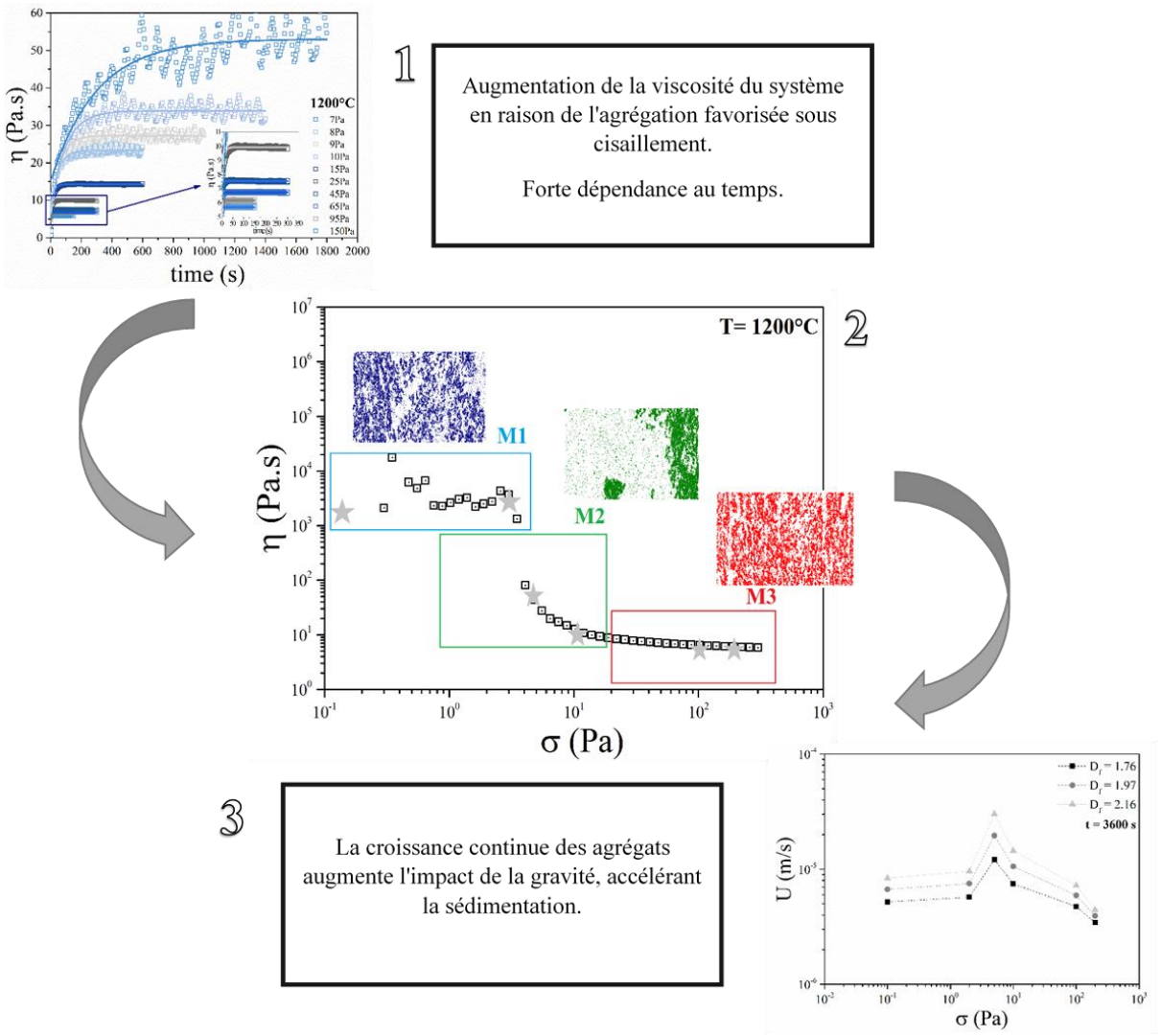

Figure 1 - Schéma de la thèse en quelques mots : Tout d'abord (1), le comportement thixotrope illustre la réorganisation des particules avec le temps, qui est directement liée à leur agrégation (2). La cinétique d'agrégation des platinoïdes est dépendante du cisaillement imposé, modifiant progressivement leur taille et par conséquent leur vitesse de sédimentation (3).

Perspectives pour les recherches futures

La présente étude sur les propriétés rhéologiques des verres nucléaires fondus contenant des platinoïdes est une conséquence de précédents projets post-doctoraux menés dans l'équipe de recherche du LDMC. L'impact du temps sur l'agrégation et la sédimentation a été exploré pour la première fois, répondant à des questions essentielles sur le sujet. Une perspective importante pour la poursuite de ce travail de recherche serait le développement d'un modèle global couplant le modèle structurel en régime permanent proposé par Hanotin *et al.*[10] et le modèle transitoire thixotrope proposé dans cette étude, afin de consolider l'impact du temps sur le comportement rhéologique de la fonte. De futures études de simulation CFD tirant parti du modèle proposé

seraient alors bénéfiques pour l'optimisation du processus de vitrification et son contrôle. Le choix de la distance entre premiers voisins, retenu comme outil mathématique pour différencier les différents types d'agrégation pourrait être étendu en prenant également en compte les voisins d'ordre supérieur (deuxième, troisième...), afin de quantifier plus précisément les différences observées par analyse d'image entre les différents scénarios d'agrégation.

En outre, la modélisation de la taille des agrégats en fonction du temps et de la contrainte de cisaillement pourrait fournir davantage d'informations sur la cinétique d'agrégation. Plusieurs paramètres peuvent affecter l'agrégation des platinoïdes dans le bain de verre. Des études précédentes ont analysé l'impact de RuO_2 seul dans le comportement rhéologique et électrique de la fonte et les effets des bulles dans des verres simplifiées [12,16–19]. Aussi, un travail intéressant serait le couplage entre la formation de bulles et l'agrégation des particules de platinoïdes dans ces verres simplifiés. Une meilleure compréhension de l'impact de l'intermétallique Pd-Te dans la cinétique globale des phénomènes impliqués pourrait également être apportée. Etant donné la littérature limitée sur la sédimentation des particules des platinoïdes dans une fonte verrière, de nouvelles études expérimentales basées sur le protocole proposé dans cette thèse permettraient de compléter encore cette étude, en considérant des contraintes de cisaillement et des plages de temps plus larges.

Références

[1] Production mondiale d'Électricité - L'énergie nucléaire dans le monde, (n.d.). https://www.cnrs.fr/cw/dossiers/dosnucleaire/darkcartes/1_production-mondiale-d-electricite.php (accessed November 3, 2021).

[2] D. Greneche, Cycle du combustible nucléaire: aval du cycle et questions génériques, Tech. l'Ingénieur. BN3564 V1 (2016).

[3] CEA, Monographie DEN - Le traitement-recyclage du combustible nucléaire usé, 2008.

[4] T. Advocat, J.L. Dussossoy, V. Petitjean, Vitrification des déchets radioactifs et appareillage, Les Tech. l'Ingénieur. 33 (2008) 0–27.

[5] G. Roth, S. Weisenburger, Vitrification of high-level liquid waste: glass chemistry, process chemistry and process technology, Nucl. Eng. Des. 202 (2000) 197–207. https://doi.org/10.1016/S0029-5493(00)00358-7.

[6] K. Uruga, T. Usami, T. Tsukada, S. Komamine, E. Ochi, Viscoplasticity of simulated high-level radioactive waste glass containing platinum group metal particles, J. Nucl. Mater. 452 (2014) 419–424. https://doi.org/10.1016/j.jnucmat.2014.05.062.

[7] R.F. Taylor, Chemical engineering problems of radioactive waste fixation by vitrification, Chem. Eng. Sci. 40 (1985) 541–569. https://doi.org/10.1016/0009-2509(85)80001-4.

[8] B. Luckscheiter, Properties and behavior of the platinum group metals in the glass resulting from the vitrification of simulated nuclear fuel reprocessing waste, J. Mater. Res. 6 (1991) 2535–2546. https://doi.org/10.1557/JMR.1991.2535.

[9] C. Simonnet, A. Grandjean, J. Phalippou, Electrical behavior of platinum-group metals in glass-forming oxide melts, J. Nucl. Mater. 336 (2005) 243–250. https://doi.org/10.1016/j.jnucmat.2004.09.019.

[10] C. Hanotin, J. Puig, M. Neyret, P. Marchal, Platinum group metal particles aggregation in nuclear glass melts under the effect of temperature, J. Nucl. Mater. 477 (2016) 102–109. https://doi.org/10.1016/j.jnucmat.2016.04.033.

[11] J. Puig, C. Hanotin, M. Neyret, P. Marchal, High temperature rheological study of borosilicate glasses containing platinum group metal particles by means of a mixer-type rheometer, J. Nucl. Mater. 469 (2016) 112–119.

https://doi.org/10.1016/j.jnucmat.2015.11.053.

[12] R.B. Nuernberg, N.M.P. Machado, D. Jouglard, L. del Campo, M. Malki, M. Neyret, The origin of hysteresis in the electrical behavior of RuO2-glass composite melts, J. Non. Cryst. Solids. 557 (2021). https://doi.org/10.1016/j.jnoncrysol.2020.120596.

[13] J. Puig, B. Penelon, P. Marchal, M. Neyret, Rheological Properties of Nuclear Glass Melt Containing Platinum Group Metals, Procedia Mater. Sci. 7 (2014) 156–162. https://doi.org/10.1016/j.mspro.2014.10.021.

[14] M. Houška, R. Žitný, Dynamics of Thixotropic Liquids and Time Dependency, in: Adv. Food Rheol. Its Appl., Elsevier, New York, 2017: pp. 47–63. https://doi.org/10.1016/B978-0-08-100431-9.00003-6.

[15] C. Allain, M. Cloitre, F. Parisse, Settling by cluster deposition in aggregating colloidal suspensions, J. Colloid Interface Sci. 178 (1996) 411–416. https://doi.org/10.1006/jcis.1996.0135.

[16] R.B. Nuernberg, N.M.P. Machado, M. Malki, M. Neyret, Electrical behavior of RuO2-glass composites: The effect of RuO2 particle size on the percolation threshold, J. Nucl. Mater. 546 (2021) 152777. https://doi.org/10.1016/j.jnucmat.2020.152777.

[17] L. Pereira, R.B. Nuernberg, O. Podda, N.M.P. Machado, A. Laplace, F. Pigeonneau, U. Kueppers, K.-U. Hess, D.B. Dingwell, A Feedback Mechanism Between Crystals and Bubbles in a RuO2- Bearing Melt, J. Non. Cryst. Solids. (2022). https://doi.org/10.1016/j.jnoncrysol.2022.121456.

[18] L. Pereira, O. Podda, B. Fayard, A. Laplace, F. Pigeonneau, Experimental study of bubble formation in a glass-forming liquid doped with cerium oxide, J. Am. Ceram. Soc. 103 (2020) 2453–2462. https://doi.org/10.1111/jace.16950.

[19] C. Simonnet, A. Grandjean, Mixed ionic and electronic conductivity of RuO2-glass composites from molten state to glassy state, J. Non. Cryst. Solids. 351 (2005) 1611–1618. https://doi.org/10.1016/j.jnoncrysol.2005.04.049.

Abstract: Rheological study of nuclear glass melts containing Platinum Group Metal aggregates

In France, borosilicate glass is used as a matrix to immobilize nuclear fission products resulting from spent fuel reprocessing. In the high-temperature vitrification process (1200 °C), most of elements to be contained react chemically with the vitrification additives to form a homogeneous glass melt. Platinum Group Metal (PGM) particles are not soluble in the melt and therefore are present as suspended particles of few microns. These particles exhibit an intense aggregation tendency and consequently the suspensions may present an anomalously high apparent viscosity. These systems are characterized by a shear-thinning and a thixotropic behaviors. The present study aims to provide important inputs for the overall rheological behavior of this system and its features through the characterization of a simulated nuclear glass melt containing 3.0 wt% (1.02 vol%) of PGM particles. A mathematical modeling of the thixotropic behavior of glass melts containing PGM particles is presented for the first time using a model similar to that proposed by Houska (Houska, 1981). This predictive model allow to describe experimental results obtained both in steady state and transient conditions. The impact of the shear stress and time on PGM aggregation degree and sedimentation kinetics is determined using an imposed-stress rheometer at high temperature and imaging analyses via Scanning Electron Microscopy (SEM). For the first time, the interplay between the rheological behavior of the system and the aggregation degree is provided, as well as the link with the particles settling. Based on the acquired experimental data, a force balance computation is executed to illustrate the different aggregation scenarios. The work provides a new input for the modeling and control of the vitrification process.

Keywords: Platinum Group Metals (PGM), Thixotropy, Aggregation, Sedimentation, Rheology.

Résumé: L'étude rhéologique de fontes verrières nucléaires contenant des agrégats de platinoïdes.

En France, les produits de fission nucléaire issus du retraitement des combustibles usés sont conditionnés au sein de matrices de verres borosilicatés. Lors du processus de vitrification à haute température (1200 °C), les éléments à confiner réagissent chimiquement avec les additifs de vitrification pour former un verre homogène. Cependant, parmi ces éléments, les platinoïdes ne sont pas solubles dans le bain de verre et restent en suspension sous forme de particules de quelques microns. Ces particules présentent une forte tendance à l'agrégation et les suspensions peuvent alors présenter une viscosité apparente anormalement élevée. Ces systèmes sont caractérisés par un comportement rhéofluidifiant et thixotrope. La présente étude vise à fournir des données importantes sur le comportement rhéologique global de ces systèmes et leurs propriétés, grâce à la caractérisation d'un verre nucléaire simulé contenant 3,0 % massique (1,02 % en volume) de platinoïdes. Une modélisation mathématique du comportement thixotrope de ce verre est présentée pour la première fois en utilisant un modèle similaire à celui proposé par Houska (Houska, 1981). Ce modèle prédictif permet la description des résultats expérimentaux obtenus à partir de mesures en régimes permanent et transitoire. L'impact de la contrainte de cisaillement et du temps sur le degré d'agrégation et la cinétique de sédimentation des particules est déterminé à l'aide d'un rhéomètre à contrainte imposée opéré à haute température et d'analyses d'images obtenues par microscopie électronique à balayage (MEB). Pour la première fois, l'interaction entre le comportement rhéologique du système et le degré d'agrégation est analysé, tout comme le lien avec la sédimentation des particules. Sur la base des données expérimentales acquises, un calcul d'équilibre des forces est réalisé pour illustrer les différents scénarios d'agrégation. Ce travail fournit des nouvelles données pour la modélisation et le contrôle du processus de vitrification.

Mots-clés : Platinoïdes, Thixotropie, Agrégation, Sédimentation, Rhéologie.